Collagenous chitinophosphatic shell of the brachiopod *Lingula*

ALWYN WILLIAMS[1], MAGGIE CUSACK[1] AND SARAH MACKAY[2]

[1]*Department of Geology and Applied Geology and* [2]*Department of Anatomy, University of Glasgow, Glasgow G12 8QQ, U.K.*

CONTENTS PAGE

SUMMARY

The structure and composition of the shell of living *Lingula* have been studied in detail to provide a measure for evaluating the evolution of the lingulid shell since early Palaeozoic times. Four constituents are identifiable at ultrastructural level. Apatite, specifically the fluorapatite francolite, occurs as coated granules, up to 10 nm in diameter, aggregated into spheroidal masses up to several microns in size, cylindroids up to 600 nm long and rare plates. Glycosaminoglycans (GAGs) are present throughout the shell as an elastic isotropic gel. Chitin is normally associated with a protein and is best seen under the scanning electron microscope after digestion of its associate by proteinases. As strands about 30 nm thick, chitin can form mats or be part of granular rods aligned as anastomosing ridges. Fibrillar collagens, with a periodicity of about 45 nm, occur mainly as sporadically developed mats throughout the body platform succession and as the core of the dorsal median septum. Elsewhere they appear sparingly as vertical and horizontal strands. At least ten proteins have been identified in the shell but it is not yet known which are covalently attached to GAGs, associated with the chitin or fabricated into membranes.

The entire integument consists of: a periostracum, about 4 μm thick, made up of closely packed fibrous tubes with axial strands presumably of chitin; a primary layer, about 40 μm thick, composed mainly of GAGs; and a mineralized secondary layer of variable thickness. The secondary layer is a succession of isotopic and isochronic laminae with thicknesses in microns compared with areas frequently of several square millimetres. Compact laminae, composed of closely packed spheroidal aggregates of apatitic granules are succeeded: by botryoidal or walled laminae, in which apatitic aggregates form botryoidal masses or vertical walls in a GAGs matrix; or by rod and plate laminae with apatitic rods accreting into anastomosing ridges disposed transversely on the body platform and radially in peripheral regions. The preponderance of the botryoid and rod laminae in the body platform and of anastomosing ridges in the lateral areas of a valve respectively explains the complex patterns of c-axis orientation of apatite obtained by X-ray diffraction. Membranous laminae, consisting of chitinoproteinaceous membranes (and sporadic collagenous mats) in GAGs, occur throughout the succession; while stratified laminae, characterized by gentle inclined, alternating organic and apatitic units, each just over a micron thick, are especially well developed (with compact laminae) at the junction with the primary layer.

Phil. Trans. R. Soc. Lond. B (1994) **346,** 223–266
Printed in Great Britain

Laminae group into well defined rhythmic sets beginning with an abrupt change from a membranous lamina to a biomineral succession founded on a compact lamina and passing gradually into a terminating membranous lamina which serves as the substrate for the next set. These rhythmic successions are secreted directly, without the intervention of extrapallial space, by outer epithelium which is anchored to the shell by variably persistent arrays of fine canals so that any cell is capable of secreting, in the right order, all the components of a rhythmic unit. When a compact lamina is being secreted apatitic granules are exocytosed through the digitate protrusions of the apical plasmalemmas of cells with clusters of large vesicles containing mottled electron-dense material and with mitochondria congregating apically. Termination of the compact lamina is marked by a sudden onset of GAGs secretion, probably from intercellular sources as well as from the cells, in which large vesicles of medium electron-dense material appear. Towards the end of a rhythmic cycle of secretion, large vesicles, which are mostly empty, and mitochondria are more dispersed throughout the cells.

Two features of phylogenetic importance have been revealed. The outer layers of the integument, the periostracum, primary layer and the underlying stratified laminar set of the secondary layer, are found in living *Discina* and *Lingula* and must have been characteristic of the ancestor of all organophosphatic brachiopods. The association of the newly discovered collagen with GAGs, apatite and chitin is probably a unique feature of the metazoan exoskeleton. It does, however, compare most closely with the uncalcified cuticle of certain protostomes, especially the priapulids, and strengthens the claim of affinities between the Priapulida and lingulide brachiopods based on their respiratory protein being haemerythrin.

1. INTRODUCTION

The geological record of *Lingula s.l.* is unexcelled among metazoans with biomineralized integuments. The genus is widely recorded in Lower Palaeozoic successions and may have been contemporaneous in the Ordovician with one of the earliest occurring brachiopods, the closely related *Lingulella* which was also a burrowing ciliary suspension feeder. Recently, Biernat & Emig (1993, p. 10) have asserted that 'no Paleozoic or Mesozoic (at least Lower Mesozoic)' lingulid species belong to *Lingula ss.* However, the distinctions drawn by them between *Lingula* and their newly founded *Lingularia* are based on changes in continuously variable morphological features like the relative length of the ventral body platform and consequently endorse the conservative nature of the *Lingula* stock. (References to fossil lingulas in this paper are made in that context.) In any event, the stock is a constant source of interest to students of evolution. G. G. Simpson (1953, p. 36), in his comparative survey of rates of evolution, cited *Lingula* as a prime example of arrested (bradytelic) evolution, as do most publications on this subject. Such references are invariably accompanied by comments on stock conservatism but seldom address two basic questions. First, has this old stock of at least 450 Ma standing truly retained its pristine genetic makeup? Secondly, how can such a conservative stock continue to thrive? Darwin (1859, p. 182) contended that had long-lived species, like those of *Lingula*, been the ancestors of the orders to which they belong, 'they would almost certainly have been long ago supplanted and exterminated by their numerous and improved descendants'. This assumption that *Lingula s.l.* is a specialized offshoot, rather than an arrested stem group within brachiopod phylogeny, fits more easily with the undeniable fact that, in terms of group longevity, *Lingula s.l.* is the most successful, skeleton-bearing metazoan ever to have evolved. Either way, the *Lingula* shell in its living and fossil state, fully merits investigation.

From a cladistic viewpoint, it has been argued that no information derived from the fossil remains of a group adds to our understanding of its phylogeny. This assertion may seem especially apposite for the *Lingula* shell which has undergone so little morphological elaboration during its evolution that to measure phylogeny by this means alone is unlikely to shed much light on the conservatism of the phenotype let alone the genotype of *Lingula*. There are, however, other, more informative measures of *Lingula* evolution than the shape of the shell or the impressions thereon of anatomical features, like muscle attachment areas and mantle canal systems. Over the past 30 years, a wealth of ultrastructural and compositional diversity has been discovered in the shell of living and fossil species; and sophisticated facilities, now becoming widely available, can be used to explore this variation which is potentially a more powerful means of assessing *Lingula* phylogeny than traditional morphological criteria.

The biochemical complexity of the organophosphatic shells of brachiopods has been suspected for well over a century (figure 1). The high organic content of the *Lingula* shell was known to Carpenter who was quoted by Blochmann (1892, p. 96) as having first identified chitin as the principal organic component. By the time Chapman (1914) had published his chemical analysis of the dried shell, it was generally accepted that the *Lingula* integument consisted of alternating layers of chitin and apatite. This view, with few refinements such as the variety of apatite involved (McConnell 1963), prevailed until 1965 when Jope published her definitive estimates of the shell composition of about twenty living and fossil brachiopod species. In this and subsequent papers (Jope 1979, 1980), she showed that the shell biochemistry of *Lingula* and other organophosphatic brachiopods is the most complex within the phylum.

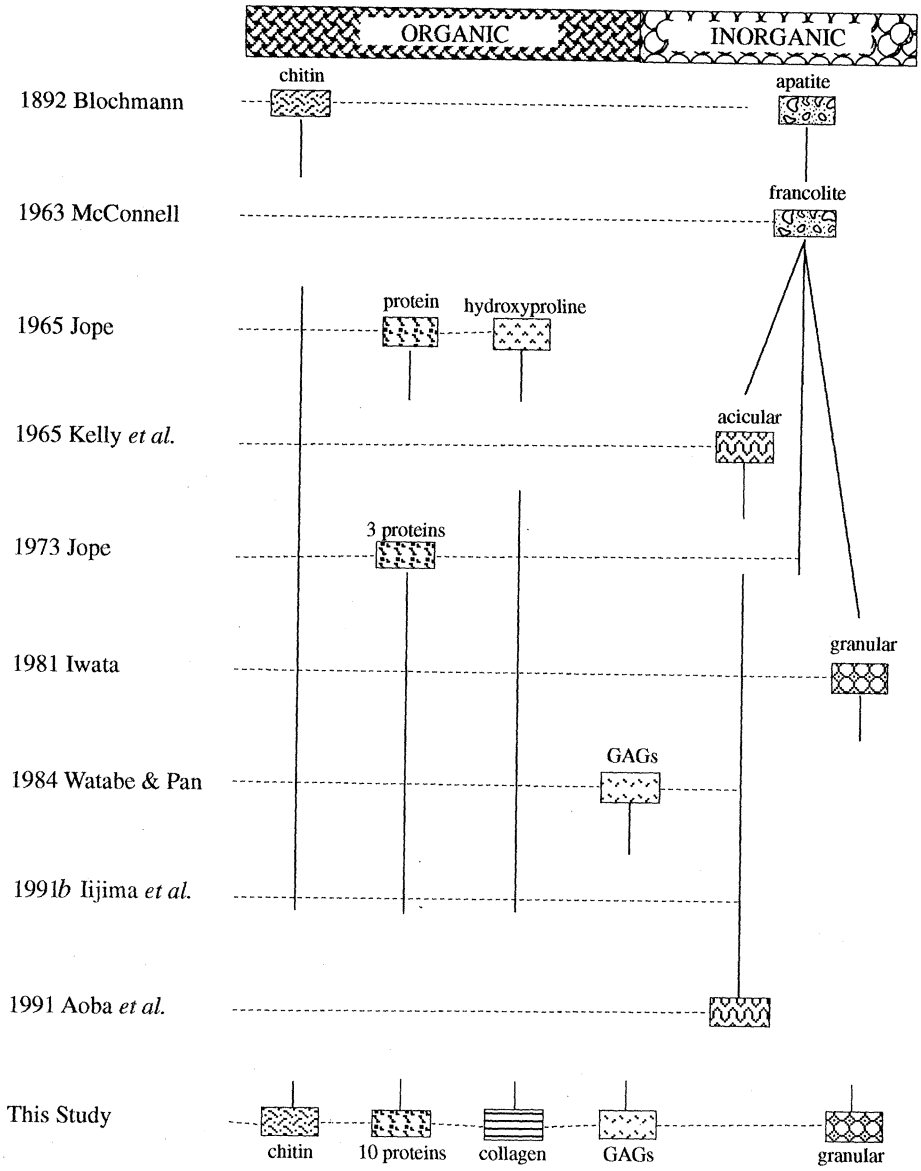

Figure 1. Chart showing the history of the identification of the known organic and biomineral components of the lingulid shell. Breaks in the continuity between the first identification of a component and confirmation of its occurrence in this study, represent investigations which were not concerned with, or failed to find, the component.

She identified at least three species of protein as well as chitin and drew attention to the presence of hydroxyproline in the organic complex although collagen had never been found within the shell. Later researches by Iwata (1981), Tuross & Fisher (1989) and Iijima *et al.* (1991*b*) confirmed and refined her findings; while Watabe & Pan (1984), investigating the related *Glottidia*, identified glycosaminoglycans (GAGs) as an important constituent of the shell. Further advances are now offered: by determining more precisely the shell components which are shown, for the first time, to include collagen; and, in the absence of any so-called 'extrapallial space', by attempting to determine the secretory history of the main components.

The biochemical complexity of the *Lingula* shell is reflected in its ultrastructural variability. This arises partly from the secretion of the shell constituents as a stratiform succession of alternating biomineralized and organic layers, more-or-less parallel with the valve surfaces, which can pass laterally and vertically into distinctive apatitic and polymer aggregates. Ultrastructural variability can also reflect the disparate strengths of the materials composing consecutive layers.

The ultrastructure of the stratiform successions has been differently interpreted. Iwata (1981, p. 38) found no evidence of an outer primary layer which, however, was later identified by Watabe & Pan (1984, p. 978) in the lingulid *Glottidia* as a distinctive mineralized zone. The reports were also at odds over the nature of the secreting epithelium with Iwata noting its cytological uniformity and Watabe & Pan its differentiation into three cell types each associated with a particular layer of the shell succession. All three authors, however, recognized a rhythmic alternation of organic and biomineralized layers. They concluded that the shell succession was built up by the accretion of its constituents out of an extra-pallial fluid and that the basic apatitic unit is an acicular crystallite

although Iwata also noted the existence of a smaller, granular particle. Not surprisingly, such variation in constituent aggregates has given rise to confusing X-ray diffraction configurations (Kelly *et al.* 1965; Aoba *et al.* 1991; Iijima *et al.* 1991*a*) with discernibly orientated acicular crystallites differently disposed in different parts of the shell. It is, however, possible to reconcile many of these conflicting observations by attempting to integrate them within a wider range of ultrastructural data as will be shown in the conclusions to this paper.

Ultrastructural successions, however, are not exclusively stratiform in disposition. Some layers consist of vertical walls of alternating organic and biomineral compositions. The secretion of these structures provides a model by which to explain the extraordinary layers of box-like apatitic compartments which characterize the shell successions of extinct organophosphatic acrotretoid brachiopods (Holmer 1989).

Ultrastructural features, resulting from the reactions of differently composed layers to stresses set up within the shell, are common. They include horizontal displacements of canals and especially microscopic folding of the periostracum and primary layer, which are subjected to stress couples (figure 4) during their migration from the mantle edge to become the substrate for the secretion of the secondary shell. During deposition of an organophosphatic shell, successive layers are secreted as elastic isotropic bodies; but, with polymerization and further maturation of their constituents, they become plastic or even brittle, dependent on the concentration and disposition of their biomineral contents and the degree of tanning of their organic components. Various strain features, indicative of the state of the media in which they occur, survive within successions as well as on the surfaces of valves. They can be distinguished from those brought about by the stresses of diagenesis and tectonism which affect shells during fossilization. Such features have only recently been studied as records of the dynamics of shell growth (Williams & Holmer 1992). The identification of such strain features in fossil shells reveals as much about the medium, in which they are cast, as the stress fields set up in the growing shell.

A synthesis of the biochemical and structural data of the living shell, in itself, would be a useful contribution to a full understanding of the biology of *Lingula*. Yet there is growing proof that many of the features described in this paper can be recognized in fossil species. Jope (1965) determined amino acid assemblages in many extinct brachiopods including a carbonate-shelled orthide of Ordovician age; and Tuross (1990) using immunological techniques identified a 40 kDa protein in fossil *Lingula*. In respect of the fossilization of ultrastructures, Holmer (1989 p. 31) has shown that the shells of Ordovician linguloids are not only stratiform but also characterized by variations in apatitic aggregation comparable with those of living species, a differentiation confirmed by our own unpublished researches on Carboniferous *Lingula s.l.* Even casts of the secreting plasmalemmas of outer epithelium on the internal shell surfaces of Cambro-Ordovician species of *Lingulella* (Curry & Williams 1983) provide as much relevant information on the degree of plasticity of the casting medium as on details of plasmalemmar surfaces of the mantle.

Given the longevity of *Lingula s.l.* and the increasing use of sophisticated equipment to explore all aspects of its durable and complex integument, it seemed to us that a wide-ranging study of the living shell could act as a measure of the degree of survival as well as the rate of evolution of various structural and compositional features of the shell of fossilized species.

2. SHELL MORPHOLOGY AND TERMINOLOGY

The shell of *Lingula* consists of a pair of gently convex, elongately elliptical valves with parallel sides (figure 2). Its colour can vary from dark brown and amber yellows to light jade greens. The brown colour, which may be apparent as growth banding, reflects different concentrations of ferric hydroxide in the periostracum (Jope 1965, H159).

The morphology of the shell is so simple (Emig 1979) that the dorsal valve (figure 3) differs from the ventral only in the absence of a median notch (pedicle groove) in the thickened posterior margin; the presence of a median septum in the middle of the valve; and some regrouping of muscle attachment areas (muscle scars). In contrast, many features, common to both valves of a mature *Lingula*, contribute to the compositional and ultrastructural differentiation of the shell. According to Kelly *et al.* (1965) and Iijima *et al.* (1991*a*), the inner laminar successions of the raised, lanceolate 'body platform',

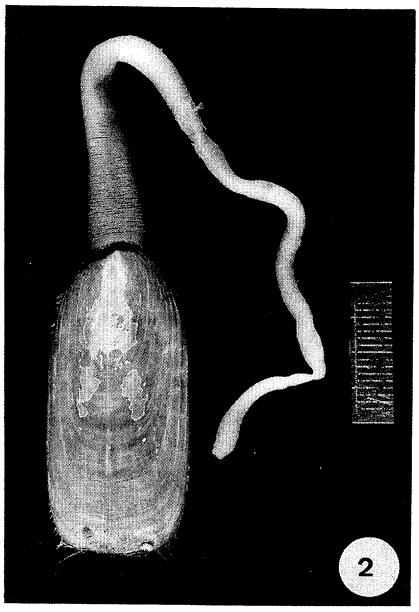

Figure 2. Dorsal view of a complete specimen of *Lingula anatina* (preserved in ethanol, 70% by volume) showing the shell in relation to the fleshy posterior stalk-like pedicle and the marginal fringe of setae; metal bar on right-hand side = 2 cm.

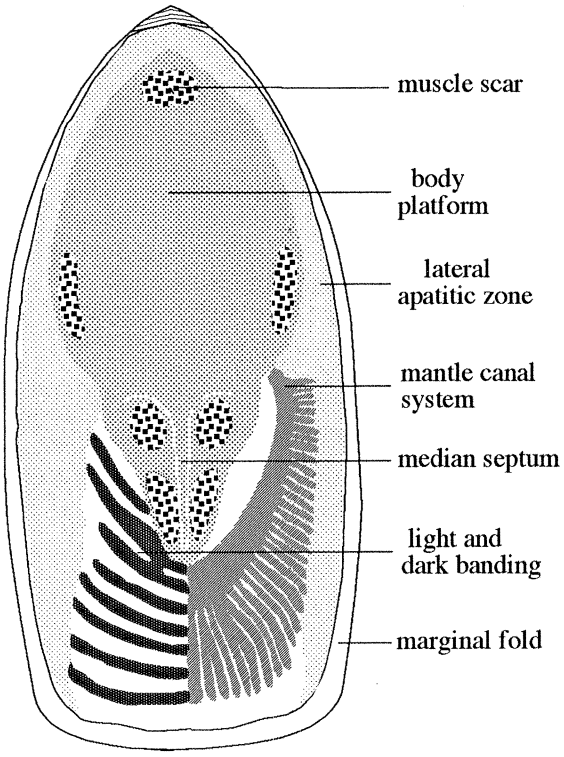

Figure 3. Stylized view of the internal morphology of the dorsal valve of *Lingula anatina* with a representation of the right anterolateral mantle canal system superimposed.

which corresponds to the main spread of the body cavity, differ from those of the flanking lateral areas in the size and orientation of their apatitic particles. The alternating dark and light concentric banding of the anterior part of the shell interior has been attributed by Blochmann (1892) to the prevalence of chitin and apatite respectively. A radial lineation, reflecting the disposition of the overlying mantle canal system, is superimposed on this concentric banding. The rounded marginal fold, which borders both valves and contains the outer mantle lobe (periostracal lobe) within a periostracal groove (figure 5), owes its structure to its organic composition.

The terminology used to describe the shell structure of *Lingula* (figure 4) is that adopted for *Discina*, another stratiform, organophosphatic brachiopod (Williams *et al.* 1992). The distinction between the outer (primary) and inner (secondary) layers of *Lingula* is sharp as is the basic unit of the shell succession, the lamina, although it now has to be more precisely defined. The laminae of *Discina* were described as structurally homogeneous (isotopic) units, secreted simultaneously (isochronic) over their entire area. Such units are also typical of *Lingula*. Yet, the edges of an isotopic unit can transgress across underlying laminae, not diachronously but as a result of changes in the components being secreted by the same patch of outer epithe-

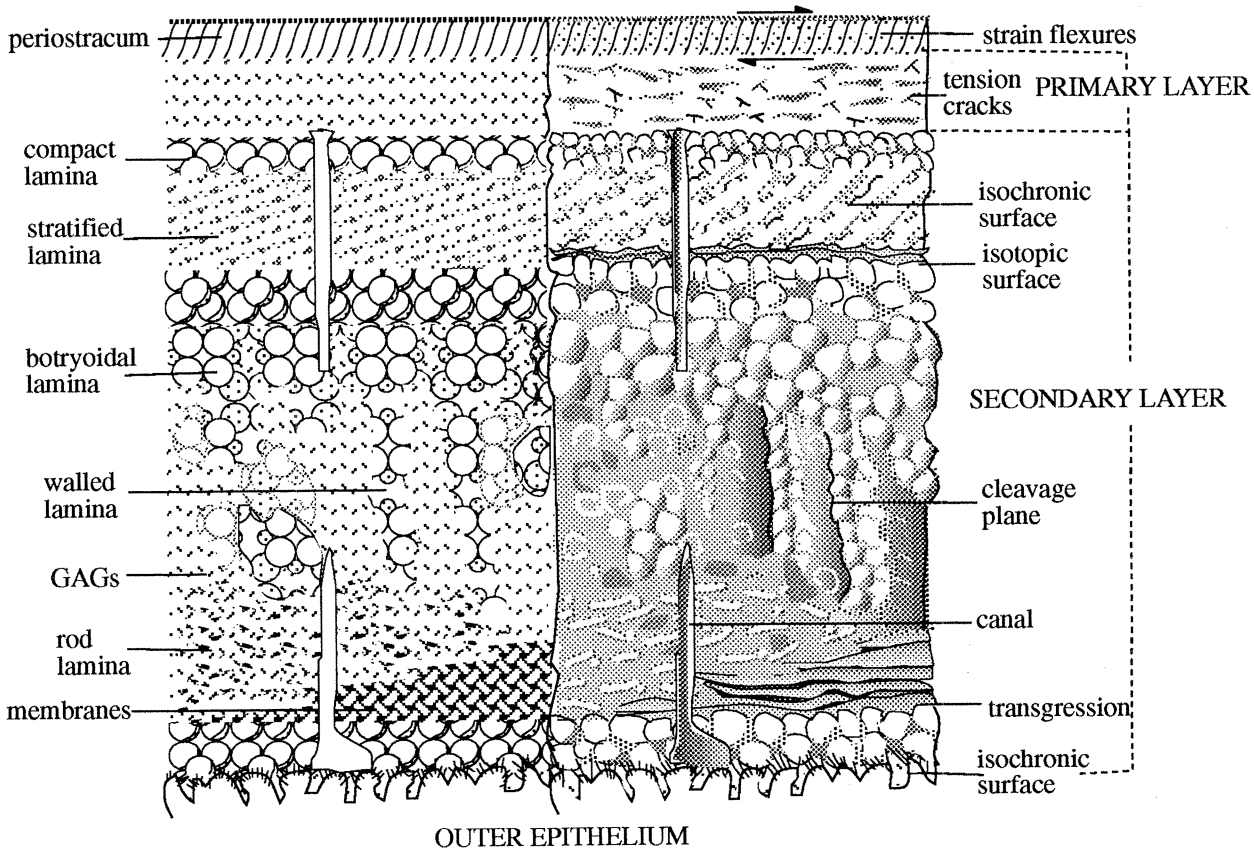

Figure 4. Diagrammatic representation of the relationship and diagnostic features of the integument of *Lingula anatina* as seen in polished and etched section (to the left) and in fracture surfaces. The opposing arrows in the top right-hand sector of the periostracum are a stress couple deduced from the plastic deformation of the outer periostracal tubes.

lium; and the term 'isochronic' is now used in this context (figure 4).

The canalicular shells of *Discina* and *Lingula* are also so alike in other respects that the terminology, used in the former genus to describe the basic unit and aggregates of apatite and the lamination, is appropriate for the latter. However, aggregation of apatite in the shell of *Lingula*, with its much higher organic content, is generally more dispersed and gives a botryoidal rather than a rubbly appearance to successions between compact apatitic and membranous organic laminae. Moreover, groups of continuous laminae, which pass laterally as well as vertically into one another, are more obviously rhythmic secretory units than their counterparts in *Discina* and are here referred to as 'sets' (figures 64 and 65). Other, minor amendments, are explained in the main part of the paper.

3. RESULTS

(*a*) *Periostracum*

The secretion, structure and composition of the periostracal cover to the shell have already been described (Williams 1977; Williams & Mackay 1978; Iwata 1981; Pan & Watabe 1989). However, new data on the periostracum warrant a brief discussion even though the layer is unlikely to survive in a fossilized state.

The layer is secreted at the mantle edge by the periostracal lobe (figures 5 and 68) on an organic substrate (pellicle). The pellicle is first exuded by lobate cell(s) on the surface of the glycocalyx adhering to the microvilli of adjacent inner epithelium. As the pellicle moves forwards around the lobe, it acts not only as a foundation for the periostracum but also as

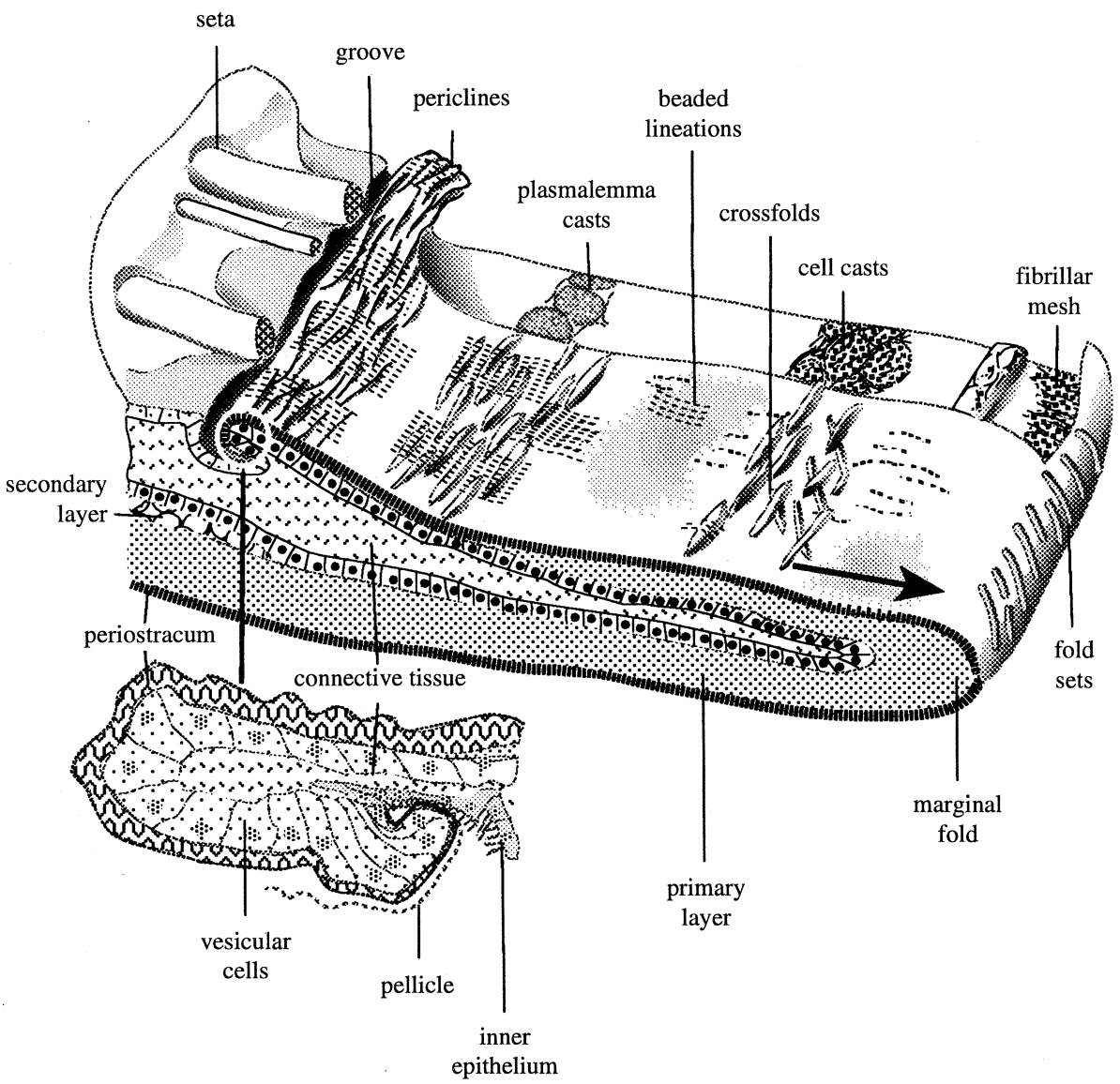

Figure 5. Stylized block section of the marginal fold of *Lingula* showing the relationship of an expanding mantle and integument, unrolling in the direction of the arrow (with an enlargement of the periostracal lobe in the bottom left hand corner). The diagram gives the location of the main superficial features on the internal surface of the marginal fold distal of its secretion on the periostracal lobe; and, on the cut-out sector along the top edge of the fold, the location of various internal microstructures including all casts associated with the primary layer and plasmalemma casts on the first-formed secondary layer.

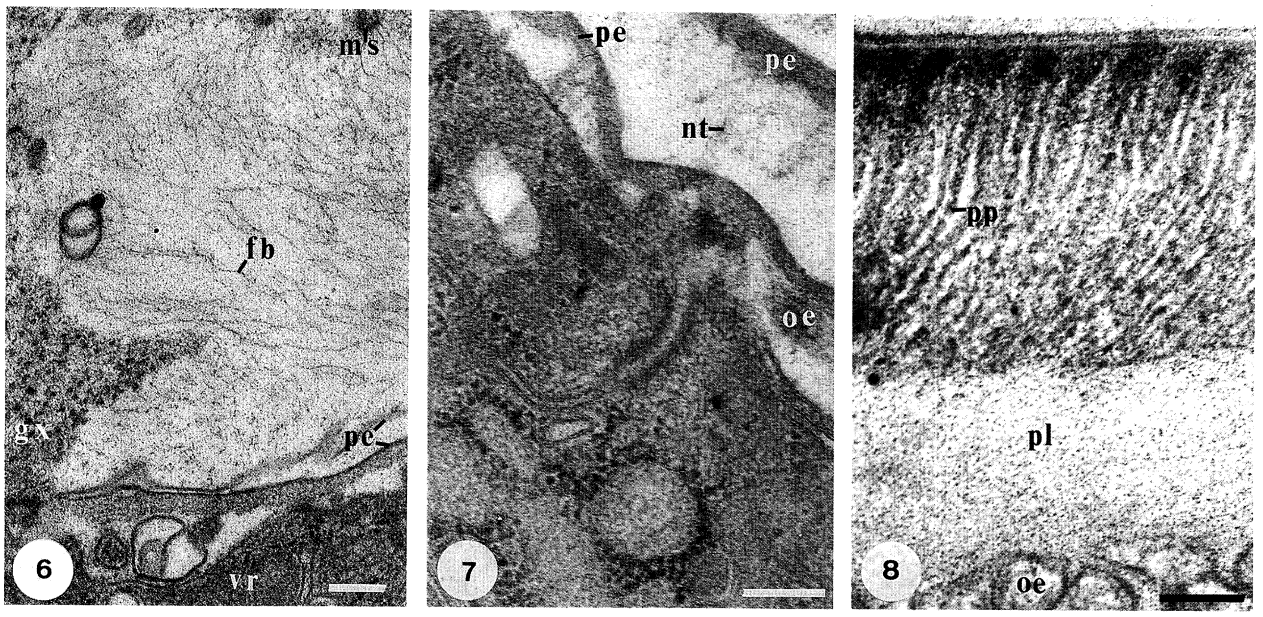

Figures 6–8. Transmission electron micrographs of sections of demineralized margins of valves of *Lingula reevii* to show the structure of the periostracum.

Figure 6. Origin of the pellicle (pe) in relation to the fibrils (fb) of the microvilli (ms) of the inner epithelium, glycocalyx (gx) and the first formed part of the periostracum underlain by vesicular cells (vr). Scale bar = 100 nm.

Figure 7. Detail of the pellicle (pe) with a network of fibrils and particles (nt) between the microvilli of inner epithelium (top right-hand corner) and the apical region of vesicular cells with finger-like protrusions (oe). Scale bar = 100 nm.

Figure 8. Detail of periostracum showing the strings of particles (pp) within electron-dense walls of the close-packed tubes, underlain by primary layer composed of GAGs (pl) and the cylindroid protrusions of the apical plasmalemma of outer epithelium (oe); the sigmoidal flexture of the walls indicates a stress couple inducing a dextral drag. Scale bar = 100 nm.

an adhesion surface for a web of fibrils arising from the tips of microvilli of more distal inner epithelium (figure 6). Simultaneously both sides of the layer polymerize. That connected with the fibrillar web becomes an electron-dense layer which can thicken distally to 100 nm; that acting as a substrate for the periostracum becomes a triple-layered membrane. Under the transmission electron microscope (TEM), the two sides are seen to diverge from the hinge at their place of origin. This separation could be an artefact but it is more likely to be a manifestation of the migration of the maturing periostracum. In sections of well-fixed, healthy specimens, an open network of medium electron-dense fibrils and granules (figure 7), bridging the gap between the two sides, could represent an ordered layer of linearly arranged constituents (figure 9) in the natural state, which is ruptured during the preparation of specimens. In any event, the inner epithelium plays a greater role than previously thought in the development of the periostracum.

The fully developed periostracum of *Lingula* is that part of the integument which is secreted on the inner surface of the periostracal lobe (figure 5). In mature valves it is seldom more than 4 μm thick and consists of two layers. The thicker, outer layer is an array of closely packed tubes between 50–60 nm in diameter (figure 8). Distally the tubes are orthogonal to the external surface but proximally are usually deflected posteriorly by stress couples (figure 4) set up by differentially migrating periostracum and secreting epithelium. The walls of the tubes are fibrous; they enclose cores of particles less than 7 nm in size, strung together as electron-dense strands and tapering basally for 500 nm or so. The thicker, inner layer, which grades insensibly into the succeeding primary layer, also contains fibrils and granules but these are usually densely scattered in an electron-lucent matrix.

The tubular layer first appears on the backward facing arch of the periostracal lobe. Immediately beneath the bounding triple membrane, single rows of three to four particles become aligned along inclined fibres about 20 nm apart. The differentiation of the outer layer must therefore involve a continuous accretion of the fibrils and particles, dispersed throughout the thickening inner layer, to form, by polymerization, the lengthening tubes and their contents. The composition of the different components is presently conjectural. Pan & Watabe (1989) reported that the same kind of periostracum of *Glottidia* gave strong positive reactions for neutral polysaccharide, GAGs, lipoprotein and chitin; glycoprotein and phenol oxidase were additionally present in the outer layer. In the present study an Alcian Blue test has confirmed the presence of acidic GAGs. Therefore, it may be assumed that the periostracal

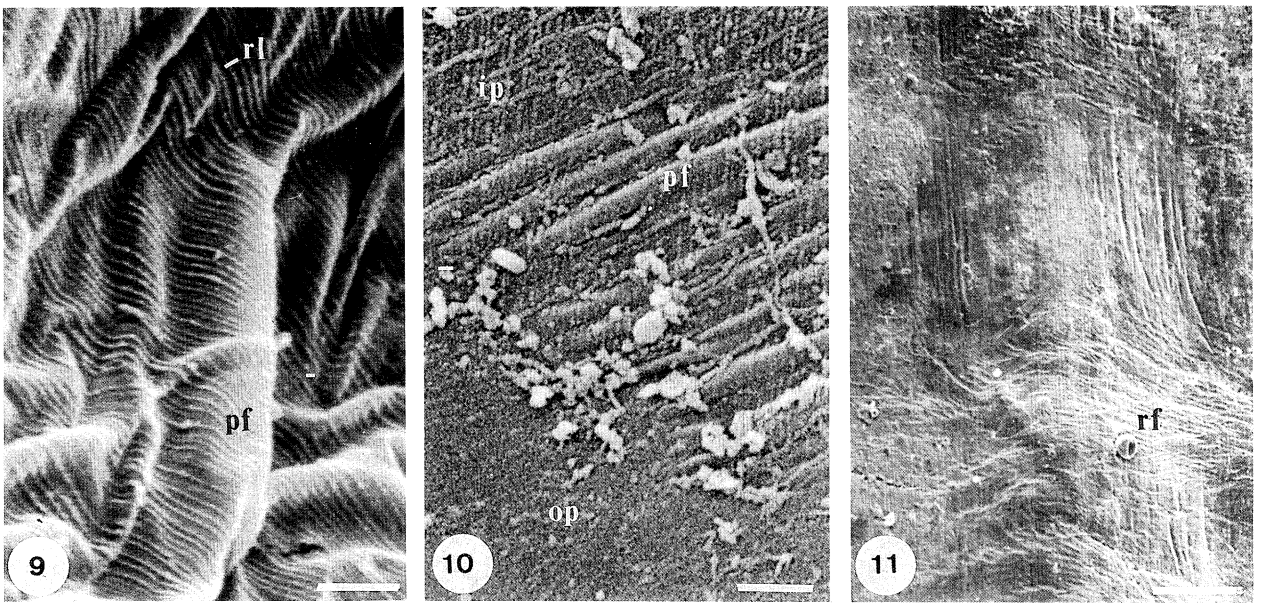

Figures 9–11. Scanning electron micrographs of gold-coated periostracal sufaces of critical point dried valves of *Lingula anatina*.

Figure 9. View of periostracum immediately distal of the periostracal groove, folded into two sets of periclines with the dominant set (pf) concentric with the groove, and ornamented by radial lineations (rl) on the inner membrane of the pellicle. Scale bar = 1 μm.

Figure 10. View of partly exfoliated inner surface of the marginal fold, showing the outer (op) and inner, lineated (ip) membranes of the pellicle with the underlying periostracum folded into impersistent periclines (pf). Scale bar = 2 μm.

Figure 11. General view of the outer side of the marginal fold showing sets of radial folds (rf) splaying towards the valve margin to the left and affecting the periostracum and underlying primary layer. Scale bar = 50 μm.

matrix is acidic GAGs and that the outer layer is a basketwork of quinone-tanned fibrous proteins containing discrete chitinous strands.

Under the scanning electron microscope (SEM), the microtopography of the periostracum appears as a mixture of features formed after, as well as during, secretion (figure 5). The periostracum, on the inward-facing surface of the periostracal lobe is normally ornamented by parallel sets of rounded, sporadically beaded lineations up to 40 nm in wavelength and between 50 and 100 nm apart (figure 9). The lineations lie orthogonal to the edge of the periostracal lobe while the periostracum is commonly thrown into rounded periclinal folds (figure 9) concentric with the edge of the lobe. The folds may be up to several microns in wavelength and affect the underlying primary layer as well. Other periclines, with axes seldom more than 5 μm long, are superficial (figure 10) and may occur as crossfolds (figure 5). Around the marginal fold, the various fold systems of the lobe give way to regular sets of folds, about 1 μm in wavelength, like creases developed in cloth under tension; but even these are generally absent from the external surface of the valve. This suggests that such fold phases are only characteristic of the periostracum and the underlying primary layer while they are still in a plastic condition.

However, fan shaped sets of fine, radial folds (figure 11) are commonly developed on the external surfaces especially in association with strong, concentric growth lines (Williams & Holmer 1992). These folds are strain figures induced by stress couples sustained throughout the polymerization of the external coats and their subsequent stiffening by apatitic secretion. An abnormal retraction of the entire periostracal lobe or damage to the shell margin can cause such stresses.

The periostracal layer, in its polymerized state, is stratiform. It consists of a succession of thin plates with a finely granular texture and poor radial cleavage and is affected by well developed desiccation cracks.

(*b*) *Subperiostracal integument: basic constituents*

The main constituents of the *Lingula* shell are well known (figure 1). The mineral component is the carbonate fluorapatite, francolite (McConnell 1963; Watabe & Pan 1984). The principal organic components are glycosaminoglycans (Watabe & Pan 1984), chitin (Jope 1965) and protein (Jope 1965, 1980; Iwata 1981; Iijima *et al.* 1991*a*). However, there is much less certainty about the form and distribution of these constituents within the shell. In particular, the shell succession is more complex than an alternation of mineralized and organic layers (Watabe 1990) as can be shown after outlining the diagnostic properties of its main constituents. The constituents were identified by procedures outlined in the Appendix, including attempts at their differential digestion and oxidation by enzymes and bleach

Table 1. *The effects of treating cleaned internal surfaces and fracture sections of the shell of* Lingula anatina *with enzymes and varying concentrations of bleach (sodium hypochlorite) by procedures described in the Appendix*

(Various concentrations of bleach (n% by volume) and five enzymes, some in combination, were used and are identified along the top row as Bl (bleach), Co (collagenase), Ch (chitinase), P-K (proteinase-K), G-C (endoproteinase Glu-C) and Su (subtilisin); the number in brackets, (n), after each enzyme(s) symbol represents the number of sets of matching pieces treated with enzymes(s) (or bleach) and buffer before examination under the SEM. The various features of the shell, which were removed or exposed by treatment, are given in the left-hand column with a bracketted figure number, (fig. *n*), alongside each feature identifying a micrograph, in which the feature is well displayed. Matching pieces which consistently showed the same effects are indicated as having undergone significant (√) or some (v) changes or no discernible change (x). Matching pieces which were affected inconclusively or which had no exposures of a stated feature are represented by blank spaces.)

		Bl (13)	Co (4)	Ch (6)	Ch & Co (3)	P-K (4)	P-K & Co (3)	P-K & Ch (3)	G-C (3)	G-C & Co (3)	G-C & Ch (3)	Su (2)
remove:												
coats of apatitic granules/spherules	(fig. 14)	√(5%)	x	x	x	√		√		x	√	√
GAGs infill	(fig. 22)	√(2%)	x	x	x	v	√	√	v	√	v	v
membranes												
as laminae	(fig. 58)	√(2%)	x	√	x			v	v			√
across canals	(fig. 85)	√(2%)		v	x			√			√	v
over mats of curved rods	(fig. 44)				x		√	√	v		x	
over anastomosing ridges	(fig. 33)	√(2%)	x	v	√			√				
mats of curved rods	(fig. 50)		x	x				x	x			
strands/hoops	(fig. 86)	√(5%)	x	x		v		x	x		√	√
canal contents	(fig. 84)	√(1%)			√	√		√	√	√	√	v
expose:												
chambers	(fig. 88)	√(1%)	x	x		√		√	√		√	√
galleries	(fig. 83)	√(1%)	x	x		√		√	√	√	√	√
botryoids	(fig. 15)	√(1%)	x	x	v	√	√	√	√	√	√	√
rods/plates	(fig. 19)	√(1%)	x	v		√		√				x

respectively (table 1). Details of their distribution and physical appearance under the electron microscope are given in expectation that some of the properties observed will prove useful in inferring the original composition and fabrics of fossilized shells.

(i) *Apatite*

The basic apatitic unit is a granule (figures 12–14) comparable, in its size of up to 10 nm and in its electron-dense coat, with that of *Discina* (Williams *et al.* 1992). At high resolutions possible with the Hitachi 900 SEM, the main difficulty in determining the nature of apatitic constituents lies in distinguishing between the smallest of these constituents and the grains of gold/palladium film deposited by shadowing. However, the interiors and cut edges of membranes lining canals in fracture sections should be mainly free of biominerals so that any granular texture is likely to be the result of shadowing. Accordingly, evenly spread films of spheroidal particles, with a uniform diameter between three and four nanometres, coating the linings of canals have been interpreted as gold/palladium grains (figure 12). Their low relief contrasts with the near spherical shapes of the apatitic granules composing the spherules and mosaics of dispersed botryoids (figure 13) or closely packed aggregates (figure 14).

At resolutions less than 10 Å, no acicular crystallites have been seen, only granules and rare prismatic plates. It is, therefore, assumed that the subrounded granules are pinacoidal plates with c-axes orthogonal to their surfaces. In sections of mineralized shell examined under the TEM, the granules are identifiable as having electron-light cores, presumably apatite, with proteinaceous electron-dense coats (figures 79 and 81). However, the organic cover is not readily digested by proteinases nor by chitinase either separately or in association with the proteinases. Even spherules, rounded aggregates of closely packed granules, are only freed of their organic matrix by oxidation in a 2–5% (by volume) bleach solution. Yet such aggregates are aligned with the fibre axes of chitin (Kelly *et al.* 1965) and it is assumed that the coat consists of layered chitin and protein which tend to mask each other.

Under the SEM at resolutions coarser than 20 nm, the spherule is the typical biomineral unit (figure 17). It averages nearly 55 nm in diameter and is coated with a protein which is partly removed by proteinase-K and sufficently oxidized by 1% bleach for the

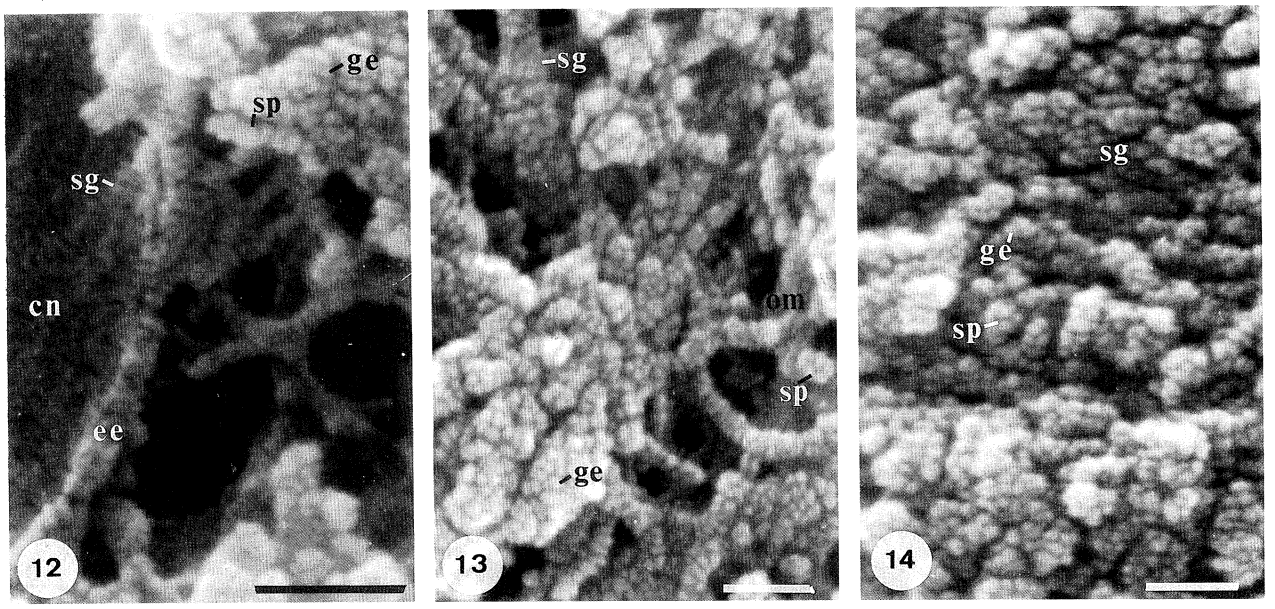

Figure 12–14. Scanning electron micrographs of gold/palladium-coated transverse, vertical fracture sections of the mid-part of a valve of *Lingula anatina* digested in subtilisin.

Figure 12. Internal surface and edge (ee) of the membranous lining of a canal (cn) showing the gold/palladium grains (sg) and the granules (ge) and spherules (sp) of apatitic botryoids on an organic framework linked with the canals. Scale bar = 50 nm.

Figure 13. Botryoids and mosaics on an organic framework (om) showing spherules (sp), granules, (ge) and gold/palladium grains (sg). Scale bar = 50 nm.

Figure 14. Close-packed spheroidal aggregates of apatite forming a compact lamina with gold/palladium grains (sg), granules (ge) and spherules (sp). Scale bar = 50 nm.

contained spherule to be dislodged from its substrate. Spherules can occur as discrete bodies but are usually closely packed into spheroidal mosaics (figures 14–16), averaging just over 210 nm in size. Mosaics, in turn, are frequently aggregated into botryoidal masses (figure 15), normally 1.5 μm in maximum diameter but exceptionally four or five times as big.

Apatitic rods (figures 18 and 19), associated with mosaics, are locally prevalent especially in the inner parts of the shell succession. They vary greatly in size but are commonly 400 nm long and 75 nm wide. They are essentially strings of spherules; and, unlike acicular crystallites, are not prismatic in habit but usually gently flexured with discernible spherules, linearly arranged. The flexible nature of these spherular rods (figures 34 and 35) and their smooth yet well delineated outlines indicate that they are sheathed in organic coats which survive treatment with the proteinases and chitinase but not with bleach (5% by volume).

Rods of a crystalline aspect do occur rarely in lenticular patches within the shell succession (figure 17), where they are disposed orthogonally to the secretory surface. They can be up to 1.5 μm long and between 200 and 500 nm in diameter increasing towards terminal domes. The domes usually split and splay outwards into twofold or fourfold arrangements of wedge-shaped plates simulating pyramidal faces of prismatic apatite. In a section digested in proteinase-K and chitinase, structures were further disaggregated into splayed bundles of rods, about 700 nm long and 40 nm thick. Even so, the spherular composition of the wedges and rods was still evident.

Apatitic blades occur, especially in some predominantly organic laminae (figures 18–20) in association with spherules, mosaics and rods. The blades are between 30 and 50 nm thick and consist of a double layer of spherules although one side may serve as a substrate for additional spherules and mosaics. They vary in area but are usually very much longer (up to 1 μm) than wide (150 nm). Many of them have fractured ends and appear to be fragments of larger units; others are tablets bounded by prismatic faces.

(ii) *Glycosaminoglycans*

The dominant organic component of the lingulid shell is glycosaminoglycans (GAGs). Sections of the shell and mantle of *Lingula*, stained with Alcian Blue, have revealed the pervasive presence of acidic GAGs and corroborate their histochemical identification in the shell of *Glottidia* (Watabe & Pan 1984). The distribution of GAGs in stained sections examined optically is clear enough to serve as a guide to their occurrences and main characteristics in shells viewed under the electron microscope. The complex, however, undergoes perceptible structural changes through dehydration as well as other forms of chemical degradation. It is also intimately associated with several microtopographic features of different origins. The characteristics and distribution of GAGs, therefore, have to be considered in the light of these complications.

GAGs act as an elastic isotropic gel in shells which, prior to shadowing, had been stored in ethanol (and transferred to distilled water in a laminar flow cabinet) or fixed in glutaraldehyde and stored in phosphate buffer (for critical point drying). On vertical fracture surfaces the gel also has a thixotropic tendency to flow so that cut laminae have smooth, rounded faces marked only by sporadic shallow pits, about 100 nm in diameter.

Dehydration is signalled by trails of short tension cracks (figure 23), seldom exceeding 500 nm in length, and patches of closely packed contraction depressions

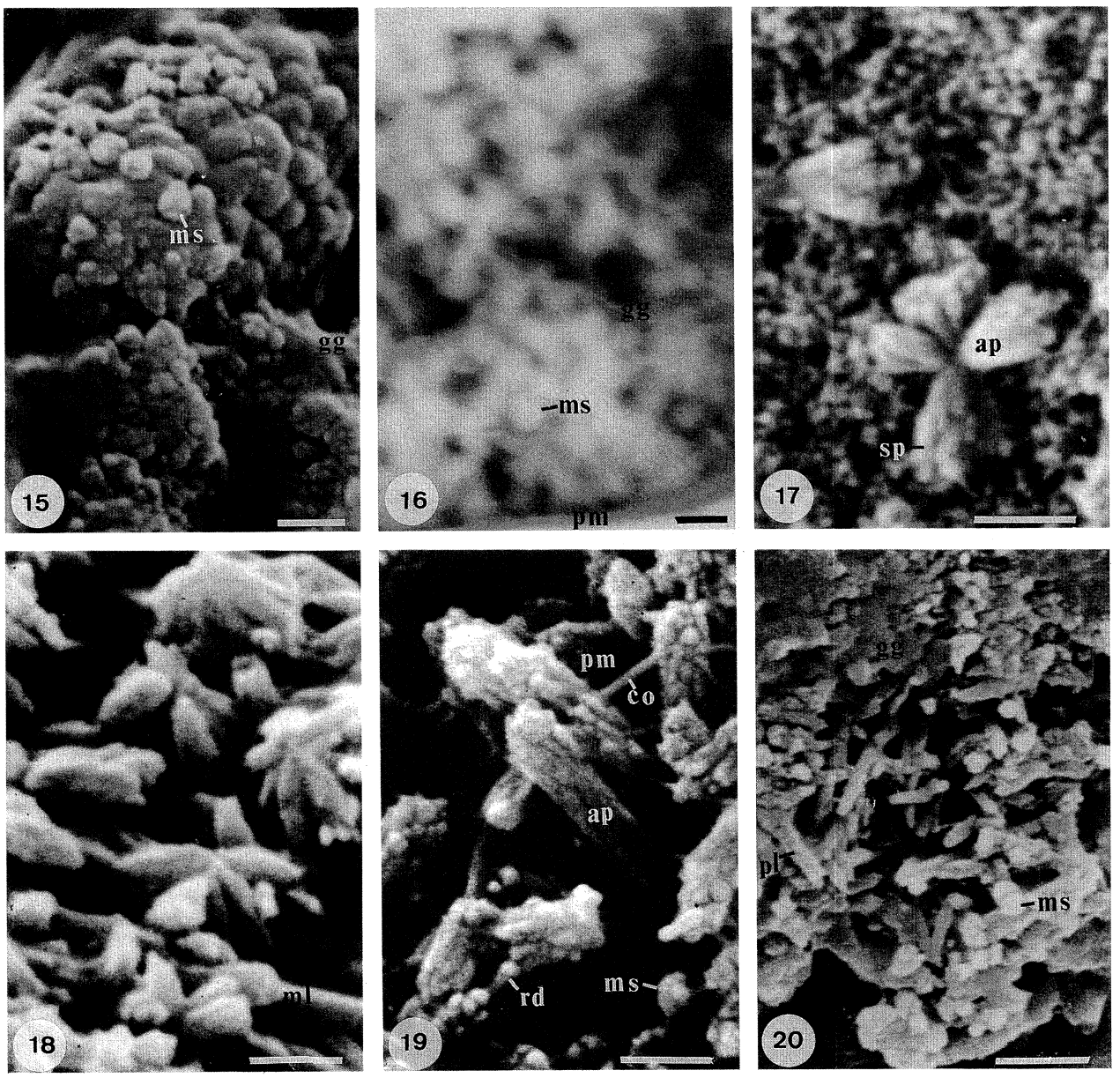

Figures 15–20. Scanning electron micrographs of gold-coated and carbon-coated (figure 16) vertical sections of valves of *Lingula anatina*.

Figure 15. Botryoidal aggregate of apatitic mosaics (ms) in a matrix of GAGs (gg) exposed in a posteromedian section of a valve treated with phosphate buffer (100 mM, pH 7). Scale bar = 0.5 μm.

Figure 16. Back scattered electron scan showing the apatitic composition of botryoids consisting of mosaics (ms) in GAGs (gg) and capped by a chitinoproteinaceous membrane (pm). Scale bar = 1 μm.

Figure 17. A split dome of apatite (in a matrix of spherular apatite and GAGs) showing the spherular texture (sp) of wedge-shaped plates (ap) exposed in a posteromedian section of a valve treated with Tris buffer (80 mM, pH 8) with $CaCl_2$ (100 mM). Scale bar = 0.5 μm.

Figures 18, 19. Mosaics (ms), plates (ap) and rods (rd) of apatite exposed in association with collagenous fibrils (co) and membranes (pm) and with membranous laminae (ml) in a submedian section of a valve digested in subtilisin. Scale bars = 0.5 μm.

Figure 20. Plates (ap) and mosaics (ms) of apatite exposed after the removal of most of the GAGs (gg) filling a chamber in a posteromedian section of a valve digested in subtilisin. Scale bar = 1 μm.

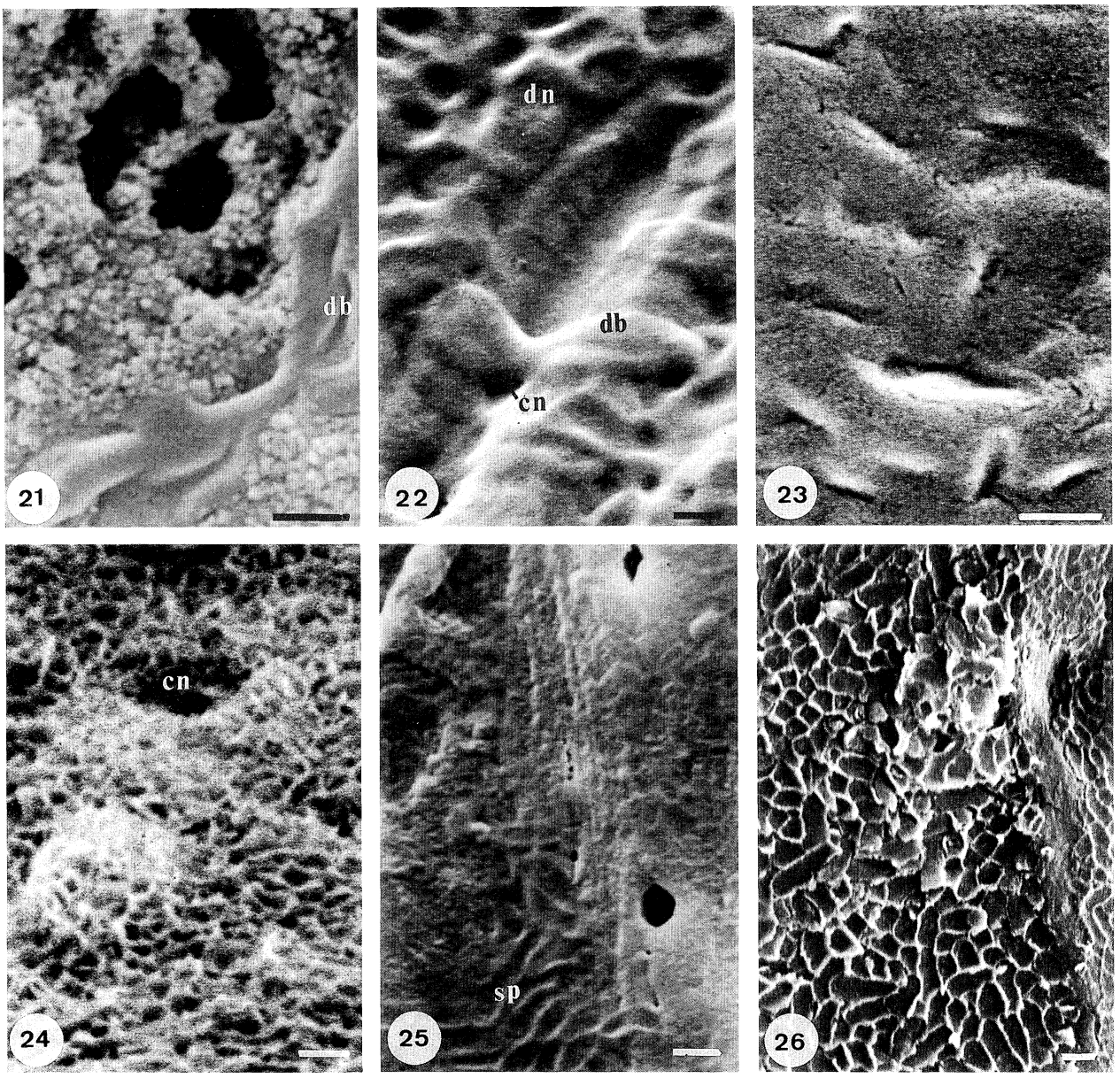

Figures 21–26. Scanning electron micrographs of gold-coated surfaces of the shell of *Lingula anatina*.

Figure 21. Residual GAGs with remnants of discoidal bodies (db) on botryoidal apatite of the internal surface of the submedial part of a valve treated with 2% bleach (by volume). Scale bar = 0.5 μm.

Figure 22. Residual GAGs with contraction depressions (dn) and discoidal bodies (db) on anastomosing ridges of apatite with canal aperture (cn) on the internal surface of the anterolateral part of a valve digested in proteinase-K. Scale bar = 0.5 μm.

Figure 23. GAGs exposed in a cut, vertical, anteromedian section of a valve digested in proteinase-K, with tension cracks and orthogonal slots of dehydration. Scale bar = 0.5 μm.

Figure 24. GAGS indented by close-packed, hemispherical hollows presumably impressed by apatitic mosaics of succeeding compact lamina, exposed on an inner facing surface with canal aperture (cn) in a cut, vertical section of a valve treated with phosphate (100 mM, pH 7) and Tris buffers (80 mM, pH 8) with $CaCl_2$ (100 mM). Scale = 0.5 μm.

Figure 25. A residual film of GAGs, indented by casts of secreting plamalemma (sp) and overlying a chitinoproteinaceous surface with a scatter of apatitic mosaics between two canal apertures, on the internal surface of the anterolateral part of a valve digested in proteinase-K. Scale bar = 1 μm.

Figure 26. A film of GAGs, indented by casts of the distal tips and sides of cylindroid protrusions of secreting plasmalemma exposed on an inward facing surface beneath a thin succession of laminae forming the internal surface of the posterolateral part of a valve treated with Tris buffer (80 mM, pH 8) with $CaCl_2$ (100 mM). Scale bar = 1 μm.

(figure 22), each up to 1 μm in diameter. However, internal surfaces may also bear features of comparable microtopography arising from other causes. Removal of outer epithelium from the shell interior exposes surfaces as they were being secreted at death. A layer of GAGs frequently provides such a surface and may be thin enough to assume the shape of more rigid underlying structures. Fibrous layers of chitin and collagen may be outlined in this way (figures 43 and 44). The latter frequently forms a network simulating contraction depressions but it invariably includes distinctive linear and arcuate branches.

A more subtle simulation of contraction features occurs when a layer of GAGs polymerizes as a cast of its secreting outer epithelium (figures 25 and 26). The secreting apical plasmalemmas are digitate with finger-like extensions, typically up to 3 μm long and 600 nm thick and frequently interspersed with clusters of vesicles up to 300 nm in diameter. Casts of these digitate tips fall within the size range of dehydration depressions and the resemblance is further enhanced by the tendency of the plasmalemmar protrusions to be arranged in hexagonal arrays. However, there are always some protrusions which are inclined or even recumbent relative to the outer epithelial plane. They give rise to curved cylindrical casts which could not be induced by dehydration.

The inner surface of a layer of GAGs may also be indented by closely packed apatitic mosaics at the base of a succeeding compact lamina. In fracture sections where such an apatitic lamina has broken away from its GAGs substrate, the casts of the mosaics form a roughly honeycomb structure (figure 24).

Except for specimens prepared in a laminar flow cabinet, GAGs surfaces, carry a variety of superficial features. Some of these are microbial in origin; others, which look like bacteria, are typically ellipsoidal with minor axes averaging 60% of the mean maximum length at 1.3 μm and proportions ranging from 25 to 80% in parallel-sided and discoidal structures respectively (figures 21 and 22). Notwithstanding such changes in shape, the bodies ('ellipsoids') are all characterized by central depressions of varying depth, bounded by rounded, thick (250 nm) rims.

Although these ellipsoids resemble bacterial rods and cocci, several characteristics preclude any connection. A microbe has a relatively strong, rigid integument and is usually surrounded by a ridge of, or a furrow within, the GAGs marking the boundary of its feeding area. Accordingly, when it is dislodged by bleach or enzymic digestion, its feeding zone is seen as a smooth concave area imprinted on the GAGs surface. In contrast, ellipsoids are flaccid bodies moulding themselves to any topographic change in their substrate (figure 22). They have no differentially developed coats so that, when they are superimposed on other ellipsoids or on epithelial imprints in GAGs, their junctions are changes in slope rather than texture. This accounts for the way ellipsoids are subject to the same kind of deformation as their GAGs substrate.

Ellipsoids are evidently composed of GAGs and are either artefacts or the products of a distinctive mode of secretion. Their characteristics favour the latter interpretation. An ellipsoid has the appearance of having been a viscous sphere squeezed so as to cause its contents to spread outwards. This would be consistent with the intrusion, between epithelium and shell, of vesicles of GAGs by intermittent exocytosis. In the light of this interpretation it is noteworthy that an average ellipsoid, 200 nm thick, could be formed from a vesicle of GAGs with a diameter of about 600 nm.

The efficacy of the various reagents used to remove GAGs from the lingulid shell is variable. The proteinases digested sufficient of the proteinaceous component of GAGs to expose most of the other components of the shell. Proteinase-K was especially effective and in association with chitinase helped to determine the characteristics of chitin. Bleach (between 2% and 5% by volume) effected a more vigorous but less selective degradation so that residual structures were seldom left intact.

Under the TEM, GAGs are most easily identified for comparative purposes in the primary layer where, according to an Alcian Blue test, it is practically the sole constituent (figure 8). In sections of this layer which had been demineralized and stained with uranyl acetate and lead citrate, the GAGs appear as a closely distributed mesh of fine fibrils and granules of medium electron-density in an electron-light matrix. GAGs in the secondary shell do not differ significantly.

(iii) *Chitin*

Chitin is the second most common organic constituent of the lingulid shell (about one-fifth of the total dry mass according to Jope (1965, p. H160)) but is the most elusive component to identify. Its presence in the shell of *Lingula* had been confirmed histochemically by the chitosan test by the mid-nineteenth century and biochemically as a hexosamine in 1965 (Jope, p. H162); while its structure as a β-chitin was first determined by X-ray diffraction by Dweltz (1961). However, its ultrastructural form and distribution have always been in doubt because it does not have a good contrast under normal staining procedures for electron microscopy (Rudall 1969; Pan & Watabe 1988). This complication has tended by default to perpetuate a widely held assumption that the shell consists of alternating layers of apatite and chitin (Blochmann 1892) although, as Iwata observed (1981, p. 40), the so-called chitin layer is not readily degraded by chitinase so that any chitin present must be masked by other organic compounds.

Rudall (1969, p. 92) obtained good images by negative staining and by shadowing layers more or less parallel to the inner surfaces of chitinous cuticles. In our studies, positive staining with uranyl acetate has frequently revealed discrete beaded fibres up to 150 nm long and aligned parallel to one another in sections of mineralized shell. The 'beads' along these fibres have been interpreted as coated granules of apatite (figure 81). Inversions of digitized images of the sections, which enhance constituents with low contrast, showed an unexpected degree of continuity

between more heavily marked strings of nodes. The nodes are believed to represent the interstices between granules and could have accommodated chitin.

Chitin is difficult to identify on its own, even under the SEM with its ultrastructural features enhanced by metal shadowing. It is usually covered with spheroids of apatite and masked by its associated protein; and the entire complex is normally submerged in GAGs. The best exposures are found on surfaces denuded by proteinases especially subtilisin and proteinase-K.

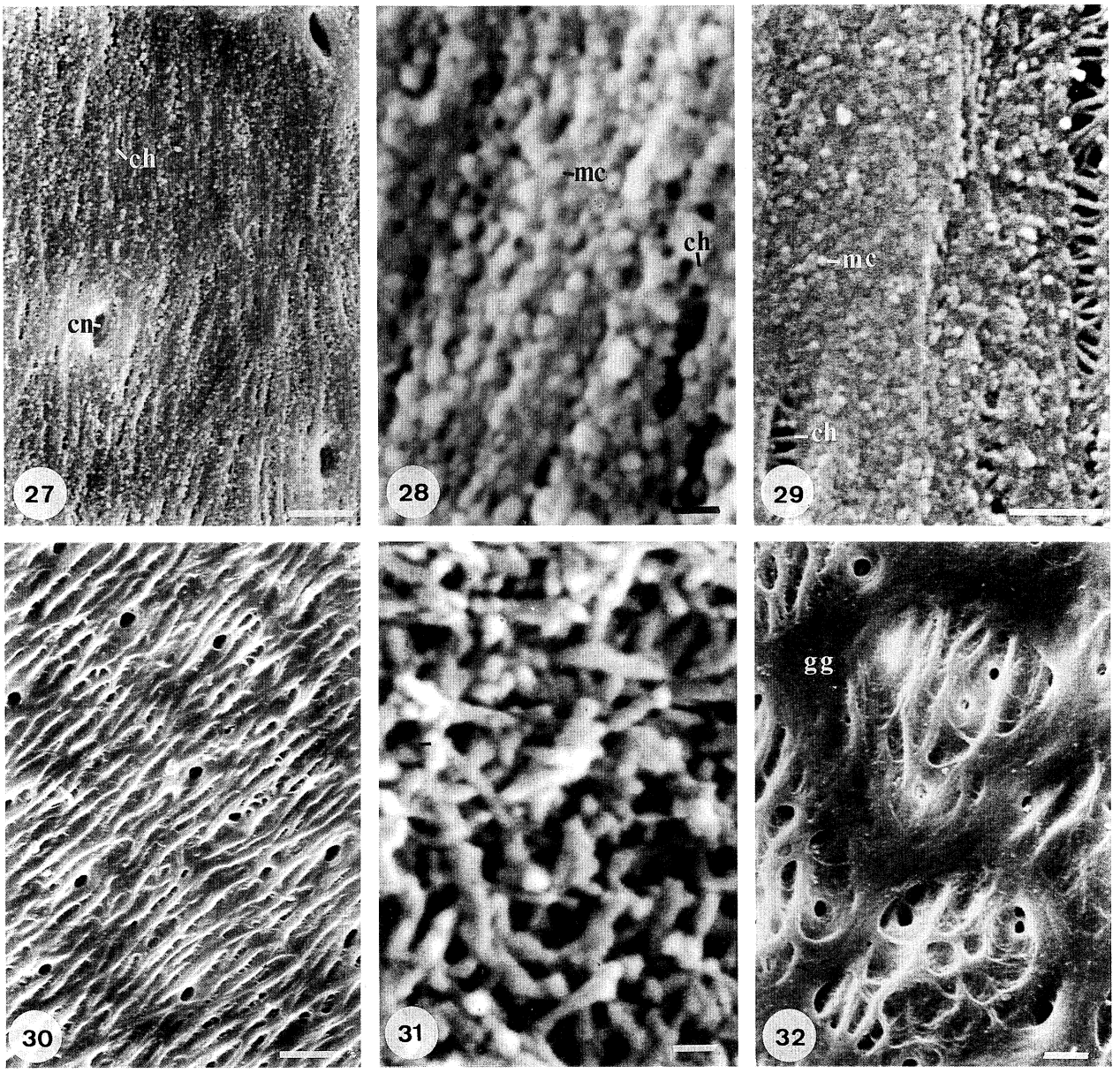

Figures 27–32. Scanning electron micrographs of gold-coated internal surfaces of the shell of *Lingula anatina*.

Figure 27. Gently flexured, lineated texture of the mid-part of a valve digested by subtilisin in a laminar flow cabinet, interpreted as consisting of chitinous fibres (ch) studded with apatitic mosaics, with canal apertures (cn) Scale bar = 2 μm.

Figure 28. Detail of the fibrous texture of figure 27, showing linear clusters of apatitic mosaics (mc) adhering to, and mainly obscuring, a network of chitin (ch). Scale bar = 200 nm.

Figure 29. Chitinous fibres (ch) coated with apatitic mosaics (mc), exposed in tension cracks in the mid-part of a valve digested in collagenase. Scale bar = 1 μm.

Figure 30. General view of anastomosing ridges exposed in the anterior part of the same valve featured in figure 27, also digested in subtilisin. Scale bar = 5 μm.

Figure 31. Short fibres treated with 5% bleach (by volume) and, therefore, probably chitin with some attached apatitic mosaics exposed in the anterolateral part of a valve. Scale bar = 200 nm.

Figure 32. General view of anastomosing ridges exposed in the posterolateral part of the same valve, featured in figure 27, and also digested in subtilisin but with enough GAGs (gg) surviving enzymic digestion to trace the outlines of outer epithelial cells. Scale bar = 2 μm.

These enzymes digest much of the pervasive GAGs and so degrade the protein associated with the chitin that the fibrous habit of the latter is revealed.

Anastomosing ridges on the internal surface of a valve (figure 30), digested by subtilisin were reduced to gently flexured lineations, up to 150 nm thick (figure 27). The lineations were studded with coated granules and spherules of apatite (figure 28) and variably separated from one another by lenticular partings, up to 5 μm or so long. These gaps are sporadically bridged by strands, about 30 nm thick, which are assumed to be part of a chitinous network compatible with the aligned spherules.

A comparable linearity of apatitic particles, parallel with, or at acute angles to, anastomosing ridges, is evident in specimens digested by subtilisin and proteinase-K; and has also been found in some control specimens treated with buffer solutions. In two specimens digested by chitinase, apatitic particles were accentuated by the partial removal of chitin. Even collagenase had so weakened the fabric of an organic layer exposed in one valve as to cause lenticular gaps, up to 5 μm or so long, to develop, which were crossed by strands, presumably chitinous, between 30 and 40 nm thick (figure 29).

In contrast to a linearly arranged chitinous framework, fragments of an apparently chitinous mesh of flexible rods, some disposed in broken circles up to one micron across, were preserved on the internal surface of a valve treated with bleach (figure 31). The fragments had broken off a succession of impersistent (presumably lenticular) plates about 40 nm thick, interleaved with layers of apatitic spherules, up to 120 nm in diameter. Should this meshwork prove to be a common arrangement of chitinous fibres associated with apatitic spherules, it would account for the occasionally observed disposition of apatitic particles in two sets of lineations at angles of about 60° to each other (figure 91). Rough cleavage can also develop within apatitic successions in two directions at about the same angle.

The use of such powerful degradants as bleach and subtilisin on shell surfaces helps to identify the microtopography of aggregated chitin fibres. On internal surfaces free of tissue, traces of hexagonally closely packed cuboidal epithelium are common as biomineralized casts of the secreting plasmalemmas (figure 32). In a fragment of one valve digested by subtilisin and in the matching piece treated with buffer, patches of their internal surfaces were studded with closely packed sets of inward projections, between 10 and 11 μm in diameter and exceptionally up to 5 μm in height (figure 36). They are assumed also to be casts of outer epithelial cells which are, however, concave inwardly. Their dominant surface features are sinuous medial ridges, up to 9 μm in length and 600 nm or more wide (figure 36). Each ridge splays into six or so radiating branches, at most 300 nm wide, which are continuous with an irregularly hexagonal network of strands, about 60 nm thick, delineating a mesh of about 400 nm (figure 37).

The catchment area of a radiating unit and associated meshwork fits the secretory plasmalemma of an outer epithelial cell. Its fabric had not been affected by subtilisin which had, however, removed any GAGs cover and at least some apatite. The resistance of this fabric to degradation has also been seen in specimens treated with bleach (5% by volume) as well as subtilisin in a laminar flow cabinet. It corroborates an assumption, drawn from the nature of the fabric, that the ridges and meshwork are a chitinoproteinaceous complex. With continuing secretion, the radiating ridges amalgamate into a transcellular network of anastomosing ridges (figures 32 and 33), the longitudinal branches of which are the medial axes of the radiating sets. In this way one of the dominant surface fabrics of the *Lingula* shell is continually developed throughout the succession.

The longitudinal branches of the anastomosing ridge system range in width from less than 500 nm to more than 5 μm but are usually between one and two microns thick (figure 36). They anastomose around lenticular spaces which are exceptionally up to 50 μm long and 5 μm wide but usually less than one-fifth of those dimensions. These gaps between the main ridges are crossed by oblique or transverse branches, commonly little more than 200 nm thick. All branches are variably coated with apatitic spherules and, even in the untreated state, frequently bear tension cracks parallel with their long axes, which presumably reflect denaturation of the chitin. Exceptionally, in two specimens treated with subtilisin, enzymic digestion dislodged enough apatitic particles to reveal a network of discontinuous partitions, about 40 nm wide, which define closely packed spaces between 70 and 300 nm in diameter (figure 38). Residues of apatitic spherules within this size range survive on parts of branches less affected by subtilisin. It is assumed that the partitions are chitinous and that they are remnants of the same kind of fabric as the honeycomb meshwork revealed by treatment with bleach (figure 31) and proteinase-K (with collagenase).

In many parts of the anastomosing ridge system, flexible rods, between 400 and 600 nm long and up to 150 nm thick become the dominant biomineral components. The rods are like those forming lenticular laminae (figures 31, 35 and 62) and are assumed also to be composed of apatitic granules with chitinoproteinaceous coats. The sequence of their deposition was revealed in exposures beneath membranous laminae which had been partly removed by subtilisin (figure 33). In the early stages, rods and spherules were aggregated around circular hollows, about one micron in diameter, which were regularly spaced in open hexagonal arrays (figures 33 and 34). Further deposition led to the development of relatively thick parallel ridges in which the rods tend to be aligned with the long axes. Hollows persisted in the alternating troughs where they were separated by transverse accumulations of both rods and spherules.

This mode of aggregation is probably typical of the anastomosing ridge system irrespective of whether rods or mosaics are the dominant biomineral

constituents. The most spectacular variant is a meanderform arrangement which is especially characteristic of muscle scars. The pattern was well developed within the outside lateral muscle scar of a valve preserved in ethanol (figures 39–41). Despite the meandering courses of the principal ridges, the general pattern is regular with the ridges themselves, about 300 nm wide, disposed in parallel sweeps

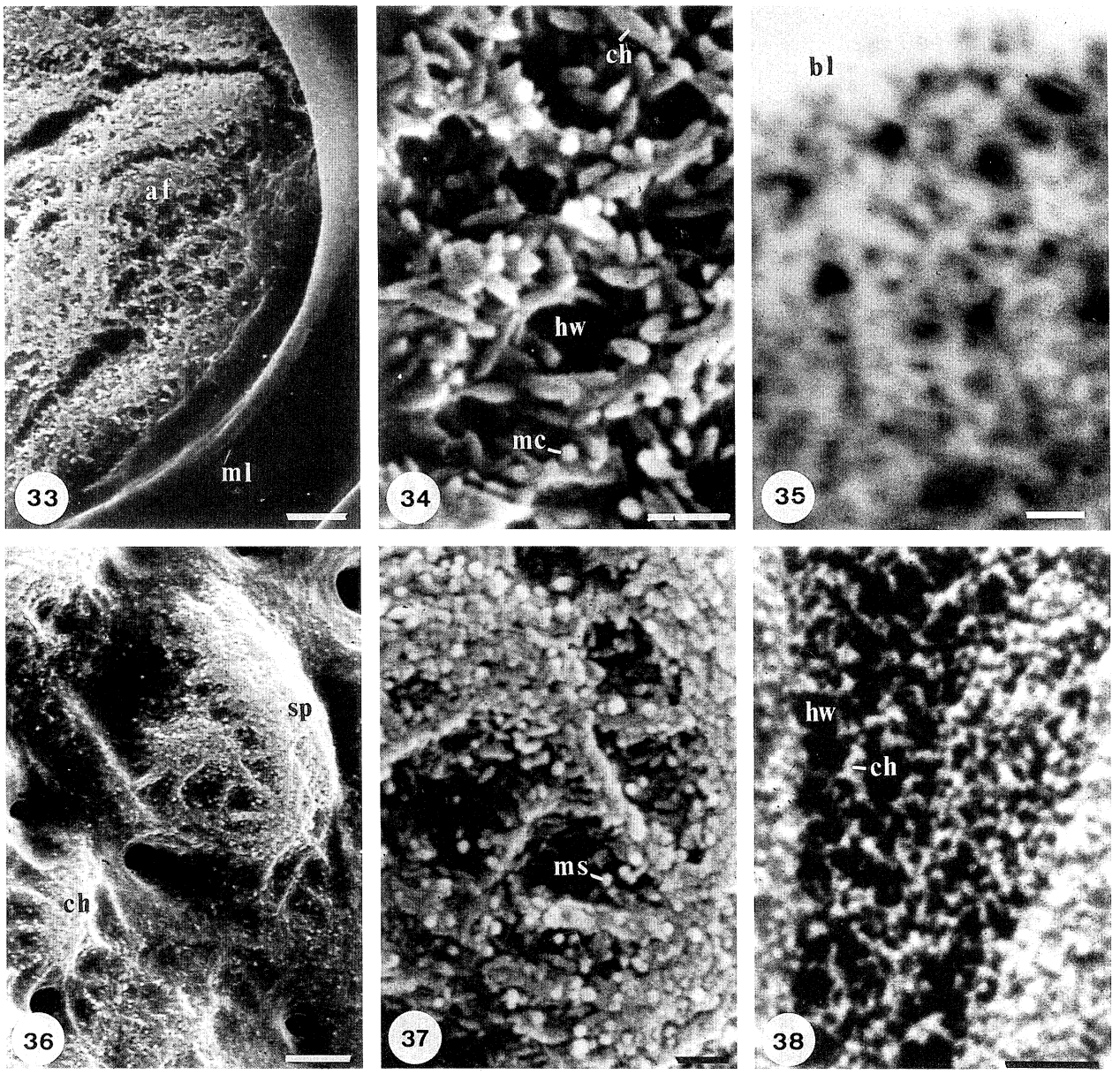

Figures 33–38. Scanning electron micrographs of gold-coated internal surfaces and a carbon-coated section (figure 35) of the shell of *Lingula anatina*.

Figures 33–34. General view of fibrous anastomosing ridges (af) arranged in a hexagonal network centrally and exposed beneath a membranous lamina (ml) in the anteromedian part of a valve digested by subtilisin; with details of the fibrous texture showing how short apatitic rods with chitin (ch) and interspersed with apatitic mosaics (mc) are assembled around hollows (hw) presumably occupied by digitations of outer epithelium (figure 34). Scale bars = 2 μm and 0.5 μm respectively.

Figure 35. Back scattered electron scan confirming the apatitic composition of rods and mosaics succeeding a botryoidal lamina (bl). Scale bar = 1 μm.

Figures 36 and 37. General view and detail of a radiating unit of ridges of proteinaceous chitin or chitin (ch) coated with apatitic mosaics (ms), which are precursory to anastomosing ridges, on the side of a subconical projection (sp) of the internal surface of the submedian part of a valve treated with phosphate buffer (100 mM, pH 7). Scale bars = 2 μm and 0.5 μm respectively.

Figure 38. Detail of radiating ridges of chitin and residual apatitic mosaics in the same valve featured in figure 36, in which subtilisin digestion has removed many mosaics leaving hollows (hw) delineated by strands of a chitin matrix (ch) showing traces of a hexagonal network. Scale bar = 0.5 μm.

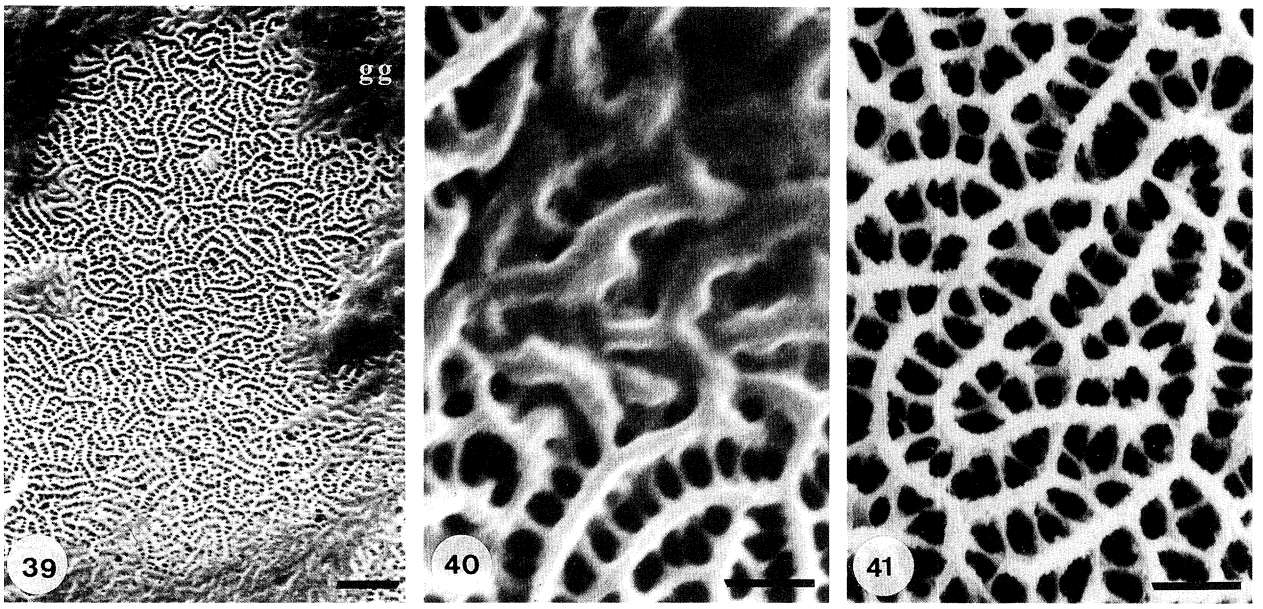

Figures 39–41. Scanning electron micrographs of a gold-coated internal surface of the posterolateral part of a valve of *Lingula anatina*, mechanically stripped of mantle and fixed in ethanol (70% by volume).

Figure 39. General view of meanderform apatitic ridges and troughs with transverse connections; traces of a GAGs cover remain (gg). Scale bar = 5 μm.

Figures 40 and 41. Detail of meanderform ridges and troughs showing a covering film of GAGs and the planospiral pattern of the meanders. Scale bars = 1 μm.

500 nm or so apart and connected by transverse bars seldom more than 100 nm wide, at intervals averaging 350 nm. No apatitic rods were seen, only spherules up to 50 nm in diameter.

(iv) *Collagen*

Collagen was first unequivocally identified on the internal surface of a valve which had been digested by proteinase-K and chitinase (figure 43). Partial

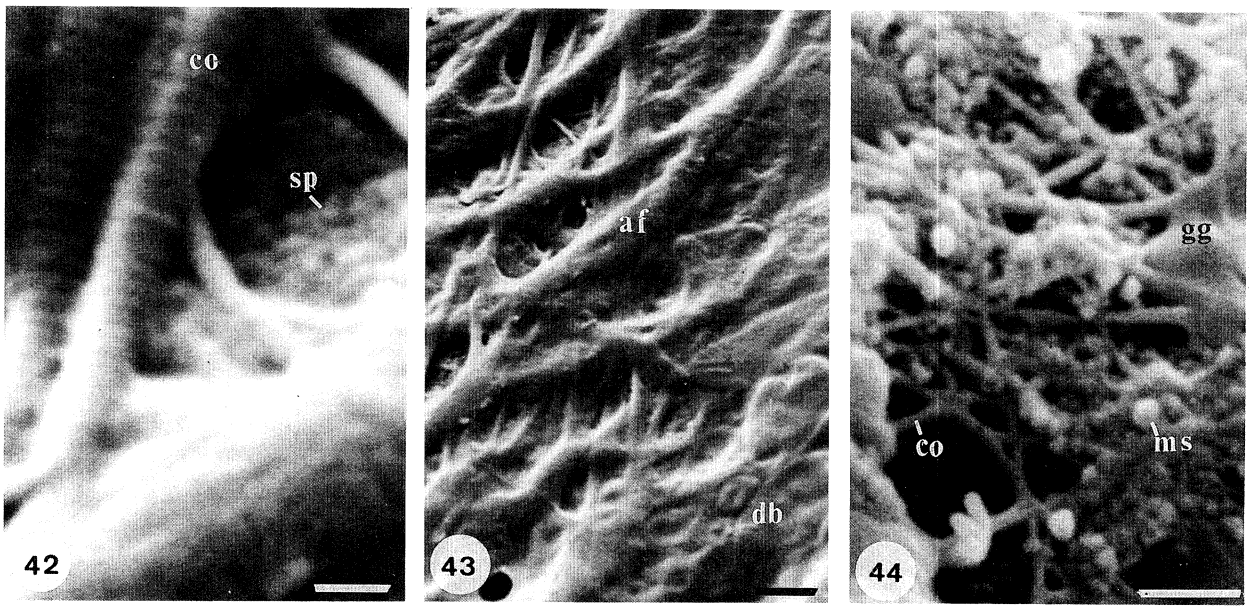

Figures 42–44. Scanning electron micrographs of gold-coated surfaces of the shell of *Lingula anatina*.

Figures 42 and 43. Detail and general view of the internal surface of the posteromedian part of a valve digested in proteinase-K and chitinase, showing collagenous fibrils (co) traversing anastomosing ridges (af), with apatitic spherules (sp), beneath an impersistent layer of GAGs with discoidal bodies (db). Scale bars = 200 nm and 1 μm respectively.

Figure 44. Partly exposed, inward facing, collagenous mat between two botryoidal laminar sets of the posteromedian part of a valve treated with phosphate buffer (100 mM, pH 7), showing fibrils of collagen (co), apatitic botryoids and mosaics (ms) and GAGs (gg). Scale bar = 0.5 μm.

degradation of a covering film of GAGs exposed a prominent set of subparallel, straight or flexured, branching rods aligned acutely to a substrate of anastomosing ridges. The rods branch laterally, usually at acute angles of about 30°, and the main rods, some of which could be traced for well over 10 μm, were significantly thicker (up to 200 nm) than the branches (80 nm). All were cross-striated with a periodicity of about 45 nm (figure 42). These collagen fibrils had not been secreted simultaneously over one surface. Fibrils of the more prominent set overlapped one another and had grown over a film of GAGs veiling an older set of fibrils, and aggregates of apatitic spherules and openings of canals (350 nm in diameter) within the lenticular spaces between the anastomosing ridges, which form the general substrate. Even the ridges were pierced, as well as overlain, by fibrils of the younger set.

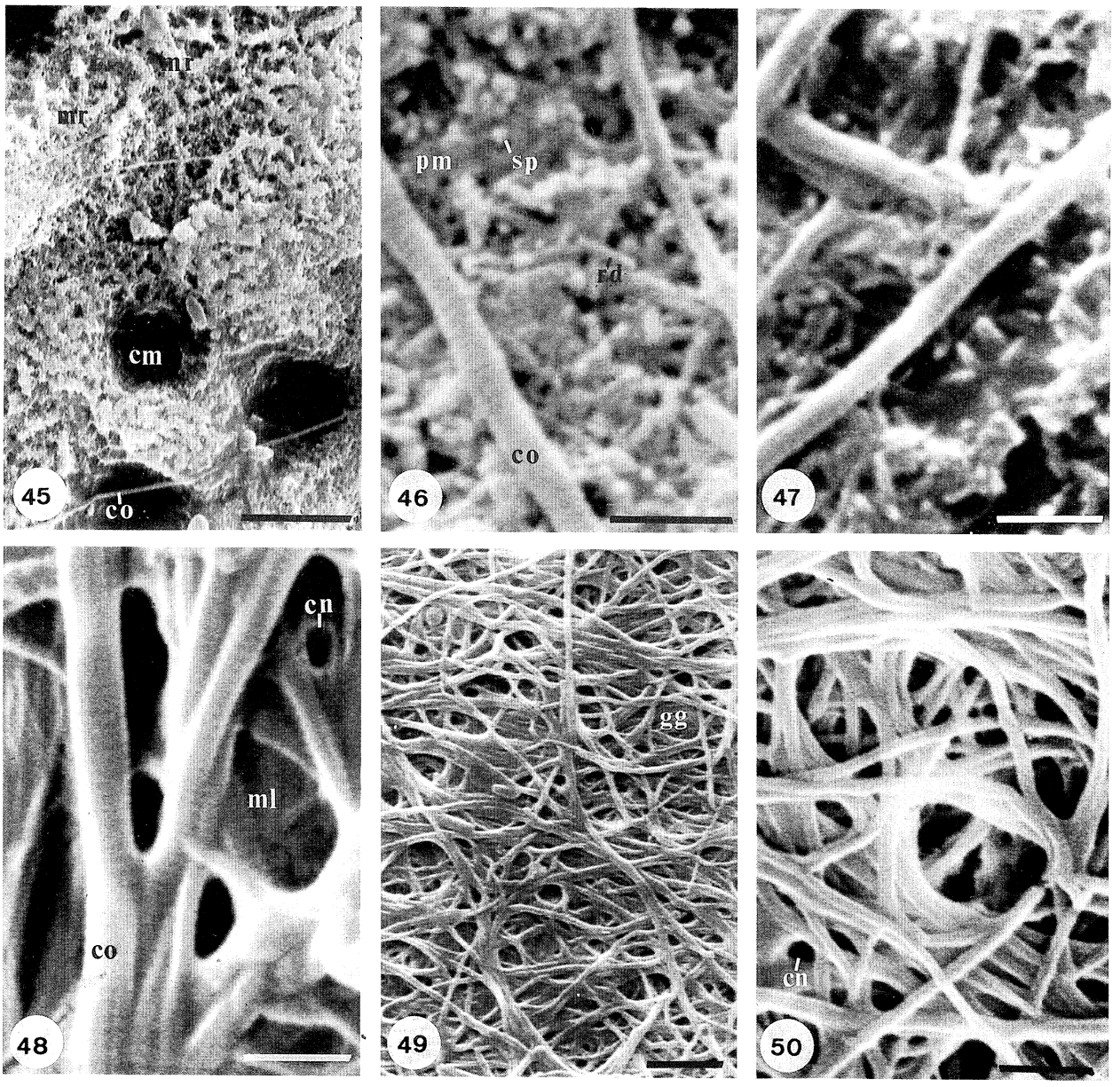

Figures 45–50. Scanning electron micrographs of gold-coated surface of the body platform of a dorsal valve of *Lingula anatina* digested in subtilisin.

Figures 45–47. General and two detailed views of the right central muscle scar showing the meanderform arrangement (mr) of chitinoproteinaceous, apatitic rods (rd) and dispersed spherules (sp) in a membranous substrate (pm), indented by chambers (cm) and overlain by collagenous fibrils (co). Scale bars = 5 μm, 0.5 μm, 0.5 μm.

Figure 48. Collagenous fibrils (co) associated with membranous laminae (ml) with canal apertures (cn) within the median cleft of the median septum. Scale bar = 0.5 μm.

Figures 49–50. General view and detail of a mat of collagenous fibrils associated with GAGs (gg) with a canal aperture (cn), and forming a broad (0.5 mm) anterolateral border to the medianly raised part of the body platform. Scale bars = 2 μm, 1 μm.

Mats of collagen fibres are periodically secreted at different horizons within the body platform. The variation of a fully developed mat on the internal surface of a platform was revealed after digestion of a mature dorsal valve by subtilisin. The fibrils, associated with the meanderform muscle scars (figure 45) and the surrounding anastomosing ridge system, tended to occur singly and sparingly (figures 46 and 47). The median septum, however, was composed mainly of bundles of fibrils, wrapped in membranes and aligned with the septum (figure 48). In contrast, the collagen fibrils at the anteromedial junction of the shell and body wall were densely packed in coils in a GAGs matrix (figures 49 and 50).

Apart from the two specimens described above, cross striations have only been seen on a few fibrils in one other valve which had been digested in endoproteinase Glu-C. However, a number of commonly occurring features are also diagnostic of collagen as identified in this study. Exposures of a group of fibrils almost invariably reveal their branching habit so that fibrils have two orders of thicknesses (with modal ranges of 30–60 nm and 100–130 nm). Individual fibres are long and flexible. They can exceed 15 μm in length and can curve to form complete hoops, up to 3 μm or so in diameter, or more elaborate tracery of three to five rays radiating from open nodes. They are also difficult to degrade by treatment with enzymes (including the type of collagenase used during this study).

By using these structural attributes as diagnostic features, mats of collagen fibrils have been identified at different horizons throughout the median zone of secondary shell successions. The mats are usually covered by GAGs and apatitic spherules but, when the cover is thin, can be recognized by the distinctive disposition of collagenous fibres in hoops and branches (figure 44). Collagens are also sparsely distributed more-or-less vertically throughout the succession and are especially well seen when crossing spaces, like canals and associated chambers and galleries, within a matrix of apatite and GAGs (figures 86–88).

No trace of collagens has yet been found in sections of either shell or secretory outer epithelium, examined under the TEM. The collagen fibrils of the connective tissue, however, have a cross-striated periodicity comparable with those within the shell (figure 72).

(*c*) *Subperiostracal integument: successions*

The subperiostracal shell of *Lingula* is a stratiform succession of laminae composed of the basic organic and biomineral components in varying proportions. The successions are complex with rapid vertical and lateral changes in the composition and structure of constituent laminae. They are well seen in transverse and sagittal vertical sections of mature valves, which have been analysed by back scattered electron scans (BSE) for phosphorus (figure 51). These surveys show that a full succession is always sharply differentiated into an outer primary layer, immediately beneath the periostracum, and a variably developed inner secondary layer making up most of the valve.

(i) *Primary layer*

The distinctive features of the primary layer include its constancy of thickness and a uniformity of structure with little variation in composition. The thickness of the layer, in the mid-regions of two valves used for this study, was within the range of 31–46 μm (mean of 40 μm) for the 15 measurements taken at intervals of 400 μm along the right half of a transverse section of one valve (figure 51). At the shell edge, the marginal fold is composed entirely of primary layer and its periostracal cover, which are easily distinguishable although the boundary between them is a rapid transition rather than a disjunct interface. The primary layer dies out just beyond the hinge of the marginal fold so that only the periostracum extends inwardly to the periostracal groove (figure 5).

The flexibility of the primary layer, which is evident in the wrinkling of its inner boundary around the marginal fold (figure 5), is diagnostic of its composition. Staining with Alcian Blue confirms that the layer is composed of acidic GAGs which, under the TEM, show up as a medium electron-dense body with a finely fibrillar structure. This identification is consistent with the appearance of the layer under the SEM. Back scattered electron scans showed a uniformly medium electron-dense band with rare traces of a fine electron-light stratification inclined inwardly at a few degrees to the primary–secondary boundary. Topographic scans reveal that sections and exposed surfaces have the characteristics of GAGs (figure 53), including wrinkling, tension cracks and sporadically occurring discoidal bodes, with rare scatters of apatitic spherules. Surfaces of sections usually fracture conchoidally; and gently inclined strata were also exposed by exfoliation of the external surface of a valve (figure 52) as microscopic scarps, parallel with surface growth lines and at intervals of about 5 μm. They were cleaved normal to the growth lines and were finely granular within a range of 50 to 70 nm.

Internal surfaces of the primary layer, exposed by the removal of mantle from within the marginal fold, are commonly the site of a circumferential, intermittent band of the larger blisters described as artefacts within a GAGs medium (figure 96).

(ii) *Secondary layer*

The primary layer is abruptly succeeded by secondary shell which is immediately distinguishable by its variable development and the complexity of its constituent laminae. The outer boundary of the secondary layer is marked by several overlapping compact laminae of apatite, lying parallel to the external surface of the valve (figure 51). Several laminae, which at their interfaces with the primary layer, are seldom more than 20 μm thick, can be traced radially for many millimetres. Each is actually the outer bounding member of a set of laminae forming a number of concentric biomineralized 'plates' approximating in outline to that of the valve at appropriate stages of growth. The outermost plate has the greatest areal contact with the primary layer. Inner plates are successively larger and overlap one another transgressively (compare figure 4) to underlie

the primary layer along discrete narrow bands concentric with the valve margin.

The sharp distinction between the primary layer and the apatitic compact laminae of the secondary shell was evident in an exposure on the posteromedian external surface of a valve (figures 5 and 54). The periostracum and primary layer had split and peeled back to reveal the fabric at different levels in the outer shell succession. The innermost exposures consisted of interconnected partitions, about 40 nm to 50 nm thick, defining closely packed polygonal areas, between 0.5 μm and 2 μm across. The floors of the polygons were fibrillar membranes with adherent apatitic spherules, between 30 nm and 100 nm in diameter, and were overlain here and there by a film of GAGs. The polygons were evidently casts of the digitate extensions of the apical plasmalemmas of the outer epithelium; and the coat of apatitic spherules, the base of a compact lamina marking the onset of the secondary shell.

The apatitic plates are separated from one another by homogeneous interleaves, usually about 15 μm thick, which, in BSE scans, are free of apatite and indistinguishable from the primary layer, with which they merge along concentric bands alternating with those formed by the apatitic plates (figure 51).

Another feature also marks the onset of the secondary layer. Canals, which densely perforate the secondary shell, contrast strongly with apatite under BSE scans. They occur along the outermost apatitic boundary of the secondary shell (figure 55) but have not been seen in the overlying primary layer. Under BSE scans, the contents of canals are indistinguishable from other organic components of the shell (including those of the primary layer). However, canals in secondary organic laminae are usually represented by electron-dense extensions into succeeding compact laminae; and the absence of any such traces along the outer boundary of the secondary layer suggests that canals originate inward of that boundary.

The variable development of the secondary layer reflects its continuous but differentiated secretion over the entire intramarginal interior of a valve. The layer is thickest posteromedianly, more or less coincident with the spread of the body cavity. It thins out radially with some differential thickening under

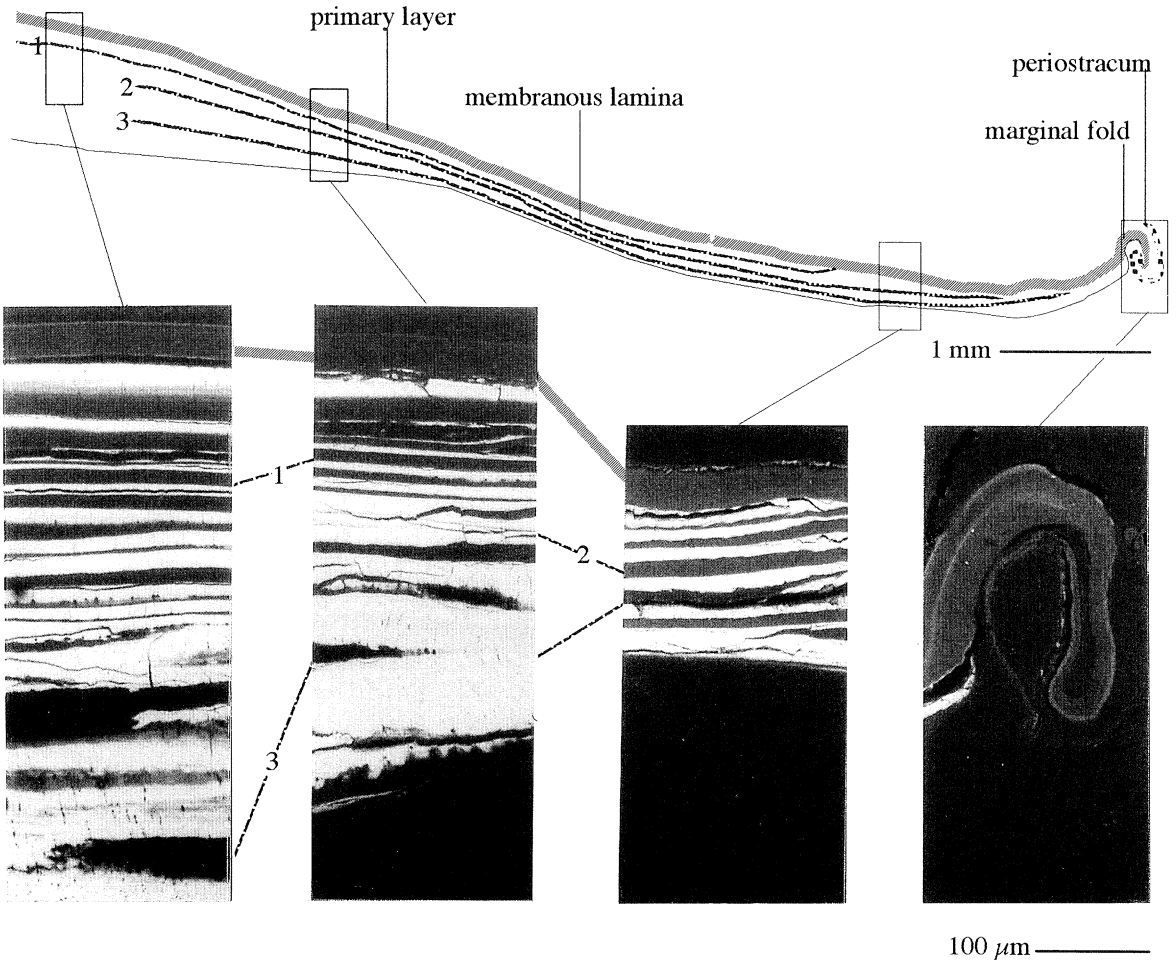

Figure 51. Composite BSE micrographs and drawing of a cut and polished transverse section of the posterior right half of a resin-mounted valve of *Lingula anatina*, coated with carbon and surveyed for a montage to show the distribution of phosphorus (white) and organic compounds (grey to black) in four correlated columns; the montage was digitized and reduced to show the extent of the primary layer and three well-developed membranous laminae (upper drawing) with lamina 3 locally overstepped by a transgressive inner compact lamina in the right-hand half of the second column from the left.

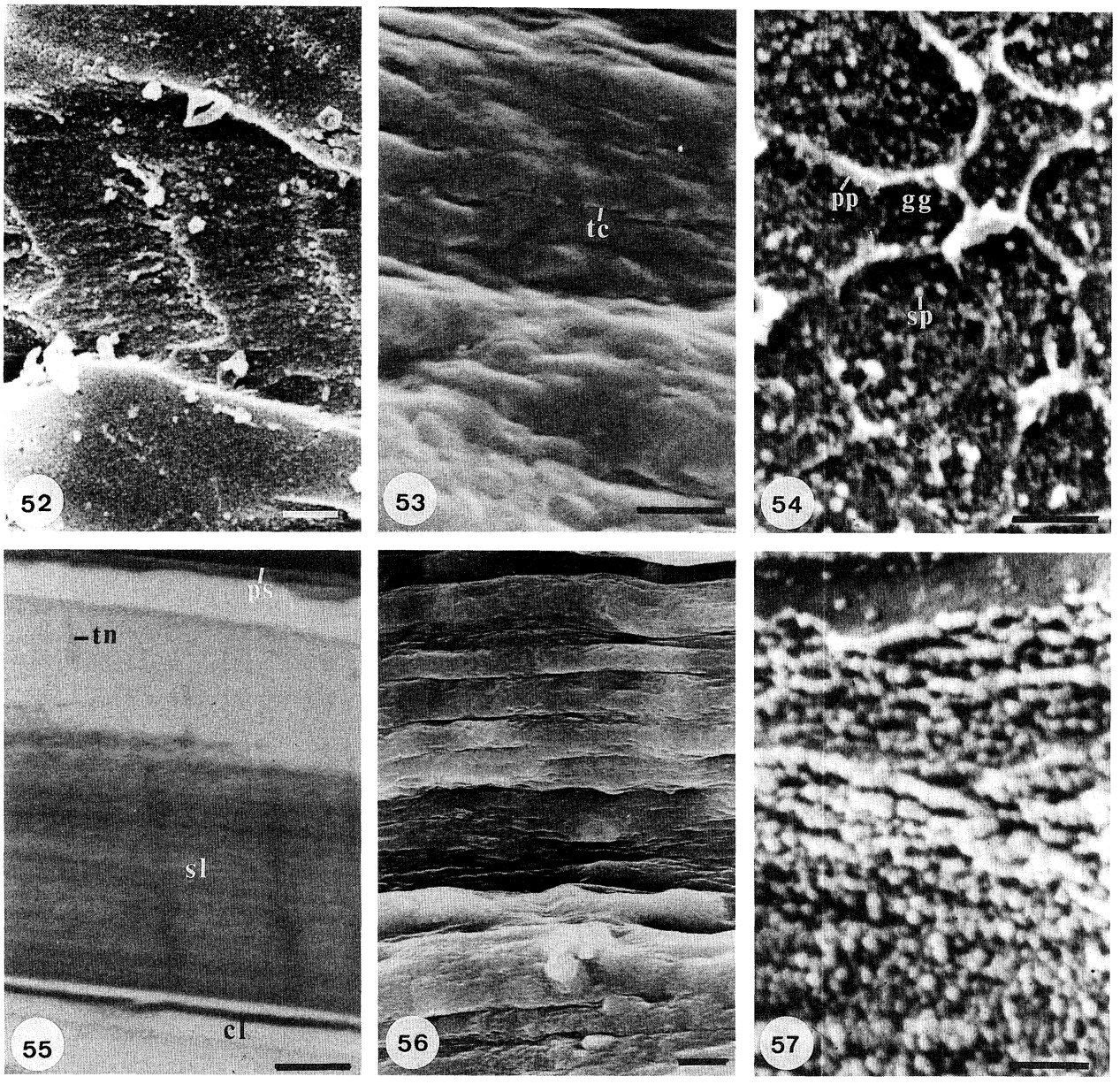

Figures 52–57. Scanning electron micrographs of gold-coated and carbon-coated (figure 55) surfaces of the shell of *Lingula anatina*.

Figure 52. Exfoliated exterior of critical point dried valve previously stored in ethanol (70% by volume) showing a finely granular, stratified and vertically cleaved primary layer composed of hardened GAGs. Scale bar = 1 μm.

Figure 53. Primary layer composed of poorly stratified GAGs with tension cracks (tc), exposed in a cut, vertical median section of the mid-part of a valve treated with MES buffer (100 mM, pH6). Scale bar = 1 μm.

Figure 54. Junction between the exfoliated primary layer and the spherular (sp) secondary layer with traces of GAGs (gg) and proteinaceous partitions (pp) deposited between the digitate protrusions of the apical plasmalemma of the secreting outer epithelium, exposed on the external surface of a critical point dried valve previously stored in ethanol (70% by volume). Scale bar = 0.5 μm.

Figure 55. Back scattered electron scan of the outer succession, exposed in a polished, transverse section of the posterior half of a resin-mounted valve, showing a stratified lamina (sl) with a terminating canal (tn) between compact laminae (cl), the top one immediately underlying the primary layer (ps). Scale bar = 10 μm.

Figure 56. Detail of outer stratified laminae consisting predominantly of GAGs with tension cracks, exposed in a cut, vertical median section of the anterior part of a valve treated with Tris buffer (80 mM, pH 8) with $CaCl_2$ (100 mM). Scale bar = 5 μm.

Figure 57. Detail of a stratified lamina showing the spherular composition of individual strata exposed in a cut, vertical submedian section of the mid-part of a valve digested in subtilisin. Scale bar = 0.5 μm.

muscle bases and in a narrow zone just within the marginal fold. The valves are thin and flexible being rigid only in the most heavily biomineralized postero-median region where laminar successions of mature shells, at more than one millimetre, are usually four or five times as thick as those in more marginal areas (figure 51).

Variations in thickness of the secondary shell are related to lateral changes in the composition of isochronic units and to differing rates of secretion from one part of the mantle to another. A lenticular set of laminae, bounded by contemporaneous marker horizons, can therefore encompass the full range of biomineralized and organic laminae by vertical and lateral passage. Such sets are best understood by first describing the composition and structure of their constituent laminae.

(iii) *Laminae*

The lamination of the secondary layer is well seen in BSE scans of polished sections, which contrast the alternating dominance of electron-light phosphatic and electron-dense organic components in successive laminae. Six kinds of laminae are identifiable, varying from wholly organic (membranous) to mainly apatitic (compact) laminae with the remaining four characterized by distinctive aggregations of the apatitic components within a predominantly organic matrix.

Membranous laminae vary in thickness from less than one micron (figure 59) to more than 40 μm (figure 51) in sections scanned by BSE, which most clearly delineate their boundaries. In such sections they are mostly indistinguishable from the primary layer; and SEM studies of unmounted fracture sections confirm that the thicker laminae consist mainly of GAGs. Yet some of the thinner membranes react more selectively than GAGs to digestion by various enzymes. These membranes, frequently occurring in stacks of four or five sheets, each less than 50 nm thick, survived treatment by subtilisin and proteinase-K better than by chitinase which tended to etch holes in them. All three enzymes, however, caused the membranes to become ductile, expanding by flow and rupturing in flaccid, stringy extensions (figure 58). These characteristics suggest that the organic laminae consist of layers of thin chitinoproteinaceous membranes which are usually masked by variable thicknesses of GAGs (figure 59).

The compact lamina (figures 60, 64 and 65) is the most persistent phosphatic marker horizon found in the secondary shell. It is composed of coated granules, spherules and rarer mosaics of apatite, which are so tightly packed that the lamina appears as a uniformly white band (figure 59) in BSE scans. In such sections, the laminar outer boundary is always sharp and unwavering while the inner boundary is a faint, undulating line marking a change to a less intensely white band, commonly speckled with dark patches of various sizes. Compact laminae can vary in thickness from less than 500 nm to more than 7 μm but median and mean estimates for 31 laminae, chosen from different parts of the secondary shell and different kinds of secretory units, were 2.2 μm and 3.2 μm respectively.

The sharpness of the outer boundary is normally enhanced by its being the interface between contiguous membranous and compact laminae (figure 60). In fact, a wholly organic lamina is almost invariably succeeded abruptly by a compact lamina which can frequently be traced for several millimetres within a mature shell succession. It is, therefore, assumed that the junction between the two laminae represents a synchronized change in the secretory régime of the same patch of outer epithelium depositing both laminae consecutively. Such a junction was well exposed on the internal surface of a valve digested by subtilisin. A chitinoproteinaceous substrate was almost covered by a layer of densely distributed, coated apatitic particles between 60 and 250 nm in size. Canals, perforating the succeeding phosphatic laminae, originated within the organic substrate and must have anchored the outer epithelium to that part of the shell during the secretion of both the substrate and its apatitic cover.

The irregular inner bounding surface of the compact lamina must also signal a change in the secretory régime although one which is less well synchronized within the outer epithelium. Correlation of sections, viewed under the SEM, indicates that this irregular bounding surface (figure 59) marks the onset of copious secretion of GAGs which are all but absent from compact laminae.

Compact laminae also occur within thick (0.5 mm or more) successions which are especially characteristic of the body platform. Here they overlie impersistent lenses of GAGs or other laminae with a high organic content; and, although they may lose their identity laterally within a short distance, their outer and inner boundaries are constant features.

Although the irregular inner bounding surface of compact laminae has been interpreted as marking the relatively sudden onset of GAGs secretion, changes leading to the characteristic configurations of apatite in other mineralized laminae are gradational. The laminae may be broadly categorized as rubbly with apatitic bodies roughly aligned horizontally or vertically; but three kinds of aggregates indicate significant deviations in the secretory cycle.

The commonest succession, grading inwardly from compact laminae, consists of apatitic spheroids which become larger and more openly distributed within the GAGs until they culminate in a zone of botryoids and mosaics suspended more or less discretely in the GAGs gel (figure 60). The terminating layers of botryoidal laminae, as seen by BSE scans, is a uniformly thick membrane (about 300 nm), presumably of a chitinoproteinaceous composition, which also acts as the substrate for the succeeding compact lamina (figure 59).

Botryoidal laminae range in thickness from 4 to 24 μm (median 12 μm for 25 laminae). They are common throughout the secondary shell but especially so in successive groups of several thicker sets within the inner part of the body platform.

Successions, grading inwardly from compact laminae and consisting of impersistent vertical walls of apatite alternating with sheets of GAGs, are generally

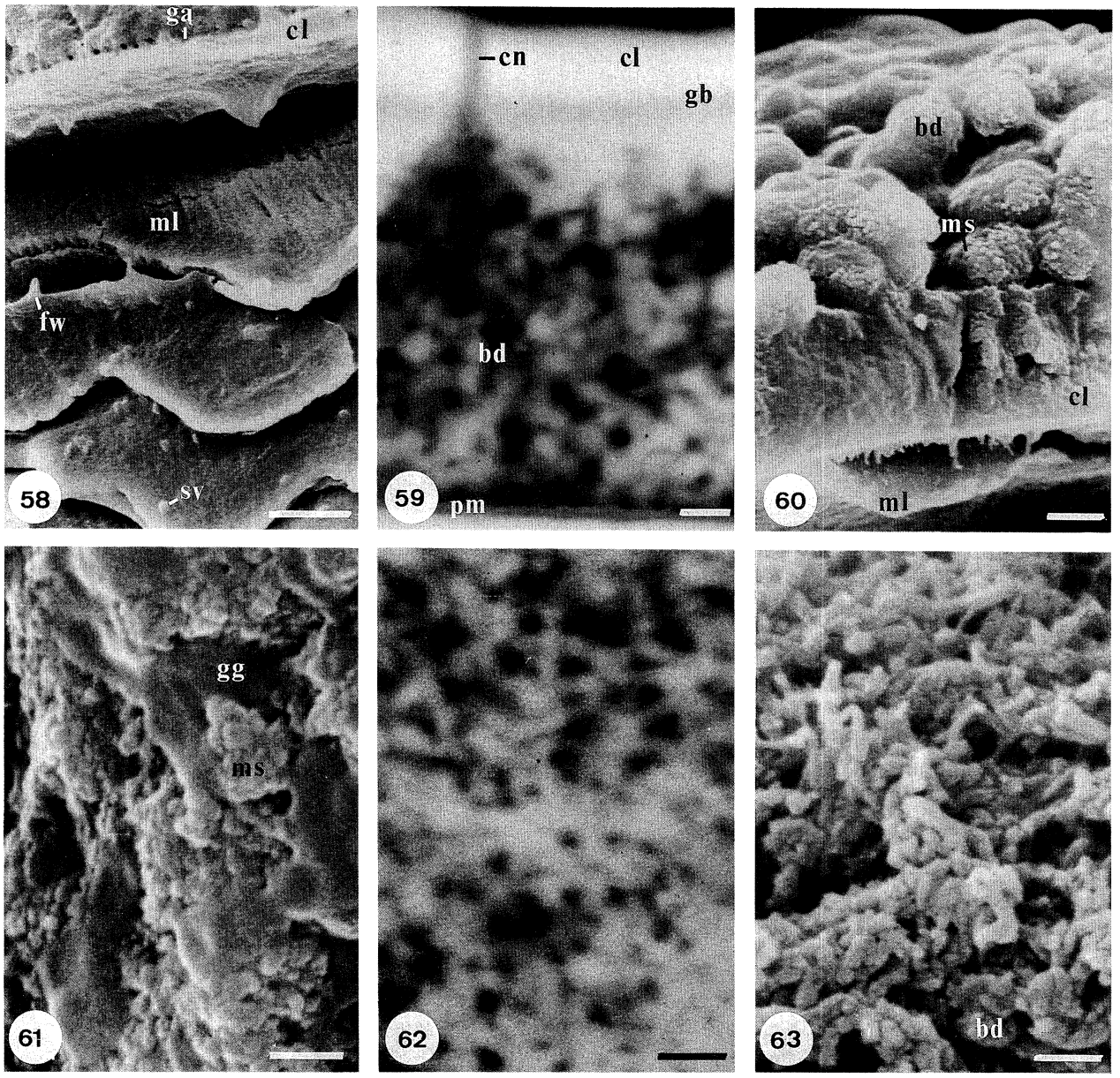

Figures 58–63. Scanning electron micrographs of gold-coated and carbon-coated (figures 59 and 62) sections of the shell of *Lingula anatina*.

Figure 58. Membranous laminae with incipient anastomosing ridges (ml) external to an apatitic compact lamina (cl) (with a row of galleries (ga) along its interface with a botryoidal lamina), exposed in a cut, vertical median section in the mid-part of a valve digested in chitinase; the laminae show signs of flow with necking (fw) and have small vesicles on their internal surfaces (sv). Scale bar = 10 μm.

Figure 59. Back scattered electron scan of a botryoidal laminar set showing a compact lamina (cl), penetrated by the organic contents of a canal (cn) and terminated by a boundary (gb) marking the onset of GAGs secretion and botryoidal clusters (bd) capped by a chitinoproteinaceous membrane (pm) exposed in a polished, transverse vertical section of the posterior half of a resin-mounted valve. Scale bar = 1 μm.

Figure 60. Botryoidal lamina (bd) composed of mosaics (ms) in a GAGs matrix succeeding a compact lamina (cl) internal of a membranous lamina (ml), exposed in a cut, vertical median section of the posterior part of a valve treated with phosphate buffer (100 mM, pH 7). Scale bar = 2 μm.

Figure 61. Walled lamina composed of alternating, highly inclined layers of ellipsoidal apatitic mosaics (ms) and GAGs (gg) and imparting a vertical cleavage on a cut, median section of the mid-part of a valve digested in collagenase. Scale bar = 0.5 μm.

Figure 62. Back scattered electron scan of a rod and plate lamina showing the disposition of linear apatitic structures (light) within an organic matrix (dark), exposed in a polished, transverse vertical section of the posterior half of a resin-mounted valve. Scale bar = 1 μm.

Figure 63. Rod and plate lamina inwardly succeeding a botryoidal apatitic zone (bd), exposed in the cut, vertical median section of the anterior part of a valve digested in proteinase-K. Scale bar = 0.5 μm.

quite thick, ranging from 5 μm to over 30 μm. These walled laminae (figure 61) are readily identifiable in broken shells as they impart a vertical cleavage to fracture surfaces (figure 65). Moreover there is a tendency for the apatitic constituents to be stacked with a vertical stratification suggesting that granules aggregated as ovoidal (figure 61) rather than spheroidal bodies. The biomineralized walls are up to 2 μm thick and, in polished sections under BSE scans, may be seen as vertical white bands intruding into a dark matrix. The alternating sheets of GAGs are discontinuous with a prevalence of lenticular patches of wrinkled exposures with discoidal bodies. They are well seen in sections of shell stained with uranyl acetate and lead citrate and viewed under the TEM (figure 74).

The walled laminae are vertical extensions of the anastomosing ridge system found on the internal surfaces of valves, with the apatitic walls corresponding to the crests of the ridges and the GAGs occurring as infills to the troughs. The lenticular distribution of GAGs in section is compatible with the way surface troughs are crossed by oblique or transverse strands of apatitic spherules which are assumed to be associated with chitin.

The laminae dominated by assemblages of rods and plates (figures 62, 63), appear to be variants of botryoidal successions. In a section digested by proteinase-K, an assemblage of rods and plates arises from a succession of botryoidal apatite overlying a compact lamina (figure 63). Many of the rods are splayed remnants of hemispherical mosaics (figure 17). They are intimately associated with organic strands, between 30 and 80 nm thick, disposed at all angles and flexible enough to form U-shaped bends. The strands are flaccid after enzymic digestion as are the membranes of the anastomosing ridges and are also assumed to be chitinoproteinaceous.

Other assemblages, exposed by treatment with subtilisin, show the same flaccid strands, studded with spherules and branching distally to support clusters of rods and mosaics in various stages of development (figures 18 and 19). In these sections, plates, bearing stalked spherules and linked to mosaics by chitinoproteinaceous strands, may be fragments of spherular monolayers, up to 100 nm thick, which form impersistent mats within the lamina; a few have hexagonal outlines and are probably pinacoids.

The remaining unit, the stratified lamina (figure 56), is as distinctive as the compact one but is more restricted in distribution. It succeeds the compact lamina marking the junction of the secondary shell with the primary layer (figure 55) although it is not always clearly differentiated into fine strata. In this part of the succession a stratified lamina is between 40 and 60 μm thick except where it feathers out against the primary layer. Stratified laminae are also found in other parts of the secondary shell succession as

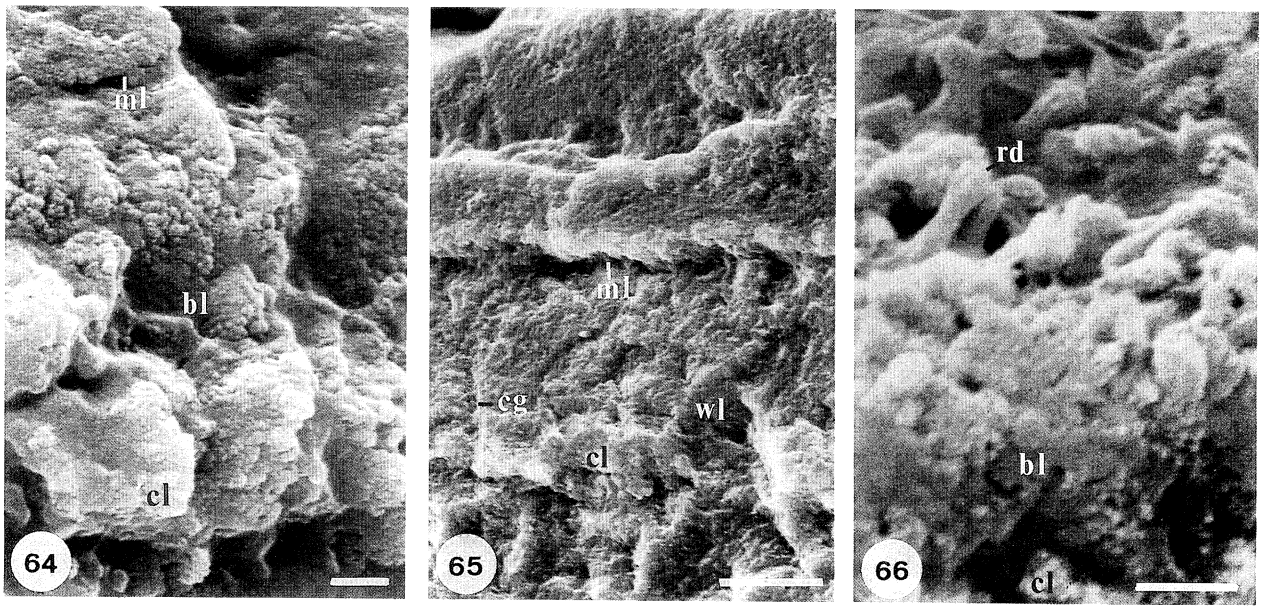

Figures 64–66. Scanning electron micrographs of gold-coated, cut, vertical sections of the shell of *Lingula anatina*.

Figure 64. Botryoidal sets of laminae, each consisting of a compact lamina (cl) passing inwardly into a botryoidal lamina (bl) and a membranous lamina (ml) which is capped by the compact lamina of the succeeding set, exposed in a posteromedian section of a valve digested in endoproteinase Glu-C and chitinase. Scale bar = 1 μm.

Figure 65. Walled sets of laminae, each consisting of a compact lamina (cl) passing inwardly into a walled lamina (wl) and a membranous lamina (ml) which is capped by the compact lamina of the succeeding set; cleavage (cg), induced by alternating walls of apatitic mosaics and GAGs, running through sets; exposed in a posteromedian section of a valve treated with phosphate buffer (100 mM, pH 7). Scale bar = 10 μm.

Figure 66. Rod and plate set of laminae consisting of a compact lamina (cl), passing inwardly through a botryoidal lamina (bl) into a lamina of rods (rd) and plates embedded in GAGs, exposed in an anteromedian section of a valve digested in proteinase-K. Scale bar = 1 μm.

impersistent lenses which are, however, much thinner at about 7 to 10 μm.

In a BSE scan, the stratification consists of pairs of darkly and lightly mottled strata, each about 3 μm (figure 55) thick. Within a group, two or three parallel trails of apatitic spherules alternate with strings of organic, electron-dense vesicular bodies up to 200 nm in diameter. The stratification is parallel to the primary–secondary interface in the mid-region of the valve; but, towards the margin, the strata are inclined inwardly up to 10° to the interface.

The strata have been exposed in an oblique fracture surface of a valve treated with subtilisin (figure 57). Under the SEM they consist of layers of spherules between 20 and 100 nm in size, which form well-ordered sheets about 70 nm thick on average and are presumably held together by a chitinoproteinaceous substrate.

(iv) *Laminar sets*

Despite the distinctiveness of individual laminae and their frequent occurrence over large areas of a valve, they are almost invariably members of one of several well-defined rhythmic sets. These sets of laminae vary from thin (20 μm), almost parallel-sided plates traceable throughout most of the outer succession of the secondary layer, to thick (150 μm or more) lenticles of more limited distribution within the inner part of the body platform.

Four different sets of laminae can be recognized within the shell succession (figure 67) although they have several characteristics in common. This suggests that the rhythmic arrangement of laminae reflects a periodicity in shell secretion. The common features include: an abrupt change from an organic to a biomineralized succession and a more gradual return from the biomineral to the organic phase at the base and top respectively of a set; the presence of the same kind of laminae at the base and top of nearly all sets; and a prevalence of lateral transitions from one set to another, especially among lenticular sets within the inner succession of the shell.

The two constant marker horizons of all sets are a basal compact and a terminating membranous lamina (figures 59 and 64–66). The interface between them in consecutive sets is sharp, even in lenticular sets within the inner succession where the membranous lamina is commonly reduced to a trace no thicker than a few hundred nanometres (compare lamina 3 in figure 51). Between these two horizons and in the presence of increasing quantities of GAGs, the proportion of variously aggregated apatite diminishes and the biomineral could be absent from terminating membranous laminae, 50 μm or so thick.

The various sets have been named after their dominant fabric. The botryoidal set is well developed throughout the shell (figure 64). Indeed, basal compact laminae usually pass rapidly through

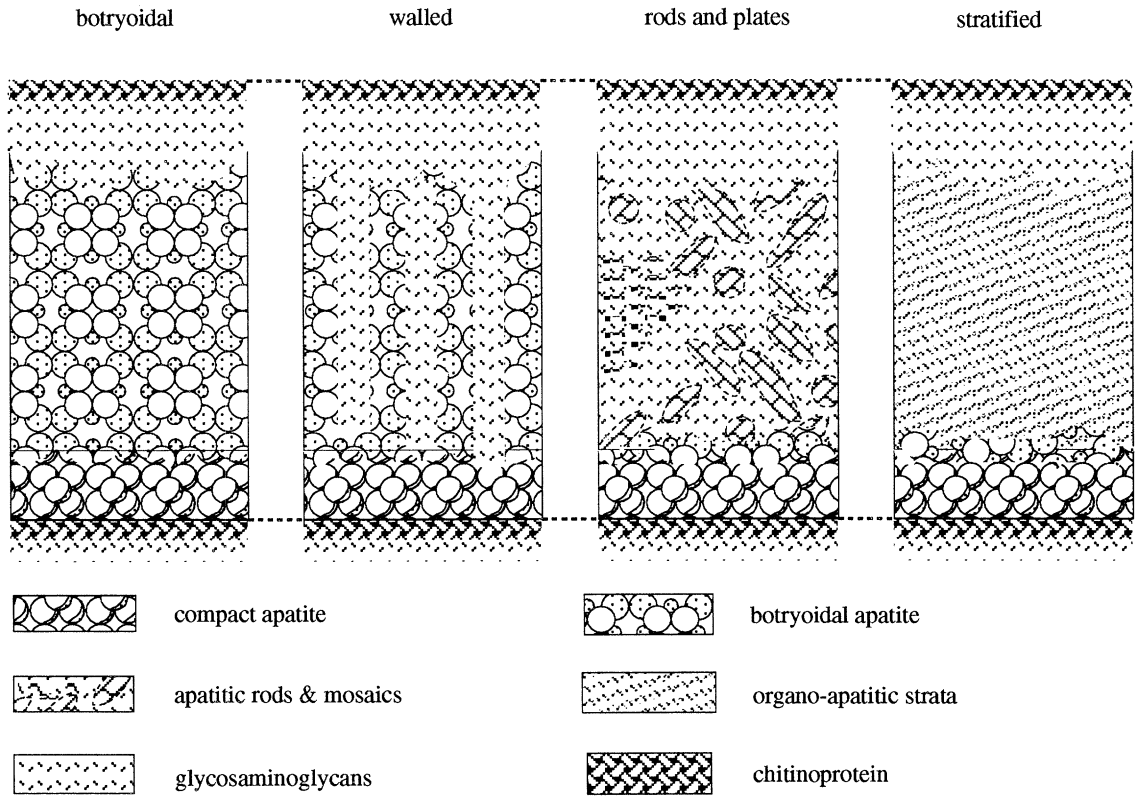

Figure 67. A graphical correlation of the four main laminar sets to show the essential rhythmic unit of secretion from a predominantly apatitic base to an exclusively organic top.

narrow botryoidal zones before becoming transformed into the vertical partitions and the less ordered rods and plates of the walled (figure 65) and rod and plate (figure 66) sets respectively. This, however, is not so for the stratified set (figures 55 and 57). Even in stratified lenticles within the inner successions of the body platform, the apatitic constituents of strata are granular or spherular and seldom aggregate into larger mosaics and botryoids.

(*d*) *Secretory epithelium*

The cells, which form a band secreting the primary layer at the marginal fold of a valve, have been taken to represent the basic cell type (figure 68) of the outer epithelium of the mantle. The primary layer has been shown by Alcian Blue staining to consist almost exclusively of GAGs which are universally although variably present throughout the entire integument of *Lingula*. Cells, which additionally secrete other organic as well as biomineralized components of the shell, may therefore be specialized variants of those secreting GAGs.

The GAGs-secreting cell is, on average, 3 μm tall with basal nuclei and highly folded lateral walls (figure 68). The basal plasmalemma bears hemidesmosomes, from which filaments extend through the cytosol. The apical plasmalemma is thrown into a series of cylindroid or digitate protrusions (figures 8 and 68), up to one micron long and 250 nm thick, similar to the secretory tubes observed in *Discina* (Williams *et al.* 1992, p. 97). There is abundant rough endoplasmic reticulum (RER) and free ribosomes and the Golgi apparatus is associated with many small vesicles, about 40 nm in size with electron-dense contents. Larger vesicles, 500 nm or so in diameter, also occur especially in the apical section where they usually contain granular electron-dense material (or, more rarely, lipids) in various stages of reconstitution and transfer in granular form to the apical plasmalemma; glycogen is common throughout. Mitochondria, which have an electron-dense matrix and tubular cristae, tend to be dispersed throughout the cells.

The vesicular cells secreting the periostracum form a concentric band peripheral to that exuding the GAGs of the primary layer (figure 68). The typical vesicular cell is distinguishable from that secreting GAGs in its variable shape for it is extensible for more than 10 μm with intercellular gaps appearing in the

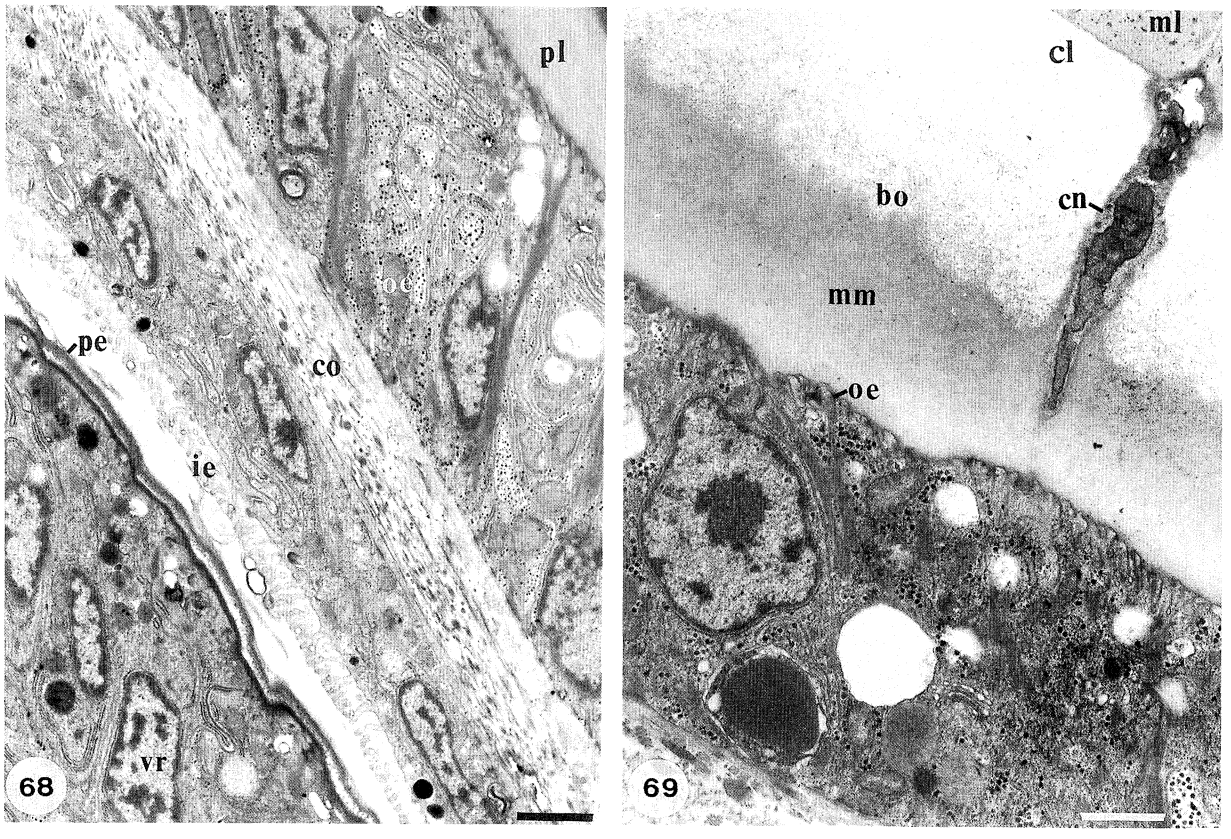

Figures 68–69. Transmission electron micrographs of demineralized valves and mantle of *Lingula anatina*.

Figure 68. Section of the marginal fold to show cuboidal outer epithelium (oe) underlying the primary layer (pl) and periostracum (top, right-hand corner), connective tissue with collagen fibrils (co), microvillous inner epithelium (ie), pellicle (pe) and vesicular cells (vr) bordering the periostracal groove. Scale bar = 1 μm.

Figure 69. Section of the shell and the secreting digitate protrusions of the apical plasmalemma (oe) showing the organic components of a botryoidal laminar set, penetrated by a canal (cn), with a chitinoproteinaceous membrane (ml) overlain by an apatitic compact lamina (cl) passing into a botryoidal zone (bo) succeeded by membranous laminae (mm). Scale bar = 1 μm.

basal region. Moreover, the protrusions of the apical plamalemma are more finger-like (figure 7) and commonly no more than 50 nm thick. The numerous vesicles can exceed one micron in size but are usually small, particularly in the vicinity of the Golgi apparatus. The most conspicuous feature of the vesicular cell, however, is the RER delineating elliptical as well as flattened cisternae around the nucleus.

The cells secreting the secondary shell vary in the distribution and development of their constituent parts. Some variation can be related to differences in the structure and composition of the laminae of the secondary shell. The cells, however, have a number of features in common, which distinguish them from cells responsible for the secretion of the primary layer and the periostracum.

The typical secondary cell is cuboidal (figures 69, 70 and 80), about 11 μm tall, with elaborately interdigitated lateral cell membranes. The cytoskeleton is normally well developed with bundles of filaments extending through the cytosol from hemidesmosomal plaques at the basal plasmalemma to digitate extensions of the apical plasmalemma, some of which are also attached by filaments to the lateral cell membranes. The Golgi apparatus is usually identified by trails of minute vesicles; RER and mitochondria are variably distributed in the apical part of the cell. Inclusions also vary in composition and distribution. Glycogen occurs widely while lipid droplets tend to cluster in the basal regions of all cuboidal cells which are normally distorted by large, closely packed aggregates (10 μm or so in size) of differently composed vesicles, up to 1.6 μm in diameter (figure 70).

In attempting to correlate consistent differences in cuboidal cells with the various laminae being secreted at death, account has to be taken of the difficulties of identifying chitin and apatite in sections prepared and stained in the normal way for TEM study. Sets of mineralized and demineralized sections were prepared to ensure study of a full range of laminae in contiguity with outer epithelium as well as within the shell succession itself. Comparison of these sections with those prepared for BSE study has helped to infer the distribution at least of apatite.

Some successions, within sections of demineralized shell stained with uranyl acetate and lead citrate, represented botryoidal and walled laminar sets (figures 69 and 74). In two successions, the membra-

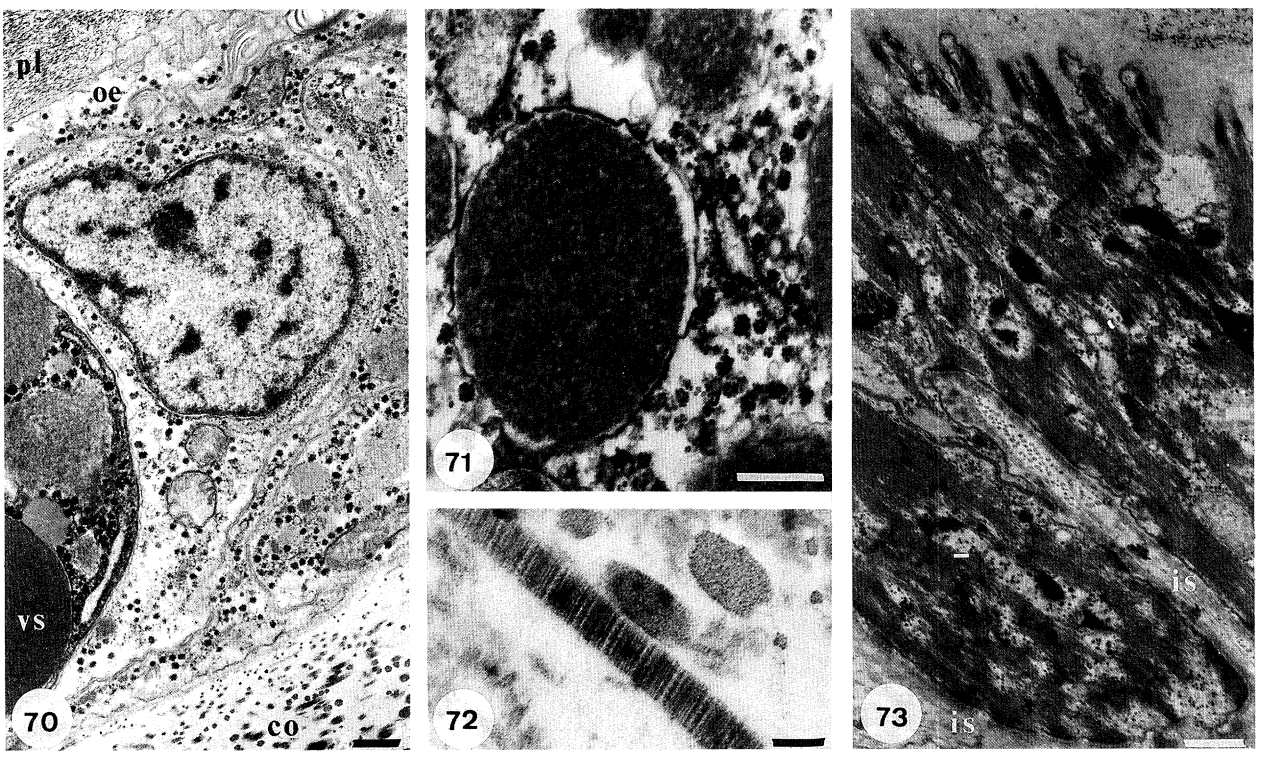

Figures 70–73. Transmission electron micrographs of sections of mineralized shell and mantle of *Lingula anatina*.

Figure 70. Section showing a rod and plate lamina (pl) secreted by digitate protrusions of apical plasmalemma (oe) of the secreting outer epithelium with a cluster of membrane-bound vesicles (vs), and connective tissue with collagen fibrils (co). Scale bar = 0.5 μm.

Figure 71. Detail of a vesicular cluster within the outer epithelium showing the mottled aspect of the vesicles and the abundance of glycogen granules and protein-coated electron-lucent components. Scale bar = 0.5 μm.

Figure 72. Detail of connective tissue showing the periodic banding of a collagen fibril. Scale bar = 100 nm.

Figure 73. Section of the outer epithelium peripheral to a muscle scar showing the pervasion of fibrils throughout the cells and the digitate protrusions of the apical plasmalemma and the intrusive sheets of connective tissue (is) between outer epithelial cells. Scale bar = 0.5 μm.

nous laminae, serving as substrate for the sets, culminated in an electron-dense band, between 10 and 20 nm thick, which can be correlated with that revealed in the BSE section (figure 59). The succeeding compact laminae are represented by closely packed circles, varying in diameter from less than 10 nm to over 50 nm (figure 75). The circles are more or less continuous electron-dense strings studded with particles, less than 5 nm in size, with electron-lucent cores; electron-dense flecks also occur sporadically. The circles have been interpreted as chitinoproteinaceous coats; and their electron-lucent interiors must have been filled with apatite, within the granular-spherular size range, before removal of apatite by EDTA.

Botryoids over one micron in size, are especially well defined by the medium electron-dense strands of the GAGs matrix at the transition into predominantly organic laminae (figure 77). The alternating walls of apatite and GAGs are also distinctive (figure 74) with the more electron-dense GAGs partitions tending to be streaked parallel with the interface between the membraneous and compact apatitic laminae, possibly indicating the presence of chitin. Chitin, as well as apatite and GAGs, has been tentatively identified in exocytosis from protrusions of apical plasmalemma (figures 76 and 79).

Some demineralized laminar successions feature swarms of needle-like structures closely distributed in an electron-light matrix of GAGs with a fine, medium electron-dense mesh of about 5 nm (figure 78). The needles, which are about 75 nm long and 10 nm thick, consist of strings of differentially stained granules or, more rarely, electron-dense surrounds with subrectangular electron-lucent cores. With the removal of apatite from such sections the stained parts of the needles can only be organic.

Sections of mineralized shell are not readily distinguishable from those which have been treated

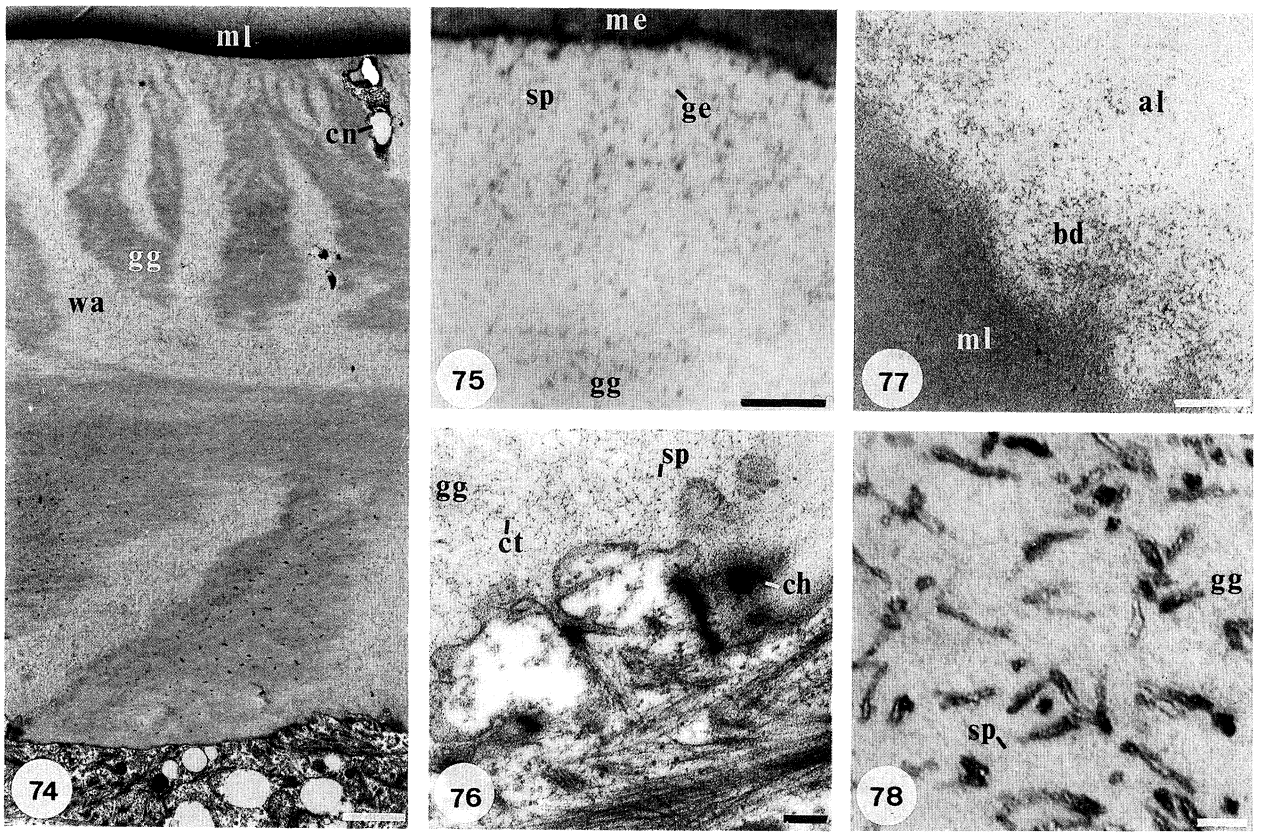

Figures 74–78. Transmission electron micrographs of demineralized valves and mantles of *Lingula anatina*.

Figure 74. Section of a walled set of laminae and secreting outer epithelium showing vesicular membranes within a canal (cn), a membranous lamina (ml) and alternating partitions of apatite (wa) and GAGs wih chitin (gg). Scale bar = 2 μm.

Figure 75. Detail of junction between a chitinoproteinous membrane (me) and a compact lamina composed of granules (ge) and spherules (sp) outlined by proteinaceous coats with chitin particles; concentrations of GAGs (gg) also occur. Scale bar = 100 nm.

Figure 76. Detail of digitate protrusions of an apical plasmalemma secreting chitinous fibrils (ch) and GAGs (gg) and apatitic granules and spherules (sp) with chitinoproteinaceous coats (ct). Scale bar = 200 nm.

Figure 77. Detail of interface between apatitic (al) and membranous (ml) laminae marked by the presence of botryoids (bd). Scale bar = 0.5 μm.

Figure 78. Detail of a demineralized lamina of rods and plates showing the chitinoproteinaceous strands associated with apatite (before it was removed by EDTA) in a GAGs (gg) matrix with outlines of spherules (sp). Scale bar = 50 nm.

with EDTA. Laminae composed of needle-like bodies are generally more intensely electron-dense although, at high magnifications, the needles, which may be 150 nm or more long, consist of electron-dense streaks threading their way through close-packed granules, about 6 nm in average size (figures 80 and 81). The granules are normally well defined, having medium electron-dense coats and electron-lucent cores and aggregating between the streaks into rounded clusters, up to 60 nm or so in diameter. The granules have been interpreted as having apatitic cores coated with chitinoprotein and closely stacked within an electron-dense, predominantly proteinaceous matrix which appears as discontinuous streaks in section.

GAGs, in sections which have not been demineralized, are remarkable only for electron-dense flecks scattered sporadically along the proteinaceous mesh; they have been interpreted as a protein.

The contents of cells contiguous with different successions vary according to whether the principal constituents of the laminae are GAGs or apatite.

The milieu of the cell secreting GAGs is crowded with glycogen granules (figure 69). The large membrane-bound vesicles, which form close-packed clusters are mostly filled with homogeneous, electron-dense glycoprotein but some are empty, especially those in the apical regions where myelin figures tend to congregate in the vicinity of the canal bases. Mitochondria and RER are relatively rare being much commoner in the middle and basal regions of the cell. Electron-dense fibrils and particles, in the low nanometre size range, pass through the apical plasmalemma as do coated granules into those localized parts where apatitic mosaics are aggregating (figure 79).

The milieu of the cell secreting a lamina with a high apatitic content (figure 70) also contains abundant glycogen granules and aggregated, large vesicles. The electron-dense contents of these vesicles, however, are mottled with electron-light granules (figure 71) and are in various stages of being reconstituted by RER with the release of large quantities of glycogen and electron-light granules which, with their electron-dense coats, are under 10 nm in size. The mitochondria associated with these vesicles have electron-dense substrates. Mitochondria with electron-light substrates are common within the apical region which also contains glycogen, electron-dense granules, myelin figures, lysosomes and some empty vesicles; fine, reticulate meshwork patches occur but RER is rare. The electron-dense granules, which are assumed to be coated apatite, are exocytosed through the apical plasmalemma together with electron-dense fibrils and particles to become aggregated into the laminar successions.

No collagen fibrils have yet been found in sections of the shell examined under the TEM. It is, however, noteworthy that outer epithelial cells of the body platform, which are pervaded by fibrils (figure 73), tend to be isolated from one another proximally by sheets of connective tissue (figure 72). Whether these intrusions are the source of the collagenous mats of the body platform, remains to be seen.

(*e*) *Canals and cavities*

The shell of *Lingula* is perforated by a densely distributed system of fine canals. Cavities in the form of enlarged chambers and horizontal galleries also occur and are usually adjuncts to the canals. These perforations and cavities complicate structural relationships of laminar successions but the part they play in shell secretion is obscure.

Canals originate immediately internal of the primary layer. Consequently any pattern to their distribution should be evident, under the SEM, in the first-formed secondary layer just within the valve margin. In this region there is a discernible radial arrangement of canals (figure 82) but without any ordered spacing between them, which can vary from 1 μm to more than 12 μm. This is to be expected as canals tend to converge with the thickening of the shell so that contiguous pairs in various stages of amalgamation can be found on internal surfaces (figures 82 and 88) and in sections. Accordingly, the number of canals extending from the apical plasmalemma of an outer epithelial cell also varies. Between two and six have been counted on surface casts of regular cuboidal epithelium exposed on the interiors of valves. The sporadic branching habit of canals is reflected in their diameter which, in 40 measurements, ranged from 180 nm to 850 nm with bimodal peaks at 530 nm and 740 nm.

Under the SEM, canals can be traced intermittently for over 50 μm within apatitic successions, with interruptions occurring at intercalated membranous laminae. At such interfaces, localized lateral disloca-

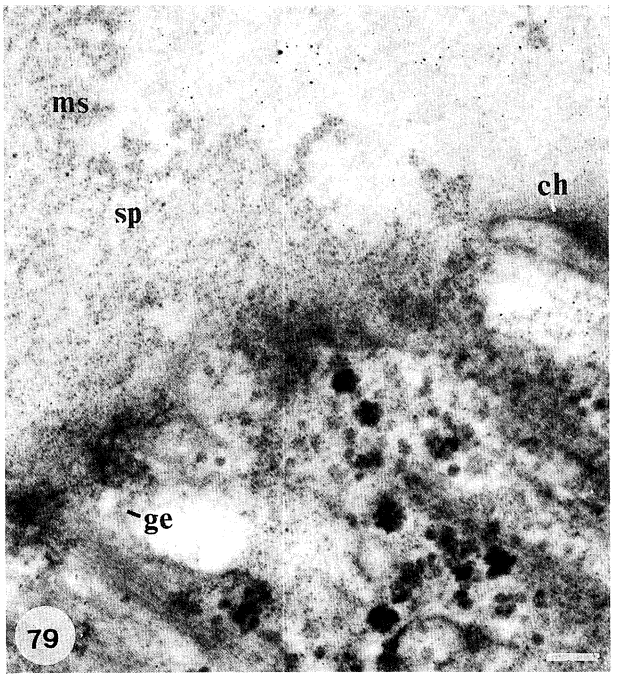

Figure 79. Transmission electron micrograph of a section of the apical plasmalemma of outer epithelium contiguous with a demineralized botryoidal lamina of *Lingula anatina* showing the exocytosis of granules (ge) and spherules (sp) to form mosaics (ms) in a GAGs matrix; chitinous fibrils (ch) were also secreted. Scale bar = 100 nm.

tions of the canal system can take place. More importantly, the canals can thicken to 1.4 μm or so and end up in chambers (figure 88), exceptionally more than 6 μm in maximum width. The chambers, which are usually lined with GAGs, may open into one or more horizontal galleries (figures 86 and 87). The latter, however, which may extend for 4 μm and can vary from 350 nm to 1.5 μm in height, are more likely to be seen in a row along the interface of two laminae (figure 58) or, half formed, as elliptical depressions developed excentrically around canals and all trailing in the same direction.

Under the TEM, the most striking aspect of canals is that they can be traced through electron-dense bands which represent membranous laminae within the shell succession (figure 69). The contents are mainly collapsed vesicular membranes and myelin figures; but coated granules of apatite aggregating into spherules also occur. Such exocytosed materials occupy much of a canal as the apical plasmalemma of the secreting outer epithelium seldom protrudes into a canal base for more than 1 μm and may even form a depression below it.

The contents of cavities in the living shell are less readily identified. The apical plasmalemma of the outer epithelium normally has a relief of more than 1 μm and can be further deformed into shapes matching the cavities. Some protuberances develop as recumbent, cylindroid extensions for up to 4 μm from the bases of canals (figure 83) whereas others form digitate mounds. The former are probably responsible for moulding the galleries; the latter, the chambers. Both types differ from canals in accommodating extensions of outer epithelium rather than exocytosed debris.

Enzymic digestion of the secondary shell is not very helpful in identifying the organic components of canal and cavity infills. The contents and membranous linings of canals are not always preserved even in the living shell, as can be confirmed by their absence from parts of sections treated with buffered solutions only. They are certainly easily removed by the proteinase enzymes (with no conclusive evidence on the efficacy of chitinase) so that canal walls in digested apatitic laminae are usually lined with spherules (figure 84). There are, however, extraneous materials which have been secreted across the pathways of canals and which survive most kinds of enzymic digestion. They include branching fibrils of collagen and membranes which restrict or cover canal openings over relatively large areas of the valve interior (figure 88). Traces of these membranes have been found on surfaces digested by chitinase and by endoproteinase Glu-C with chitinase; but they are best seen in specimens treated with buffered solutions only (figure 85). The membranes, which are normally coated with GAGs, are assumed to be chitinoproteinaceous.

Collagen fibrils and membranes also cross cavities especially galleries where vertical membranes (figures 86 and 87), partly digestible in chitinase, can occur in groups of two or three. Cavity walls are usually coated with GAGs which are likely to be the main infill of these spaces in the living shell.

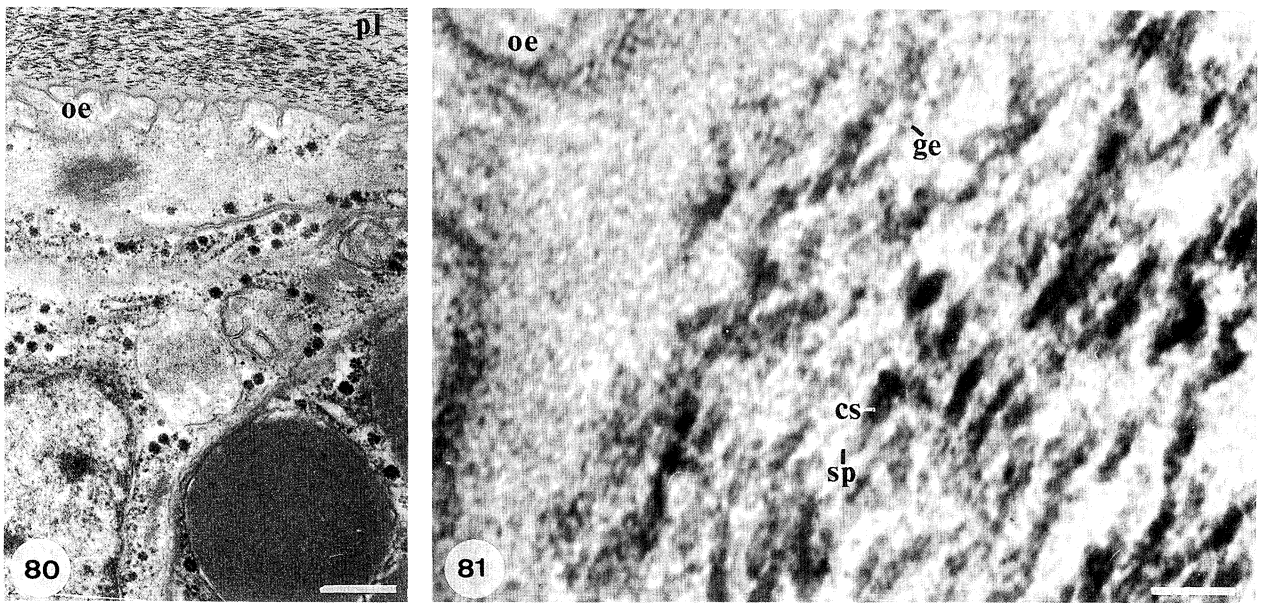

Figures 80–81. Transmission electron micrographs of a section of mineralized shell and secreting mantle of *Lingula anatina* stained with uranyl acetate and lead citrate.

Figure 80. Section of a rod and plate lamina (pl) with its secreting epithelium showing flattened protrusions of the apical plasmalemma (oe), glycogen granules, free ribosome particles, mitochondria and mottled vesicles. Scale bar = 0.5 μm.

Figure 81. Detail of the junction between the apical plasmalemma (oe) and the rod (and plate) lamina composed of granular (ge) and spherular (sp) apatite with coats of medium electron-dense protein and chitin particles, arranged linearly with strands of electron-dense material, assumed to be chitinoproteinaceous (cs). Scale bar 50 nm.

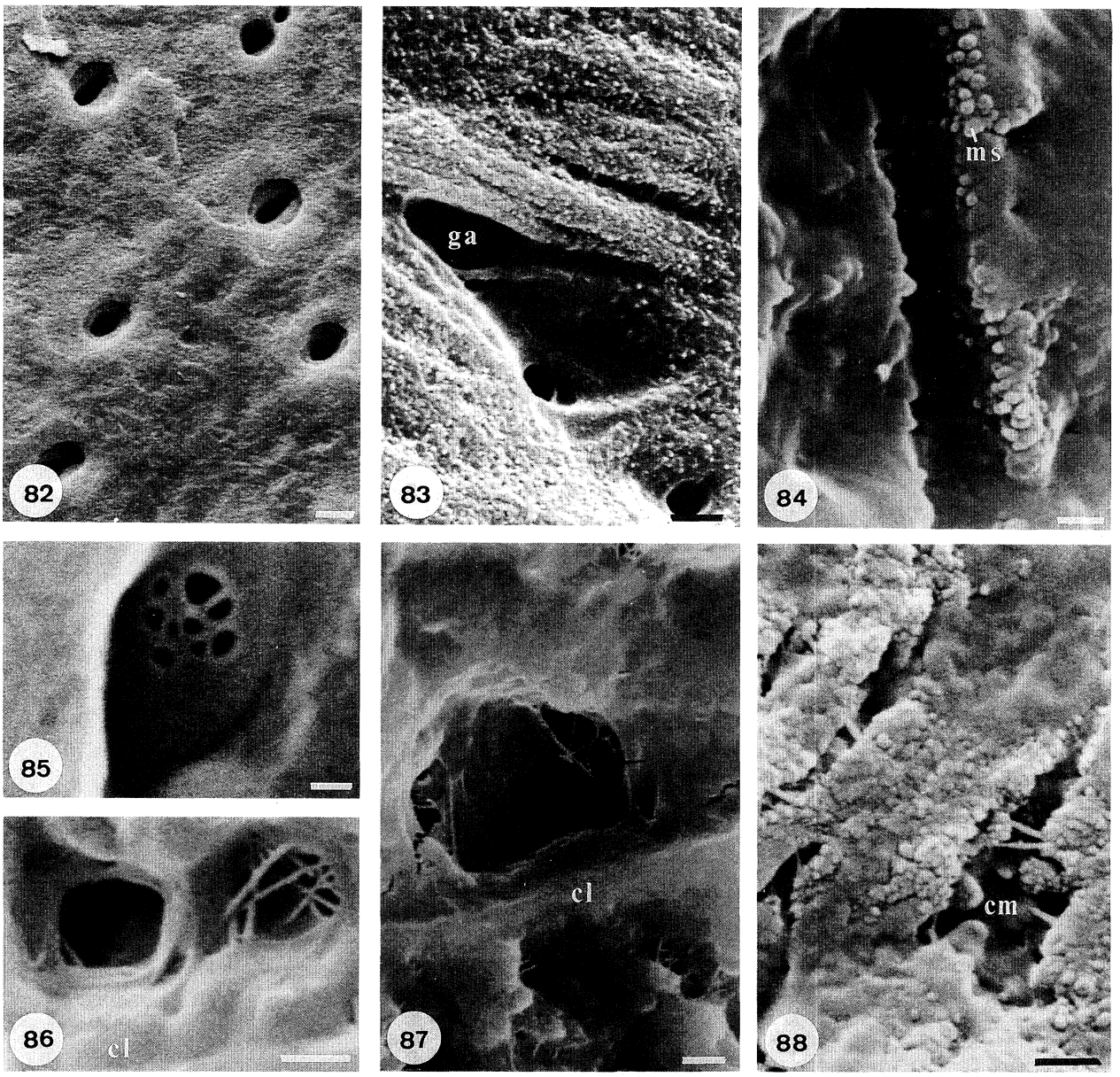

Figures 82–88. Scanning electron micrographs of gold-coated surfaces of the shell of *Lingula anatina*.

Figure 82. Radially arranged canal apertures in an apatitic compact lamina exposed on the internal surface of the mid-part of a valve digested in chitinase, with a converging pair of canals near the top right-hand corner. Scale bar = 2 μm.

Figure 83. Detail of a membrane-lined canal aperture in an apatitic compact lamina (with closely packed mosaics) exposed on the internal surface of the mid-part of a valve treated with phosphate buffer (100 mM, pH 7), with the beginnings of a horizontal gallery (ga) trailing laterally from the expanded opening of the canal, crossed by a collagen fibril strand. Scale bar = 1 μm.

Figure 84. Detail of a canal wall studded with mosaics (ms) in a botryoidal lamina exposed in a cut, vertical, posteromedian section of a valve digested in endoproteinase Glu-C. Scale bar = 0.5 μm.

Figure 85. Detail of a transverse membrane within the aperture of a canal in a compact lamina exposed on the internal surface of the mid-part of a valve treated with Tris buffer (80 mM, pH 8) with $CaCl_2$ (100 mM). Scale bar = 200 nm.

Figure 86. Detail of the openings of two horizontal galleries crossed and framed by collagenous fibrils immediately inward of an apatitic compact lamina (cl) exposed in a cut, vertical, median section in the mid-part of a valve digested in chitinase. Scale bar = 0.5 μm.

Figure 87. Transverse membrane across a horizontal gallery within a botryoidal lamina and immediately internal of an apatitic compact lamina (cl), exposed in a cut, vertical, median section in the mid-part of a valve digested in chitinase. Scale bar = 1 μm.

Figure 88. Detail of a vertical chamber intruded by mosaics (cm) and branching canals, all crossed by collagenous strands within a botryoidal lamina exposed in a cut, vertical posteromedian section of a valve treated with phosphate buffer (100 mM, pH 7). Scale bar = 1 μm.

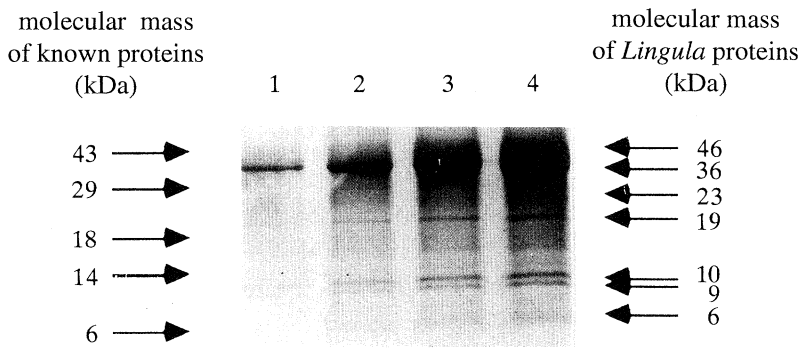

Figure 89. SDS PAGE analysis of the mineral-associated proteins from valves of *Lingula anatina*; the soluble fraction of the mineral-associated proteins was fractionated by SDS PAGE in a 15% polyacrylamide gel using the method of Schägger & Von Jagow (1987); Coomassie Brilliant Blue-R revealed the mixture of proteins present.

(*f*) *Protein analysis*

The mineral-associated proteins, extracted from *Lingula* valves and fractionated by sodium dodecyl sulphate polyacrylamide gel electrophoresis (SDS PAGE), are presented in figure 89. A complex mixture of proteins is present, ranging in size from 6 kDa to 46 kDa. In lanes three and four of figure 89 , several of the protein bands are overloaded but this serves to display the proteins present in very low levels. In total, there are at least ten proteins present. The Minitan filtration system employed in the purification procedure was fitted with filters of 10 kDa molecular mass cut-off. This cut-off is dependent on the conformation of the protein molecules so that the presence of proteins of molecular mass below 10 kDa is not surprising. Larger protein molecules, including collagen, are likely to remain in the insoluble fraction of the preparation. The work described in this paper, using proteinases to degrade specific proteins, indicated that a complex protein population may be present and this is confirmed by SDS PAGE. To begin characterization of the proteins, those fractionated by SDS PAGE were electroblotted onto ProBlott™ membrane and the amino acid composition of individual proteins determined as described in section (e) of the Appendix. The amino acid composition of seven of the mineral-associated proteins from *Lingula* valves are presented in table 2.

4. CONCLUSIONS

Before drawing any conclusions on the secretion and phylogeny of the *Lingula* shell, account has to be taken of the conflicting interpretations of its lamination and composition, which are currently in vogue. There are certainly grounds for dispute. Over the past 30 years, the shell of *Lingula* has been more widely studied than those of other brachiopods, or of most other marine invertebrates. In particular, the complexity of the shell (including its biochemical similarities with bone) and its supposed structural and compositional stability throughout most of the Phanerozoic, have stimulated multidisciplinary interest, frequently with seemingly contradictory results in three fundamental aspects

Table 2. *Amino acid composition of mineral-associated proteins from the shell of* Lingula anatina
(Amino acids are stated as residues per 100 amino acid residues.)

amino acid	molecular mass of protein						
	46 kDa	36 kDa	23 kDa	19 kDa	10 kDa	9 kDa	6 kDa
D/N	6.08	9.68	8.98	7.38	9.88	9.65	5.18
E/Q	8.45	20.93	11.72	14.52	22.73	17.27	15.05
S	12.14	7.74	7.23	8.63	6.16	6.68	7.46
G	24.53	4.5	9.68	11.03	9.17	6.14	7.46
H	1.35	0.83	0.89		2.08	2.21	
R	2.44	4.61	3.04	2.81	2.83	2.37	4.18
T	5.69	5.61	5.42	4.16	3.89	7.36	
A	10.53	13.06	12.51	15.86	9.82	9.64	14.4
P	5.21	2.27	5.26	3.63	4.19	6.29	4.08
Y	1.47	1.08	1.29	1.38	1.59	2.04	2.63
V	7.26	6.26	12.09	10.65	7.13	7.22	18.93
M		0.27					
I	5.04	5.73	6.78	7.33	5.22	7.46	7.32
L	4.38	8.89	6.43	5.92	5.42	5.54	6.27
F	2.66	1.76	4.15	2.94	4.96	5.8	2.75
K	2.74	6.74	4.49	3.75	4.88	4.31	

of invertebrate biomineralization. They are: the presence of hydroxyproline and the distribution of other organic compounds in the shell; the mode of shell accretion; and the nature of the basic biomineral unit. Some of these can now be reconciled as a result of this investigation.

(*a*) *Reconciliation of previous results*

When Jope (1965, p. H161) first identified hydroxyproline in organophosphatic brachiopod shells, she commented on its role in the synthesis of collagen. Later she noted (1977) that proteins of the *Lingula* shell did not contain glycine in sufficient quantities relative to the hydroxyproline to suggest the presence of collagen. In the absence of any evidence of exoskeletal collagen (including an X-ray diffraction scan of decalcified shell by Kelly *et al.* (1965, p. 339)), she concluded that the entire protein complex in the *Lingula* shell is exclusively part of a laminated chitinoproteinaceous system (1980, p. 85). Iwata (1981, p. 49) also noted that the histochemical reactions of the organic constituents of the mineralized layers of *Lingula* were similar to those of collagen which he was unable to find and which he thought might exist in an amorphous form. Tuross & Fisher (1989, p. 327) confirmed the presence of hydroxyproline in *Lingula* valves but failed either to demonstrate or rule out the occurrence of collagen in the shell. More recent accounts (Watabe 1990, p. 43) have continued to refer to the presence of hydroxyproline but without any indication as to the nature of its occurrence within the shell.

The significance of the presence of hydroxyproline in shell analyses has now been resolved. The amino acid is indicative of the occurrence of fibrillar collagen within the shell. The fibrils, however, are sparingly developed and form mats only sporadically, mainly within the successions of the body platform. The failure of clostridial collagenase to digest collagen in the *Lingula* valves is in accordance with the findings of Krane (1970) working with bone. Krane reported that even clostridial collagenase was ineffective against collagen in the presence of the mineral phase.

The systematic exploration by Jope (1969, 1973, 1979) of the organic content of the brachiopod shell culminated with her identification of several distinct proteins, three in significant quantities (1979, p. 171). Iwata also analysed the amino acid content of the *Lingula* shell but was more intent on determining compositional differences between the 'organic' and 'mineralized' layers. However, he did not separate the layers for analysis but conducted his investigation on the assumption that the body platform is largely mineralized and the marginal areas mainly organic (p. 45). On this basis, Iwata found that the 'organic' part of the shell contained hexosamine with some protein in the form of fibrils less than 10 nm long (p. 49) while the organic matrix of the body platform had collagenous affinities. There was no reaction to chitinase, which prompted Iwata (p. 40) to suggest that chitin might be masked by scleroprotein. GAGs were first identified in *Glottidia* by Watabe & Pan (1984, p. 977) who found that they are present throughout the lingulid shell although those of the mineralized layers, which probably have a role in apatite crystallization, are morphologically different from those of the organic layers.

In their attempt to determine more precisely the distribution of the various constituents of the *Lingula* shell, Iijima *et al.* (1991*b*) separated finely ground, organic and mineralized layers by floatation. They found that glucosamine was equally present in both layers while galactosamine was present only in the organic layers which also had a lesser concentration of acidic amino acid and a lower proportion of chitin:protein than mineralized laminae.

This current work describes the extraction of at least ten different proteins. They are present in various amounts, some being relatively minor components of the mixture. Jope (1977) described the extraction of three proteins from *Lingula* valves on the basis of carboxy-end group analysis but, using SDS PAGE, resolved only two bands of molecular masses, 90 kDa and 50 kDa. More proteins have been extracted in this study probably because the valves were ground to a fine powder prior to demineralization in EDTA, which is likely to improve extraction. Demineralization was carried out at 4°C with agitation for seven days. The tangential flow system used in this study removes EDTA most efficiently allowing improved resolution by SDS PAGE. Tuross (1990) described the extraction of a 40 kDa protein from *Lingula* valves. This protein is likely to be the 36 kDa protein described here as SDS PAGE is not a precise means of determining molecular mass.

The amino acid composition of seven of the *Lingula* proteins is presented in table 2. Unfortunately, aspartic acid (D) and asparagine (N) and glutamic acid (E) and glutamine (Q) cannot be distinguished by such analyses so it is not possible to determine comparative numbers of acidic and basic residues with any accuracy. However, the level of E/Q is much higher than any other amino acid in each case but especially in the 36 kDa and the 10 kDa proteins. These may be acidic proteins but further work using isoelectric focusing and protein sequencing will be necessary to test this possibility. Glycine levels are fairly low for each protein other than the 46 kDa protein.

The structural relationship between the shell and mantle of *Lingula* is another issue requiring clarification. Iwata (1981, p. 42) assumed that outer epithelium is physically separated from the shell by an extrapallial space containing a fluid, in which exocytosed materials are assembled for accretion onto the internal surface of the shell. This arrangement is characteristic of molluscs (Simkiss & Wilbur 1989, p. 230) and is accepted as the mechanism for *Lingula* (Watabe 1990, p. 43).

No such extrapallial space was found in this study of the *Lingula* shell and mantle. Transgressions of one lamina across another, which are frequently seen in shell successions under the SEM (figure 51), can also be found along the interface between shell and outer epithelium in sections under the TEM. Such sharp

changes can occur within the space of a few cells and, together with the existence of a densely distributed canal system anchoring mantle to shell, confirm that digitations of the apical plasmalemmas of outer epithelium directly secrete the shell intruded by them. Aggregation of apatitic units and polymerizing organic constituents do take place in embayments of the apical plasmalemmas; but the contents of these spaces are really an integral part of the advancing shell front.

In discussing the nature of the basic apatitic unit, reference has to be made to its form in various laminae. Unfortunately different terminologies are used to describe the same laminar successions as is shown in figure 90. The one used here (Williams *et al.* 1992, p. 87) has the advantage of being solely descriptive, without implication of ordered successions. The poor correlation between the A- and B-zones of Iwata and the laminar sets of Williams *et al.* is due, in our opinion, to the former succession being less representative than the latter of *Lingula* lamination as a whole, especially in showing the A-zone (the equivalent of the anastomosing ridge system) as the prevalent fabric.

In his study of *Lingula* biomineralization, Iwata (1981 pp. 41–42) concluded that two forms of apatite are secreted. In compact laminae (C-zone), apatite occurs as granules up to 50 nm in diameter. In other mineralized laminae, apatite takes the form of acicular crystallites, up to 200 nm long and arranged subparallel to one another in anastomosing ridge systems (A-zone) but irregularly in other laminae (B-zone). In contrast, Watabe (1990, p. 42) favoured the spherulite as the basic crystalline unit, although he described it as composed of acicular crystallites between 5 and 20 nm long. Aoba *et al.* (1991, p. 461) also figured acicular crystallites from the *Lingula* shell and commented on how they precipitated in aggregates.

X-ray diffraction studies (Kelly *et al.* 1965; Iijima *et al.* 1991*a*,*b*) further suggest that the basic apatitic unit is an acicular crystallite. Both investigating teams explored the orientation of apatite relative to the organic framework of the shell and published diagrams mapping the orientation of crystallites in the plane of the dorsal valve.

Kelly *et al.* (1965) found that the c-axes of apatitic crystals were usually aligned parallel to the plane of the shell but varied considerably in orientation relative to the shell margins and in the strength of definition (figure 91). In the posteromedian zone, equivalent to the body platform, c-axes were transverse or disposed in two directions and even inclined to the shell surface. In lateral areas, c-axes tended to be normal to the valve margin but in the anteromedian sector, they were ill-defined and as disorientated as in the posteromedian area. Removal of apatite by EDTA showed that the β-chitin configuration was orientated in the same way as the apatite had been so that the polysaccharide chain lay parallel with the c-axes of the apatitic components. However, reflections indicated that the crystallites were no more than 20 nm in size, increasing to 100 nm or so in the lateral areas. Concurrent electron microscopic studies confirmed that the smallest particles, at about 5 nm, were rounded and enveloped by organic material. Fractionation of the mineral components suggested that three other grades existed: needle-shaped particles with organic envelopes about 30 nm long; closely packed acicular crystallites at about 100 nm in length; and larger, rectangular aggregations. The diagrammatic representation of the findings of Iijima *et al.* (1991*a*,*b*) differed from that of Kelly *et al.* (1965) (figure 91) only in ascribing diffuse reflections of the median area to a high organic content and in showing the orientation of the c-axes of apatite and the fibre-axes

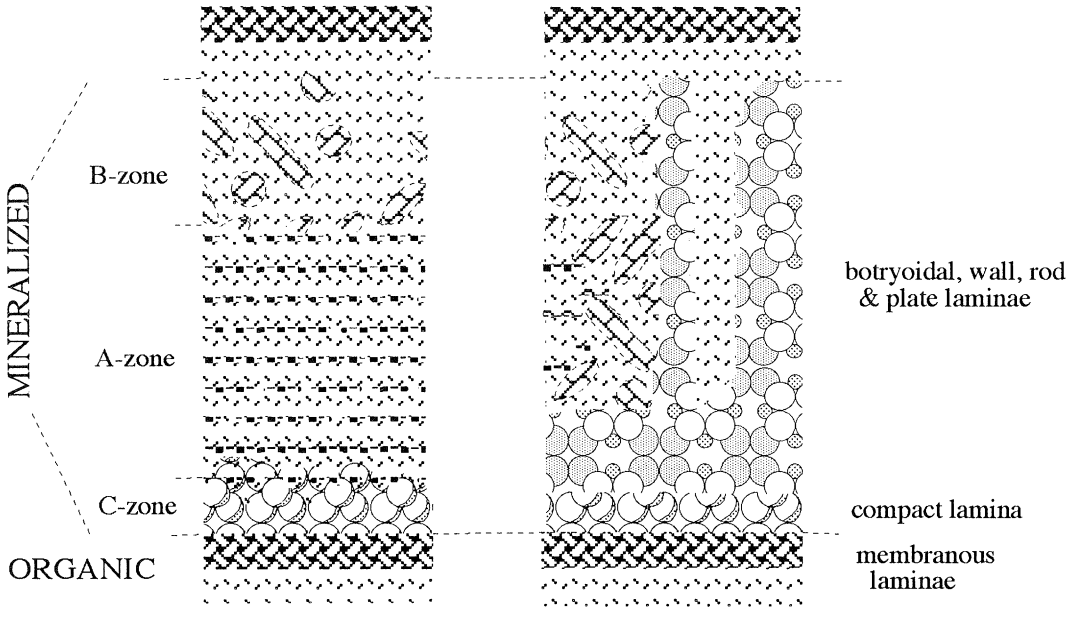

Figure 90. A terminological correlation of a composite laminar set of the shell of *Lingula anatina* as described in this paper (right-hand side) with the mineralized and organic layers as understood by Iwata (1981, p. 41); the patterned characterization of the various laminae is the same as that for figure 67.

of β-chitin to have been closely parallel with the growth vectors of posterolateral areas.

Colleagues in the University of Glasgow have undertaken X-ray diffraction (XRD) checks on shell and sections of *Lingula* on our behalf. Dr Allan J. Hall, in a powder and fragment analysis of the body platform, obtained a profile almost identical with that published by Iwata (1981). The peaks of the profile were small on a highly erratic background, probably through the 'presence of organic matter as well as the small size of the crystallites' (personal communication). The preferred orientation of the c-axis was in the plane of the valve. Dr John R. Fryer, after examining sections of lateral areas under an ABT002B microscope at 200 Kv, reported that 'the apatite in the sections of the *Lingula* shell is francolite in a very fine polycrystalline state with c-axis orientation discernible only in localized areas' (personal communication).

At first sight, the results presented here appear to be at variance with the prevailing view that the basic apatitic unit is a hexagonal prism up to 200 nm or so long. The results are based on systematic scans of interiors and sections of valves at resolutions of about 20 nm, well within the size range of described acicular crystallites. Yet the most frequently occurring basic unit is the coated granule, comparable with those seen by Kelly *et al.* (1965) under the TEM and aggregated into spheroidal bodies up to several microns in diameter. Rods and plates also occur but the former are generally too flexured to be single prisms of apatite while the latter are hexagonal in outline not rectangular as described by Kelly *et al.* (1965). The discrepancy can be resolved by comparing the distribution of internal structural lineations with the orientations of c-axes of apatite as plotted by Kelly *et al.* (1965) and Iijima *et al.* (1991*a*,*b*) on the interior of a dorsal valve (figure 91).

The structural lineations consist of anastomosing ridge systems and alternating light and dark bands of mineralized and GAGs-covered surfaces respectively, which mark concentric arcs of growth peripheral to the anterior part of the platform. The distribution of the long axes of the ridges is strikingly similar to that of the c-axes. On the platform, the ridges run transversely and, at the muscle scars, are frequently meanderform (figure 39). Lateromedianly sets of ridges may be superimposed at angles to one another (right-hand side of figure 91, see figure 30). Towards

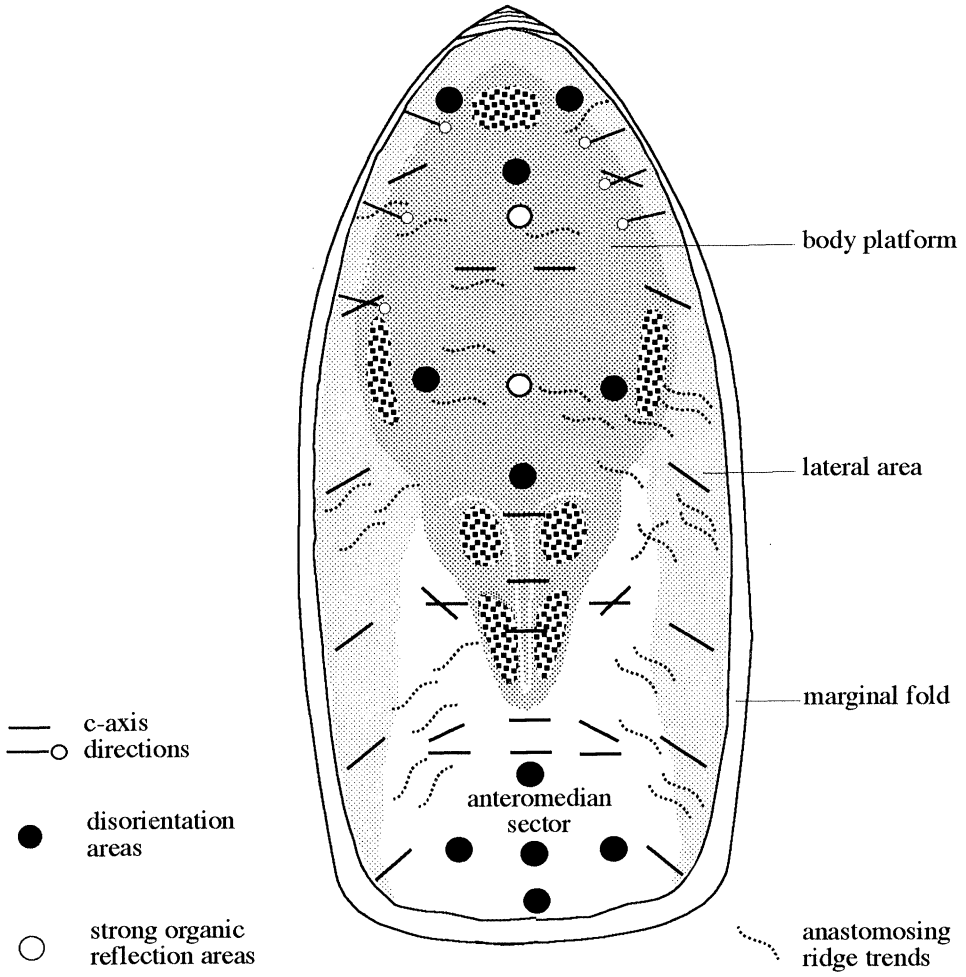

Figure 91. The interior of a dorsal valve of *Lingula anatina* showing the orientation of apatitic crystallites, for which c-axis directions have been determined, relative to the trends of anastomosing ridges; the c-axes represented by lines ending in circles are those plotted by Iijima *et al.* (1991*b*, p. 435), which were not co-incident with those mapped by Kelly *et al.* (1965, p. 339); the trends of the ridges are a compilation of observations of a number of interiors seen under the SEM.

the margin of a valve, however, ridges become aligned orthogonal to the track of the growing edge as represented by the light and dark banding.

The density distributions of spheroidal and linear aggregates of apatite are also different. The platform of a mature valve is greatly thickened (figure 51) by localized secretion of lenticles of botryoidal laminae, sporadically interleaved with collagenous mats. X-ray diffraction analysis of such a succession would reveal zones of disorientation where granular apatite is aggregated into spheroids bodies and would also reflect the collagen. These complications would tend to obscure c-axis directions of apatite within any anastomosing ridges which are interleaved with the thicker botryoidal laminae.

In the lateral areas, however, anastomosing ridges become a dominant fabric and their orientation matches the radial disposition of distal branches of the mantle canal system (figure 3). The apatitic components are mainly rods up to 600 nm long with some spherules (figures 33 and 34). The rods lie more or less parallel with the long axes of the ridges and are probably the structures identified by Kelly *et al.* (1965) as acicular crystallites. There are, however, difficulties in interpreting the rods as aggregates of prisms. Under the SEM, some are arcuate and others slightly nodular; all are coated. Under the TEM, the rods appear as acicular bodies, up to 150 nm or more long, composed of electron-dense, linear cores surrounded by granular bodies (figures 80 and 81). On our assumption that the granules, not the cores, are the apatitic units of the ridges, their crystallographic alignment in linear arrays within chitinoproteinaceous coats would account for their beaded appearance in the solid state and their XRD reflections as prisms.

It is noteworthy that the orientation of anastomosing ridges in the lateral areas of the *Lingula* shell matches the radial disposition of fine distal branches of the mantle canal systems (figure 3). Moreover the anteromedian sectors, which contain negligible quantities of disorientated apatite (figure 91) are the most flexible parts of the shell, which in life form a biconvex funnel accommodating the three setal pseudosiphons fashioned for the exchange of water within the mantle cavity (figure 93).

(*b*) *Inferred secretion of the Lingula shell*

Despite the complexity of the *Lingula* shell, the rhythmic nature of its laminar sets (figure 67) and the comparatively uniform cell structure of its associated epithelium (figures 68–73) suggest that its secretion is a simple process. The rhythm is initiated by the sudden bulk secretion of coated granules of apatite, virtually to the exclusion of organic constituents, which, however, become dominant towards the end of the cycle. This increase in the organic content culminates in the secretion of a chitinoproteinaceous membrane(s) (and/or a collagenous mat on the body platform) which serves as the substrate for the next influx of apatite.

Iwata (1984, p. 48) has discussed the possible causes of the alternation of mineralized and organic layers as understood by him and earlier researchers (figure 90). The longevity of *Lingula*, which exceeds five years (Yatsu 1902; Chuang 1961), prompted him to suggest that alternate successions could reflect annual and seasonal cycles as well as other environmental and physiological factors. Seasonal and circadian rhythms do have a role in shell secretion; laminar sets traceable throughout a succession (figure 51) could reflect the former and the fine units of a stratified laminar (figure 55), the latter. This issue, however, is complex as even apatitic secretion could be triggered by more than one factor; and is beyond the scope of this paper.

There are two notable aspects to a rhythmic unit. First, it is widespread enough to be secreted over a large area, if not the entire spread, of outer epithelium lining a valve. Secondly, the anchoring of the epithelium to the shell by canals (figure 69) means that a single cell can secrete in sequence that part of an entire rhythmic set, to which it is attached. Rhythmic changes in the secretory activities of the mantle are, therefore, a cyclical régime (figure 92).

One such cycle begins with the secretion of apatitic granules by cells, like those shown in figure 70, with large vacuoles of electron-dense materials (figure 71) and mitochondria congregating in the apical region. These coated granules, made up, at least in part, of reconstituted contents of the vesicles, are exocytosed through apical plasmalemmas onto a membranous substrate (terminating the preceding cycle). They aggregate in spherules and mosaics in a sparse chitonoproteinaceous matrix (figure 75) to form a compact lamina.

The compact lamina is terminated by the sudden secretion of GAGs which share an undulating interface with compacted apatitic spheroids. This phase of the cycle is marked within cells by the presence of numerous small vesicles and a few large ones being emptied of their medium electron-dense contents in the apical region (figure 69). There is also evidence to suggest that GAGs are exuded through intercellular spaces. Outer epithelial cells are frequently delineated on internal surfaces of the shell by ridges of GAGs replacing intercellular boundaries (figure 32).

Half way through the cycle, shell secretion is at its most diverse with walls, botryoids or rods and plates of apatite being assembled within a flood of GAGs, usually with some chitin. All three components may be simultaneously secreted by a single cell (figures 76 and 79), the chitin in fibrillar form after aggregation of particles within the apical region. The exocytosis of rods involves the linear aggregation of granules and spherules around electron-dense chitinoproteinaceous strands (figures 80 and 81) and their alignment into anastomosing ridges in the manner described for those shown in figure 34. Deposition of the meanderform ridge system (figure 39) proceeds in the same way as exoskeletal growth in the brain coral.

By the end of the cycle, little or no apatite is being secreted and the cells are like those shown in figures 68 and 69 with scattered, large vesicles, mainly empty of contents. Mitochondria are no longer congregated in the apical region although the role of these organelles

in shell secretion is unknown. The section in figure 69 is particularly apposite as it shows an almost complete succession of a rhythmic set of laminae. Only a sealing membrane, to serve as a substrate for the next cycle, is absent; and the cell, mainly with empty large vesicles but with others basally situated being filled with electron-dense and mottled materials, is in a precursory state for the next cycle. A confirmatory BSE scan of a complete cycle is shown in figure 59.

(*c*) *Phylogenetic significance of the Lingula shell*

Several structural and compositional characteristics of the shell of living *Lingula* are likely to prove phylogenetically important once fossil lingulids are better known. Two features, however, immediately provide further information on the skeletal succession of the ancestral brachiopod and its affinities with other early metazoan protostomes.

A stratified laminar set underlying a well-defined primary layer is characteristic not only of *Lingula* but also of another living brachiopod, *Discina* (Williams *et al.* 1992, p. 93). The secondary layers of these two organophosphatic genera are different in detail although the coated granule is the basic biomineral in both. The genera also share many anatomical and developmental features (Nielsen 1991, p. 25) and are widely recognized as having evolved from a common ancestor in early Phanerozoic times. The divergence evidently took place after the acquisition of an organophosphatic integument and its differentiation into a periostracum, an outer primary layer composed of GAGs and a thin secondary layer made up of inclined strata.

The discovery of fibrillar collagen in the *Lingula* shell is phylogenetically significant associated, as it is, with GAGs, apatite and chitin. The four constituents are universally or widely characteristic of eumetazoans but their presence in a mineralized integument is rare, if not unique. Only the uncalcified cuticles of certain protostomes (Richards 1984; Storch 1984) compare in their organic constituents with the brachiopod phosphatic shell. The cuticle closest to the *Lingula* integument is that of the Priapulida (Welsch *et al.* 1992). The priapulid cuticle probably contains chitin, has an inner layer of sulphated GAGs and stains for collagen which, in subepidermal sites, is striated with a periodicity of 47 nm, closely comparable with that of the fibrils in the *Lingula* shell. It is also significant that, apart from general anatomical considerations, the respiratory protein of both phyla is haemerythrin (Runnegar & Curry 1992) and that

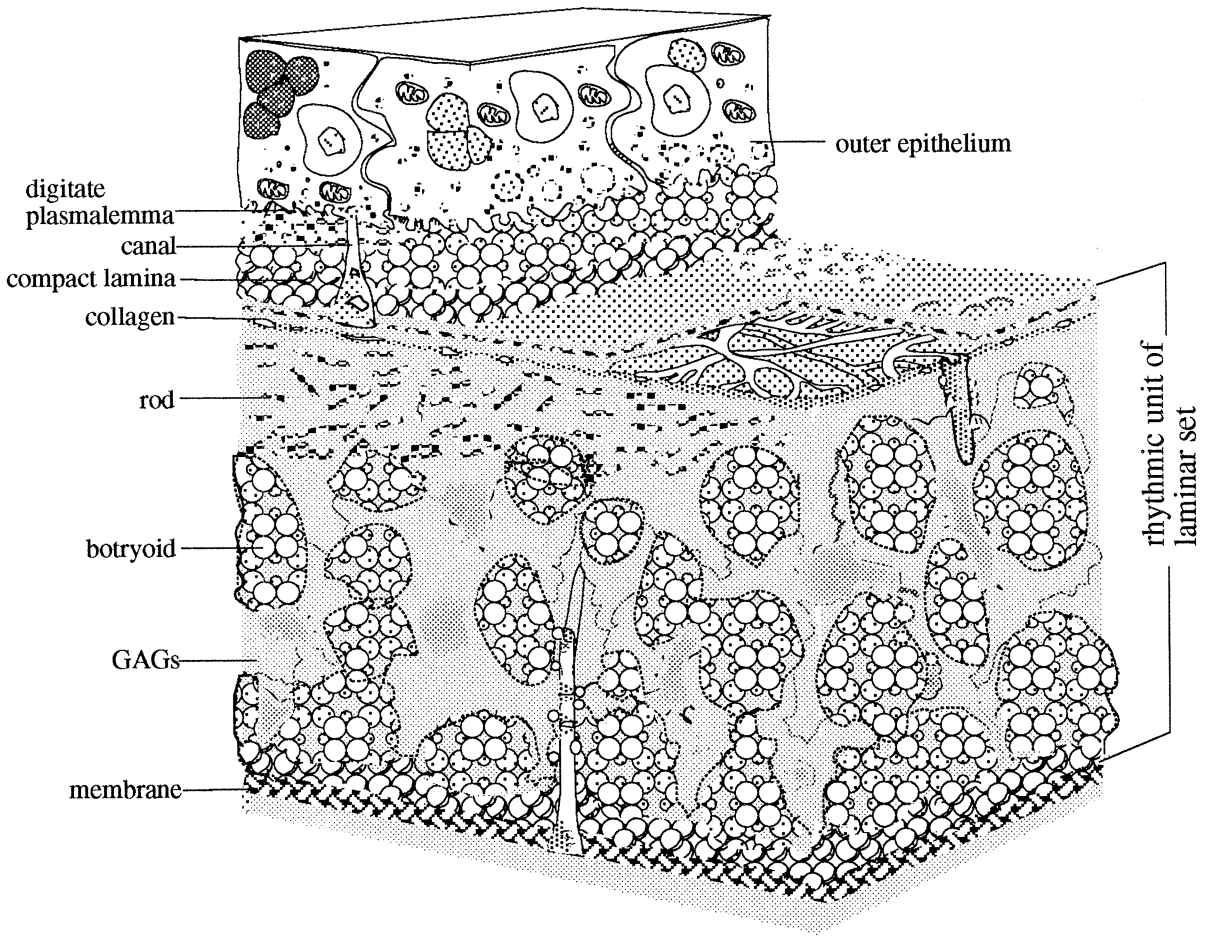

Figure 92. Diagrammatic representation of a laminar set of the shell of *Lingula anatina* showing a complete rhythmic unit of secretion with the base of the compact lamina marking the onset of a decreasing cycle of apatitic secretion and the base of the botryoidal lamina the first exudation of an increasingly preponderant GAGs matrix.

comparison of their ribosomal RNA places them both within the same major division of the protostomes (Conway Morris 1993).

In such a phylogeny, a biomineralized integument would have evolved out of a chitino-collagenous cuticle; and if phosphatic secretion represents a process of tissue detoxification (Degens *et al.* 1985), the secretory régime of *Lingula* is a set of periodic cycles of detoxification superimposed on rhythmic cuticular successions consisting of frameworks of chitin and collagen filled with GAGs.

This secretory régime provided *Lingula*, quite early in eumetazoan history, with a shell which was well constructed for its burrowing and feeding habits. The valves which, with pedicle, are like a double-bladed shovel (figure 2), are selectively strengthened by apatitic secretion posteromedially and laterally to serve respectively as protective 'mail armour' plates for the body and as ploughshares for slicing through the sediment (figure 93). Yet biomineralization does not render the impregnated parts of the shell brittle. The basic unit, an apatitic granule, is organically coated as are all its discrete aggregates which are mostly suspended, like domes and rafts of lubricated ball bearings in films of GAGs doubling up as a safeguard against intertidal desiccation. Even the anteromedial sectors of the valves, which are all but free of apatite, have a vital role in the life of *Lingula*. As the most flexible parts of the shell, they bend outwards in feeding to form a biconvex funnel accommodating three pseudosiphons, fashioned out of setae, for the circulation of water-borne nutrients within the mantle cavity.

The correlation between the rarity of apatite in the anteromedial sectors of the shell and the disposition of the setal pseudosiphons may also throw some light on

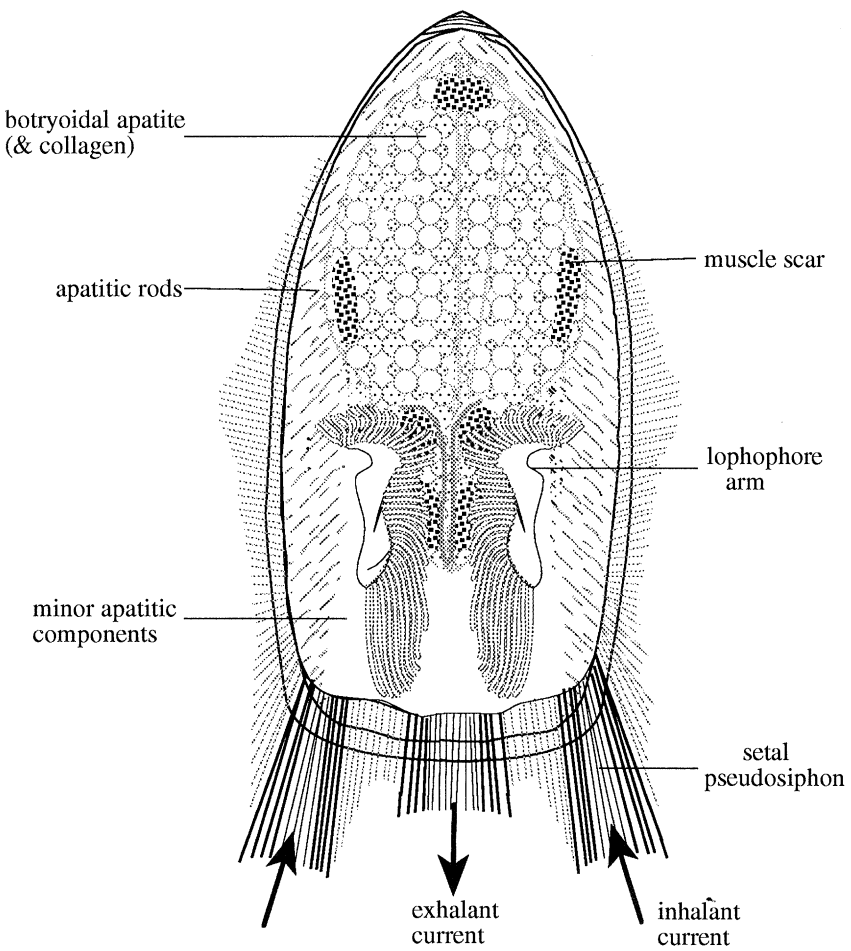

Figure 93. Diagrammatic representation of the disposition of setae and lophophore arms relative to the distribution of apatite in a dorsal valve of *Lingula*. The medial laminae of botryoidal apatite serve as mail armour for the soft body parts; the lateral apatitic rods strengthen the margins which slice burrows in the substrate; and the almost complete absence of apatite from the flexible anteromedial sector of the integument facilitates the formation of triple setal pseudosiphons.

the evolution of the feeding apparatus of *Lingula*. Emig (1990, p. 233), having noted that degradation and abrasion cause the valves of *Lingula* to 'disappear in 2 to 3 weeks', concluded that fossilization of *Lingula* shells can only occur through 'catastrophic' burial. No details were given about the conditions governing such a rapid dissolution of the shell, which is at variance with our own casual observations on dead shells in aquaria. More importantly, there is abundant geological evidence of complete, disarticulated valves of *Lingula* (*s.l.*) occurring on bedding surfaces of siltstones and sandstones which accumulated under normal conditions of sedimentation. However, in the shell of Palaeozoic species, like those of *L.* cf.*squamiformis* Phillips from the Carboniferous Limestone Series of W. Scotland, apatitic laminae do extend throughout the anteromedial sectors of both valves. This suggests that the anteromedial sectors of the shells of some extinct species were less flexible than those of modern *Lingula* and, therefore, less well-adapted to accommodating any pseudosiphonal system that may have then existed.

Many of the specimens of *Lingula* used in this study were collected in the field by AW; and we are indebted to Professor Alison Kay of the University of Hawaii at Honolulu for arranging facilities for collecting *L. reevii*; and to Professor Juichi Yanagida of the University of Kyushu and the Director of the Marine Station at Yanagawa, Kyushu for facilities and for assistance in obtaining supplies of *L. anatina*. The latter sample was looked after for some days, and later supplemented by Dr Kazuyoshi Endo of the Imperial University of Tokyo and we are grateful to him as we are to Dr Mark James who sent us samples collected on our behalf in Queensland, Singapore and Hong Kong. Our studies were conducted in our respective departments and we are grateful for all the assistance we have received, especially from Mr Peter Aynsworth and Mr Douglas McLean of the Department of Geology and Applied Geology. In addition we were fortunate to have access to a number of sophisticated facilities in many departments of the University; and we should like to express our appreciation of help we received from Dr John L. Fryer of the Department of Chemistry, Mr Douglas McIntyre and Mr David Gourley of Electronics and Electrical Engineering, Dr Laurence Tetley of the Electron Microscopy Centre, Dr Allan J. Hall of Geology and Applied Geology, Professor John Chapman and Dr Laurence Garvie of Physics and Dr Ian Montgomery of Physiology. We greatly benefitted from discussions with Professor Alastair Wardlaw of Microbiology and Dr Douglas MacKenzie of the Dunstaffnage Marine Laboratory at Oban about microbes and artefacts found in sections of *Lingula*. Finally, we thank various funding bodies for contributing towards the costs of travel and the use and purchase of equipment: A.W. and M.C. have received financial support from the Royal Society; A.W. and S.M. from the NERC; and A.W. from British Petroleum, the Carnegie Trust for the Universities of Scotland, the Leverhulme Trust and the Royal Society of Edinburgh.

REFERENCES

Aoba, T., Miake, S., Shimoda, S., Prostak, K., Moreno, E.C. & Suga, S. 1991 Dental apatites in vertebrate species: morphology and chemical properties. In *Mechanisms and phylogeny of mineralization in biological systems* (ed. S. Suga & H. Nakahara), pp. 459–463. Tokyo: Springer-Verlag.

Biernat, G & Emig, C.C. 1993 Anatomical distinctions of the Mesozoic lingulide brachiopods. *Acta Palaeont. Polonica* **38**, 1–20.

Blochmann, F. 1892 *Untersuchungen über den bau der Brachiopoden*. (124 pages.) Jena: Verlag von Gustav Fischer.

Chapman, F. 1914 Notes on shell-structure in the genus Lingula, Recent and Fossil. *R. Micros. Soc. Jour.* 28–31.

Chuang, S.H. 1961 Growth of the postlarval shell of *Lingula unguis* (L.) (Brachiopoda). *Proc. zool. Soc. Lond.* **137**, 299–310.

Conway Morris, S. 1993 The fossil record and the early evolution of the Metazoa. *Nature, Lond.* **361**, 219–224.

Curry, G.B. & Williams, A. 1983 Epithelial moulds on the shells of the early Palaeozoic brachiopod *Lingulella*. *Lethaia* **16**, 111–118.

Darwin, C. 1859 *On The origin of the species by means of natural selection or the preservation of favoured races in the struggle for life*. (298 pages.) The Folio Society edition (1990).

Degens, E.T., Kasmierczak, J. & Ittekkot, U. 1985 Cellular responses to Ca^{2+} stress and its geological implications. *Palaeontologica* **30**, 115–135.

Drapeau, G.R. 1976 Protease from *Staphylococcus aureus*. *Meth. Enzymol.* **45**, 469–475.

Dweltz, N.E. 1961 The structure of β-chitin. *Biochim. biophys. Acta* **51**, 283–294.

Ebeling, W., Henrich, N., Klockow, M., Metz, H., Orth, H.D. & Lang, H. 1974 Proteinase K from *Tritirachium album* Limber. *Eur. J. Biochem.* **47**, 91–97.

Emig, C.C. 1978 A redescription of the Inarticulate Brachiopod *Lingula reevii* Davidson. *Pacific Sci.* **32**, 31–34.

Emig, C.C. 1979 Three species of *Lingula* from the Queensland Coast. *Mem. Qld Mus.* **19**, 381–391.

Emig, C.C. 1990 Examples of post-mortality alteration in Recent brachiopod shells and (paleo)ecological consequences. *Mar. Biol.* **104**, 233–238.

Holmer, L.E. 1989 Middle Ordovician phosphatic inarticulate brachiopods from Västergötland and Dalarna, Sweden. *Fossil Strata* **26**, 1-1-72.

Iijima, M., Moriwaki, Y. & Kuboki, Y. 1991*a* Orientation of apatite and the organic matrix in *Lingula* shells. In *Mechanisms and phylogeny of mineralization in biological systems* (ed. S. Suga & H. Nakahara) Tokyo: Springer-Verlag.

Iijima, M., Takita, H., Moriwaki, Y. & Kuboki, Y. 1991*b* Difference of the organic component between the mineralized and the non-mineralized layers of *Lingula* shell. *Comp. Biochem. Physiol.* **98A**, 379–382.

Iwata, K. 1981 Ultrastructure and mineralization of the shell of *Lingula unguis* Linné, (Inarticulate Brachiopod). *J. Faculty Sci. Hokkaido Univ.* **4**, 35–65.

Jope, H.M. 1965 Composition of brachiopod shell. In *Treatise on invertebrate palaeontology*, vol. (H) (*Brachiopoda*) (ed. R. C. Moore), p. H159–H162. Kansas: Geological Society of America & University of Kansas Press.

Jope, H.M. 1969 The protein of brachiopod shell – III. Comparison with structural protein of soft tissue. *Comp. Biochem. Physiol.* **30**, 209–224.

Jope, H.M. 1973 The protein of brachiopod shell – V. N-terminal end groups. *Comp. Biochem. Physiol.* **45B**, 17–24.

Jope, M. 1977 Brachiopod shell proteins: their function and taxonomic significance. *Am. Zool.* **17**, 133–140.

Jope, M. 1979 The protein of brachiopod shell – VI. C-terminal end groups and sodium dodecyl sulphate-polyacrylamide gel electrophoresis: molecular constitution and structure of the protein. *Comp. Biochem. Physiol.* **63B**, 163–173.

Jope, H.M. 1980 Phylogenetic information derivable from

fossil brachiopods. In *Biogeochemistry of amino acids* (ed. P. E. Hare, T. C. Hoering & K. King Jr) New York: John Wiley & Sons.

Kelly, P.G., Oliver, P.T.P. & Pautard, F.G.E. 1965 The shell of *Lingula unguis*. In *Proc. 2nd European Symposium on Calcified Tissue*, pp 337–345.

Krane, S. M. 1970 Degradation of collagen in connective tissue diseases. Rheumatoid arthritis. In *Dynamics of connective tissue macromolecules* (ed. P. M. C. Burleigh & A. R. Poole), pp. 309–326. North-Holland Publishing Company.

Markland, F.S. & Smith, E.G. 1971 Subtilisin: primary structure, chemical and physical properties. In *The enzymes*, vol III (*Hydrolysis: peptide bonds*), 3rd edn (ed. P. D. Boyer), pp. 562–606. New York: Academic Press.

McConnell, D. 1963 Inorganic constituents in the shell of the living brachiopod *Lingula*. *Geol. Soc. Am. Bull.* **74**, 363–364.

Nielsen, C. 1991 The development of the brachiopod *Crania (Neocrania) anomala* (O. F. Müller) and its phylogenetic significance. *Acta Zool, Stockh.* **72**, 7–28.

Pan, C.-M. & Watabe, N. 1988 Shell growth of *Glottidia pyramidata* Stimpson (Brachiopoda: Inarticulata). *J. exp. mar. Biol. Ecol.* **119**, 43–53.

Pan, C.-M. & Watabe, N. 1989 Periostracum formation and shell regeneration in the lingulid *Glottidia pyramidata* (Brachiopoda: Inarticulata). *Trans. Am. Microsc. Soc.* **108**, 283–298.

Pfannenstiel, H.-D. 1982 Modified axonemes and ciliary membranes in three polychaete species. *Cell. Tiss. Res.* **224**, 181–188.

Richards, K.S. 1984 Cuticle. In *Biology of the integument*, vol. 1 (*Invertebrates*) (ed. J. Bereiter-Hahn, A. G. Matoltsy & K. S. Richards), pp. 310–319. Berlin: Springer-Verlag.

Rowell, A.J. 1965 Inarticulata. In *Treatise on invertebrate palaeontology*, vol. (H) (*Brachiopoda*) (ed. R. C. Moore), p. H260–H296. Kansas: Geological Society of America & University of Kansas Press.

Rudall, K.M. 1969 Chitin and its association with other molecules. *J. Polymer Sci.* **28**, 83–102.

Runnegar, B. & Curry, G.B. 1992 Amino acid sequences of hemerythrins from Lingula and a priapulid worm and the evolution of oxygen transport in the Metazoa. *Proc. 29th International Geological Congress (Abs)* vol. **2**, p. 3–46, Kyoto, Japan.

Schägger, H. & Von Jagow, G. 1987 Tricine-sodium dodecyl sulphate-polyacrylamide gel electrophoresis for the separation of proteins in the range from 1 to 100 kDa. *Analyt. Biochem.* **166**, 368–379.

Seifter, S. & Harper, E. 1970 Collagenases[1]. In *Methods in enzymology*, vol. XIX (*Proteolytic enzymes*) (ed. G. E. Perlman & L. Lorand), pp. 613–635. New York: Academic Press.

Simkiss, K. & Wilbur, K.M. 1989 *Biomineralization cell biology and mineral deposition*. (337 pages.) San Diego: Academic Press.

Simpson, G.G. 1953 *The major features of evolution*. (4–34 pages.) New York: Columbia University Press.

Storch, V. 1984 Echiura and Sipuncula. In *Biology of the integument*, vol. 1 (*Invertebrates*) (ed. J. Bereiter-Hahn, A. G. Matoltsy & K. S. Richards), pp. 368–375. Berlin: Springer-Verlag.

Tuross, N. 1990 A 40 kD Protein in Modern and Fossil Lingula. *The Sixth International Symposium on Biomineralization* (Abs), Odawara, Japan.

Tuross, N. & Fisher, L.W. 1989 The proteins in the shell of *Lingula*. In *Origin, evolution and modern aspects of biomineralization in plants and animals* (ed. R. E. Crick), pp. 325–328. New York: Plenum Press.

Watabe, N. & Pan, C.-M. 1984 Phosphatic shell formation in atremate brachiopods. *Am. Zool.* **24**, 977–985.

Watabe, N. 1990 Calcium phosphate structures in invertebrates and protozoans. In *Skeletal biomineralization: patterns, processes and evolutionary trends*, vol. 1 (ed. J. G. Carter), pp. 35–44. New York: Van Nostrand Reinhold.

Welsch, U., Erlinger, R. & Storch, V. 1992 Glycosaminoglycans and fibrillar collagen in Priapulida: a histo- and cytochemical study. *Histochemistry* **98**, 389–397.

Williams, A. 1977 Differentiation and growth of the brachiopod mantle. *Am. Zool.* **17**, 107–120.

Williams, A. & Holmer, L.E. 1992 Ornamentation and shell structure of acrotretoid brachiopods. *Palaeontology* **35**, 657–692.

Williams, A., Mackay, S. & Cusack, M. 1992 Structure of the organo-phosphatic shell of the brachiopod *Discinisca*. *Phil. Trans. R. Soc. Lond.* B **337**, 83–104.

Williams, A. & Mackay, S. 1978 Secretion and ultrastructure of the periostracum of some terebratulide brachiopods. *Proc. R. Soc. Lond.* B **202**, 191–209.

Yatsu, N. 1902 On the development of *Lingula anatina*. *Tokyo Imper. Univ. Coll. Jour.* **17**, 11–12.

Received 9 November 1993; revised 25 March 1994; accepted 29 April 1994

APPENDIX: MATERIALS AND METHODS

Two species of *Lingula* have been used in our researches. Specimens of *Lingula anatina* Lamarck, from intertidal silts in Ariake Bay near Yanagawa, N. Kyushu, Japan, and of *L. reevii* Davidson (Emig 1978) from intertidal carbonate muds at Coconut Island, Honolulu, were collected by one of us (A.W.) and brought back alive to Glasgow. They were kept in an aquarium on a diet of 'Liquifry Marine' in an aerated solution of Instant Ocean sea salt at normal salinity and appropriate temperatures until they were required for laboratory studies. Specimens of *L. anatina* were also collected by Dr M. A. James from Magnetic Island, Queensland (Emig 1979), and Starfish Bay, Hong Kong. The samples received from Dr James had been fixed within a day or so of collecting in isopropanol or in glutaraldehyde (3% by volume made up in phosphate buffer (0.1 M, pH 7.2 containing sodium chloride ($30\,g\,l^{-1}$)).

The samples were collected for more extensive study than the biomineralization of the shell. Moreover, shell secretion is known to be affected by environmental factors; and, as most research on the biomineralization of *Lingula* is being undertaken in Japan, it was decided to concentrate on the samples from Kyushu. Accordingly, the results and illustrations given here are based on specimens of *L. anatina* from Ariake Bay with conspecific material from Queensland and Hong Kong used for critical point dried preparations and *L. reevii* for the secretion of the periostracum. It is noteworthy that studies of other lingulas have not revealed any structural or biochemical differences.

(*a*) *Preparation of materials for the* TEM

Living *Lingula* were maintained in an aquarium until the time of fixation. On removal from the aquarium, shells were allowed to snap shut around a

wooden stick to provide an opening for fixative to penetrate. Animals were fixed by two hours immersion in 3% glutaraldehyde in 0.1 M phosphate buffer containing 3% sodium chloride. After several buffer rinses each specimen was cut into pieces with a razor blade. Cuts were made so that areas from the anterior, posterior, middle and lateral regions could be compared. Then, some specimens were transferred to EDTA ($10\,g\,l^{-1}$) for demineralization, after which EDTA was washed out in 0.2 M sucrose. The EDTA treatment was omitted for fully mineralized specimens. All specimens were post-fixed in 1% osmium tetroxide buffered to pH 7.2 with phosphate buffer, dehydrated through an ascending alcohol sequence and embedded in Spurr's resin. Thin sections were cut on a Reichert E ultramicrotome using a Diatome diamond knife. Sections stained with an aqueous solution of uranyl acetate and lead citrate were examined on either a Jeol JEM 100S or Philips 301 transmission electron microscope.

(*b*) *Preparation of materials for the* SEM

All valves of *Lingula* used for SEM studies had been stored in ethanol (70% by volume) at 4°C for varying periods after the removal of soft tissue for RNA and haemerythrin extraction. Previous researches on the organophosphatic shell of *Discina* (Williams *et al.* 1992) had shown that the most informative way of studying its ultrastructure under the SEM was to scan prepared surfaces and sections of valves in the natural state. Sections, cut with dissecting scissors in the preferred direction, provide three-dimensional views of shells and facilitate studies of the bounding surfaces as well as the internal structure of constituent laminae. After such specimens had been prepared according to the procedures outlined below, they were coated with gold or gold/palladium dependent on whether they were to be viewed under the Cambridge 360 or the Hitachi 900 for resolutions down to 100 Å and 7 Å respectively.

At high magnifications and at resolutions attainable with the Hitachi 900, the grain of the gold/palladium film became discernible even when shadowing was limited to two 30-second bursts, at 10 and 20 mA. The grain size was homogeneous at about 4 nm which is within the range established by TEM studies for the apatitic constituents of the shell. However, this granular sputter is distinctive in its uniformly low relief (figure 12) compared with the bold relief of granules composing the very much larger apatitic spherules and mosaics.

The main complications of using unmounted shell to determine its ultrastructure result from the chemical characteristics of its principal organic component, glycosaminoglygans.

In the earlier stages of this study, cut pieces of a valve, chosen for differential treatment, were sonicated for 3 min. in Milli Q^{TM} water. After treatment, the sectioned valve was stored in Milli Q water for periods of usually less than two days, when it was dried on lens cleaning tissue and mounted on stubs for coating within twelve hours of mounting. Under the SEM, the effects of the drying out of the valve were evident in the cracked state of the GAGs gel, although this condition actually serves as a reliable diagnostic feature of the gel. Moreover, two kinds of vesicles, distinguishable in size and location, also occurred sporadically on exposures of GAGs and had to be considered as intrinsic features.

The smaller, hemispherical vesicles averaged 1.7 μm in diameter (figure 94). They were widely scattered on sections and internal surfaces, especially of the inner laminae. Some were contained by radiating, narrow folds of GAGs, others by flattened bands or hoops about 200 nm wide (figure 95).

The larger vesicles were almost invariably more than 3 μm in diameter and occasionally exceeded 15 μm. They occurred as sporadically distributed clusters within the hinge of the marginal fold of the valves (figure 96). They were hollow hemispheres with a thin coat of GAGs indented by dehydration depressions and tension cracks.

We concluded that all such vesicles are artefacts. All develop within GAGs containing discoidal bodies (described in §3*b*(ii) which can become greatly stretched to form the hoops of some smaller vesicles. The size difference may be related to the nature of their media. At its margin, a valve is composed largely of GAGs in a plastic state which would not narrowly constrain the development of vesicles. In more heavily biomineralized successions of the secondary shell, however, vesiculation would be constricted within a less flexible framework of apatite. Both kinds of vesicles were induced during the preparation of specimens for electron microscopy and are, therefore, comparable with artificial distensions of polychaete cilia (Pfannenstiel 1982).

Within the time taken to prepare specimens in the manner outlined above, exposures of GAGs were also liable to microbial settlement.

The commonest bacteria were rods, about 2 μm long and 700 nm thick, associated with cocci, up to 4 μm in diameter. We concluded that they were *post mortem* contaminants which, under normal laboratory conditions, could colonize an uncoated shell within a few days of treatment. However, traces of another microbe also occurred but more rarely and on internal surfaces only. These were rods with long flagella, 5 μm or so in overall length, which morphologically compare with the obligate, anaerobic thiopneutes. Their presence within the shell milieu of a brachiopod which burrows in anoxic sediments, merits further study.

To test the assumptions that vesiculation and microbial settlement are promoted by the length of time taken to prepare specimens in normal laboratory conditions, a pair of valves were processed in the same way but without delay and in a near sterile environment. The valves, which had been stored in ethanol, were each cut into three pairs of matching pieces and incubated overnight in a laminar flow chamber with the six pieces of one valve kept in ethanol or Milli Q^{TM} water and the six of the other digested in subtilisin (0.5 M in 100 mM phosphate buffer, pH 7) or retained in ethanol (70% by

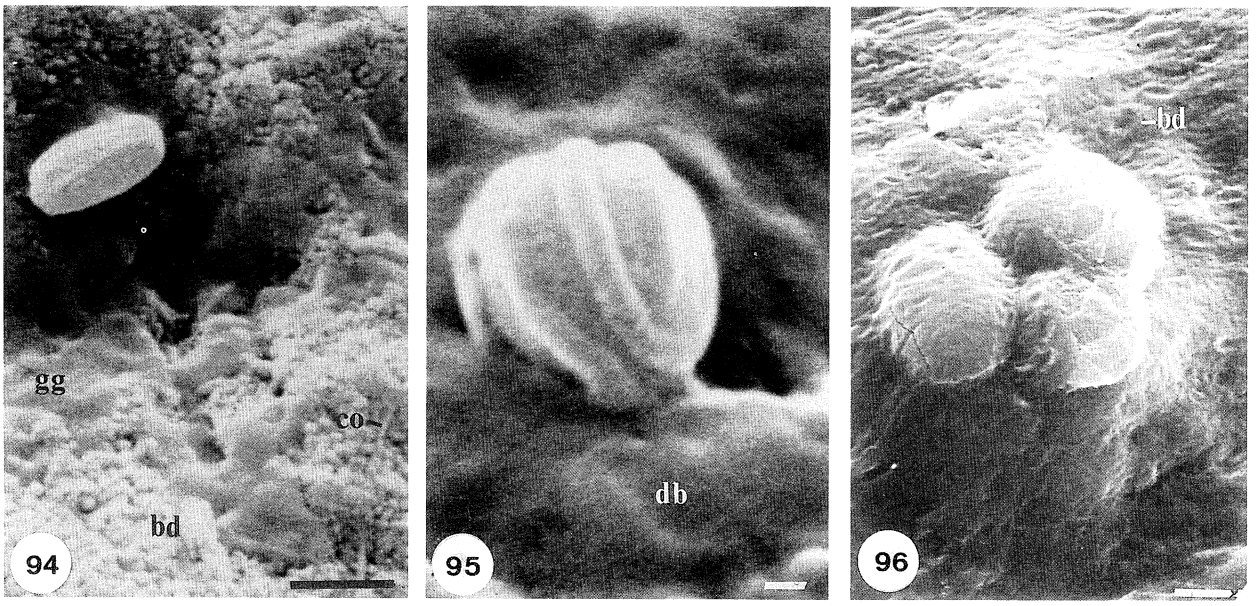

Figures 94–96. Scanning electron micrographs of gold-coated, extrinsic objects in the shell of *Lingula anatina*.

Figure 94. Banded vesicle developed in GAGs (gg) on a cut, vertical section of the body platform of a valve digested in subtilisin, with botryoidal apatite (bd) and collagen (co). Scale bar = 1 μm.

Figure 95. Hooped vesicle in GAGs with discoidal bodies (db) on a cut, vertical median section of the mid-part of a valve treated with MES buffer (100 mM, pH 6). Scale bar = 200 nm.

Figure 96. A cluster of large vesicles developed in GAGs with discoidal bodies (bd), on the internal surface of the marginal fold of a valve treated with phosphate buffer (100 mM, pH 7). Scale bar = 2 μm.

volume). Autoclaved instruments were used, within the chamber, to mount all pieces on stubs which were then immediately shadowed with gold for examination under the SEM. No bacteria or vesicles were seen, while the GAGs bore fewer signs of contraction, even in those pieces of shell digested by subtilisin. Such evidence confirms the desirability of near sterile conditions for the preparation of unmounted specimens and suggests that vesiculation is brought about by osmotic pressures (Pfannenstiel 1992).

The bilateral symmetry of *Lingula* facilitates the checking of various chemical and enzymic reactions on the shell. The valves can be cut medially along their sagittal axes with the assurance that the structural details of one half are mirrored in the other half (figure 97). However, the composition of a mature valve varies radially from a relatively thick, posteromedian zone with a strongly apatitic inner shell to a comparatively thin, mainly organic succession towards the edge of the valve (figure 93). Chemical or enzymic treatment of a valve interior could, therefore, result in different reactions in the posteromedian and marginal zones and even in the transitional areas between them.

The effects of these changes in shell composition can be assessed by cutting a valve transversely into three parts, each consisting of a pair of matching pieces on either side of the medial cut. In this way, six pieces of a valve can be incubated in three different enzymes and their buffers; and three valves are required to ensure that all three enzymes have been used to digest the posterior, median and anterior parts of a valve. A possible disadvantage to this apportionment of a valve is that the medial sections could be dominated by the exaggerated growth of median ridges especially in dorsal valves. Accordingly, valves were also sliced obliquely in transverse arcs as shown in figure 97. Oblique cuts increased access to interlaminar boundaries and facilitated checks on the representativeness of sagittal and transverse sections.

In all, five enzymes have been used to digest the *Lingula* shell, separately and in paired combinations. Some incubations were repeated and 15 valves were so

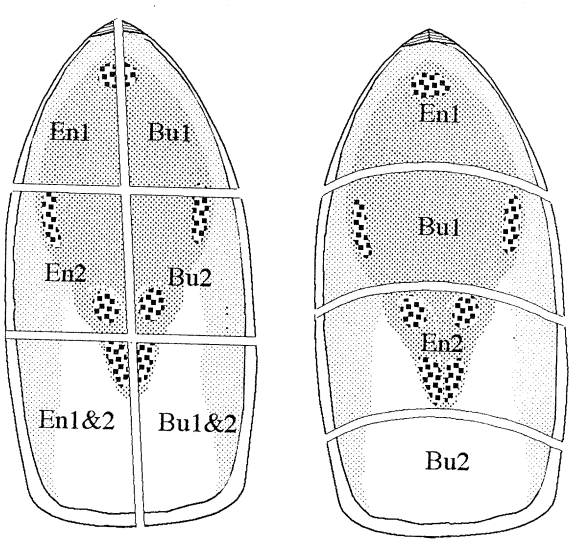

Figure 97. Two ways of cutting valves of *Lingula anatina* to provide matching sections (and also matching internal surfaces in the case of the left valve) for incubation with enzymes (En) and their buffers (Bu).

treated. In addition, another four valves had been apportioned in the same way and treated with various concentrations of bleach and incubating controls (ethanol and Milli Q^{TM} water). All valves used in this way were mature and varied in sagittal length between 35 and 50 mm.

(*c*) *Chemical and enzymic treatment of specimens*

Natural surfaces and cut or fracture sections of valves of *Lingula* were subjected to various treatments in order to identify, and determine the distribution of, the principal organic and biomineral components of the shell.

(i) *Sodium hypochlorite treatment*

Non-specific degradation of the organic components of the *Lingula* shell was achieved by incubating valves at 22°C for 24 h with an aqueous solution of sodium hypochlorite. To determine the concentration of sodium hypochlorite resulting in degradation of organic material without destruction of the shell fabric, a pair of *Lingula* valves were cut into pieces of eight; and the four pairs of portions for each valve incubated with sodium hypochlorite at 0, 1, 2 or 5% by volume in different sequences for matching pairs. The portions were incubated with sodium hypochlorite for 24 h at 22°C before being rinsed in Milli Q^{TM} water.

(ii) *Enzymic digestion*

The five enzymes used ito identify various organic components of the *Lingula* valve *in situ* were as follows.

Two serine proteinases, subtilisin and proteinase-K, with broad range specificity for hydrolysis were used to locate proteinaceous material. Subtilisin (E.C.3.4.21.14) cleaves peptide bonds at the carboxylic side of neutral and acidic residues (Markland & Smith 1971). Subtilisin from *Bacillus licheniformis* was employed at a concentration of 0.5 mM in sodium dihydrogen phosphate buffer (100 mM, pH 7). Proteinase-K (E.C.3.4.21.14) cleaves peptide bonds adjacent to the carboxylic group of aliphatic and aromatic amino acids (Ebeling *et al.* 1974). Proteinase K from the fungus *Tritirachium album* was applied at concentrations of 0.1 and 0.5 mM in sodium dihydrogen phosphate buffer (100 mM, pH 7).

A third serine proteinase, with narrow range specificity, was used in an attempt to identify proteins with substantial proportions of acidic residues. Endoproteinase Glu-C (E.C.3.4.21.19) or V8 protease from *Staphylococcus aureus* cleaves peptide bonds at the carboxylic end of both aspartic acid and glutamic acid residues when used in sodium dihydrogen phosphate buffer (100 mM, pH 7) (Drapeau 1976). Endoproteinase Glu-C was employed at 0.5, 1.2 mM and 12 mM.

Collagenase (E.C.3.4.24.3) cleaves collagen molecules between the X and G residues in the sequence -P-X-G-P-Y-, where P and G are proline and glycine residues respectively and X and Y are any amino acid residues (Seifter & Harper 1970). Collagenase from *Clostridium histolyticum* was applied at concentrations of 6, 15 and 35 mM in Tris buffer (80 mM, pH 8) with $CaCl_2$ (100 mM).

Chitinase (E.C.3.2.1.14) from *Serratia marcesens* dissolved in MES [2-(*N*-morpholino) ethanesulphonic acid] buffer (100 mM, pH 6) was used at concentrations of 0.15, 0.5 and 1 mM.

Valve portions were incubated with buffered enzymes or enzymes alone for 72 h at 22°C. At 24 h intervals, all solutions were replaced. After the 72 h incubation, valve portions were rinsed with Milli Q^{TM} water.

As previously described, each valve was cut into six pieces of similar size, a total of twelve portions from a complete shell. Paired portions were incubated with enzyme (or a mixture of enzymes) and with its buffer (or a mixture of appropriate buffers) (figure 97).

One pair of valves was cut in this way and the effects of subtilisin, chitinase, proteinase K and endoproteinase Glu-C were examined. The enzymes were applied alone and in combinations and the appropriate buffers were applied to complementary portions of valve.

Four pairs of valves were used in another programme. Two pairs were treated to examine the effects of chitinase, collagenase and proteinase K, alone and in paired combinations, as well as buffers and combinations of buffers. The other two pairs were incubated with the same series of enzymes and buffers except that the broadly specific proteinase-K was replaced by the narrowly specific endoproteinase Glu-C.

Obliquely cut valves were also incubated in enzymes and appropriate buffers. In this programme the effects of chitinase, collagenase and endoproteinase Glu-C, alone and in paired combinations, as well as buffers and combinations of buffers were examined.

(*d*) *Crystallographic analysis*

Apart from the powder preparations used by Dr Hall in his X-ray diffraction analysis of a *Lingula* valve, electron dispersive studies to determine crystallographic and fibre axes of apatite and chitin required resin-impregnated sections of the shell.

(i) *Scanning techniques*

Resin-mounted block sections were used for energy dispersive x-ray (EDX) analysis and back scattered electron (BSE) detection. All valves mounted in resin had first been physically stripped of soft tissue and stored in ethanol prior to use. The sections were obtained by impregnating valves with London Resin under low atmospheric pressures and, after polymerization of the resin, by cutting the blocks in the preferred plane with a diamond wheel, polishing the surface with fine alumina (Gamma 100) and coating the prepared surfaces with carbon.

(ii) *Transmission techniques*

Body tissue was removed and valves stored in ethanol (70% by volume). After rinsing in sterile Milli Q^{TM} water, a valve was cut into four transverse sections and organic tissue digested with 0.5 mM

subtilisin in phosphate buffer for 24 h. Samples were thoroughly rinsed in Milli Q™ water and transverse sections cut further to give central and lateral pieces. They were then dehydrated through an ascending alcohol series and embedded in Spurr's resin. For STEM examination 50 nm sections were cut; for X-ray diffraction, dark grey sections (approximately 10 nm) were cut.

(*e*) *Extraction and purification of mineral-associated proteins*

Body tissue was stripped from the shell and fine sandpaper used to remove the periostracum and any adherent body tissue. Loosened material was detached by sonicating three times (three minutes each time) in a water-bath with Milli Q™ water. The shell is perforated by fine canals (and rare chambers and galleries up to several microns in size) which contain vesicular membranes and other exocytosed materials. These structures, however, do not contribute significantly to the organic contents of a cleaned shell. The apertures of 19 canals exposed in 1500 μm^2 of a typical internal surface of a lamina of compact apatite, which had been treated with chitinase, occupied less than 1% of the area.

The cleaned valves were allowed to dry, cut into small pieces with dissecting scissors and ground to a fine powder using a Teema mill. Ethyl diamine tetra acetate (EDTA, 20% by volume, pH 8) was added to the shell powder at a ratio of 20 millilitres per gram of shell. The mixture was then incubated at 4°C with agitation for seven days. After centrifugation (20 000 *g* for one hour), the supernatant was concentrated 16-fold and the EDTA removed using the Minitan™ tangential flow filtration system from Millipore. The Minitan™ system was fitted with 10 kDa cut-off filters. The supernatant was concentrated a further tenfold and desalted in a Minicon concentrator from Amicon. The proteins were fractionated by sodium dodecyl sulphate polyacrylamide gel electrophoresis (SDS PAGE). Small gels (9 cm×7 cm) of 0.75 mm thickness containing 15% polyacrylamide were prepared according to Schägger & Van Jagow (1987). Glycine which is used in most SDS PAGE systems was replaced by tricine. Samples for electrophoresis were heated at 100°C for 4 min in an equal volume of sample buffer containing Tris-HCl (0.15 M, pH 6.8), β-mercaptoethanol (0.2 M), SDS (0.1% by mass), glycerol (30% by volume) and the tracking dye, Bromophenol Blue (0.0002% by mass). Molecular mass standards were included on every gel. Electrophoresis of samples in the small gel system required a constant voltage of 100 V for 2 h.

After electrophoresis, a constant voltage of 50 V was applied for 30 min to transfer the proteins from the polyacrylamide gel onto ProBlott Membrane in Caps buffer (10 mM, pH 11, containing methanol, 10% by volume). The membrane was washed briefly with water and then with methanol before staining with Coomassie Brilliant Blue-R (0.1% by mass) in destain for 1 min. Background staining was reduced with an aqueous dilution of methanol (50% by volume).

The amino acid composition of the pure proteins immobilized on ProBlott membrane was determined by loading samples directly onto the 410-H amino acid analyser with automatic hydrolysis from Applied Biosystems. Fractions of the membrane that contained no protein were also analysed to determine the background level of contaminants present. This background level was then subtracted from the absolute values.

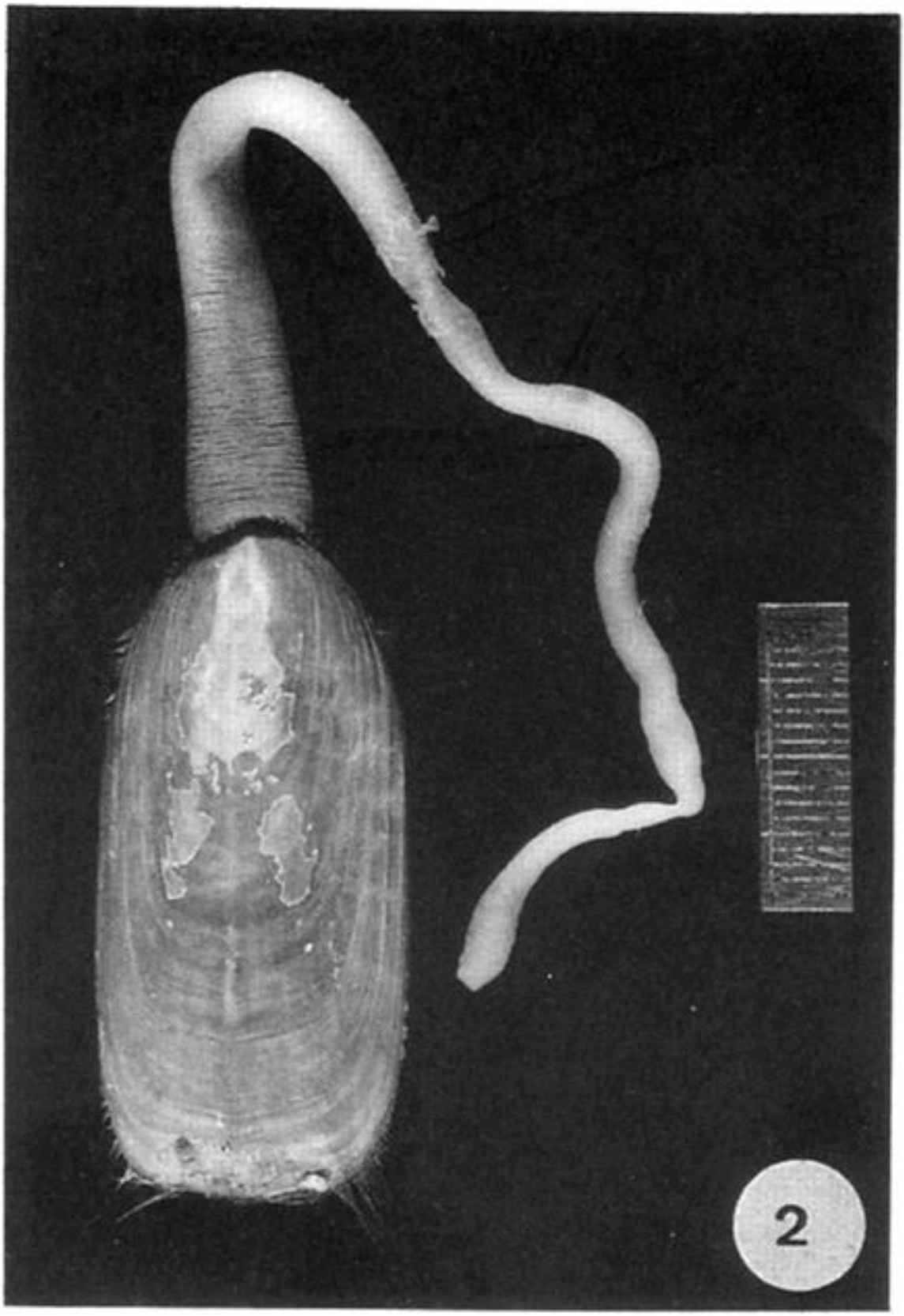

Figure 2. Dorsal view of a complete specimen of *Lingula anatina* (preserved in ethanol, 70% by volume) showing the shell in relation to the fleshy posterior stalk-like pedicle and the marginal fringe of setae; metal bar on right-hand side = 2 cm.

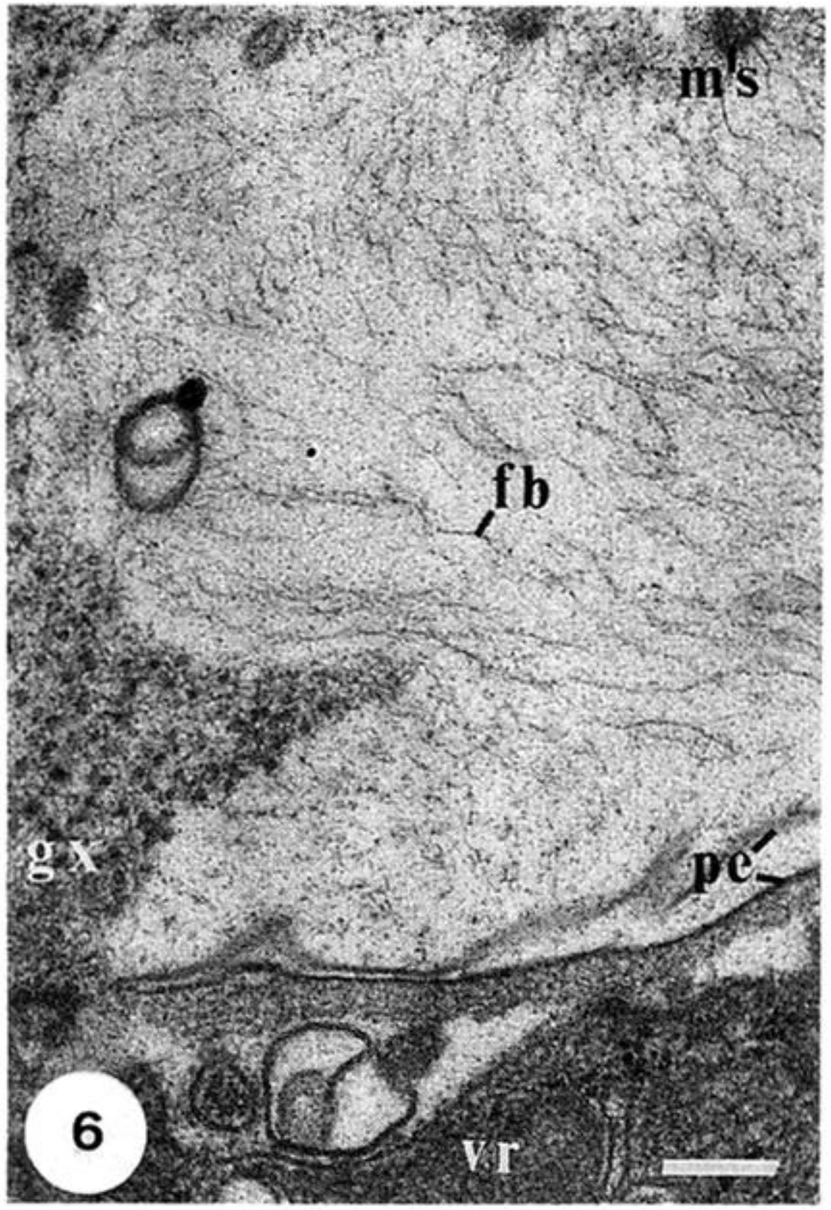

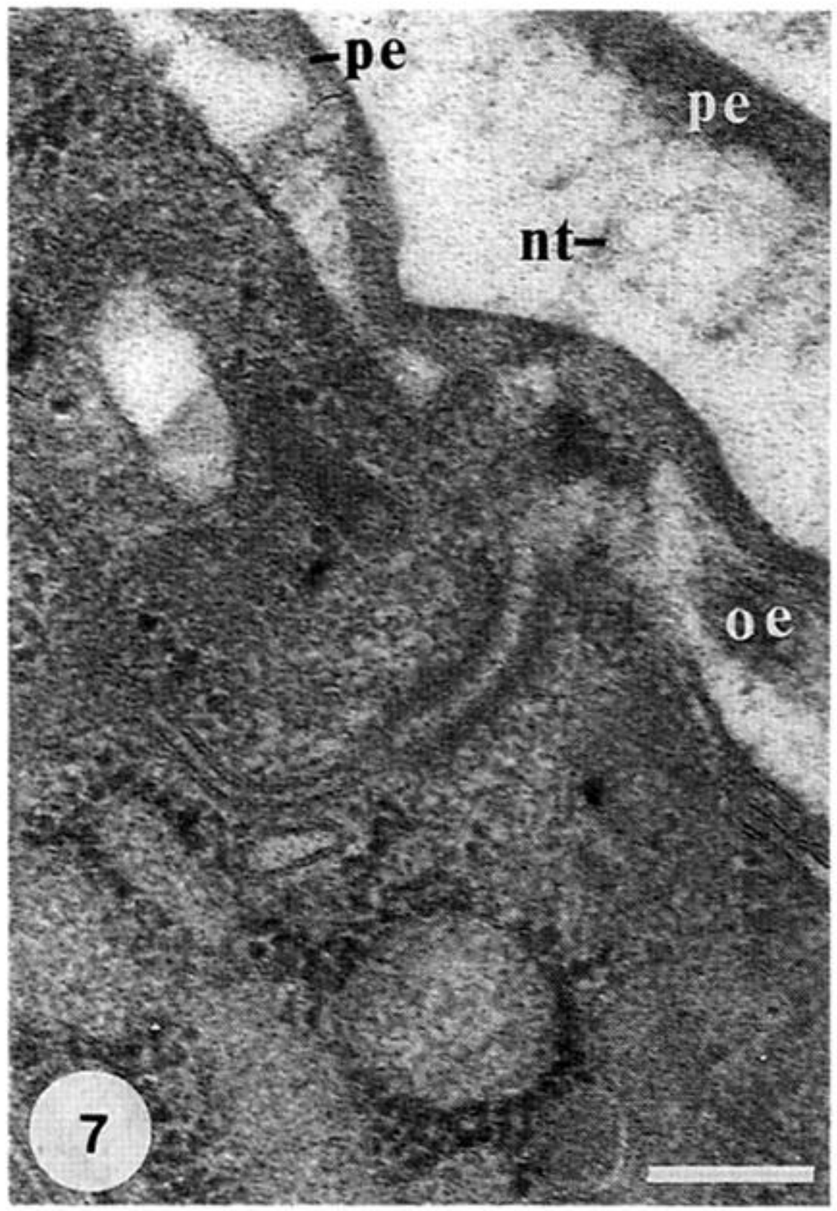

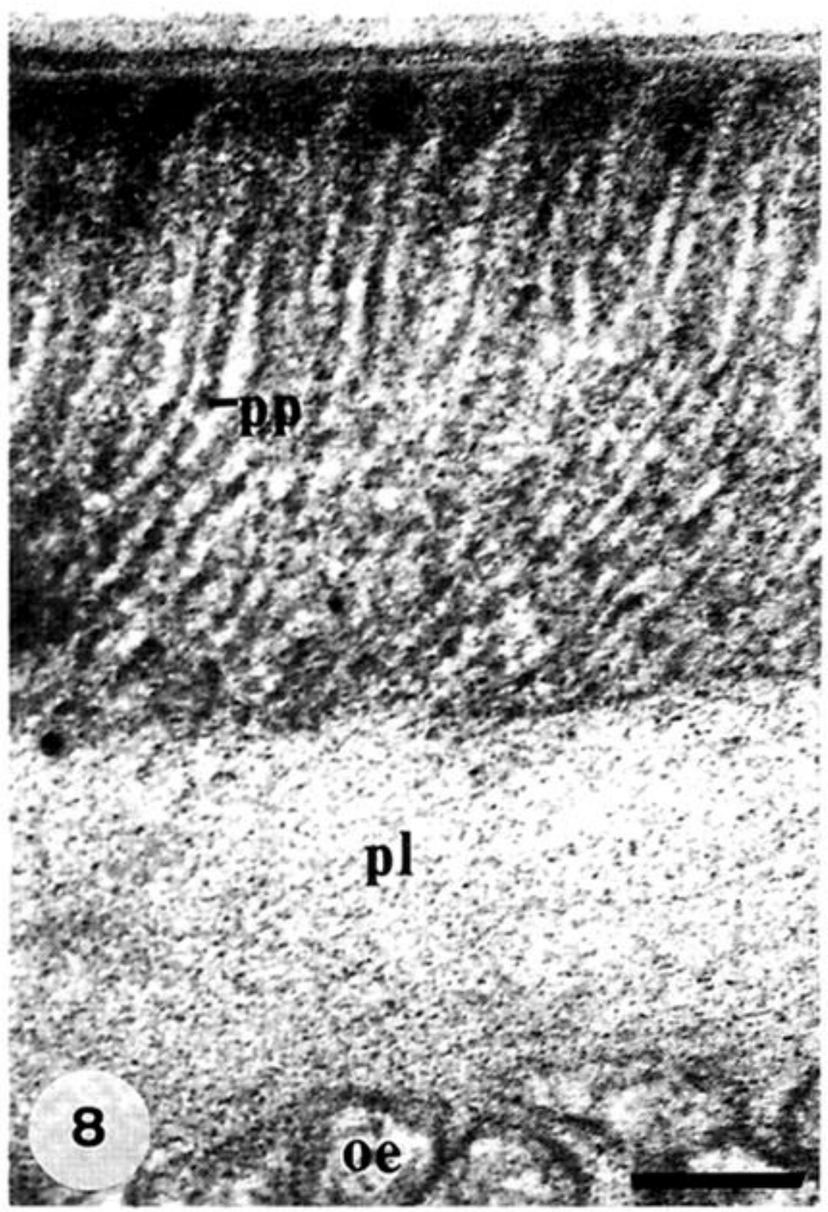

Figures 6–8. Transmission electron micrographs of sections of demineralized margins of valves of *Lingula reevii* to show the structure of the periostracum.

Figure 6. Origin of the pellicle (pe) in relation to the fibrils (fb) of the microvilli (ms) of the inner epithelium, glycocalyx (gx) and the first formed part of the periostracum underlain by vesicular cells (vr). Scale bar = 100 nm.

Figure 7. Detail of the pellicle (pe) with a network of fibrils and particles (nt) between the microvilli of inner epithelium (top right-hand corner) and the apical region of vesicular cells with finger-like protrusions (oe). Scale bar = 100 nm.

Figure 8. Detail of periostracum showing the strings of particles (pp) within electron-dense walls of the close-packed tubes, underlain by primary layer composed of GAGs (pl) and the cylindroid protrusions of the apical plasmalemma of outer epithelium (oe); the sigmoidal flexture of the walls indicates a stress couple inducing a dextral drag. Scale bar = 100 nm.

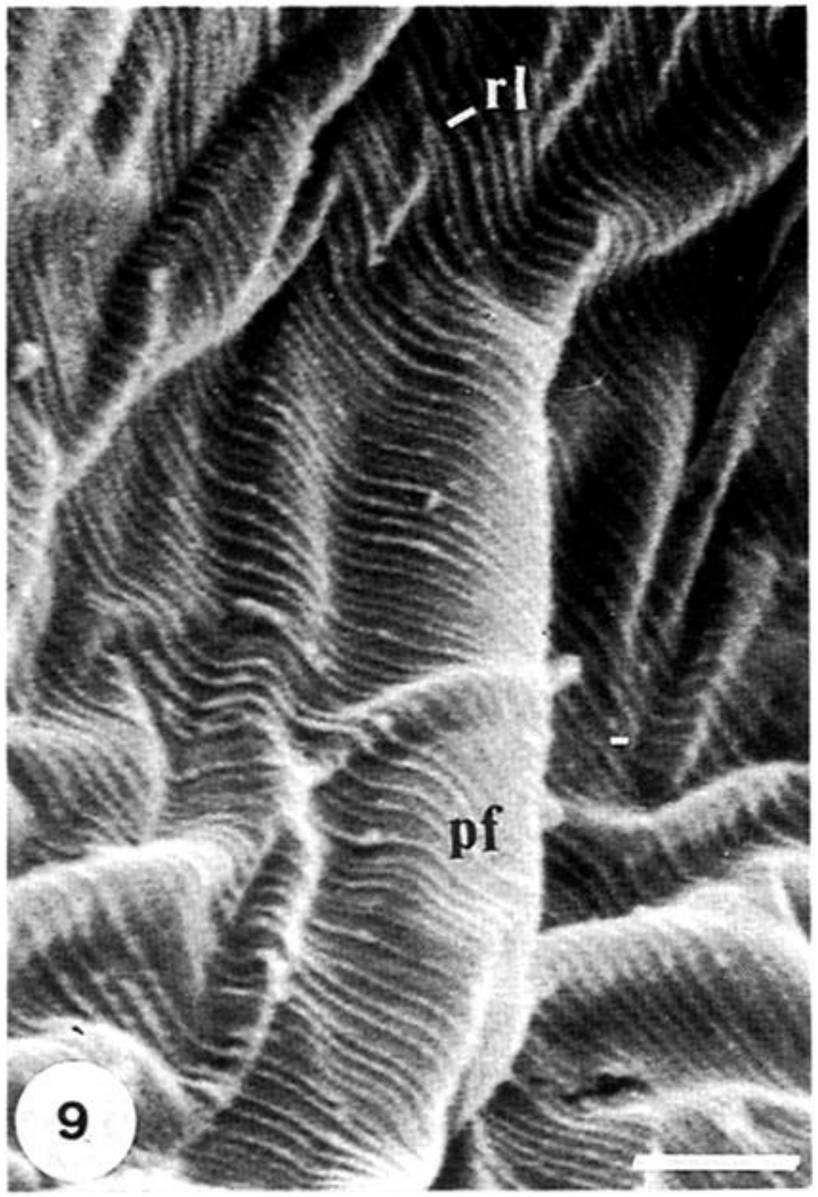

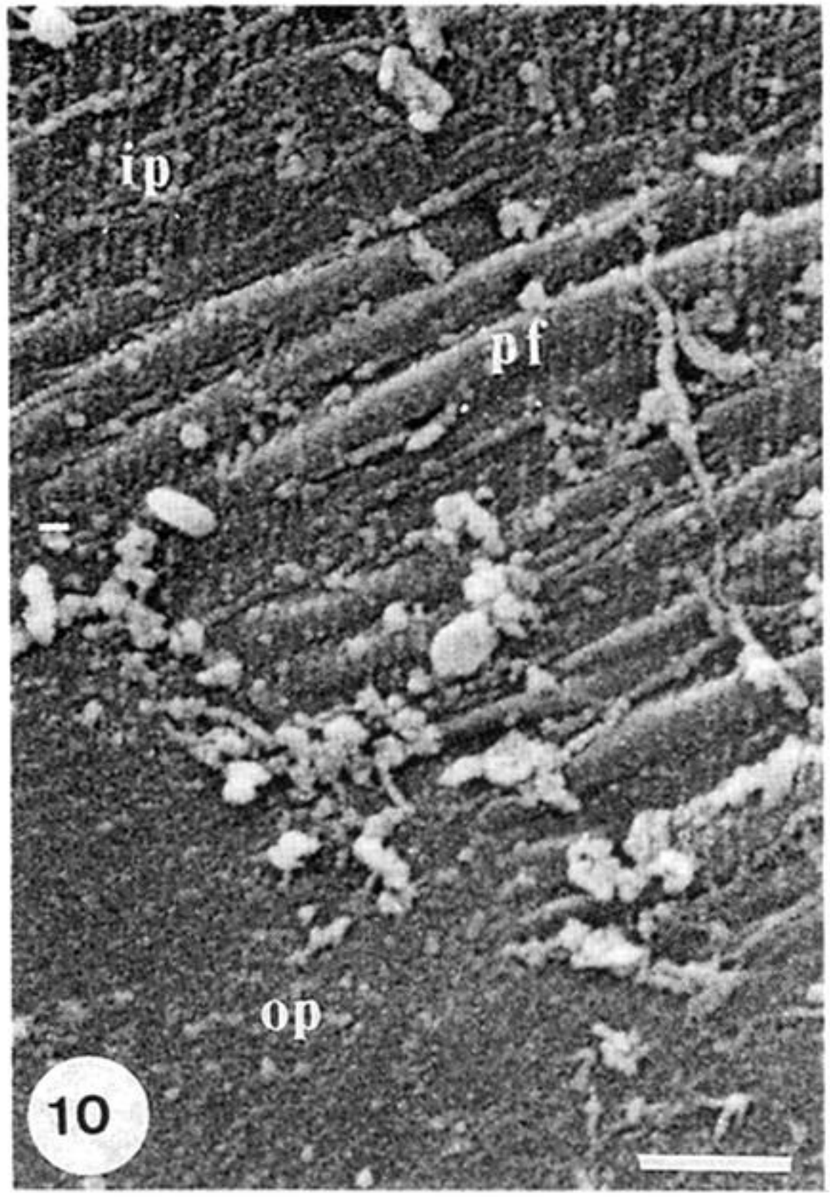

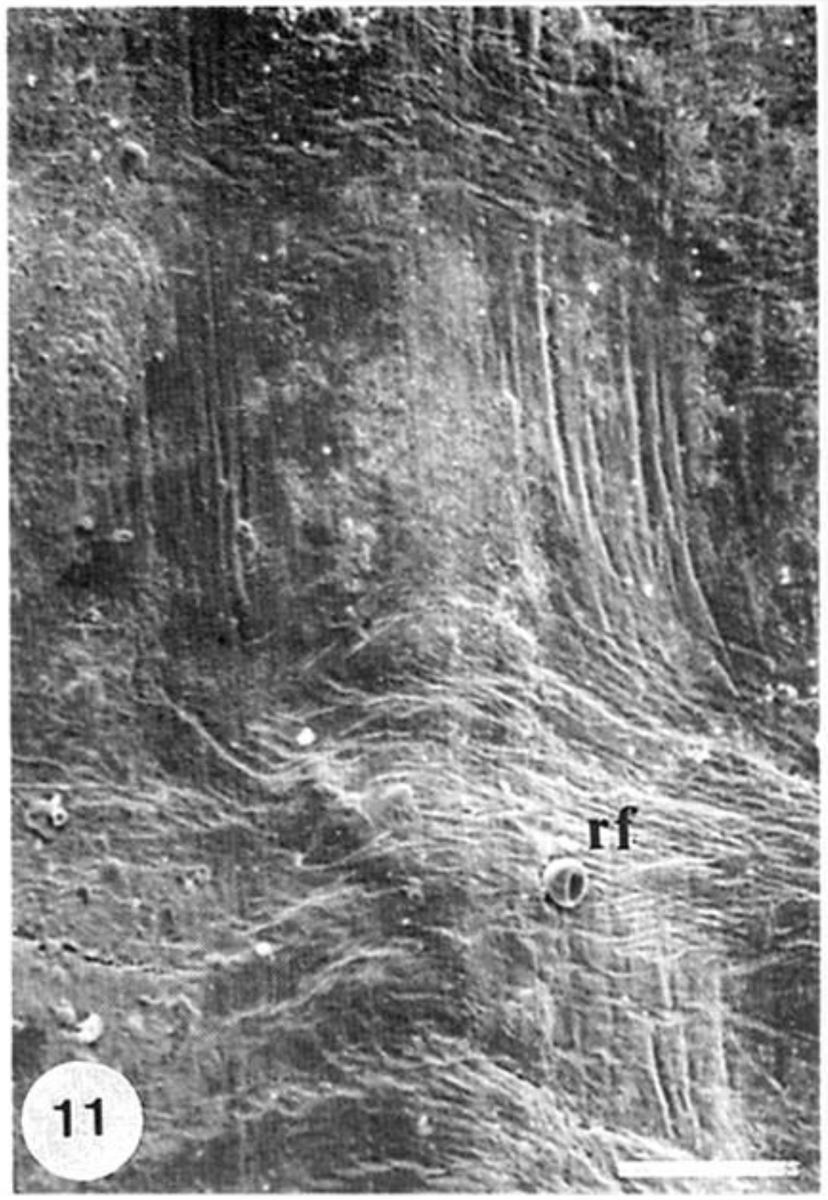

Figures 9–11. Scanning electron micrographs of gold-coated periostracal sufaces of critical point dried valves of *Lingula anatina*.

Figure 9. View of periostracum immediately distal of the periostracal groove, folded into two sets of periclines with the dominant set (pf) concentric with the groove, and ornamented by radial lineations (rl) on the inner membrane of the pellicle. Scale bar = 1 μm.

Figure 10. View of partly exfoliated inner surface of the marginal fold, showing the outer (op) and inner, lineated (ip) membranes of the pellicle with the underlying periostracum folded into impersistent periclines (pf). Scale bar = 2 μm.

Figure 11. General view of the outer side of the marginal fold showing sets of radial folds (rf) splaying towards the valve margin to the left and affecting the periostracum and underlying primary layer. Scale bar = 50 μm.

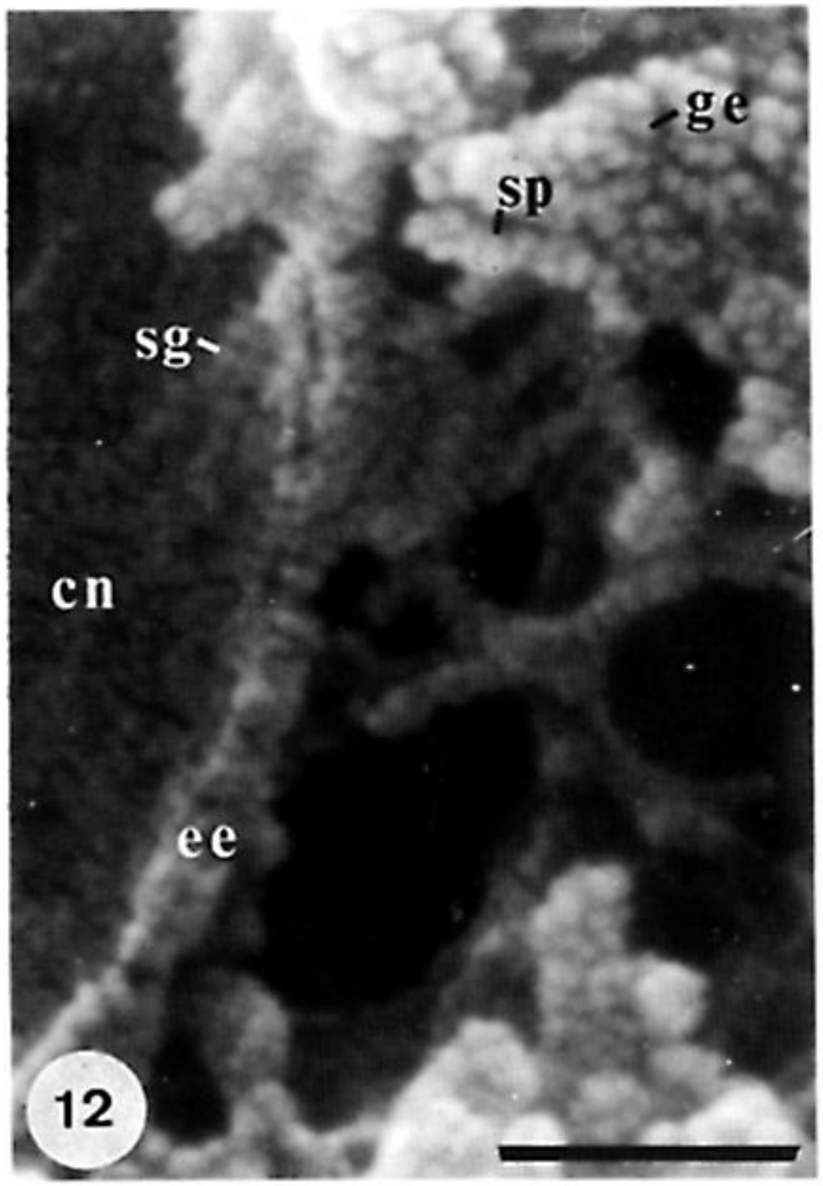

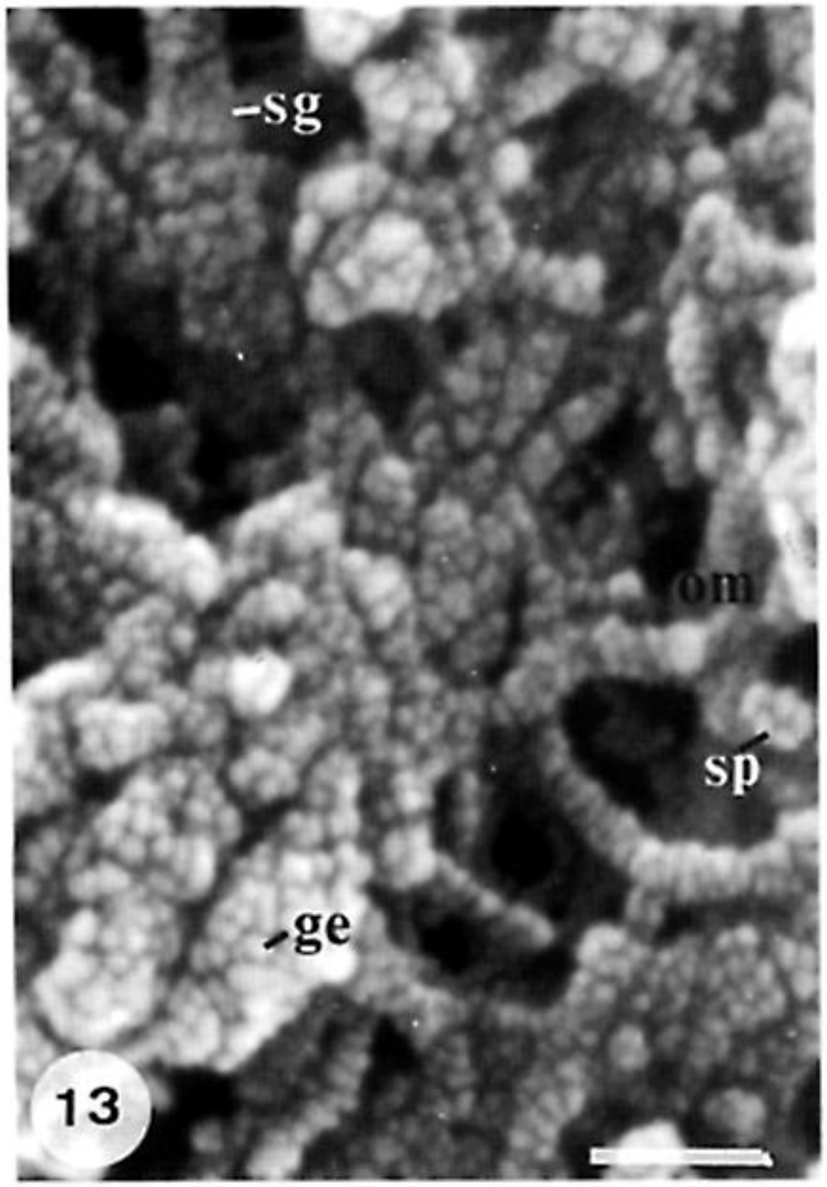

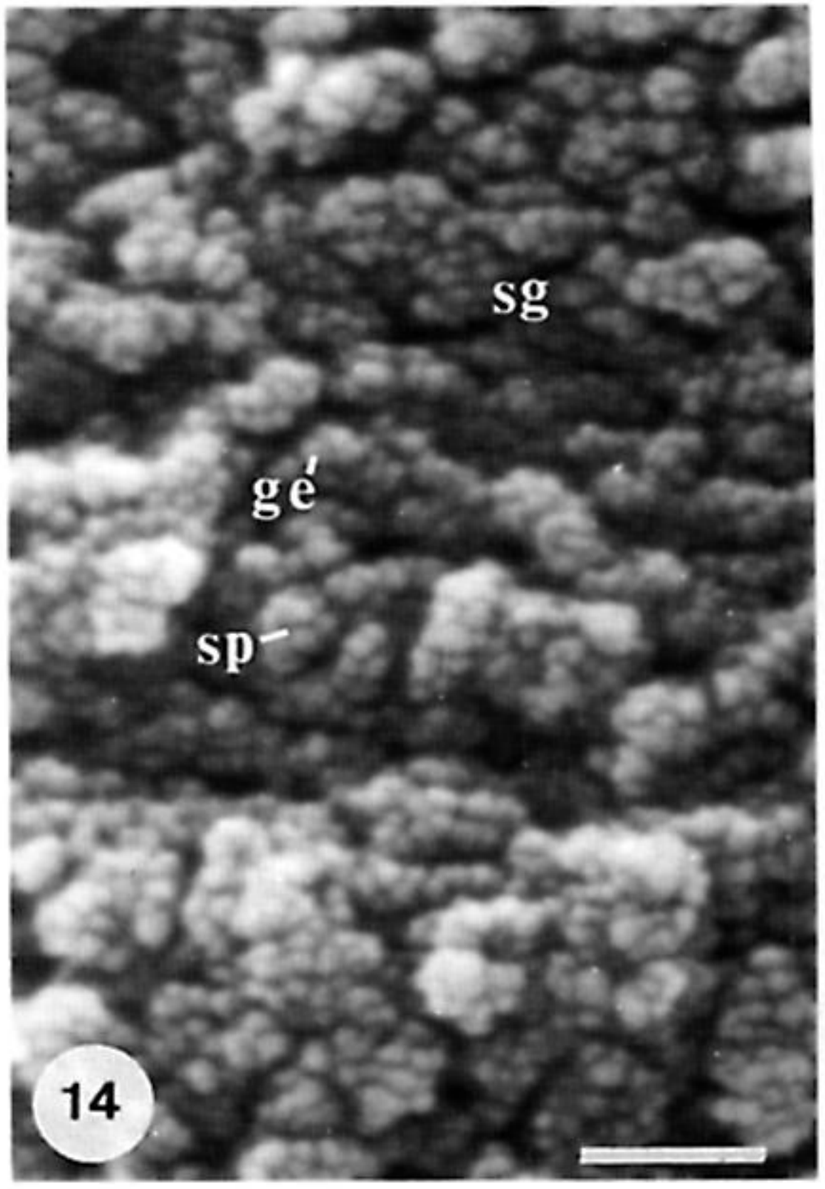

Figure 12–14. Scanning electron micrographs of gold/palladium-coated transverse, vertical fracture sections of the mid-part of a valve of *Lingula anatina* digested in subtilisin.

Figure 12. Internal surface and edge (ee) of the membranous lining of a canal (cn) showing the gold/palladium grains (sg) and the granules (ge) and spherules (sp) of apatitic botryoids on an organic framework linked with the canals. Scale bar = 50 nm.

Figure 13. Botryoids and mosaics on an organic framework (om) showing spherules (sp), granules, (ge) and gold/palladium grains (sg). Scale bar = 50 nm.

Figure 14. Close-packed spheroidal aggregates of apatite forming a compact lamina with gold/palladium grains (sg), granules (ge) and spherules (sp). Scale bar = 50 nm.

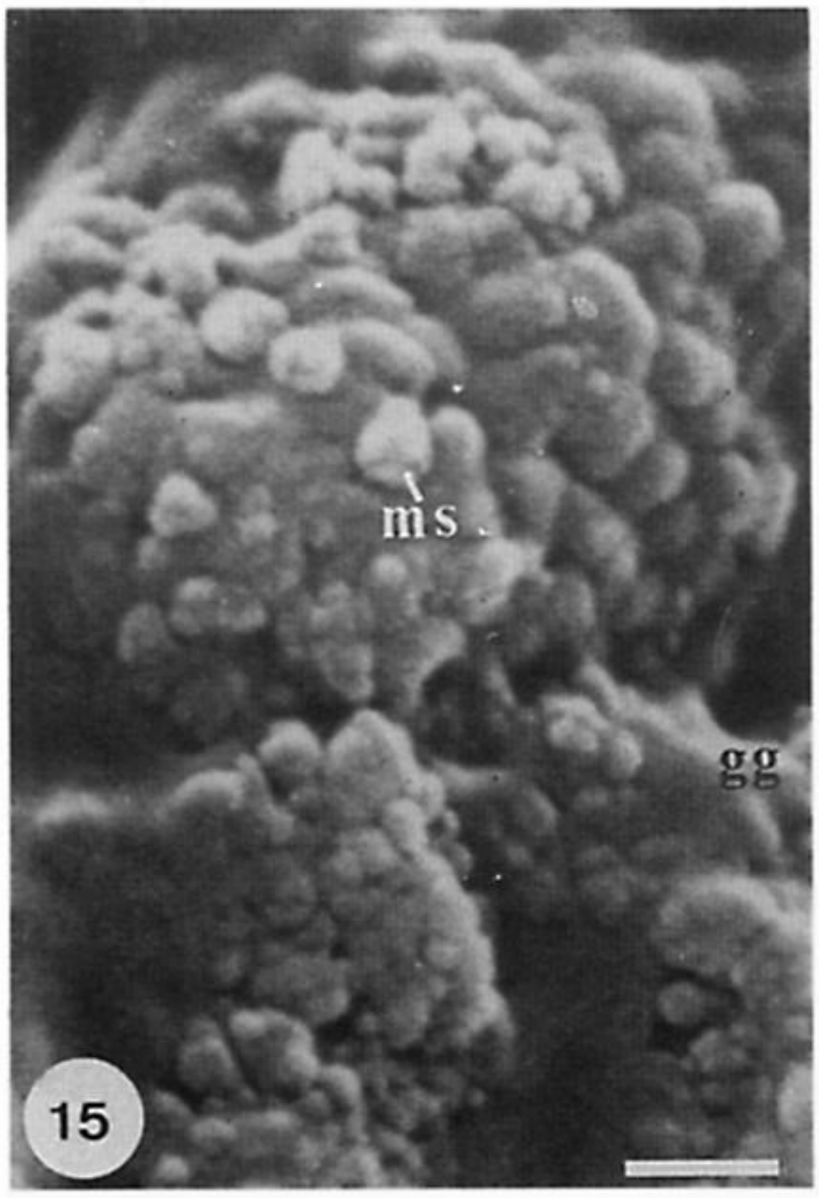

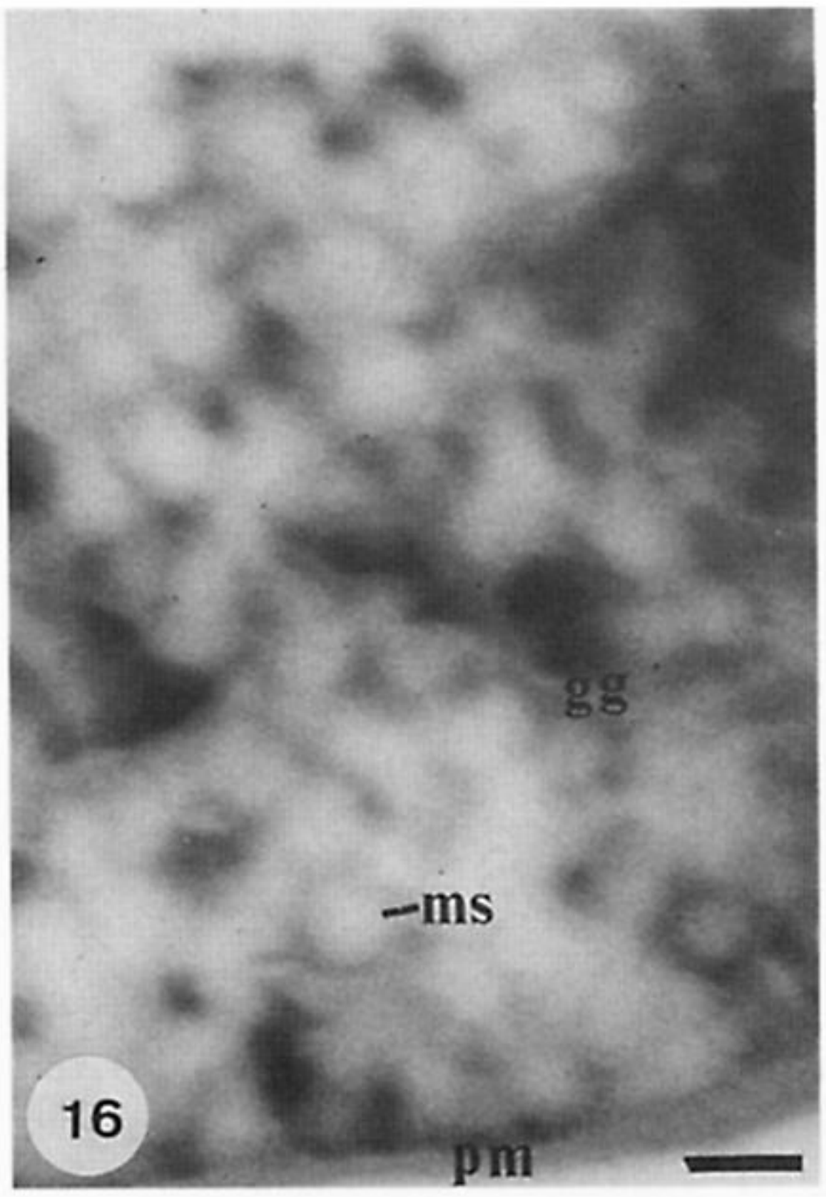

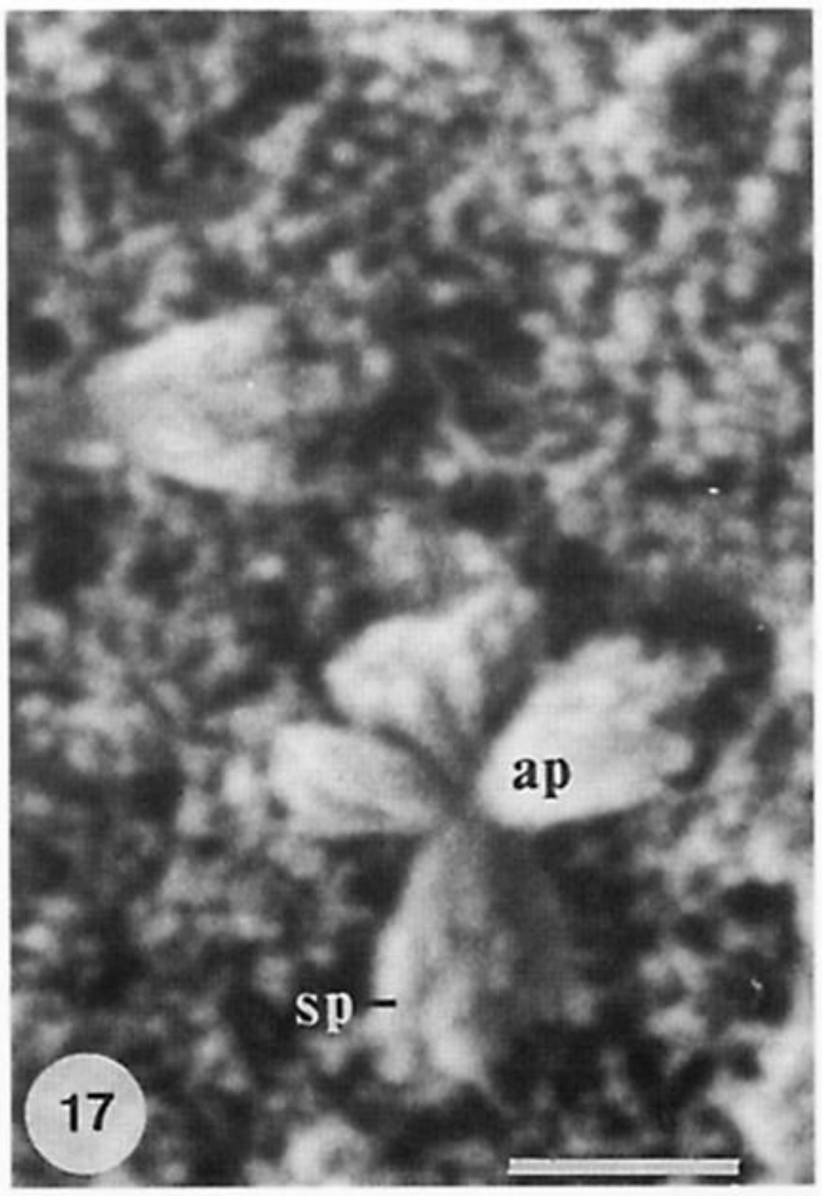

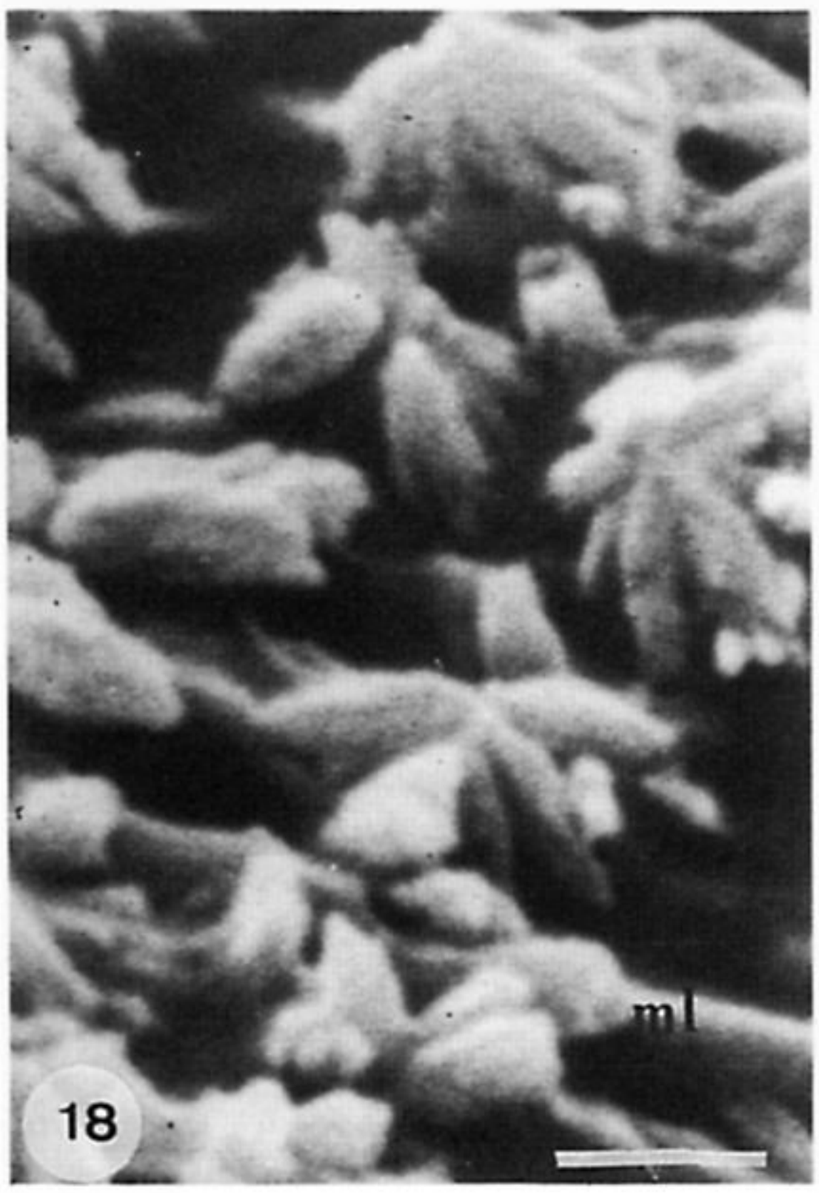

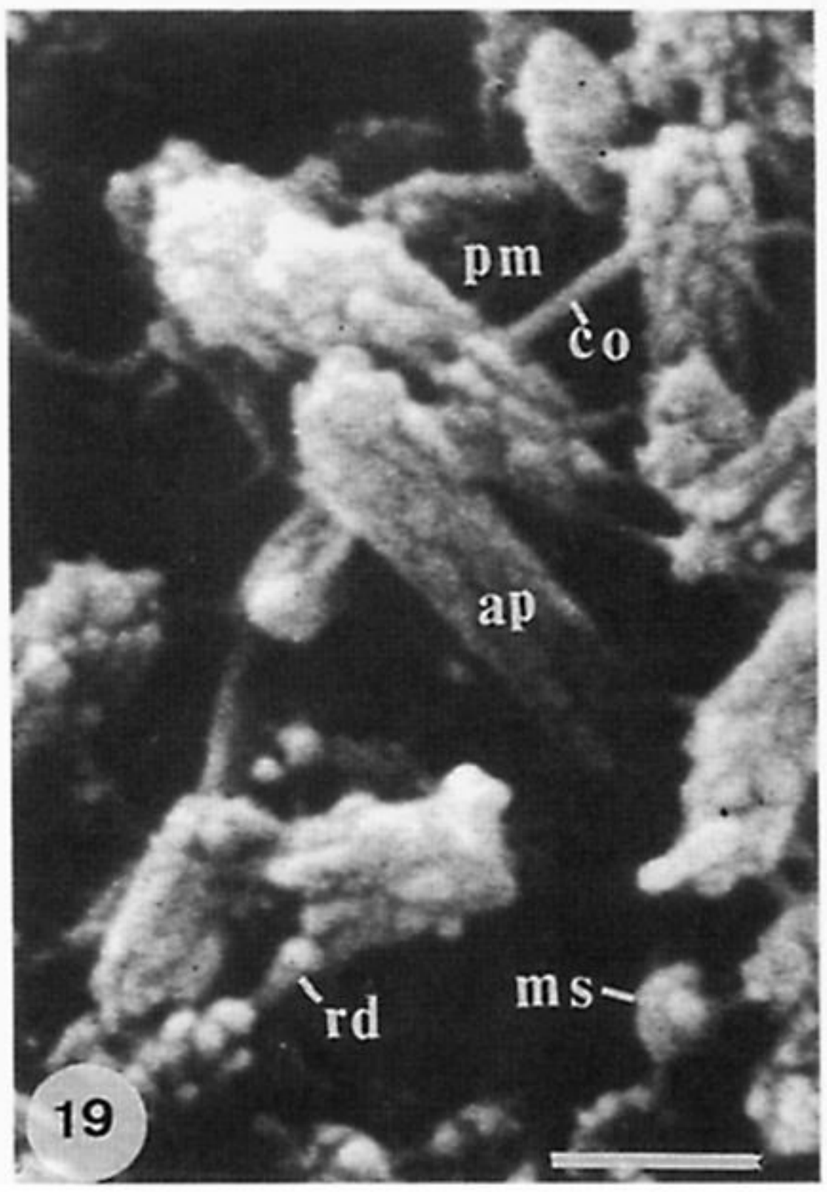

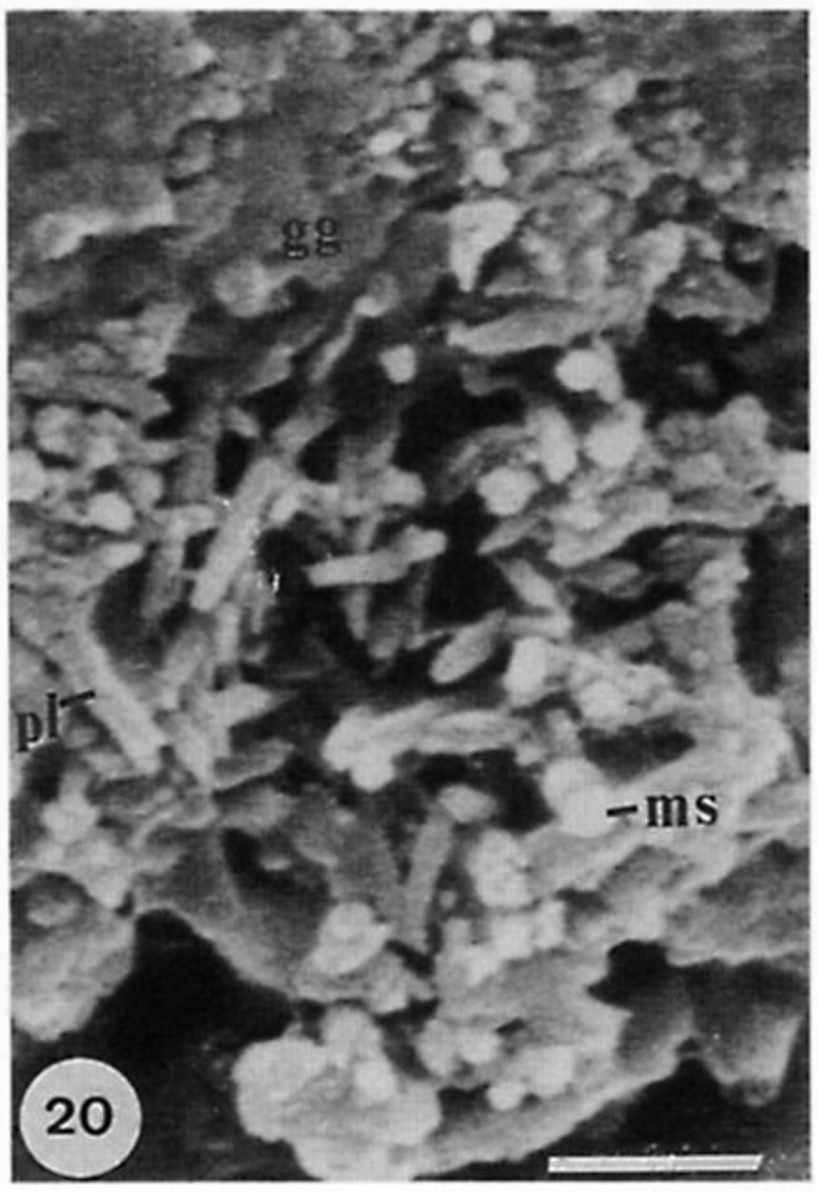

Figures 15–20. Scanning electron micrographs of gold-coated and carbon-coated (figure 16) vertical sections of valves of *Lingula anatina*.

Figure 15. Botryoidal aggregate of apatitic mosaics (ms) in a matrix of GAGs (gg) exposed in a posteromedian section of a valve treated with phosphate buffer (100 mM, pH 7). Scale bar = 0.5 μm.

Figure 16. Back scattered electron scan showing the apatitic composition of botryoids consisting of mosaics (ms) in GAGs (gg) and capped by a chitinoproteinaceous membrane (pm). Scale bar = 1 μm.

Figure 17. A split dome of apatite (in a matrix of spherular apatite and GAGs) showing the spherular texture (sp) of wedge-shaped plates (ap) exposed in a posteromedian section of a valve treated with Tris buffer (80 mM, pH 8) with $CaCl_2$ (100 mM). Scale bar = 0.5 μm.

Figures 18, 19. Mosaics (ms), plates (ap) and rods (rd) of apatite exposed in association with collagenous fibrils (co) and membranes (pm) and with membranous laminae (ml) in a submedian section of a valve digested in subtilisin. Scale bars = 0.5 μm.

Figure 20. Plates (ap) and mosaics (ms) of apatite exposed after the removal of most of the GAGs (gg) filling a chamber in a posteromedian section of a valve digested in subtilisin. Scale bar = 1 μm.

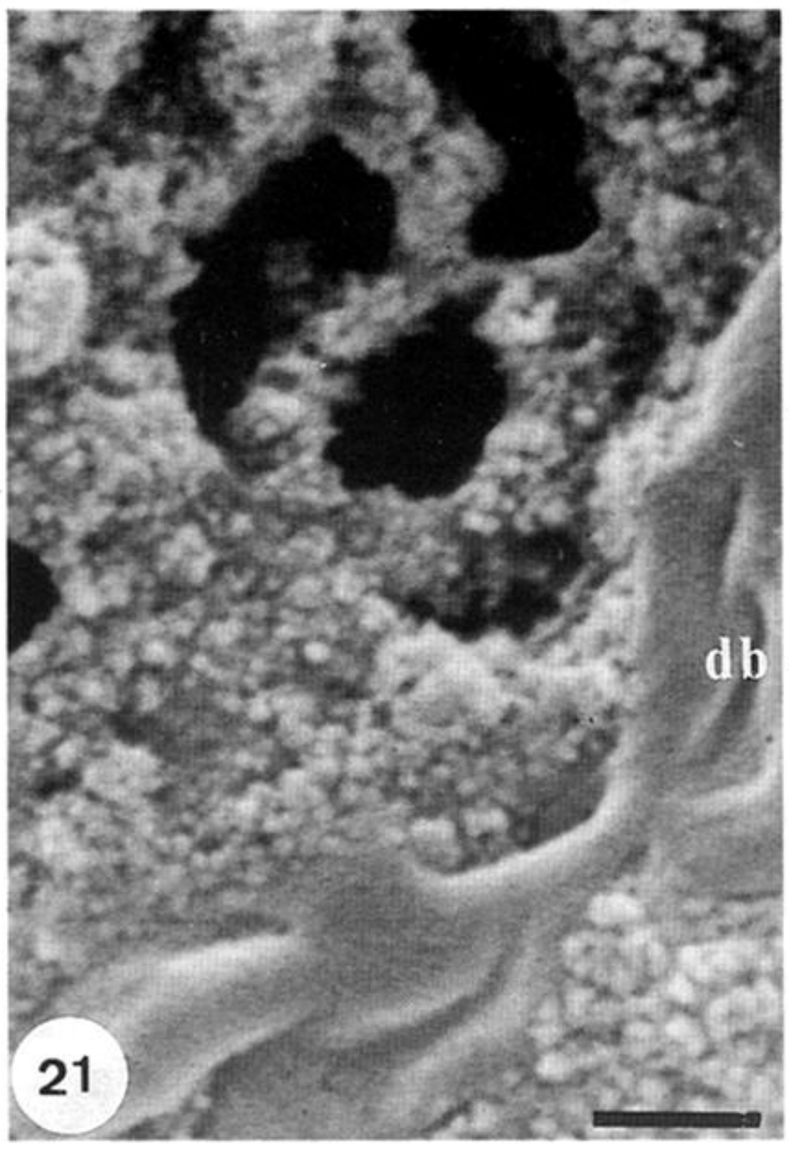

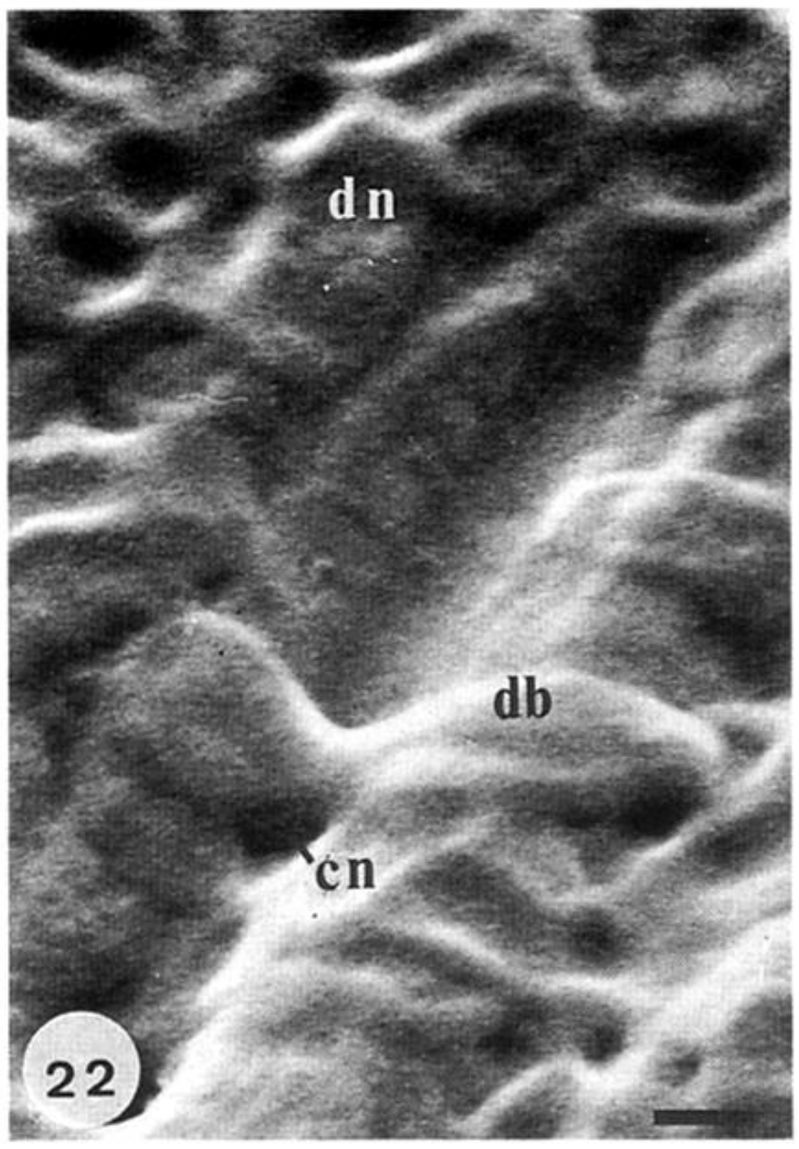

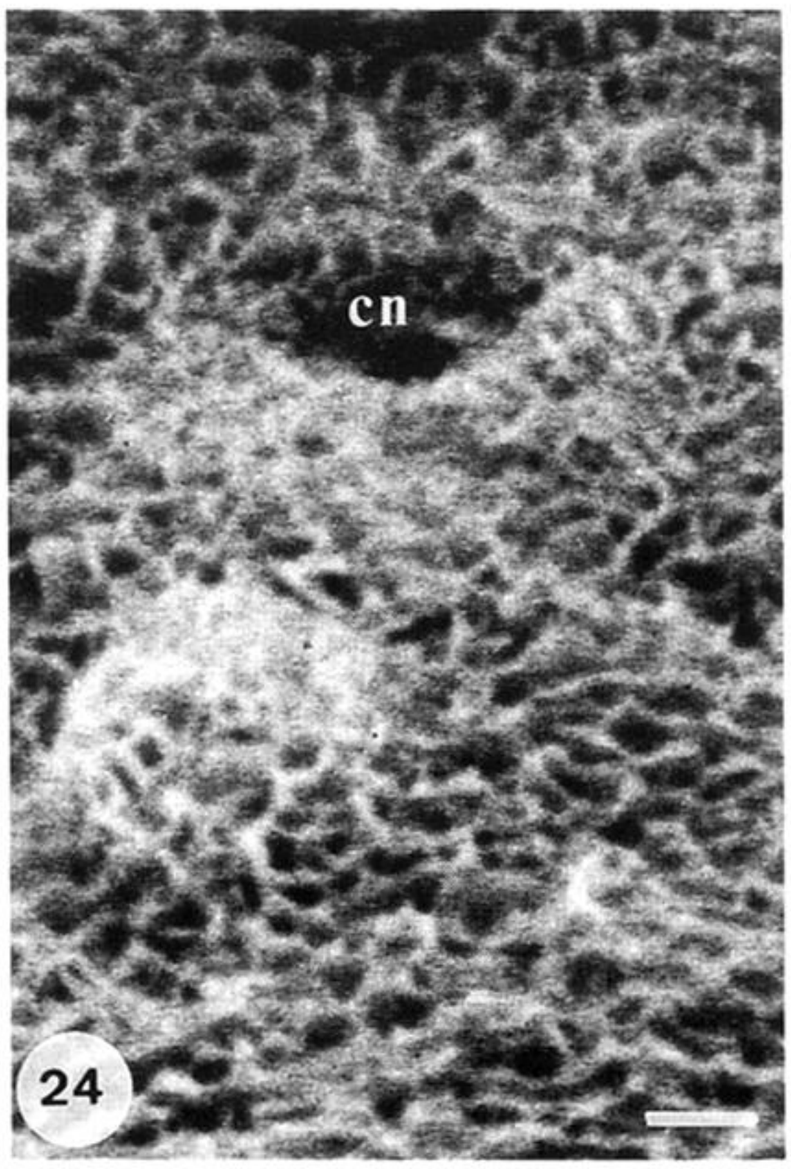

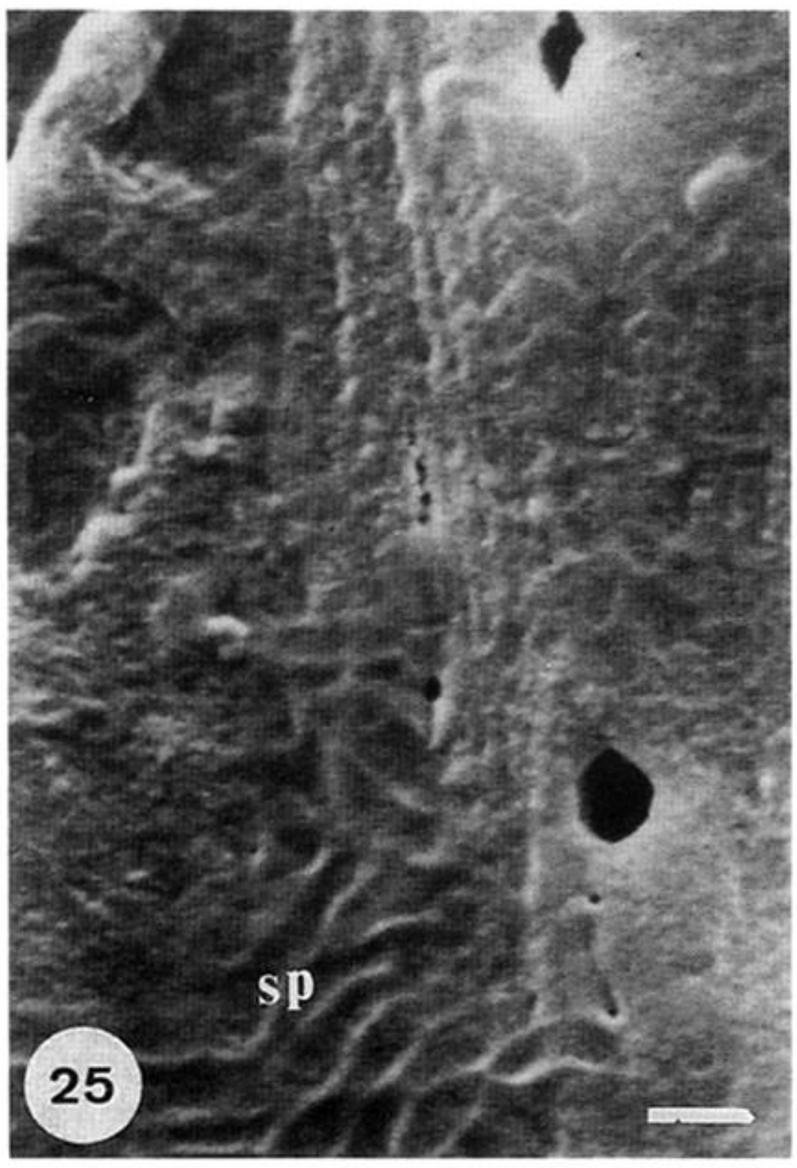

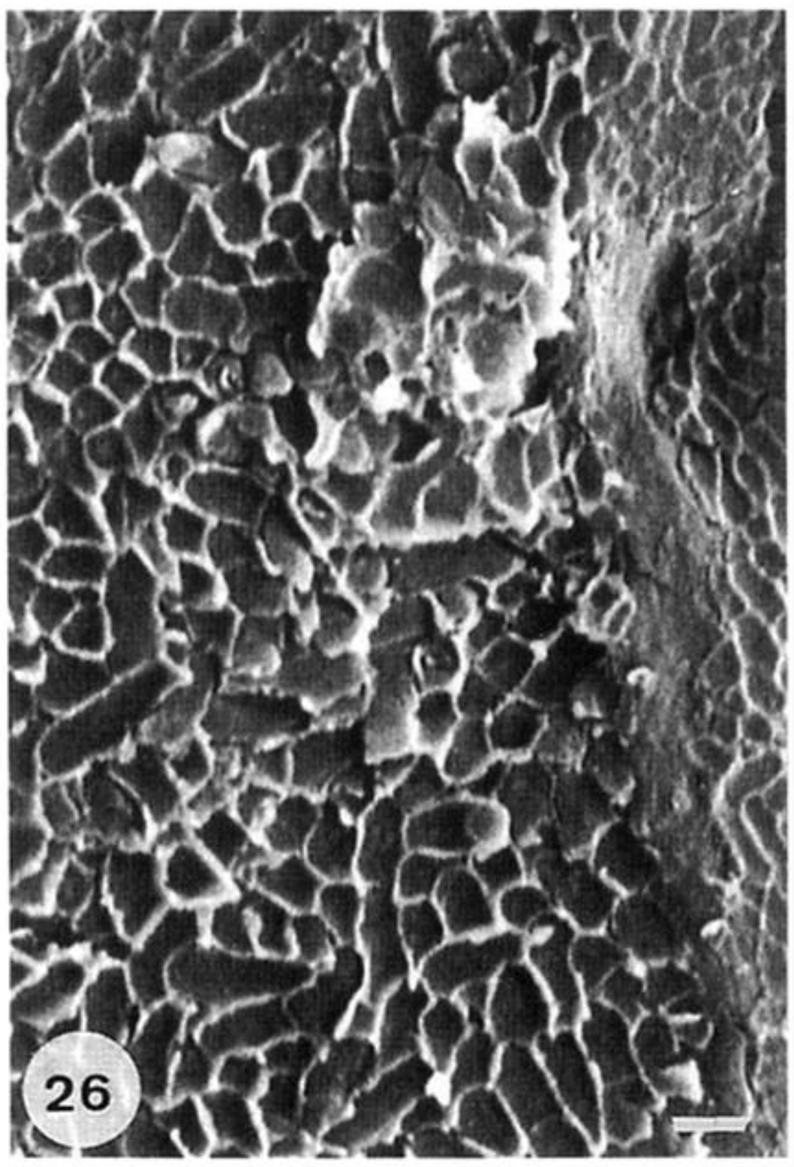

Figures 21–26. Scanning electron micrographs of gold-coated surfaces of the shell of *Lingula anatina*.

Figure 21. Residual GAGs with remnants of discoidal bodies (db) on botryoidal apatite of the internal surface of the submedial part of a valve treated with 2% bleach (by volume). Scale bar = 0.5 µm.

Figure 22. Residual GAGs with contraction depressions (dn) and discoidal bodies (db) on anastomosing ridges of apatite with canal aperture (cn) on the internal surface of the anterolateral part of a valve digested in proteinase-K. Scale bar = 0.5 µm.

Figure 23. GAGs exposed in a cut, vertical, anteromedian section of a valve digested in proteinase-K, with tension cracks and orthogonal slots of dehydration. Scale bar = 0.5 µm.

Figure 24. GAGS indented by close-packed, hemispherical hollows presumably impressed by apatitic mosaics of succeeding compact lamina, exposed on an inner facing surface with canal aperture (cn) in a cut, vertical section of a valve treated with phosphate (100 mM, pH 7) and Tris buffers (80 mM, pH 8) with $CaCl_2$ (100 mM). Scale = 0.5 µm.

Figure 25. A residual film of GAGs, indented by casts of secreting plamalemma (sp) and overlying a chitinoproteinaceous surface with a scatter of apatitic mosaics between two canal apertures, on the internal surface of the anterolateral part of a valve digested in proteinase-K. Scale bar = 1 µm.

Figure 26. A film of GAGs, indented by casts of the distal tips and sides of cylindroid protrusions of secreting plasmalemma exposed on an inward facing surface beneath a thin succession of laminae forming the internal surface of the posterolateral part of a valve treated with Tris buffer (80 mM, pH 8) with $CaCl_2$ (100 mM). Scale bar = 1 µm.

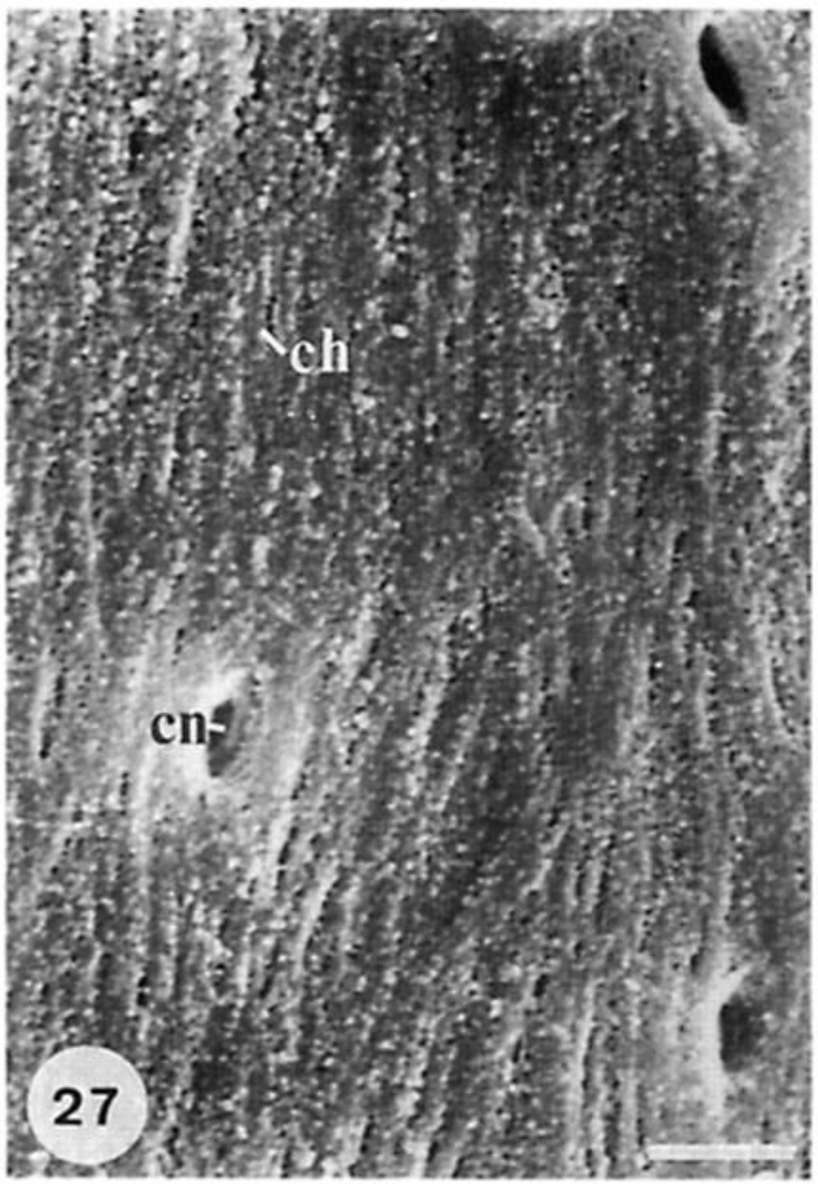

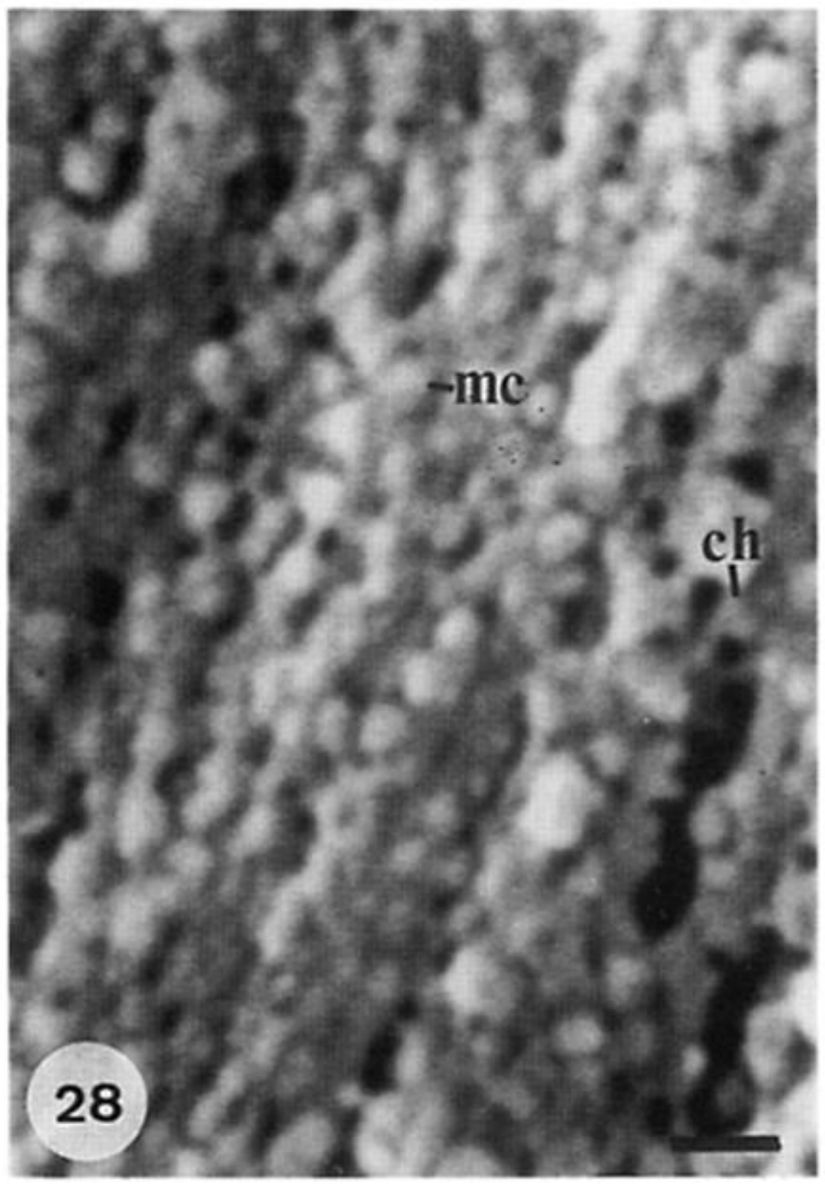

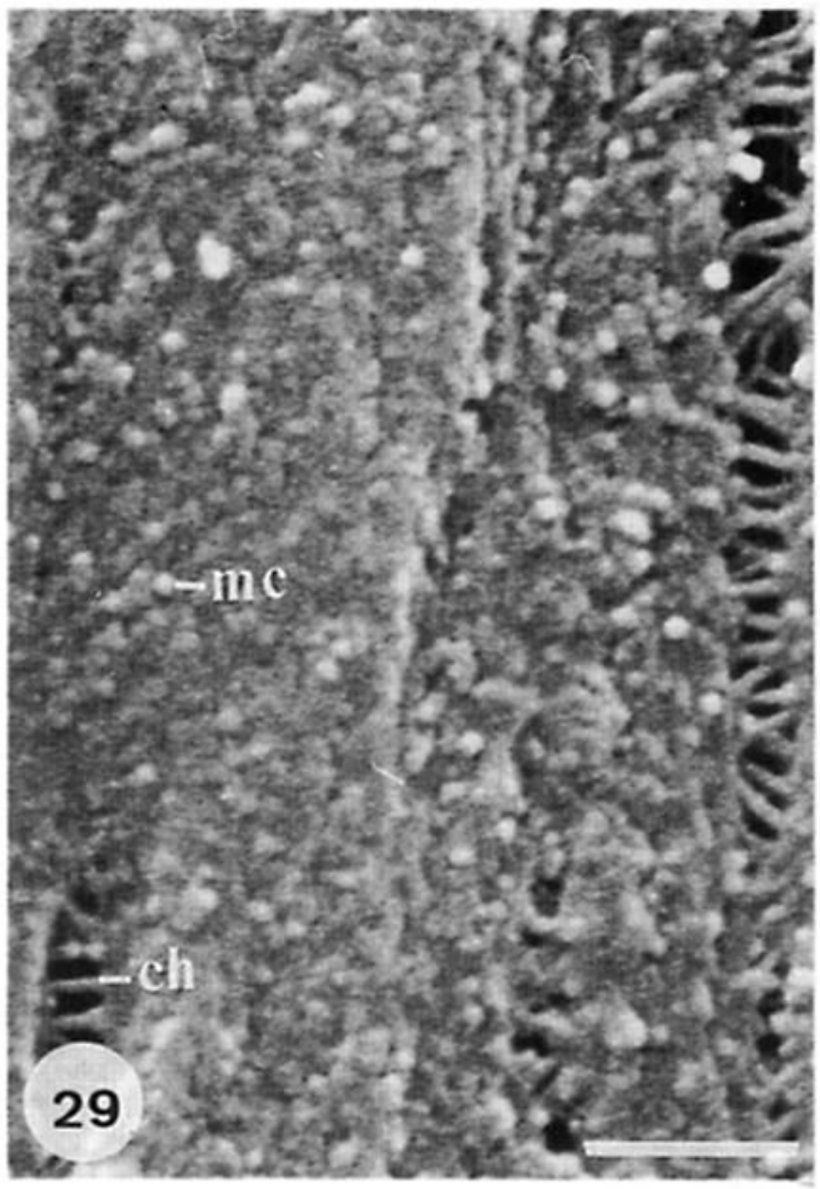

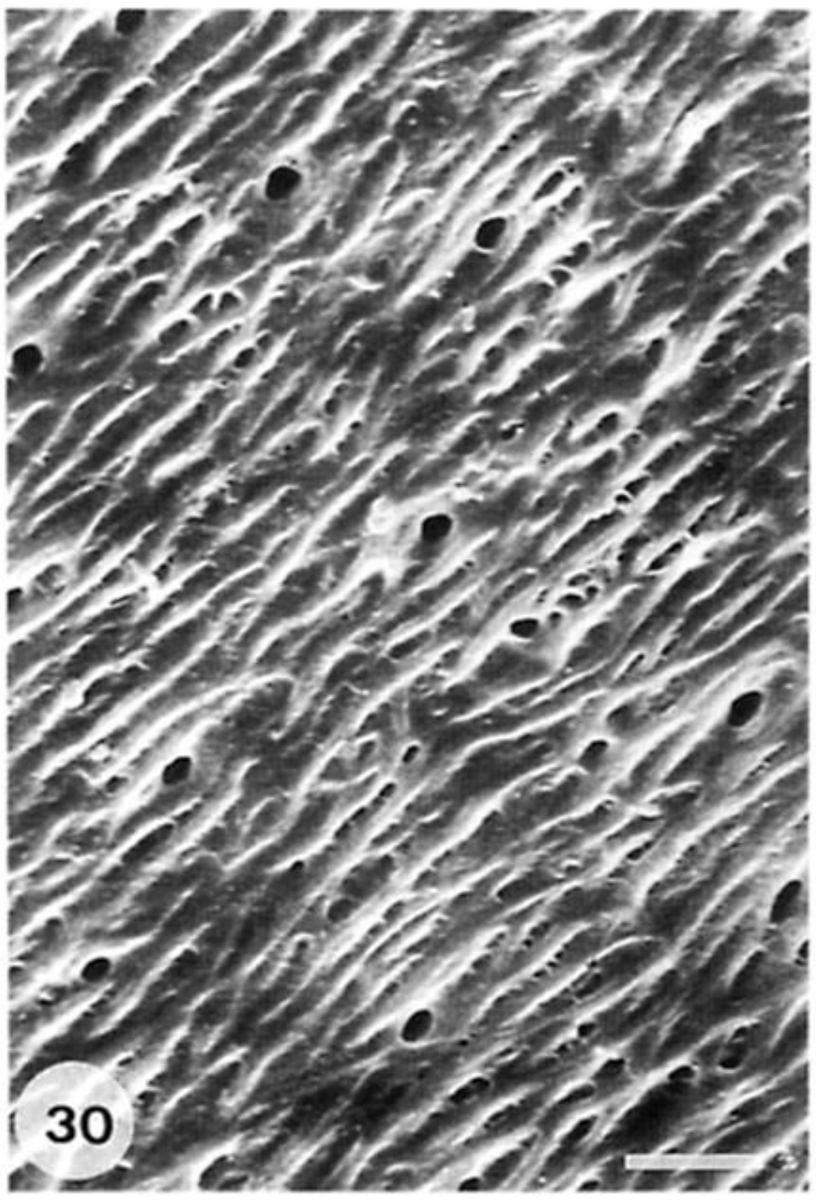

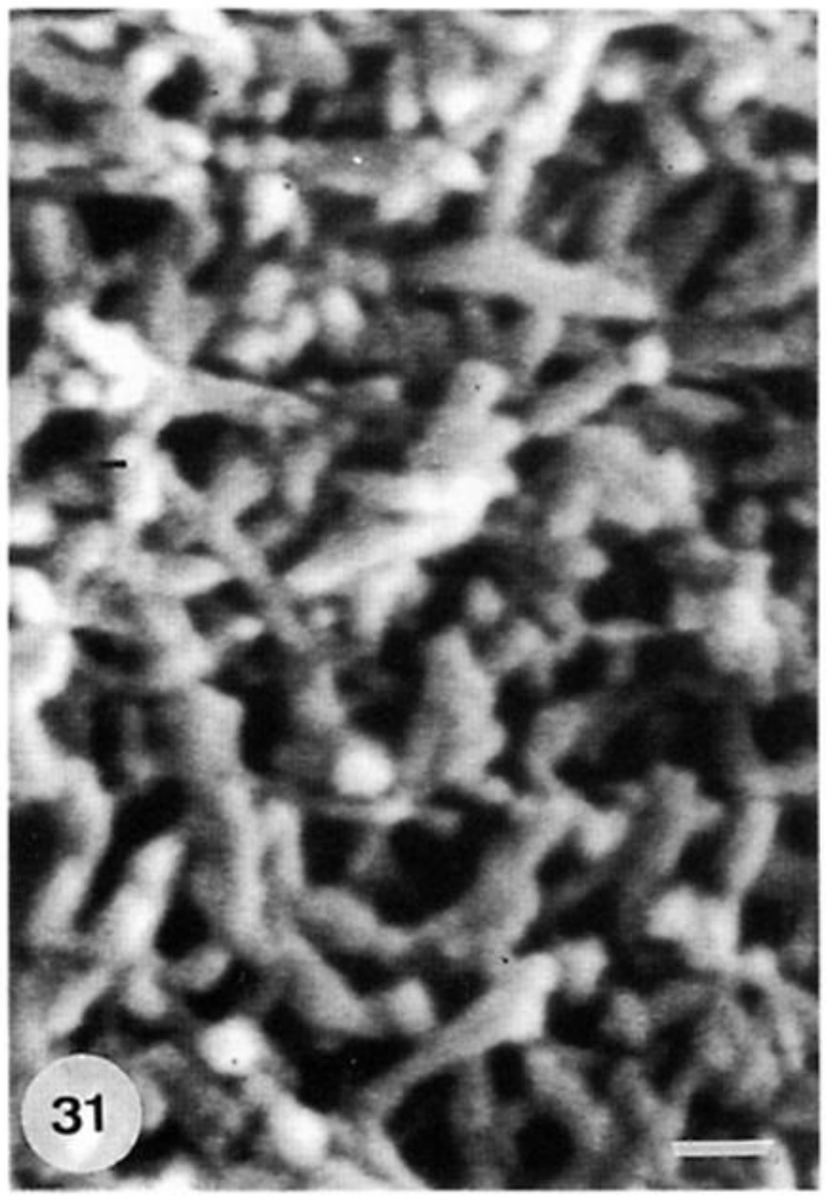

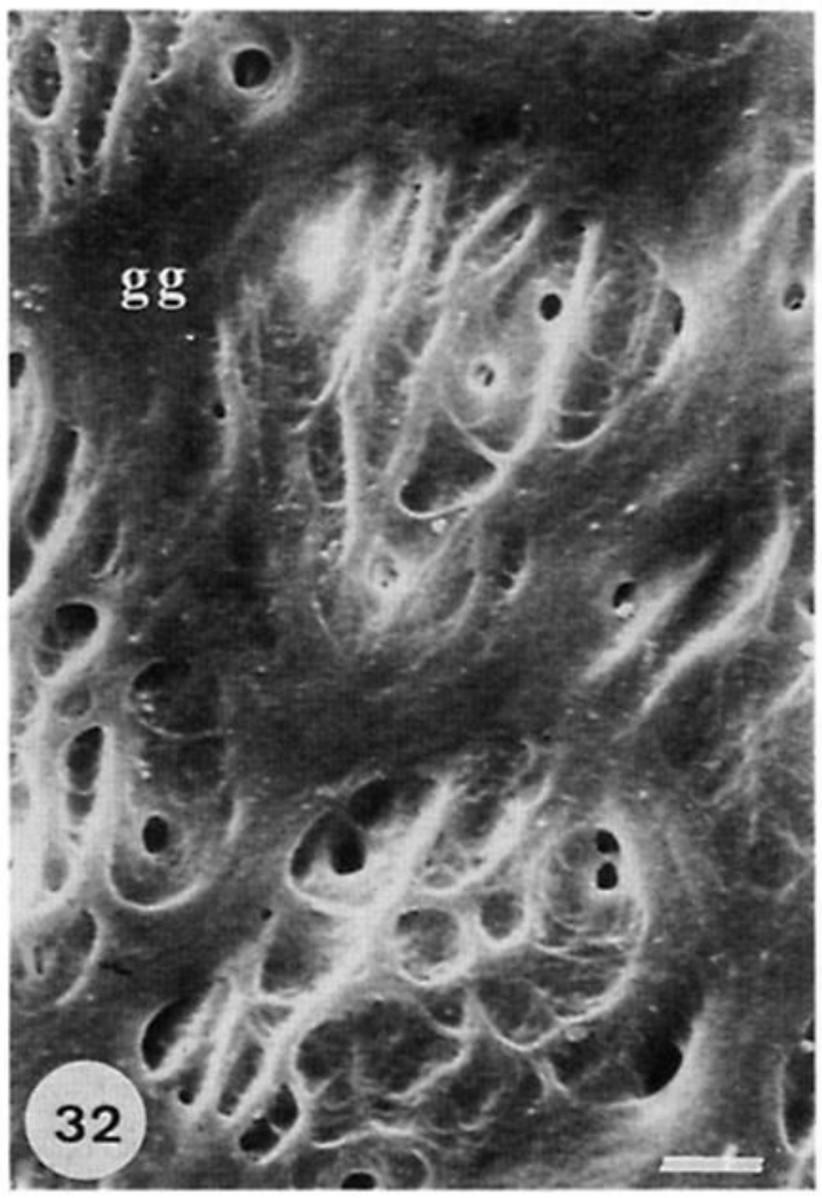

Figures 27–32. Scanning electron micrographs of gold-coated internal surfaces of the shell of *Lingula anatina*.

Figure 27. Gently flexured, lineated texture of the mid-part of a valve digested by subtilisin in a laminar flow cabinet, interpreted as consisting of chitinous fibres (ch) studded with apatitic mosaics, with canal apertures (cn) Scale bar = 2 μm.

Figure 28. Detail of the fibrous texture of figure 27, showing linear clusters of apatitic mosaics (mc) adhering to, and mainly obscuring, a network of chitin (ch). Scale bar = 200 nm.

Figure 29. Chitinous fibres (ch) coated with apatitic mosaics (mc), exposed in tension cracks in the mid-part of a valve digested in collagenase. Scale bar = 1 μm.

Figure 30. General view of anastomosing ridges exposed in the anterior part of the same valve featured in figure 27, also digested in subtilisin. Scale bar = 5 μm.

Figure 31. Short fibres treated with 5% bleach (by volume) and, therefore, probably chitin with some attached apatitic mosaics exposed in the anterolateral part of a valve. Scale bar = 200 nm.

Figure 32. General view of anastomosing ridges exposed in the posterolateral part of the same valve, featured in figure 27, and also digested in subtilisin but with enough GAGs (gg) surviving enzymic digestion to trace the outlines of outer epithelial cells. Scale bar = 2 μm.

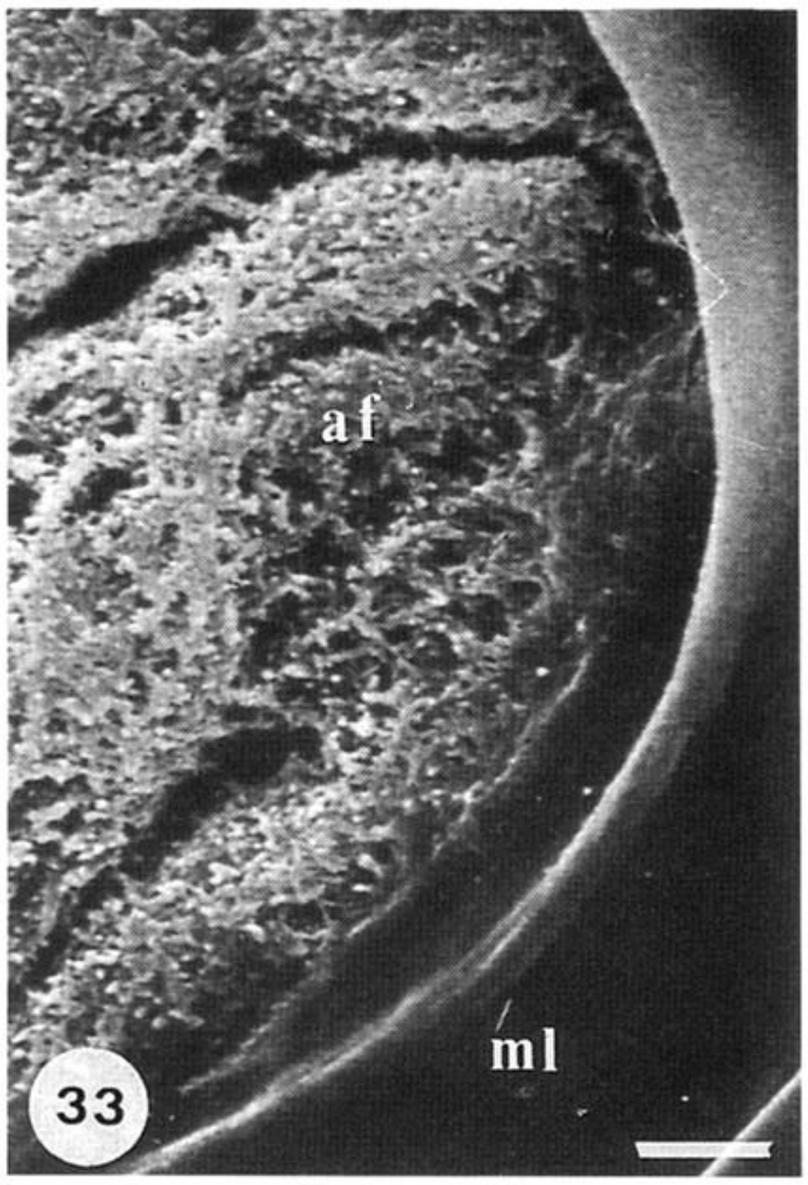

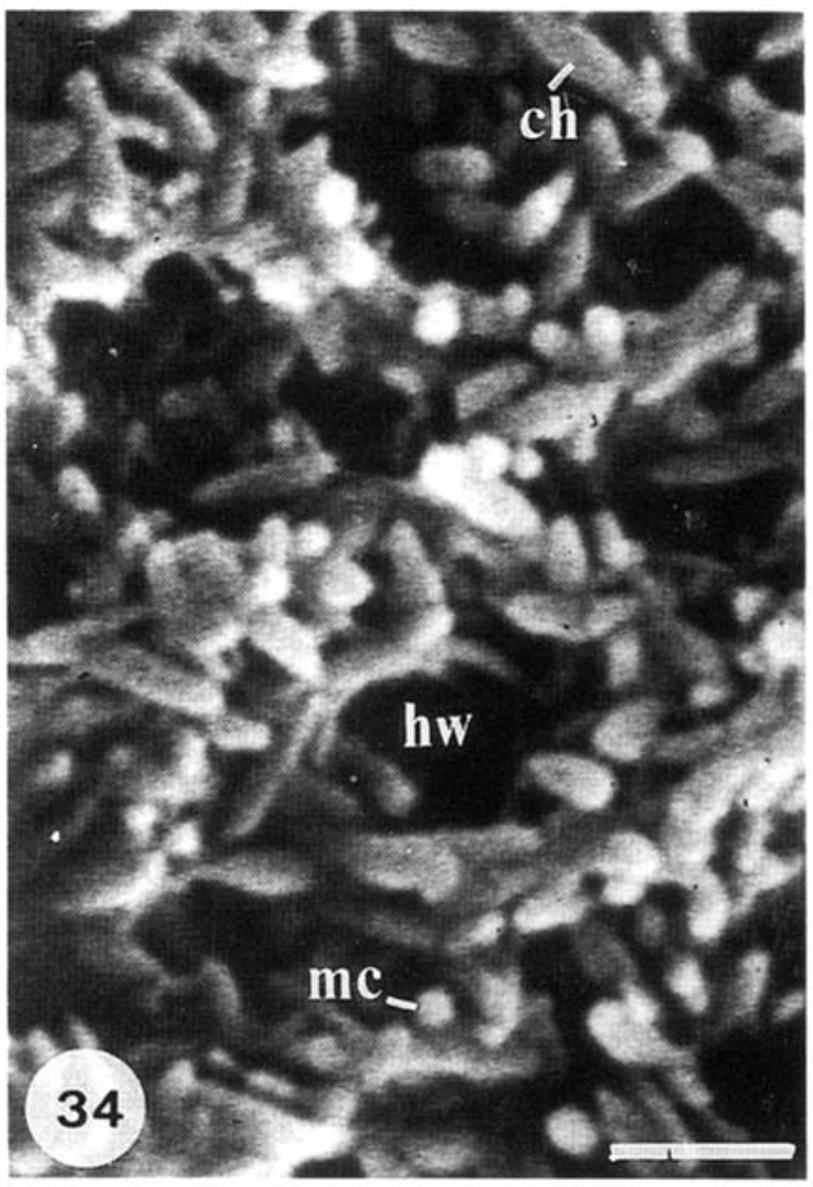

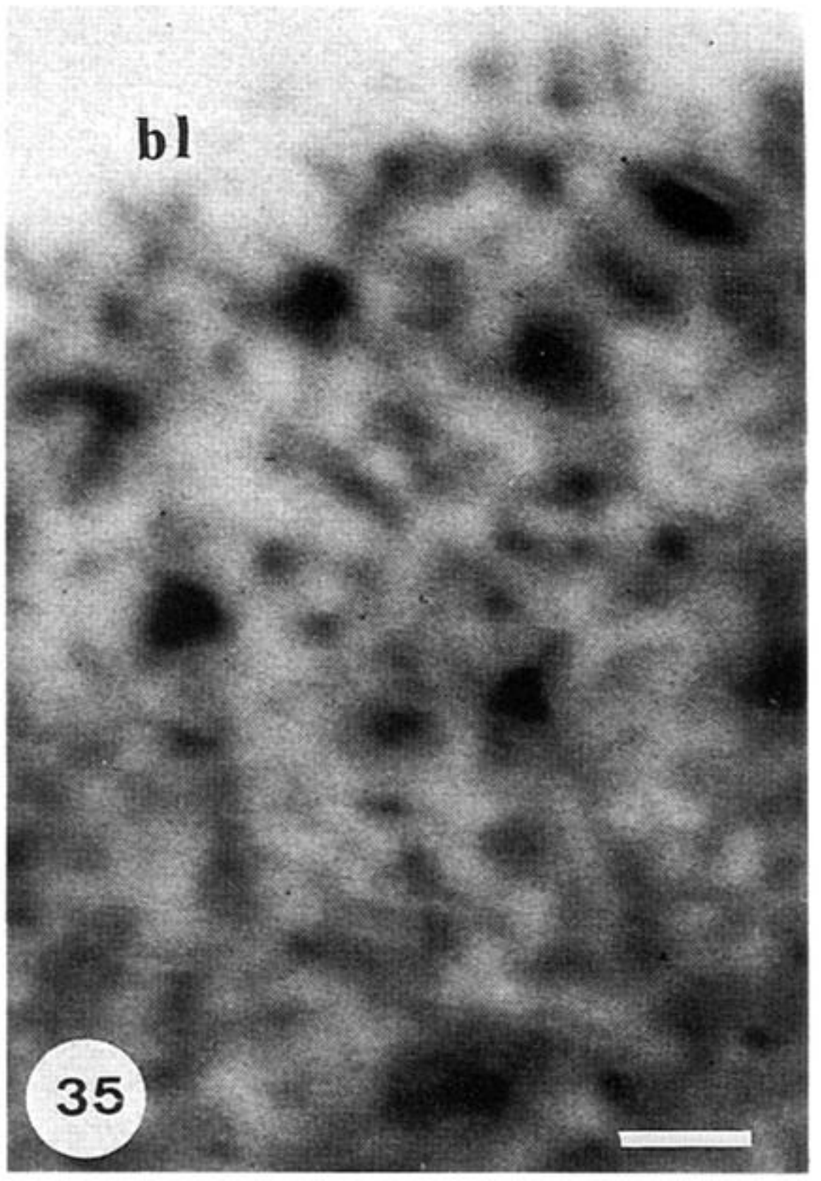

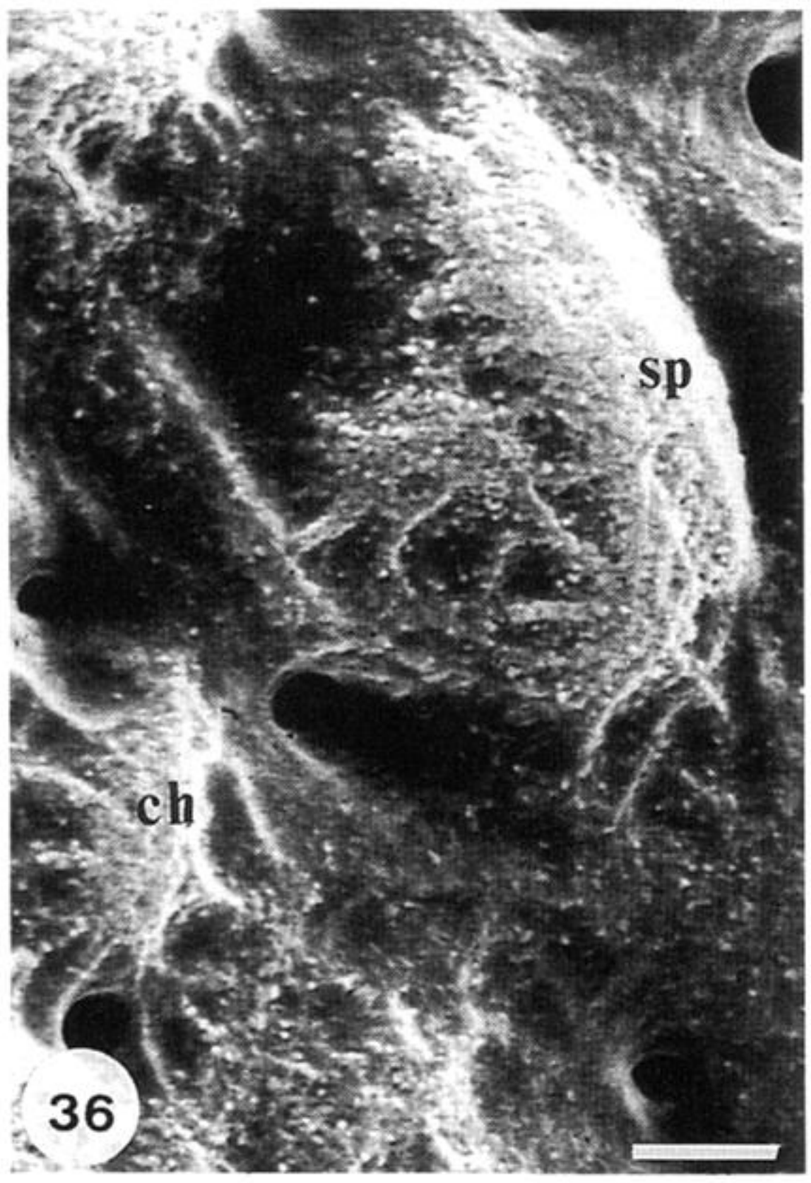

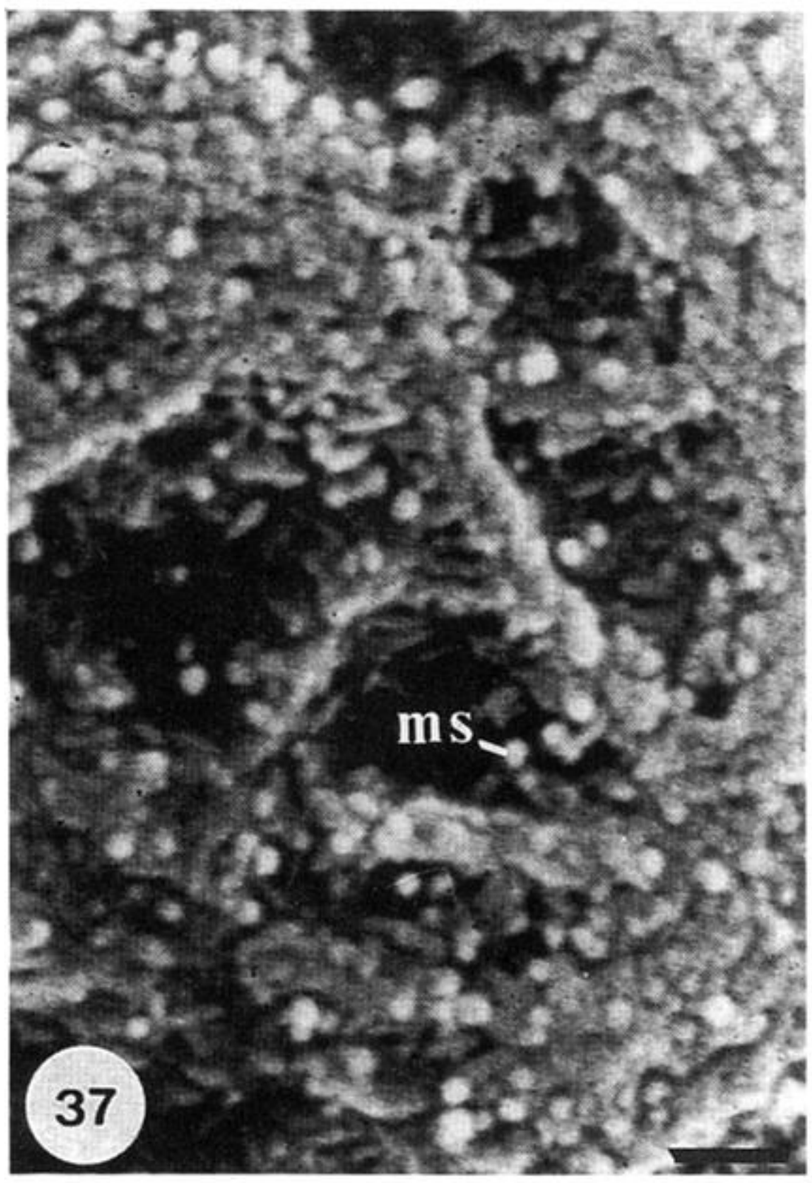

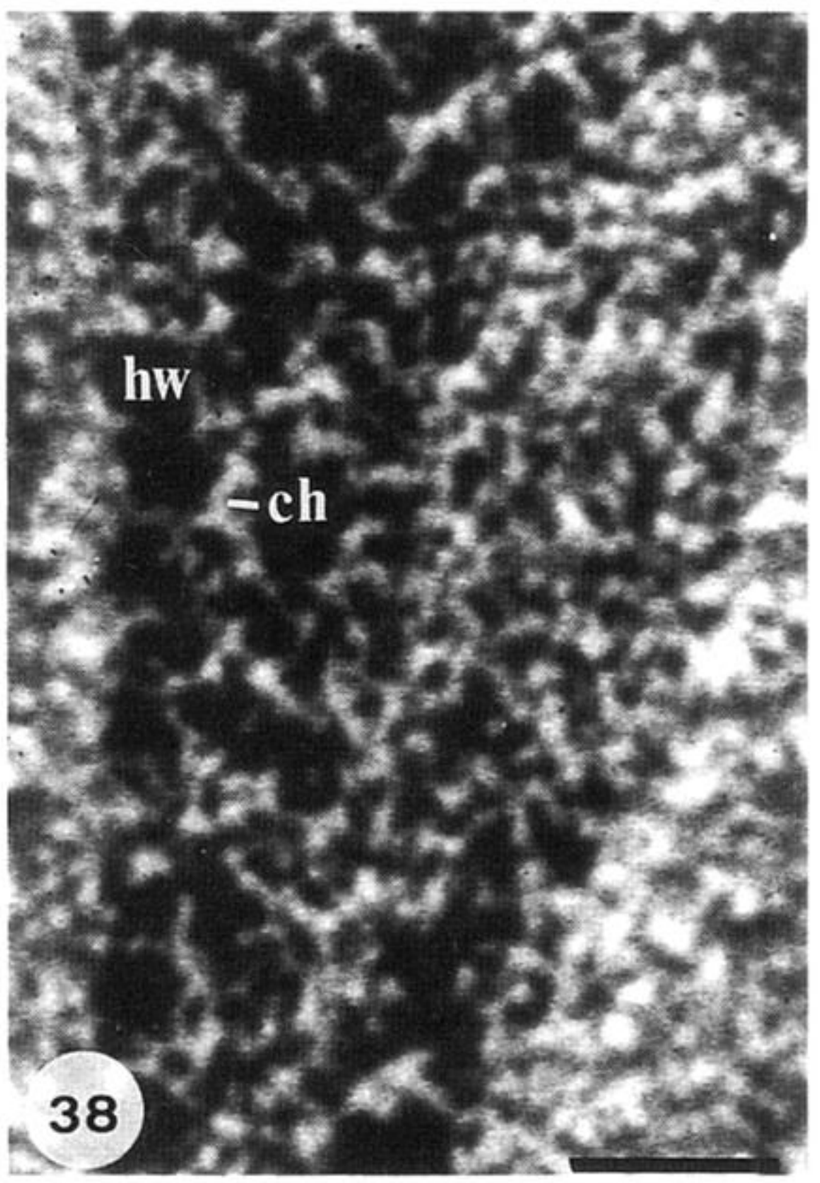

Figures 33–38. Scanning electron micrographs of gold-coated internal surfaces and a carbon-coated section (figure 35) of the shell of *Lingula anatina*.

Figures 33–34. General view of fibrous anastomosing ridges (af) arranged in a hexagonal network centrally and exposed beneath a membranous lamina (ml) in the anteromedian part of a valve digested by subtilisin; with details of the fibrous texture showing how short apatitic rods with chitin (ch) and interspersed with apatitic mosaics (mc) are assembled around hollows (hw) presumably occupied by digitations of outer epithelium (figure 34). Scale bars = 2 μm and 0.5 μm respectively.

Figure 35. Back scattered electron scan confirming the apatitic composition of rods and mosaics succeeding a botryoidal lamina (bl). Scale bar = 1 μm.

Figures 36 and 37. General view and detail of a radiating unit of ridges of proteinaceous chitin or chitin (ch) coated with apatitic mosaics (ms), which are precursory to anastomosing ridges, on the side of a subconical projection (sp) of the internal surface of the submedian part of a valve treated with phosphate buffer (100 mM, pH 7). Scale bars = 2 μm and 0.5 μm respectively.

Figure 38. Detail of radiating ridges of chitin and residual apatitic mosaics in the same valve featured in figure 36, in which subtilisin digestion has removed many mosaics leaving hollows (hw) delineated by strands of a chitin matrix (ch) showing traces of a hexagonal network. Scale bar = 0.5 μm.

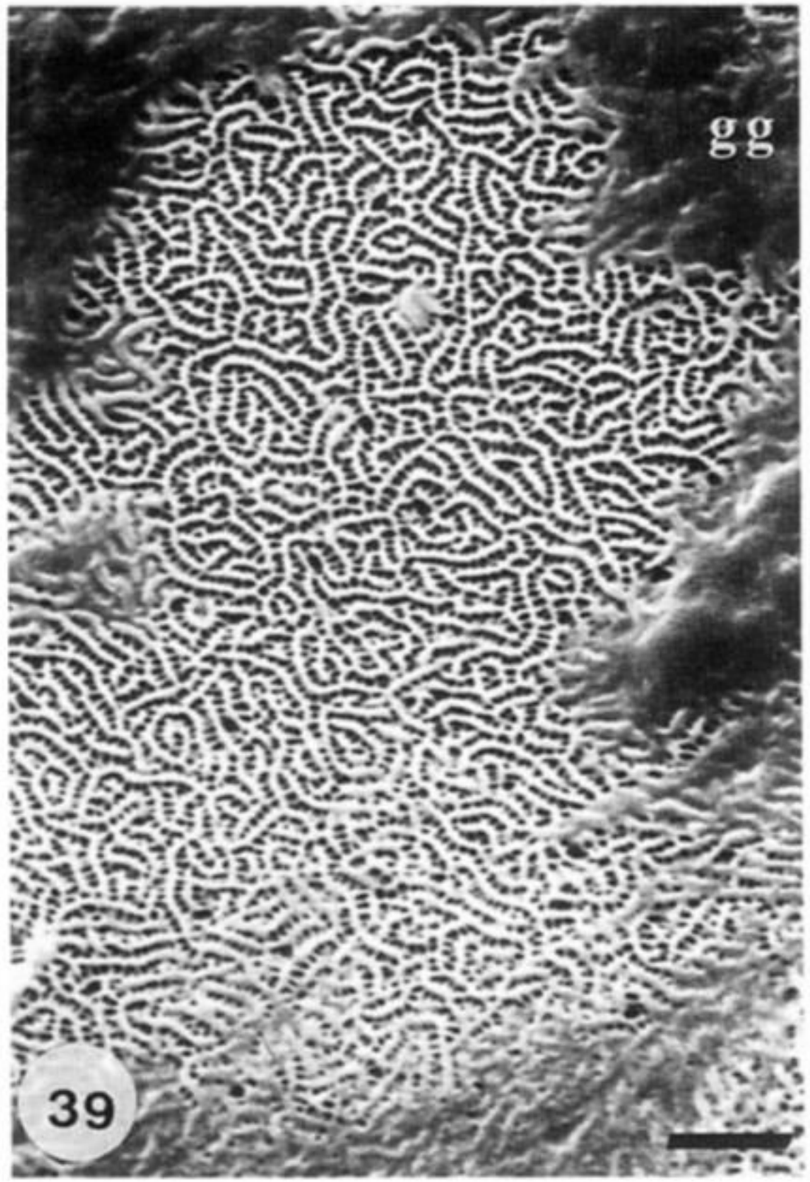

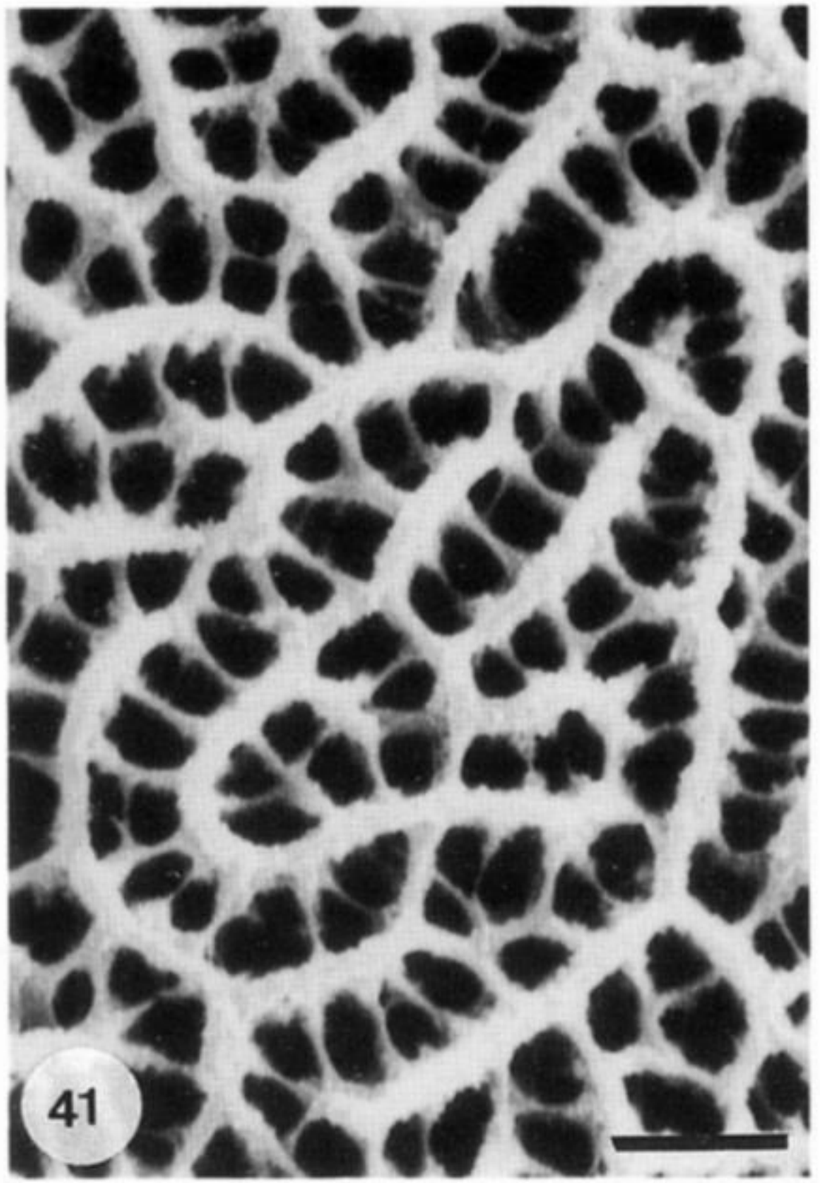

Figures 39–41. Scanning electron micrographs of a gold-coated internal surface of the posterolateral part of a valve of *Lingula anatina*, mechanically stripped of mantle and fixed in ethanol (70% by volume).

Figure 39. General view of meanderform apatitic ridges and troughs with transverse connections; traces of a GAGs cover remain (gg). Scale bar = 5 μm.

Figures 40 and 41. Detail of meanderform ridges and troughs showing a covering film of GAGs and the planospiral pattern of the meanders. Scale bars = 1 μm.

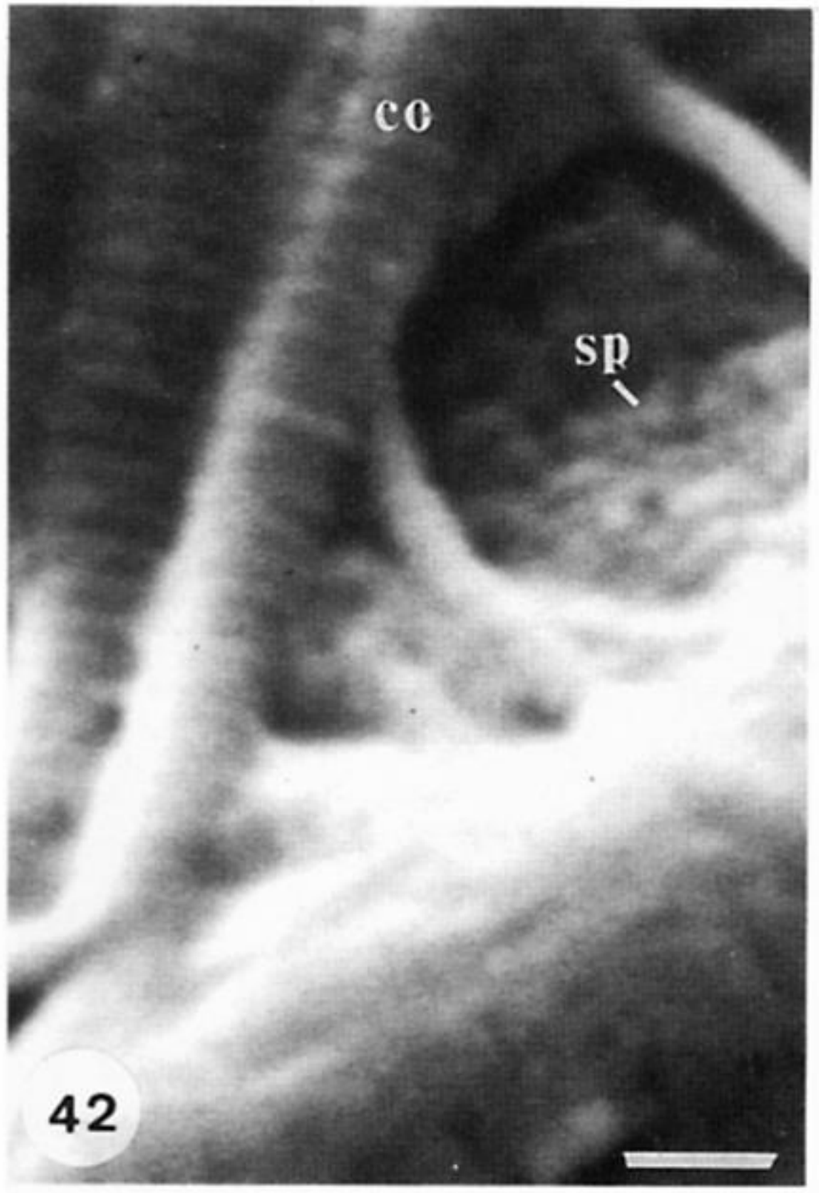

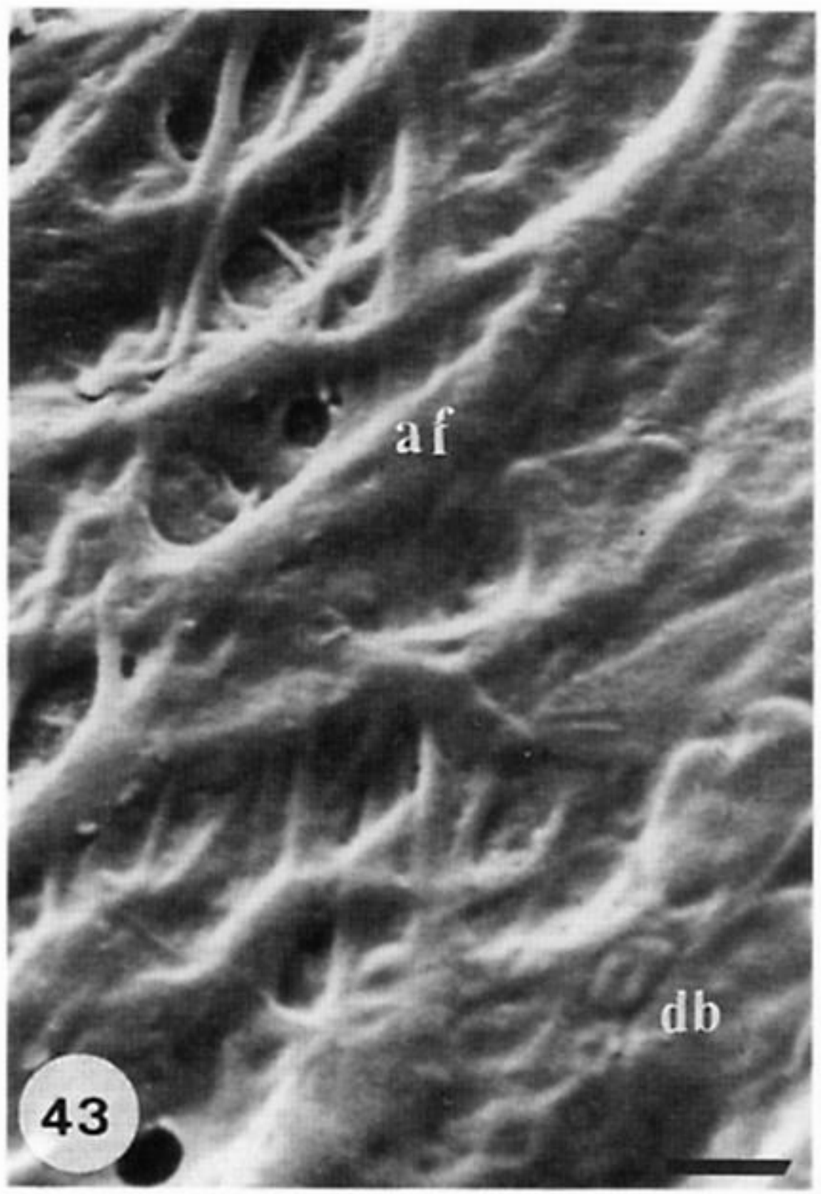

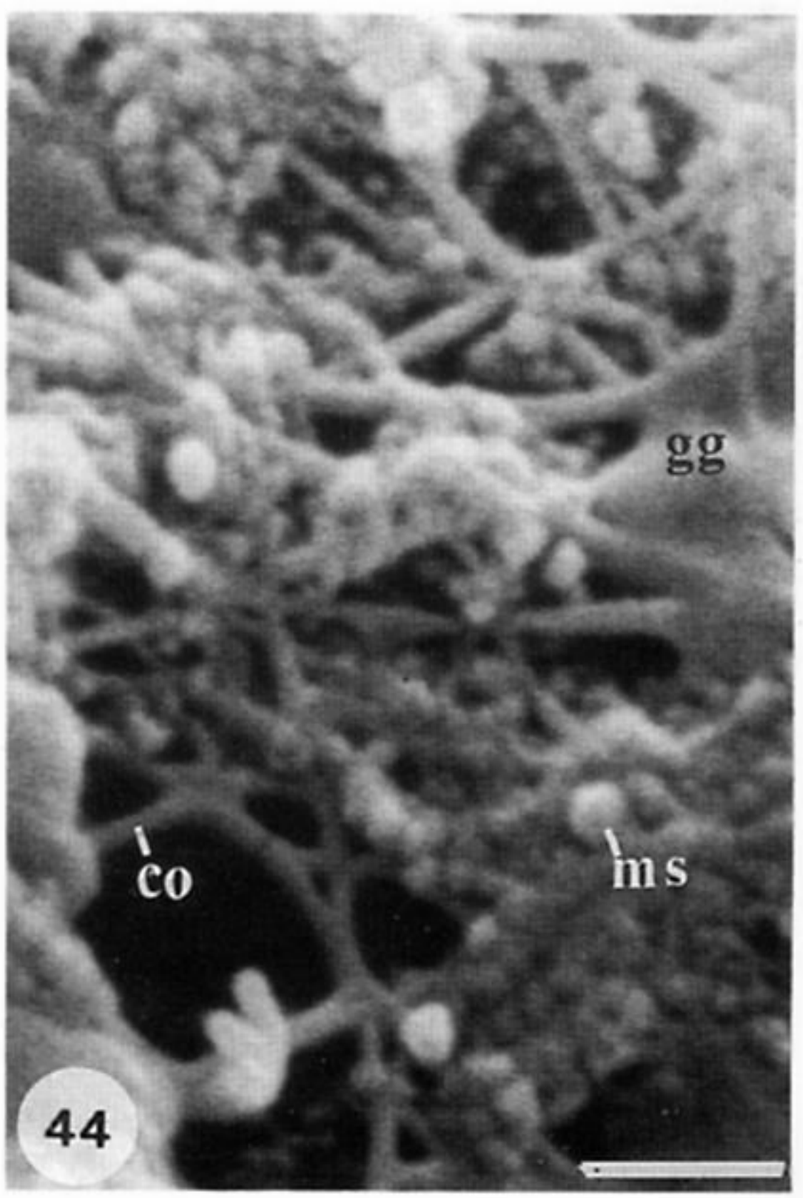

Figures 42–44. Scanning electron micrographs of gold-coated surfaces of the shell of *Lingula anatina*.

Figures 42 and 43. Detail and general view of the internal surface of the posteromedian part of a valve digested in proteinase-K and chitinase, showing collagenous fibrils (co) traversing anastomosing ridges (af), with apatitic spherules (sp), beneath an impersistent layer of GAGs with discoidal bodies (db). Scale bars = 200 nm and 1 µm respectively.

Figure 44. Partly exposed, inward facing, collagenous mat between two botryoidal laminar sets of the posteromedian part of a valve treated with phosphate buffer (100 mM, pH 7), showing fibrils of collagen (co), apatitic botryoids and mosaics (ms) and GAGs (gg). Scale bar = 0.5 µm.

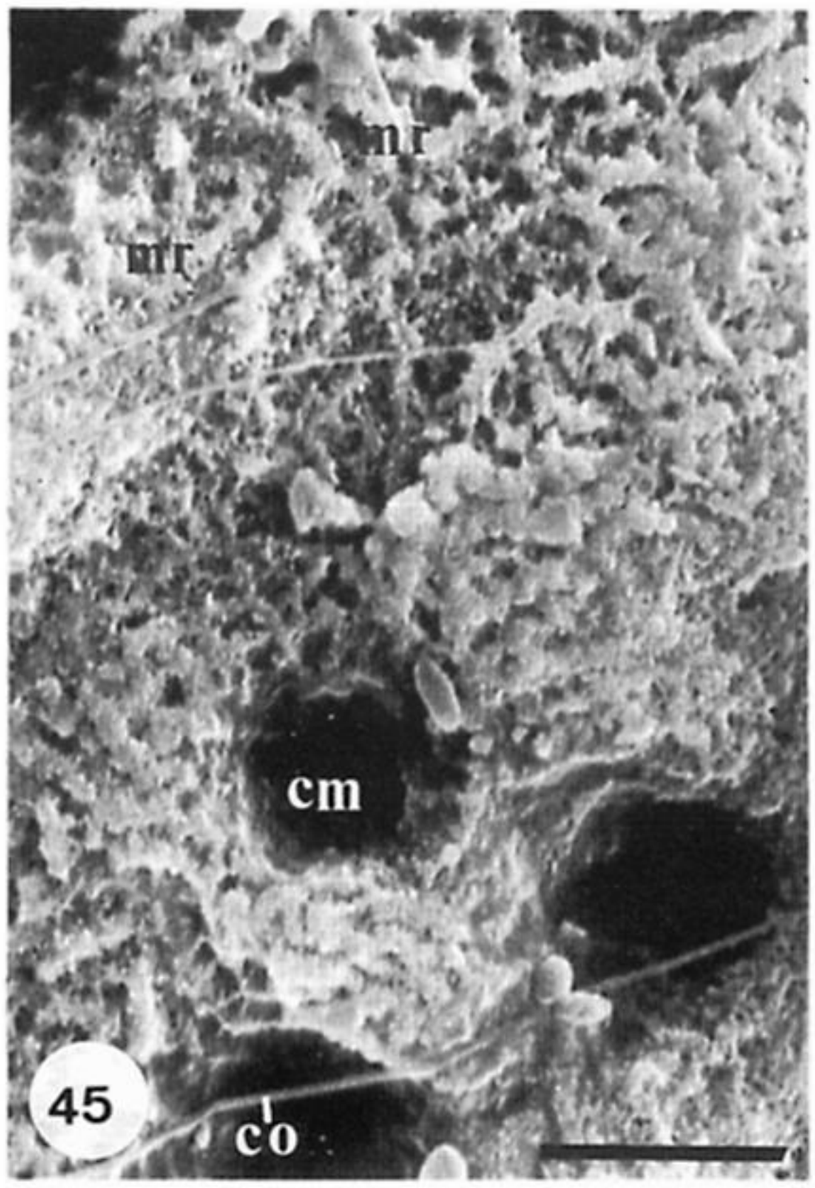

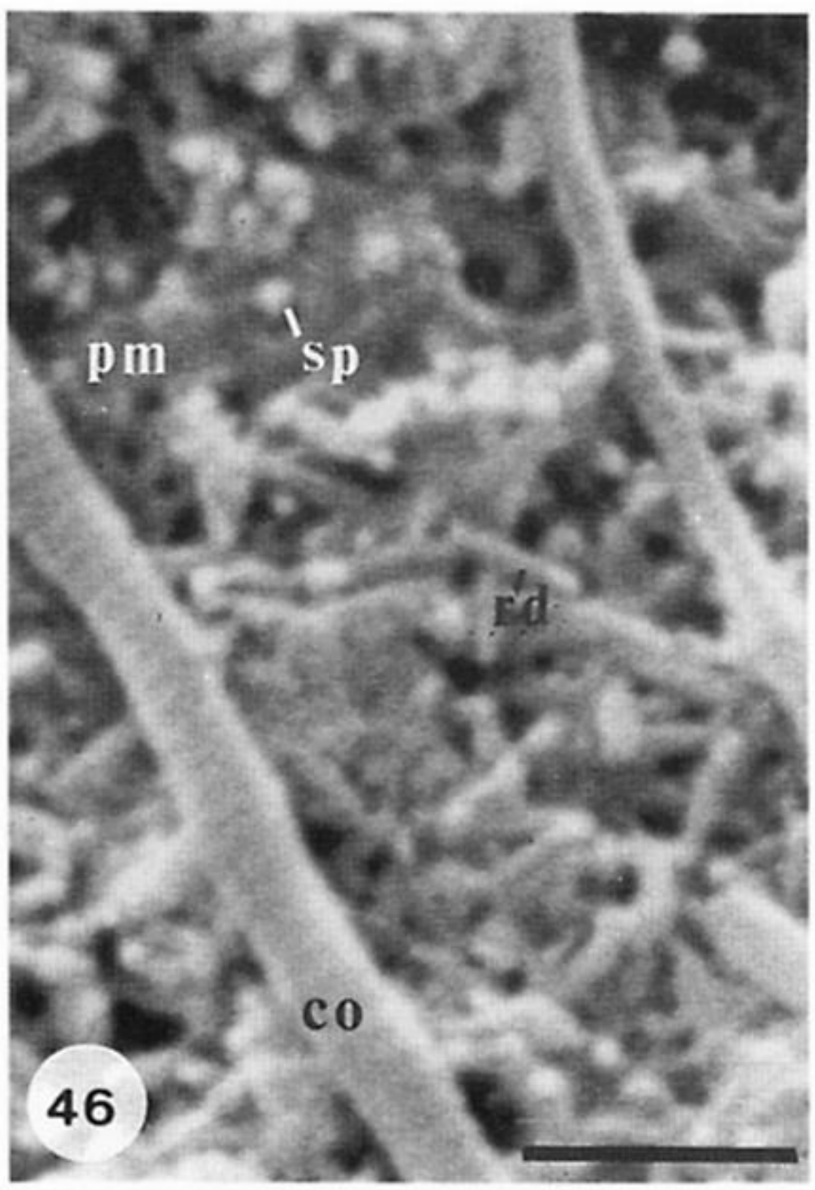

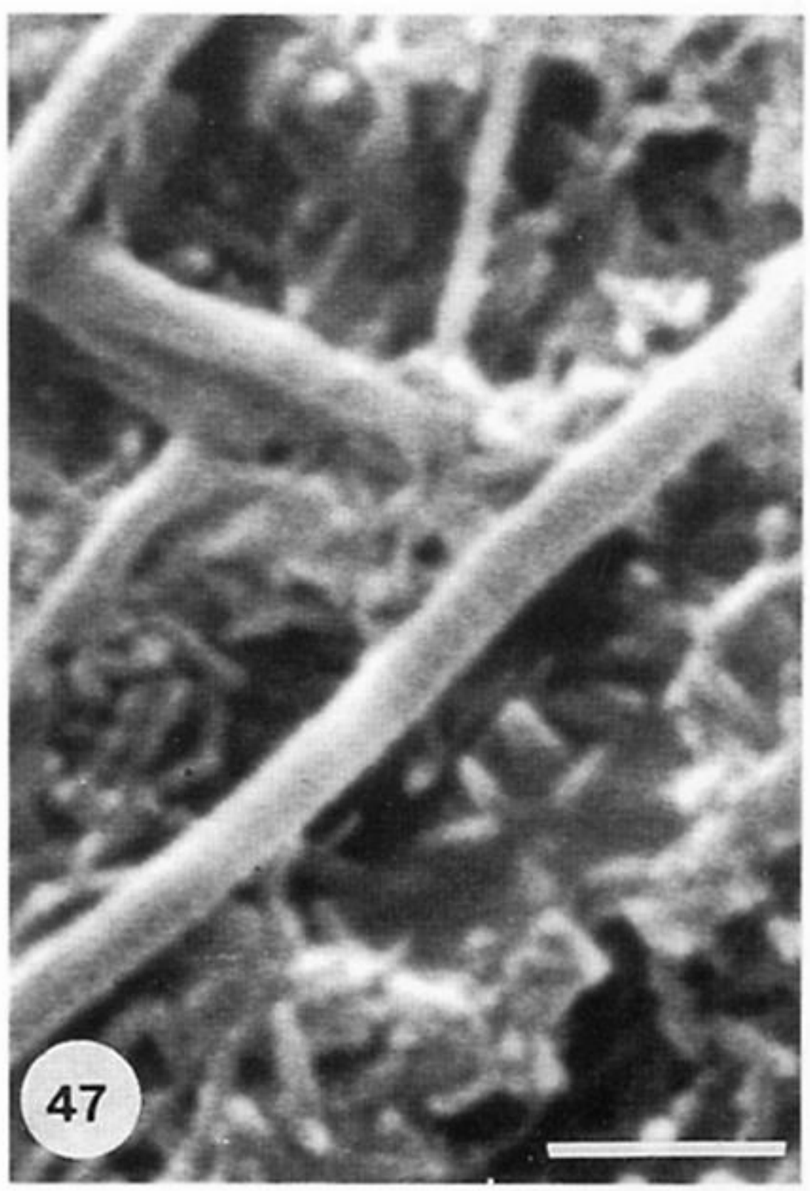

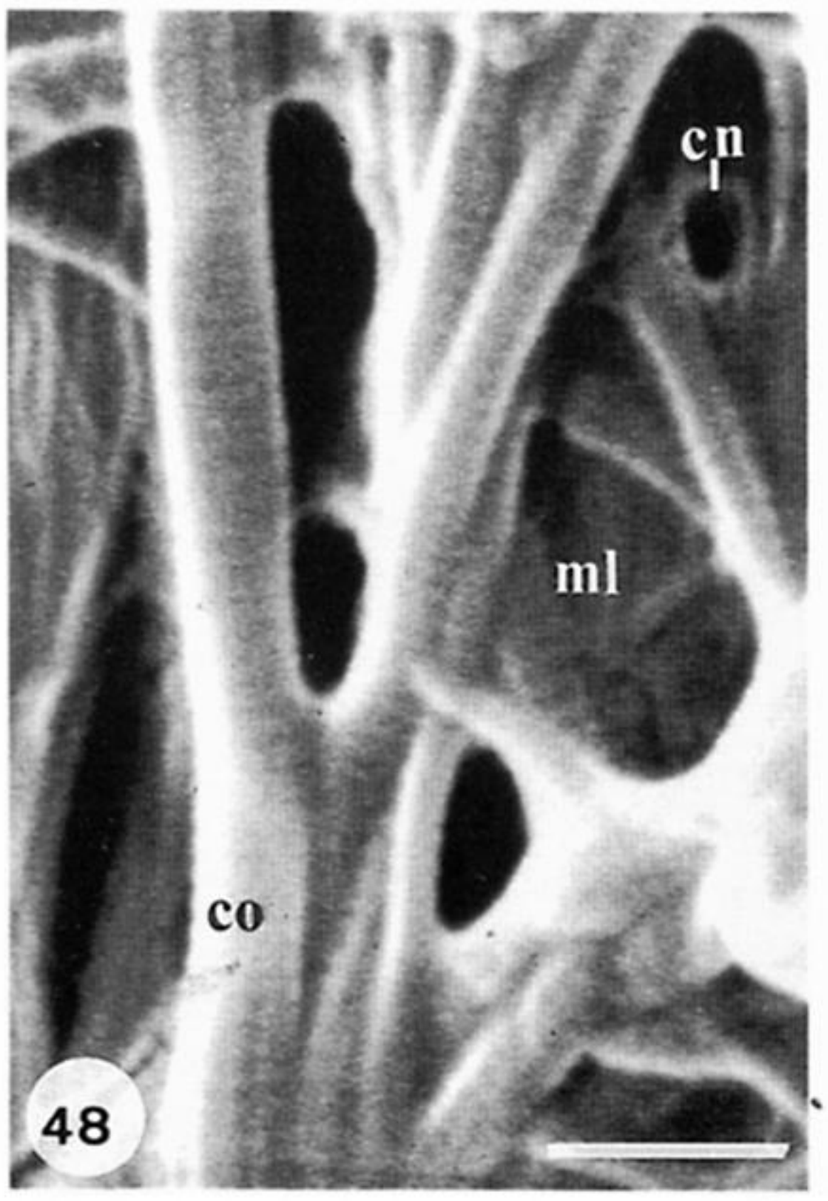

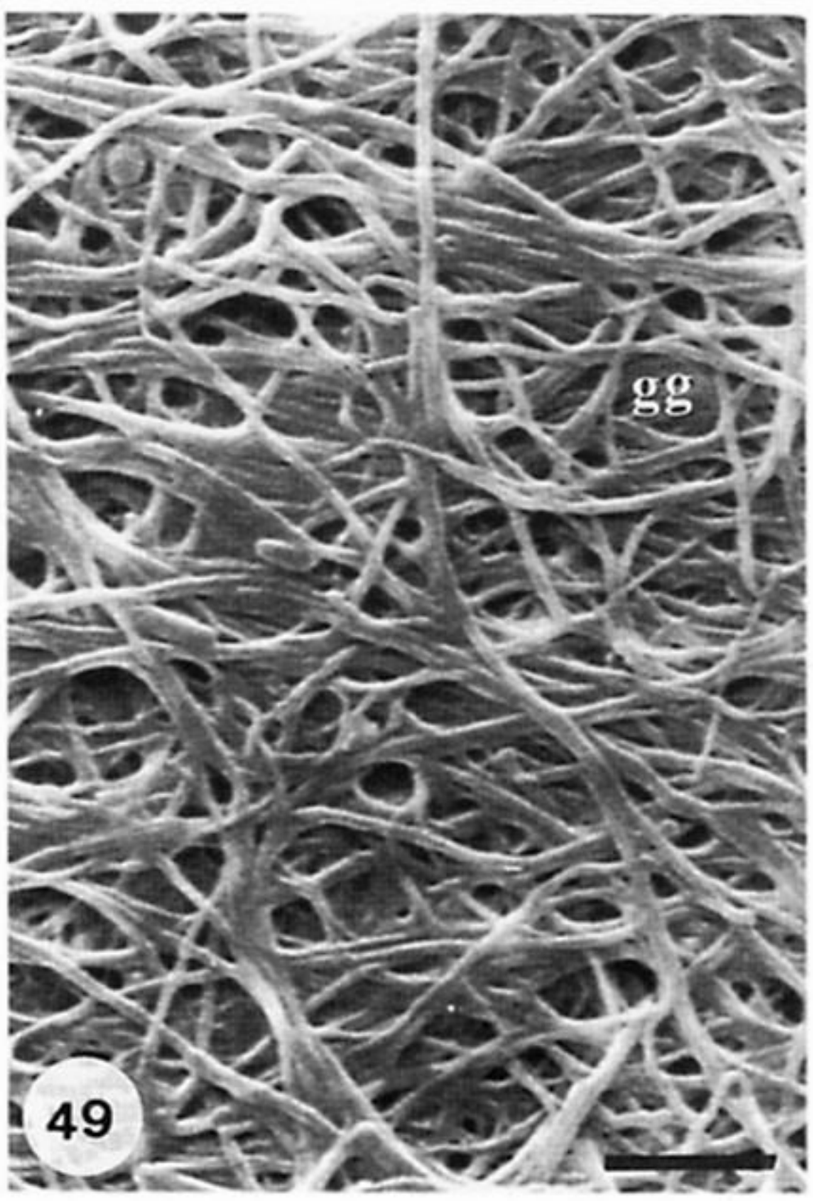

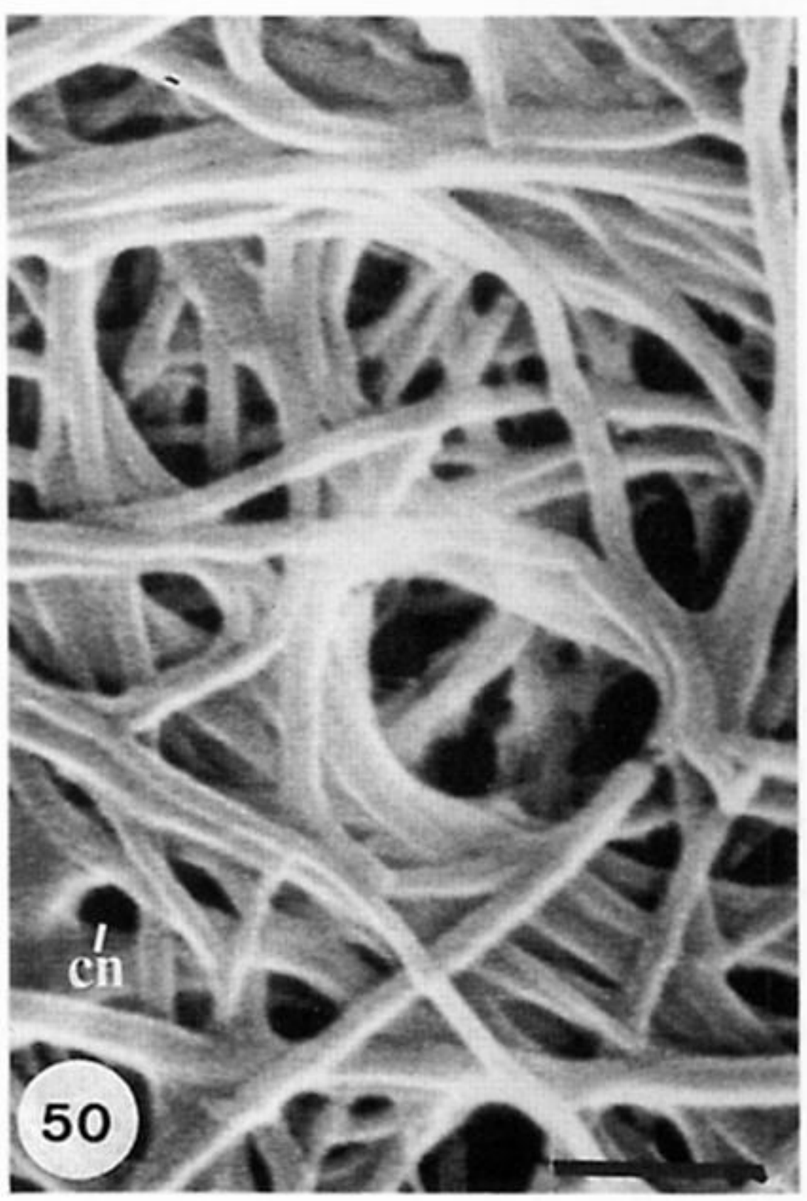

Figures 45–50. Scanning electron micrographs of gold-coated surface of the body platform of a dorsal valve of *Lingula anatina* digested in subtilisin.

Figures 45–47. General and two detailed views of the right central muscle scar showing the meanderform arrangement (mr) of chitinoproteinaceous, apatitic rods (rd) and dispersed spherules (sp) in a membranous substrate (pm), indented by chambers (cm) and overlain by collagenous fibrils (co). Scale bars = 5 μm, 0.5 μm, 0.5 μm.

Figure 48. Collagenous fibrils (co) associated with membranous laminae (ml) with canal apertures (cn) within the median cleft of the median septum. Scale bar = 0.5 μm.

Figures 49–50. General view and detail of a mat of collagenous fibrils associated with GAGs (gg) with a canal aperture (cn), and forming a broad (0.5 mm) anterolateral border to the medianly raised part of the body platform. Scale bars = 2 μm, 1 μm.

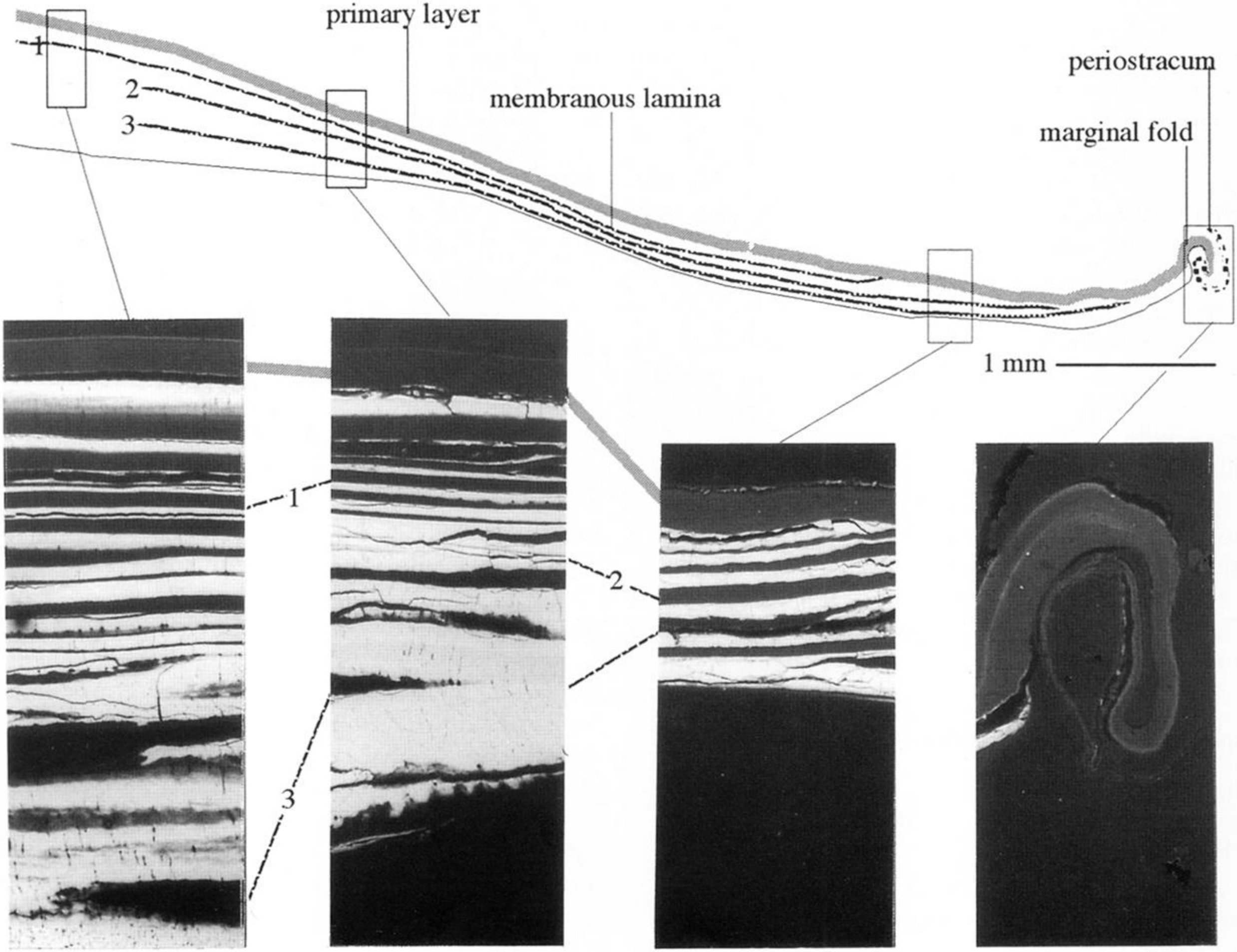

Figure 51. Composite BSE micrographs and drawing of a cut and polished transverse section of the posterior right half of a resin-mounted valve of *Lingula anatina*, coated with carbon and surveyed for a montage to show the distribution of phosphorus (white) and organic compounds (grey to black) in four correlated columns; the montage was digitized and reduced to show the extent of the primary layer and three well-developed membranous laminae (upper drawing) with lamina 3 locally overstepped by a transgressive inner compact lamina in the right-hand half of the second column from the left.

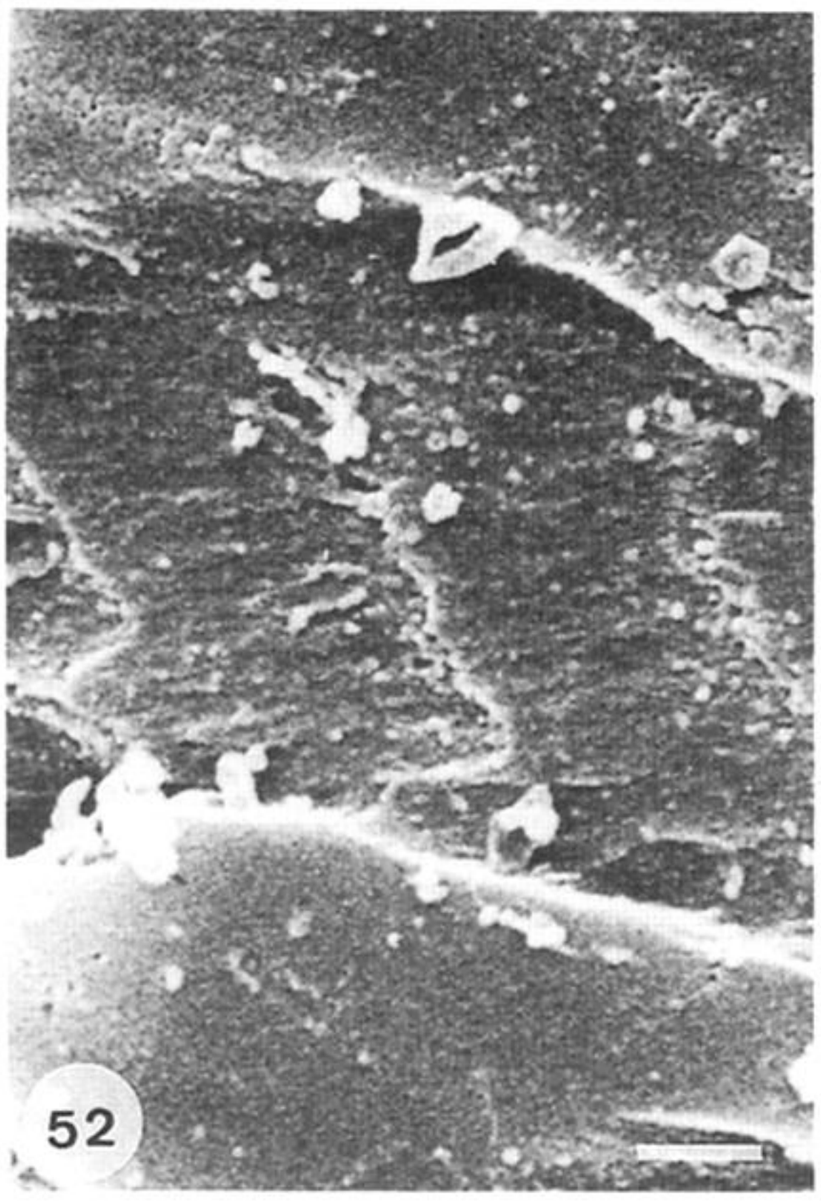

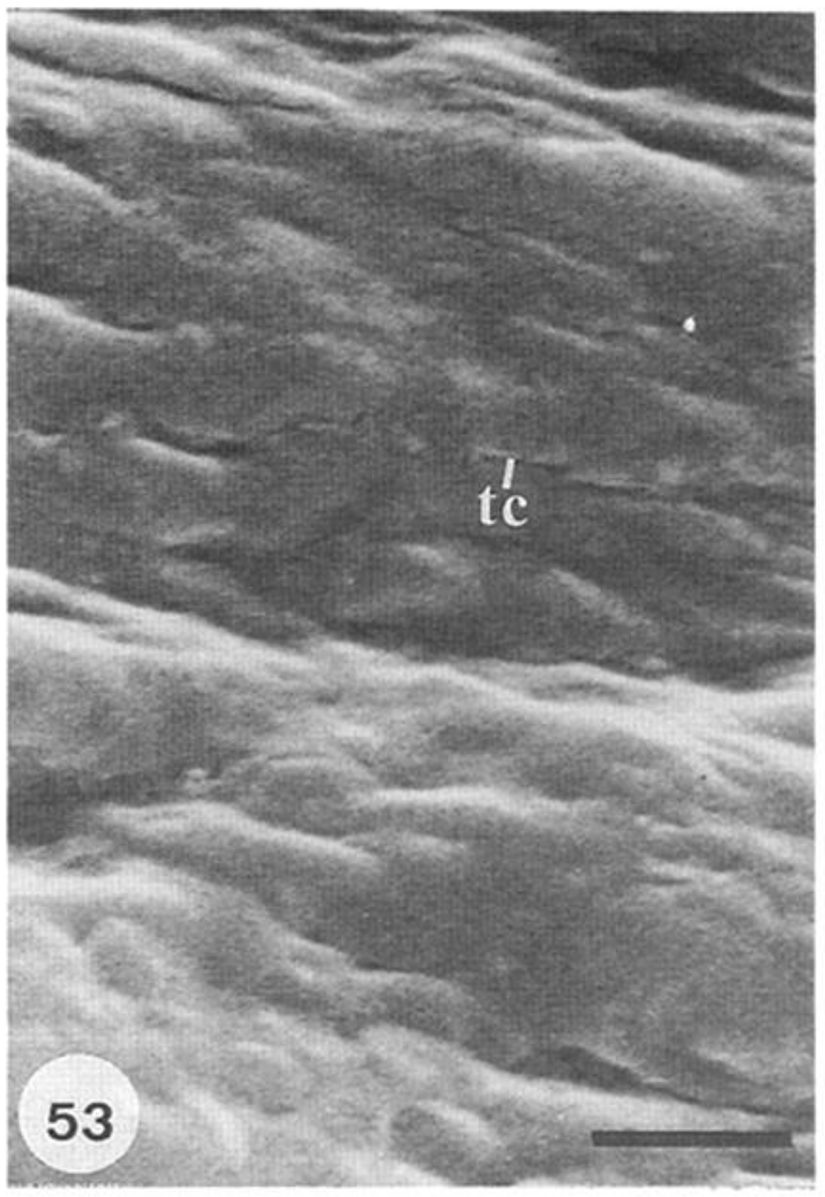

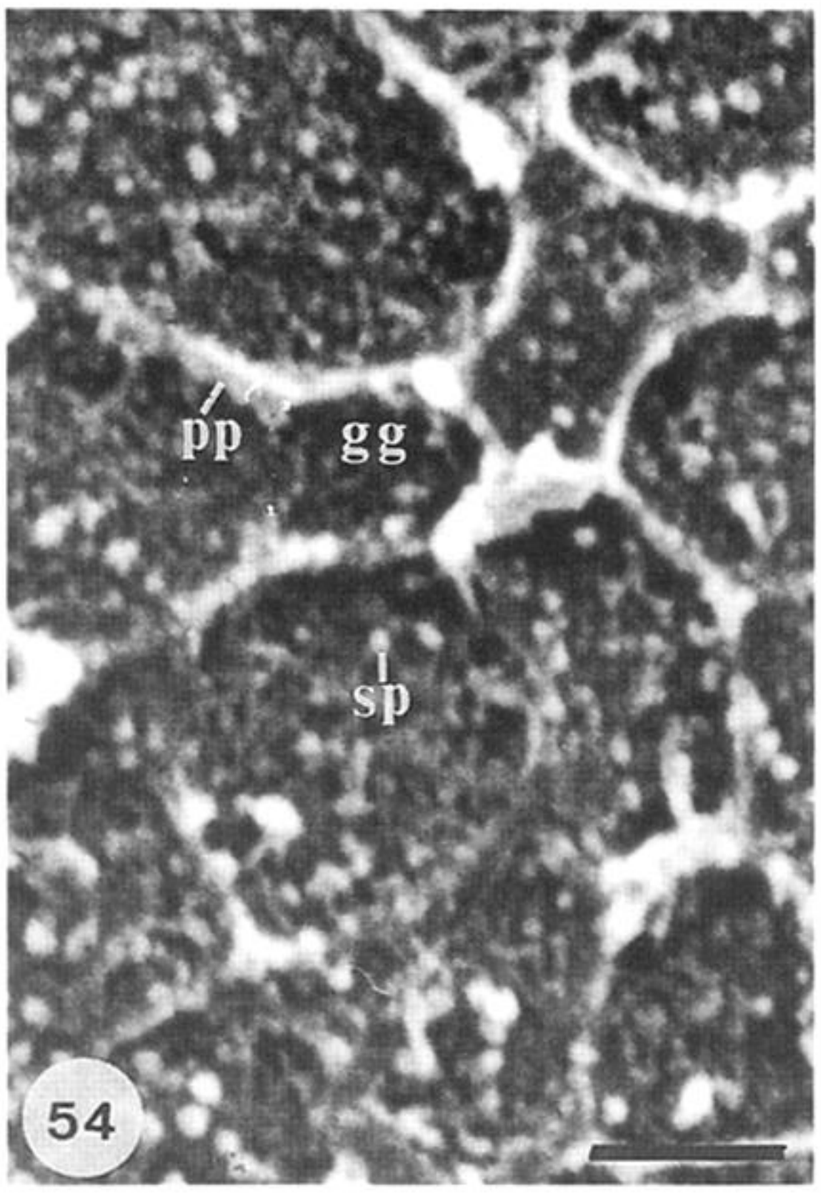

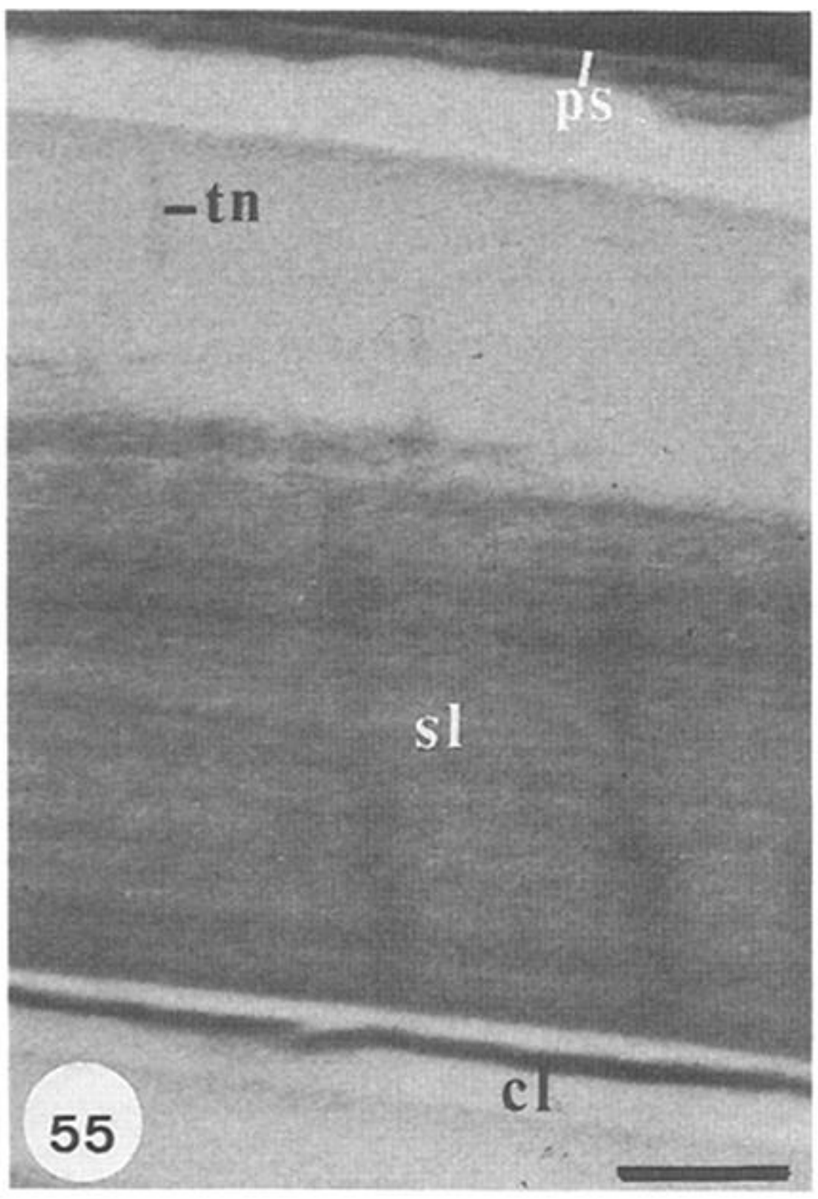

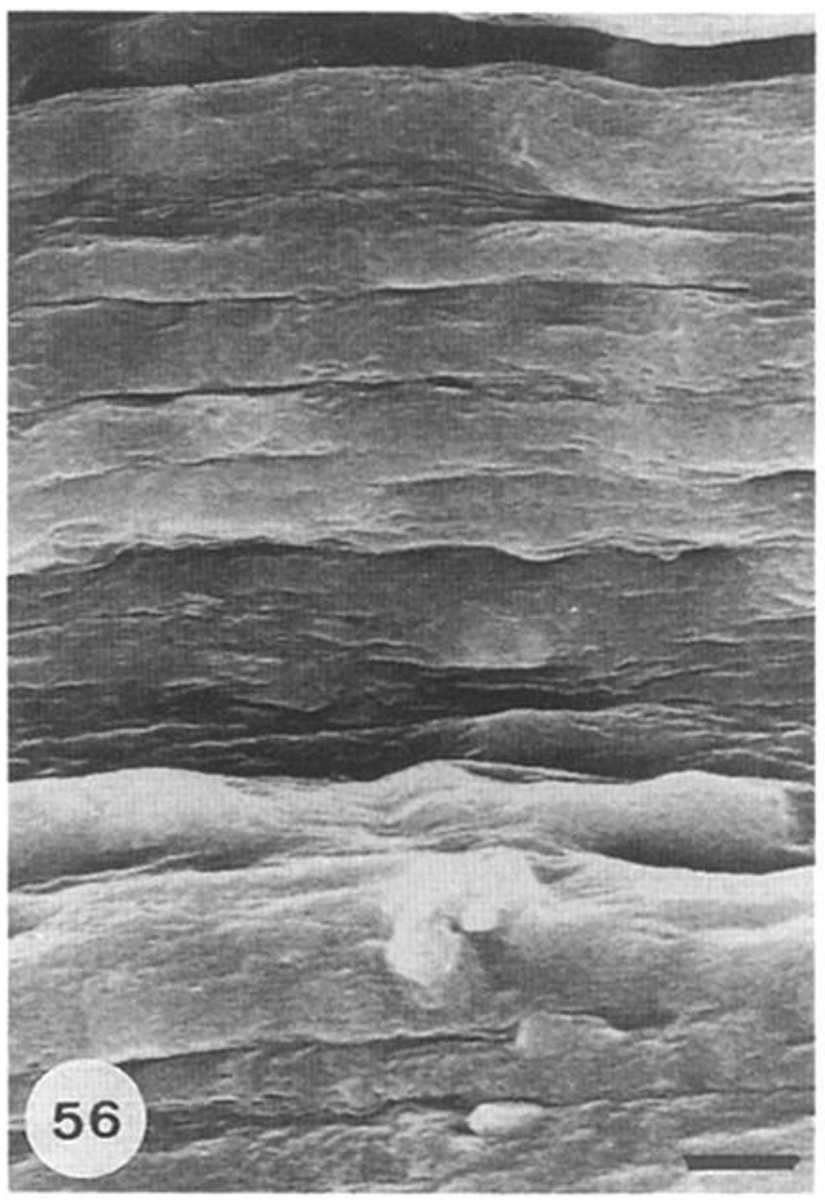

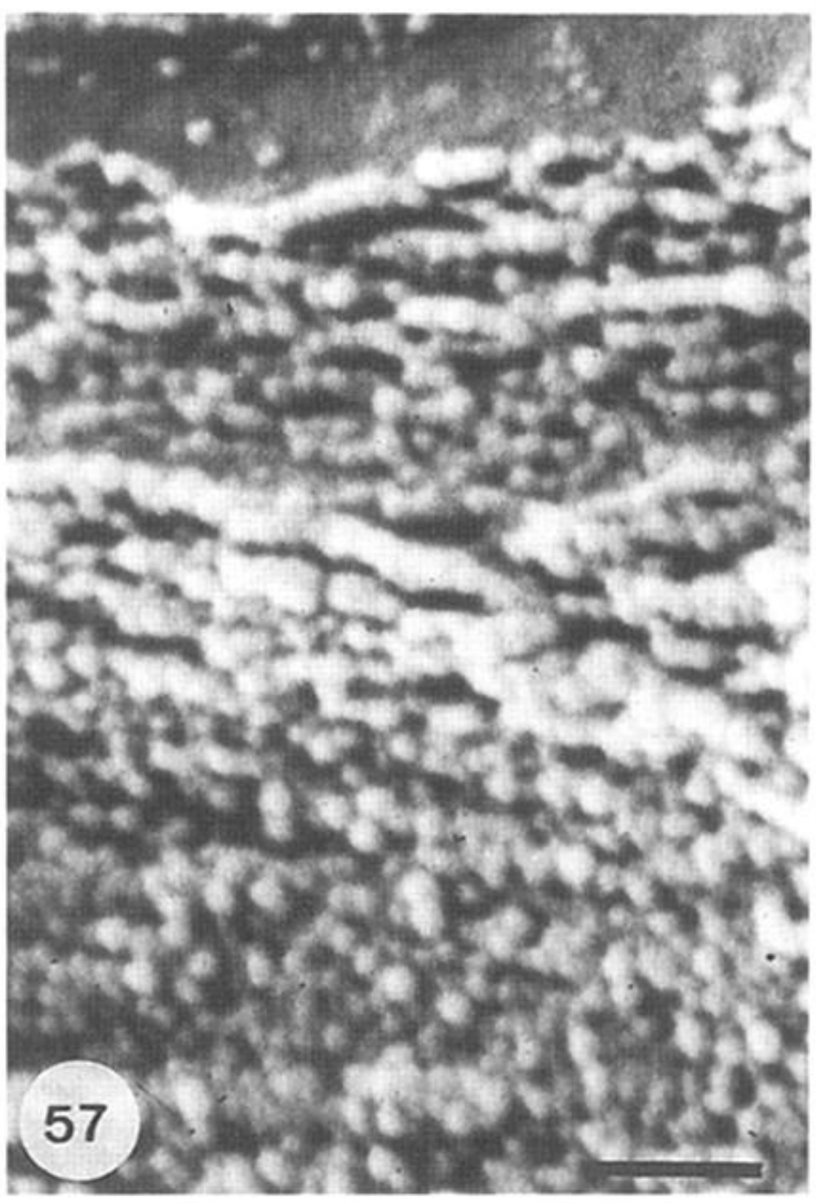

Figures 52–57. Scanning electron micrographs of gold-coated and carbon-coated (figure 55) surfaces of the shell of *Lingula anatina*.

Figure 52. Exfoliated exterior of critical point dried valve previously stored in ethanol (70% by volume) showing a finely granular, stratified and vertically cleaved primary layer composed of hardened GAGs. Scale bar = 1 μm.

Figure 53. Primary layer composed of poorly stratified GAGs with tension cracks (tc), exposed in a cut, vertical median section of the mid-part of a valve treated with MES buffer (100 mM, pH6). Scale bar = 1 μm.

Figure 54. Junction between the exfoliated primary layer and the spherular (sp) secondary layer with traces of GAGs (gg) and proteinaceous partitions (pp) deposited between the digitate protrusions of the apical plasmalemma of the secreting outer epithelium, exposed on the external surface of a critical point dried valve previously stored in ethanol (70% by volume). Scale bar = 0.5 μm.

Figure 55. Back scattered electron scan of the outer succession, exposed in a polished, transverse section of the posterior half of a resin-mounted valve, showing a stratified lamina (sl) with a terminating canal (tn) between compact laminae (cl), the top one immediately underlying the primary layer (ps). Scale bar = 10 μm.

Figure 56. Detail of outer stratified laminae consisting predominantly of GAGs with tension cracks, exposed in a cut, vertical median section of the anterior part of a valve treated with Tris buffer (80 mM, pH 8) with $CaCl_2$ (100 mM). Scale bar = 5 μm.

Figure 57. Detail of a stratified lamina showing the spherular composition of individual strata exposed in a cut, vertical submedian section of the mid-part of a valve digested in subtilisin. Scale bar = 0.5 μm.

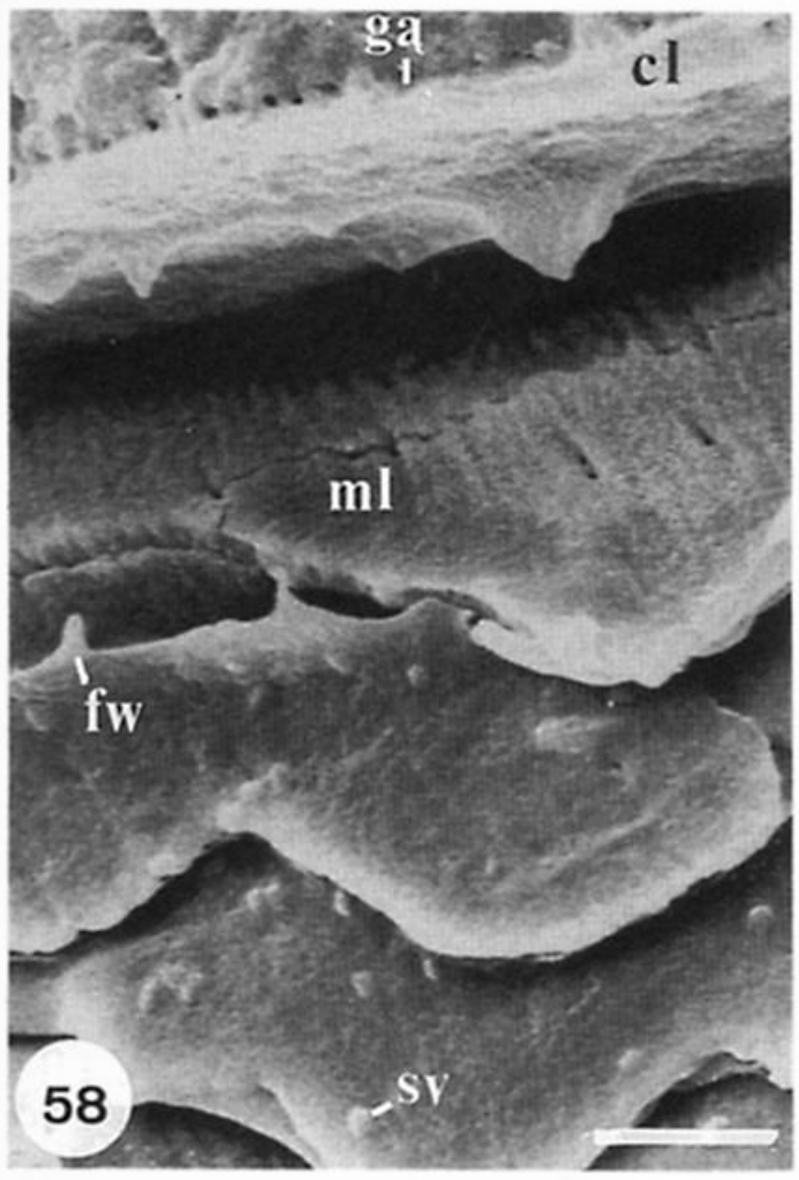

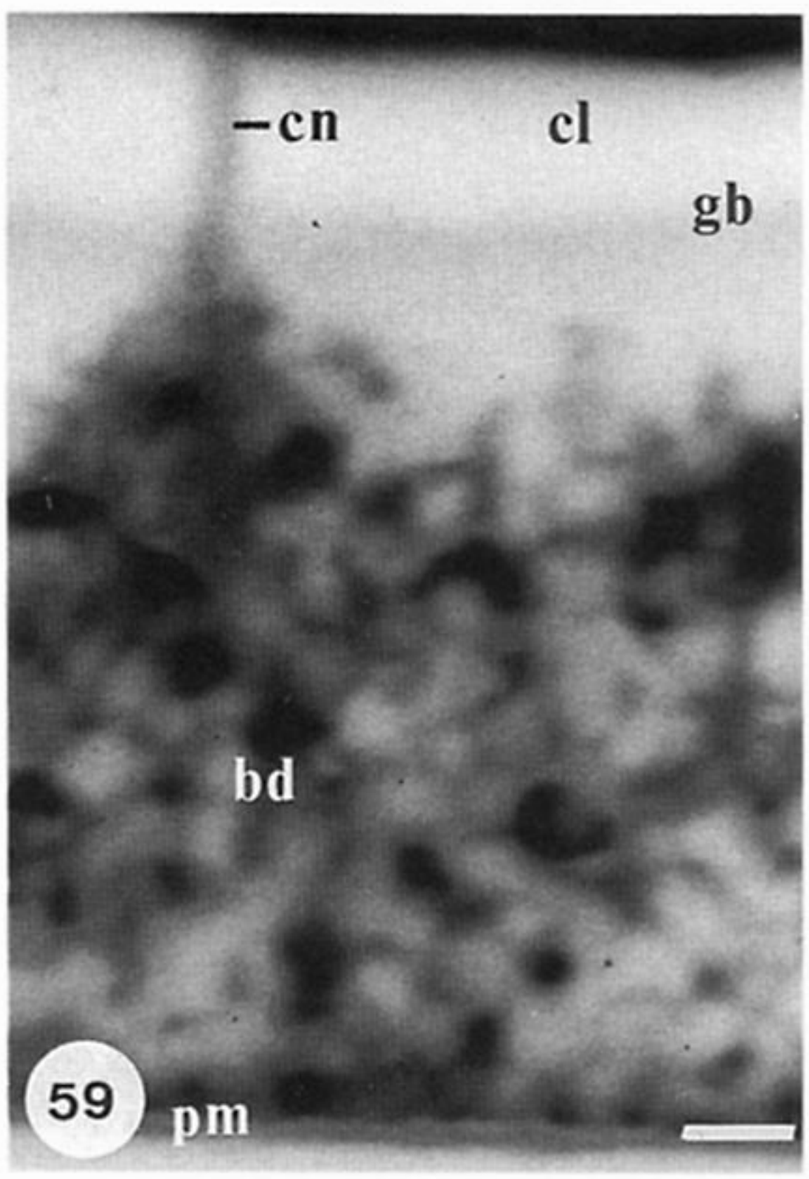

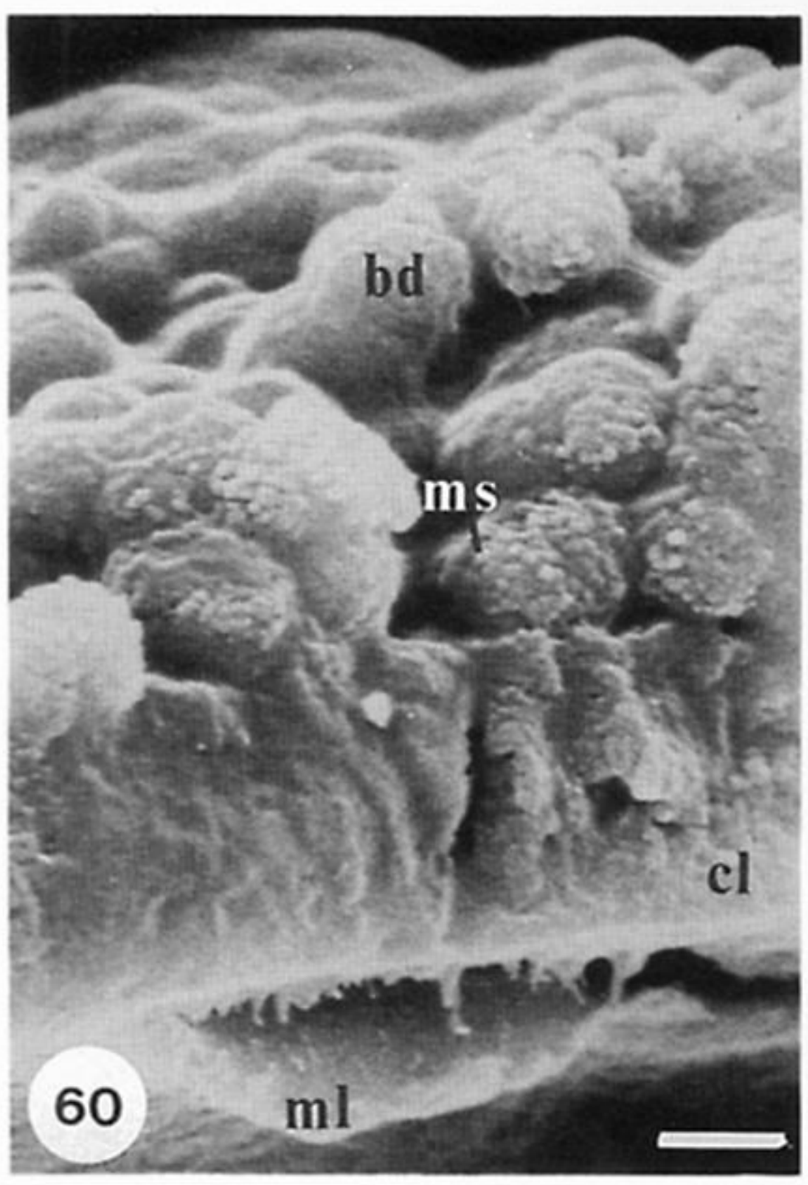

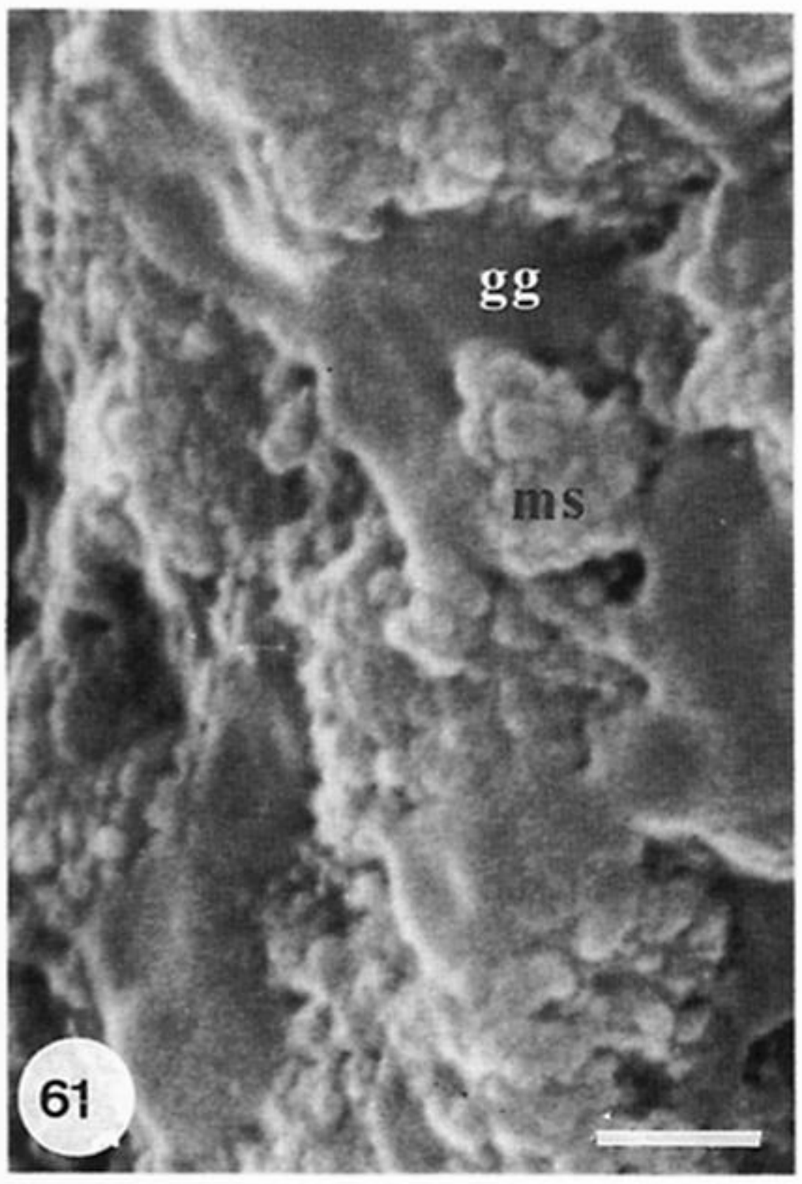

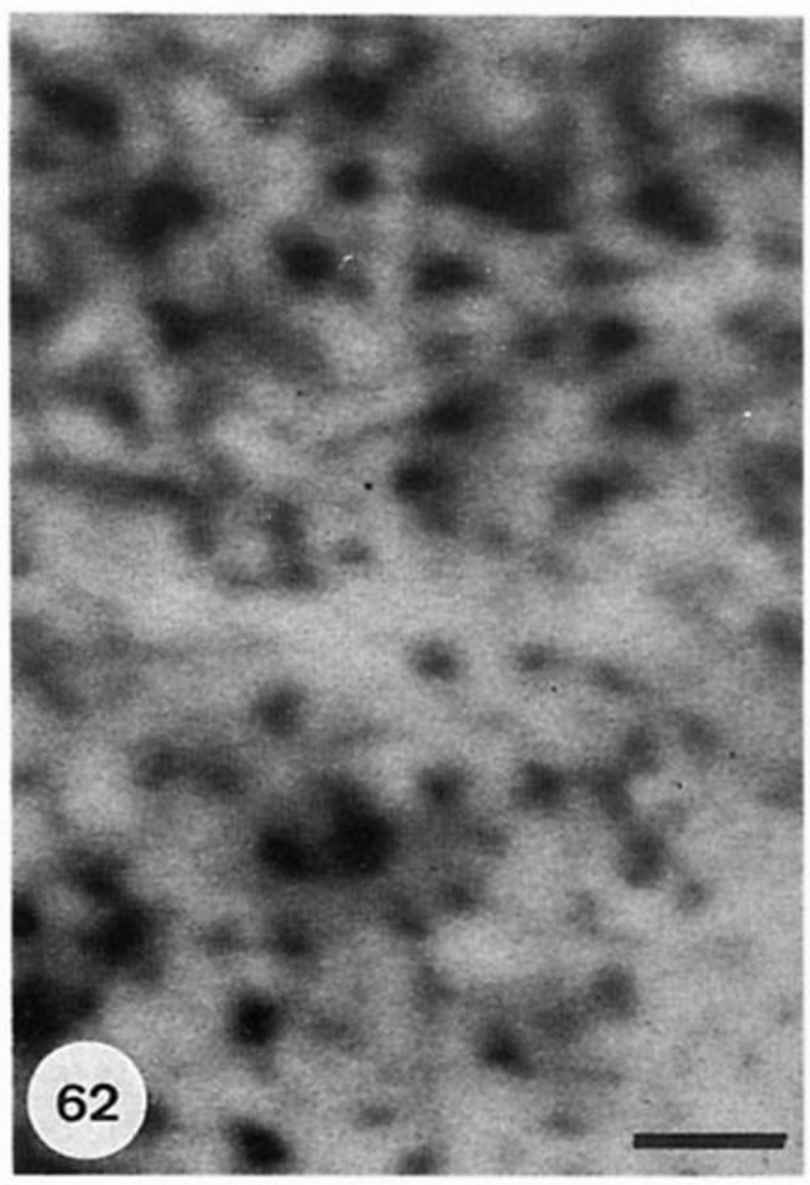

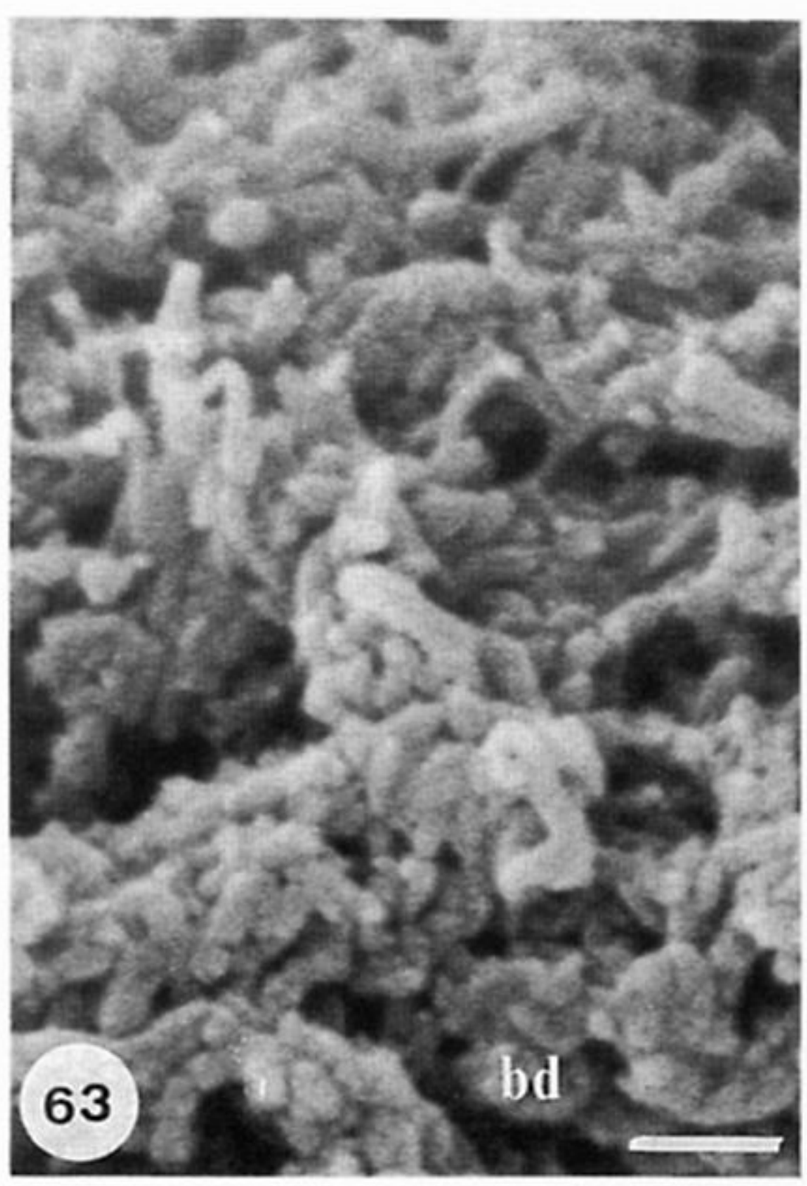

Figures 58–63. Scanning electron micrographs of gold-coated and carbon-coated (figures 59 and 62) sections of the shell of *Lingula anatina*.

Figure 58. Membranous laminae with incipient anastomosing ridges (ml) external to an apatitic compact lamina (cl) (with a row of galleries (ga) along its interface with a botryoidal lamina), exposed in a cut, vertical median section in the mid-part of a valve digested in chitinase; the laminae show signs of flow with necking (fw) and have small vesicles on their internal surfaces (sv). Scale bar = 10 μm.

Figure 59. Back scattered electron scan of a botryoidal laminar set showing a compact lamina (cl), penetrated by the organic contents of a canal (cn) and terminated by a boundary (gb) marking the onset of GAGs secretion and botryoidal clusters (bd) capped by a chitinoproteinaceous membrane (pm) exposed in a polished, transverse vertical section of the posterior half of a resin-mounted valve. Scale bar = 1 μm.

Figure 60. Botryoidal lamina (bd) composed of mosaics (ms) in a GAGs matrix succeeding a compact lamina (cl) internal of a membranous lamina (ml), exposed in a cut, vertical median section of the posterior part of a valve treated with phosphate buffer (100 mM, pH 7). Scale bar = 2 μm.

Figure 61. Walled lamina composed of alternating, highly inclined layers of ellipsoidal apatitic mosaics (ms) and GAGs (gg) and imparting a vertical cleavage on a cut, median section of the mid-part of a valve digested in collagenase. Scale bar = 0.5 μm.

Figure 62. Back scattered electron scan of a rod and plate lamina showing the disposition of linear apatitic structures (light) within an organic matrix (dark), exposed in a polished, transverse vertical section of the posterior half of a resin-mounted valve. Scale bar = 1 μm.

Figure 63. Rod and plate lamina inwardly succeeding a botryoidal apatitic zone (bd), exposed in the cut, vertical median section of the anterior part of a valve digested in proteinase-K. Scale bar = 0.5 μm.

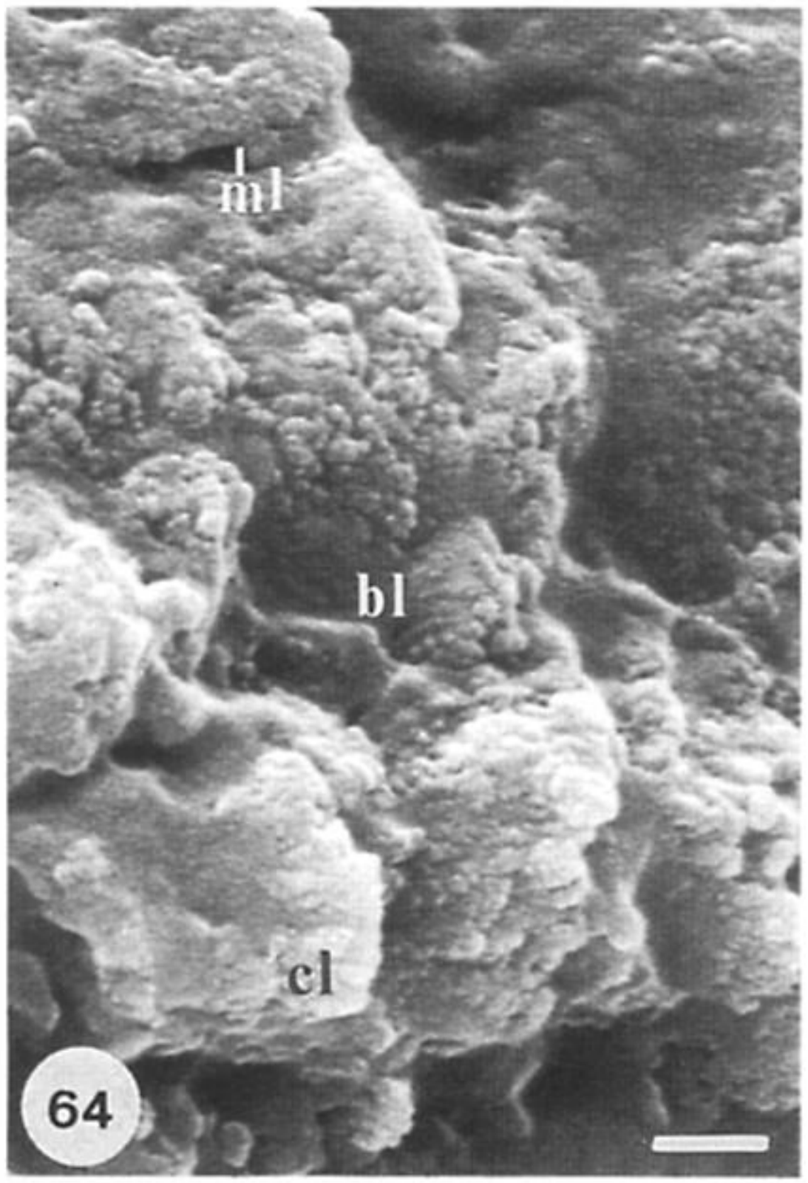

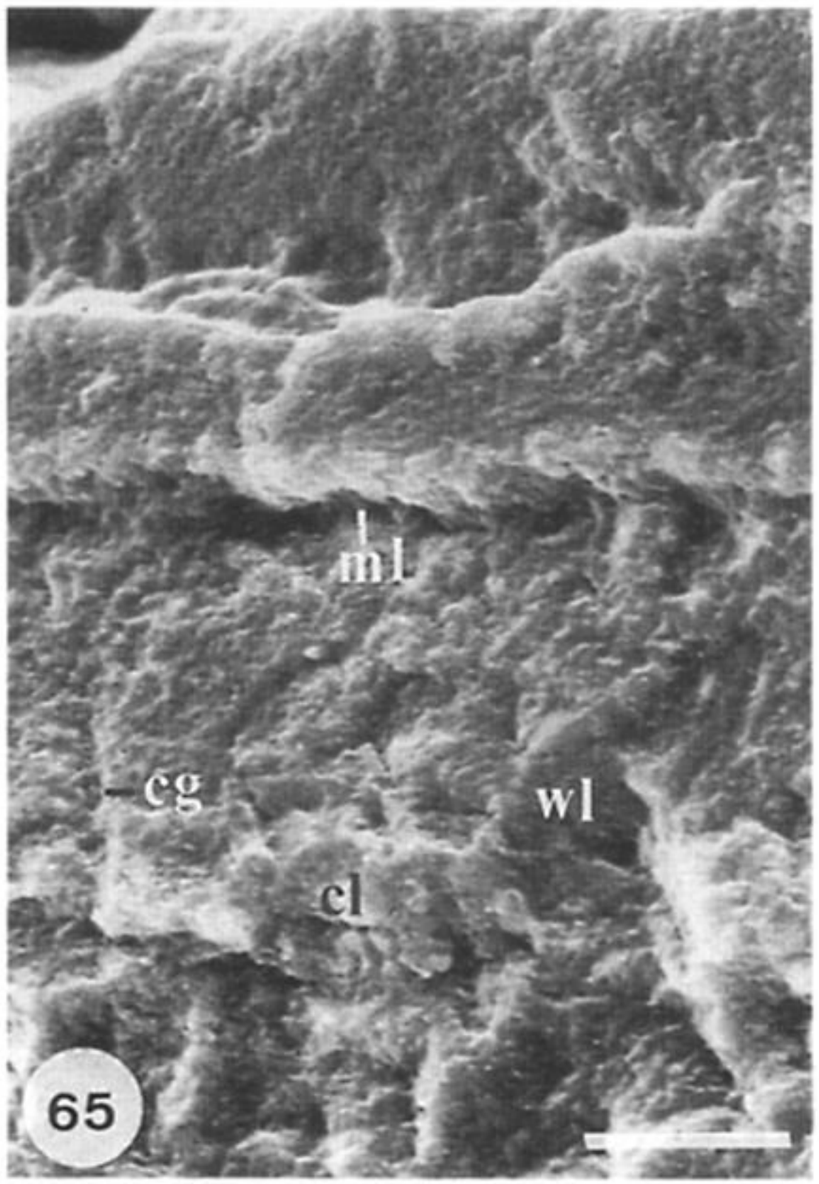

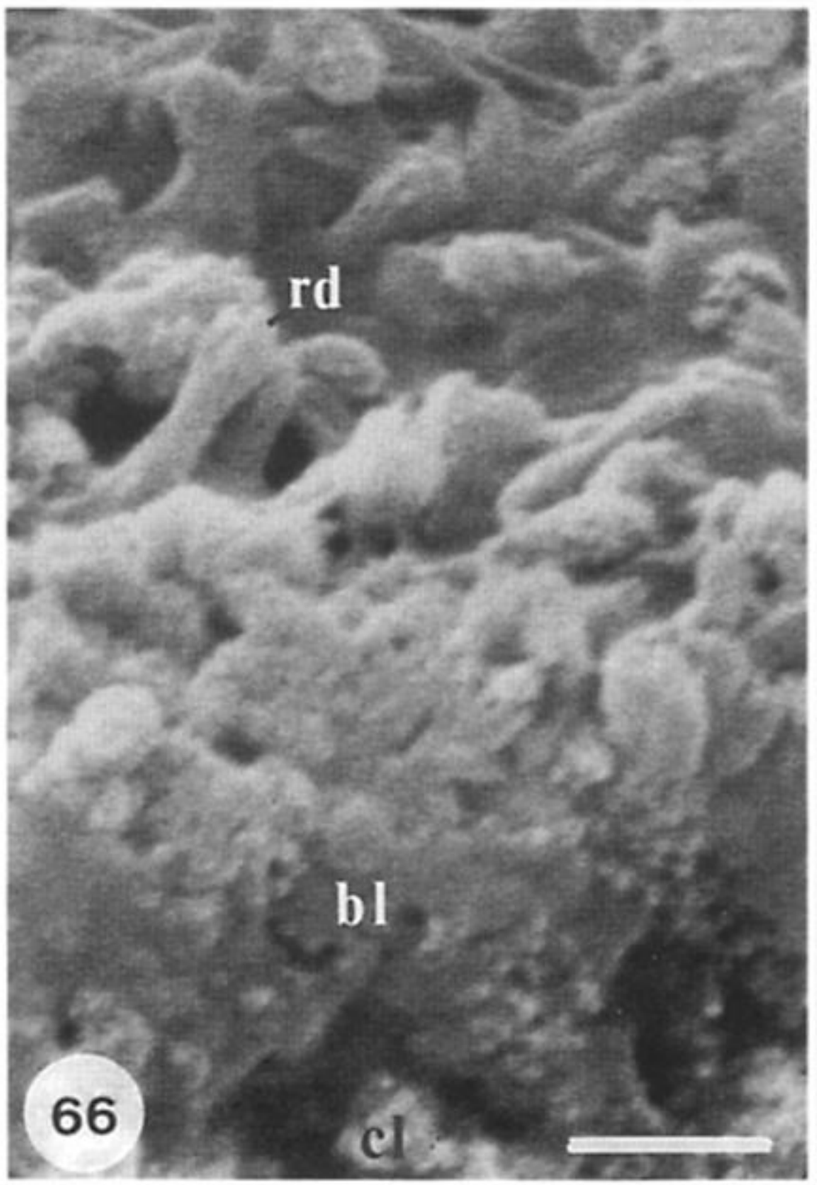

Figures 64–66. Scanning electron micrographs of gold-coated, cut, vertical sections of the shell of *Lingula anatina*.

Figure 64. Botryoidal sets of laminae, each consisting of a compact lamina (cl) passing inwardly into a botryoidal lamina (bl) and a membranous lamina (ml) which is capped by the compact lamina of the succeeding set, exposed in a posteromedian section of a valve digested in endoproteinase Glu-C and chitinase. Scale bar = 1 μm.

Figure 65. Walled sets of laminae, each consisting of a compact lamina (cl) passing inwardly into a walled lamina (wl) and a membranous lamina (ml) which is capped by the compact lamina of the succeeding set; cleavage (cg), induced by alternating walls of apatitic mosaics and GAGs, running through sets; exposed in a posteromedian section of a valve treated with phosphate buffer (100 mM, pH 7). Scale bar = 10 μm.

Figure 66. Rod and plate set of laminae consisting of a compact lamina (cl), passing inwardly through a botryoidal lamina (bl) into a lamina of rods (rd) and plates embedded in GAGs, exposed in an anteromedian section of a valve digested in proteinase-K. Scale bar = 1 μm.

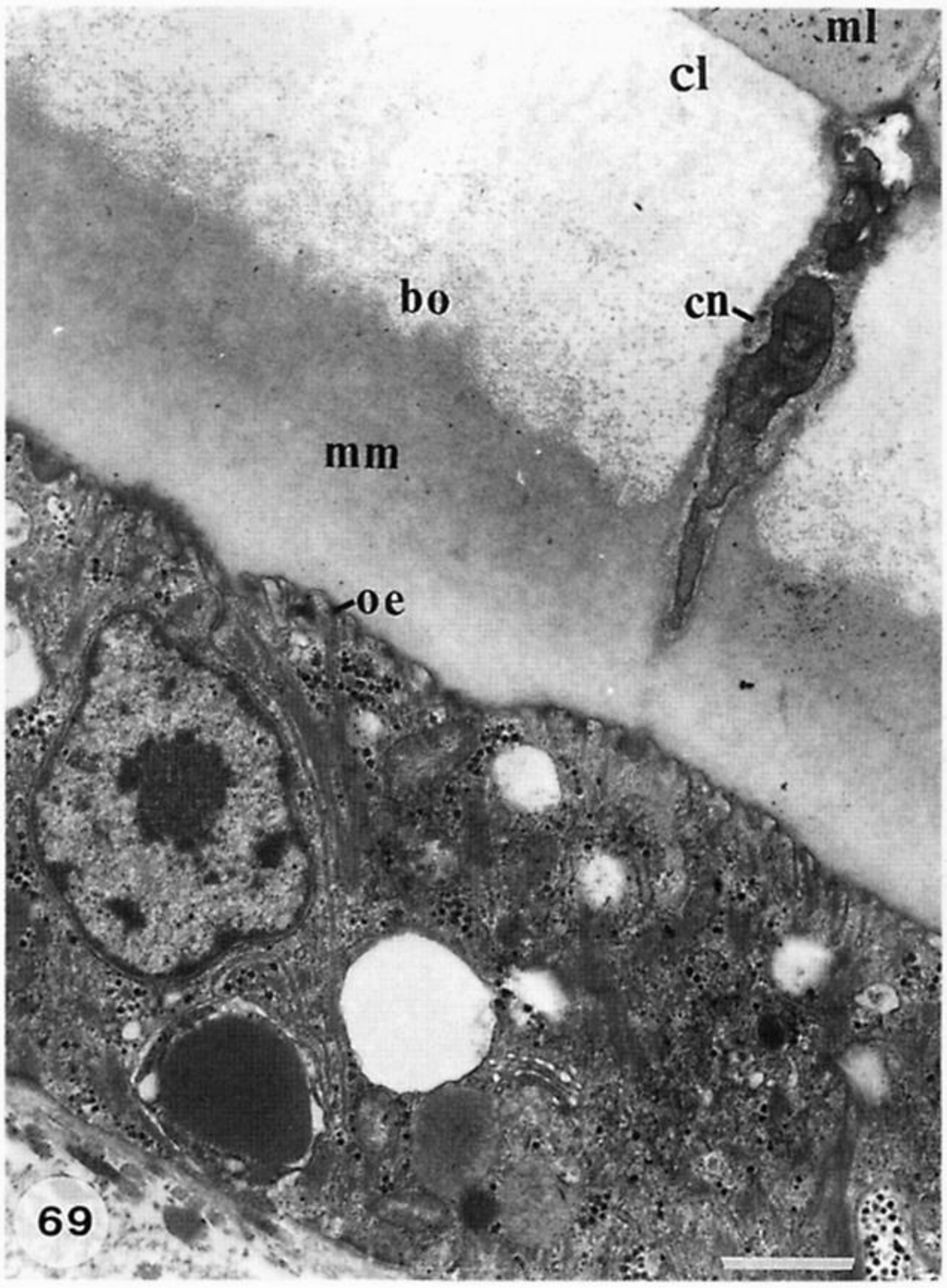

Figures 68–69. Transmission electron micrographs of demineralized valves and mantle of *Lingula anatina*.

Figure 68. Section of the marginal fold to show cuboidal outer epithelium (oe) underlying the primary layer (pl) and periostracum (top, right-hand corner), connective tissue with collagen fibrils (co), microvillous inner epithelium (ie), pellicle (pe) and vesicular cells (vr) bordering the periostracal groove. Scale bar = 1 μm.

Figure 69. Section of the shell and the secreting digitate protrusions of the apical plasmalemma (oe) showing the organic components of a botryoidal laminar set, penetrated by a canal (cn), with a chitinoproteinaceous membrane (ml) overlain by an apatitic compact lamina (cl) passing into a botryoidal zone (bo) succeeded by membranous laminae (mm). Scale bar = 1 μm.

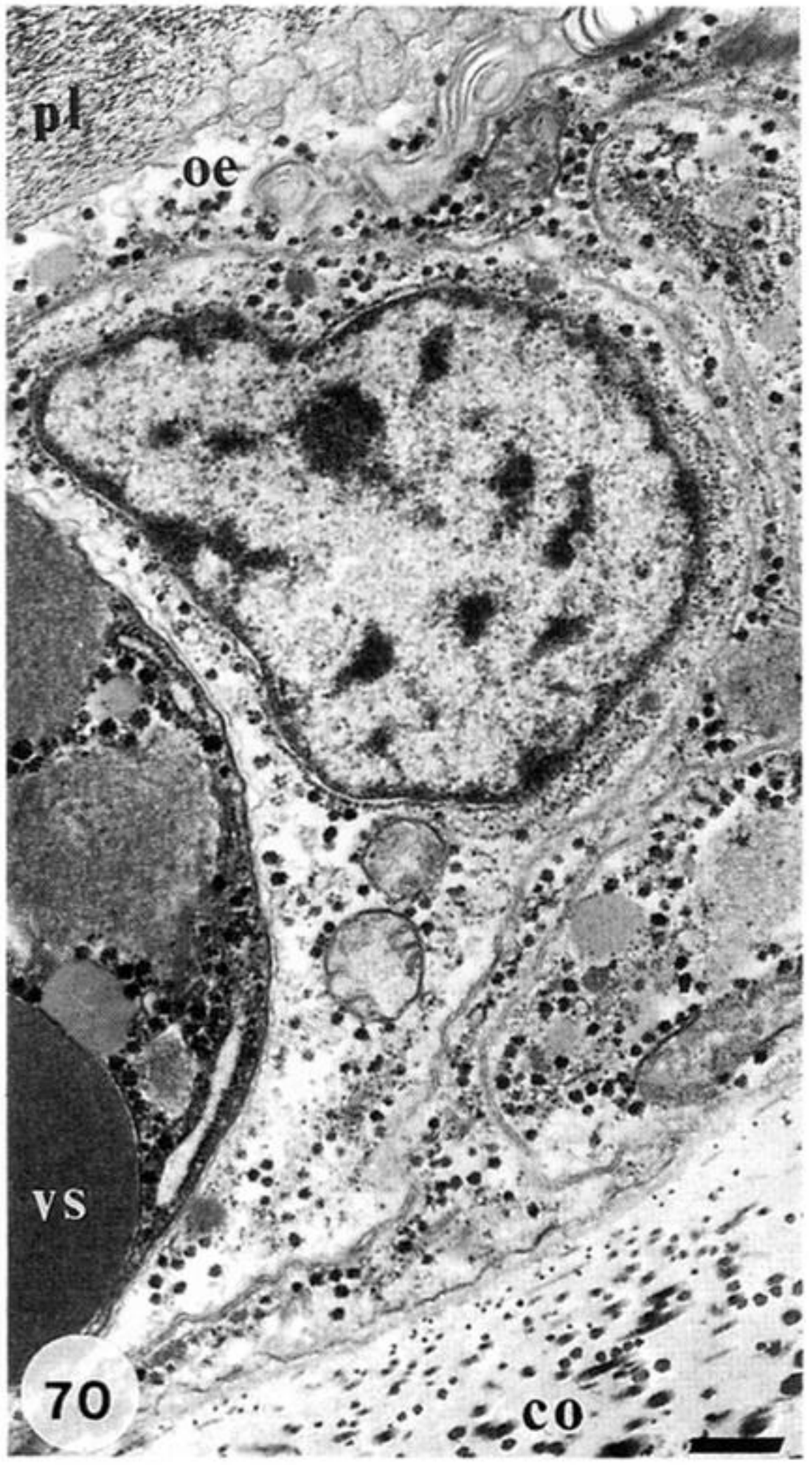

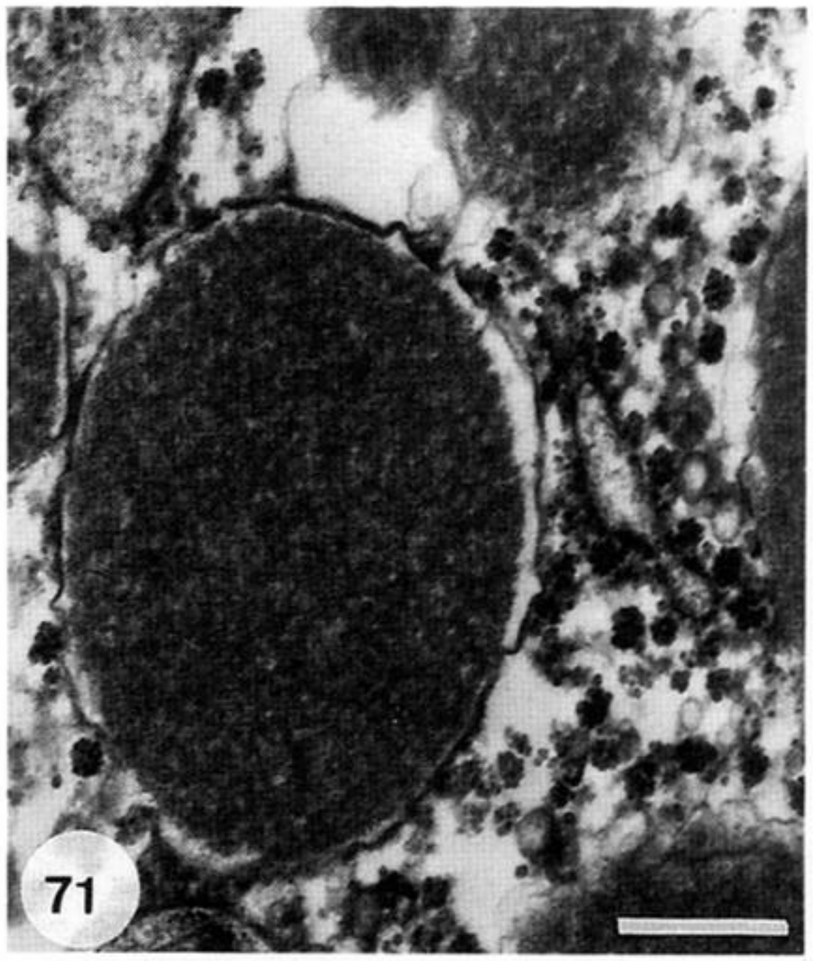

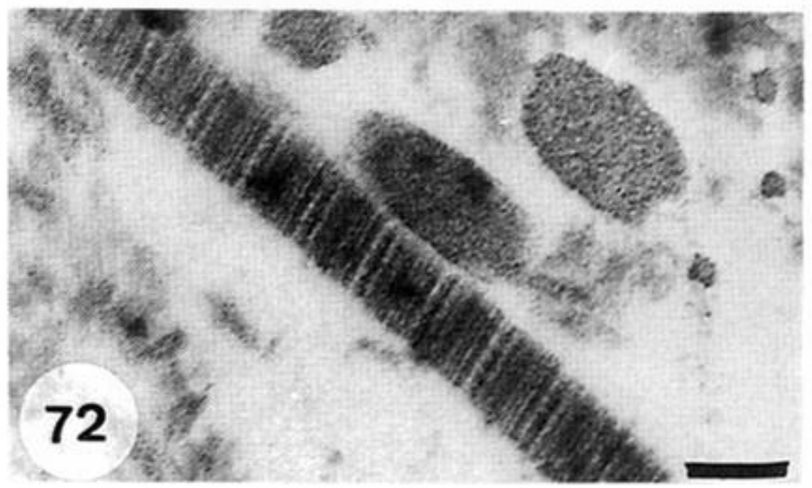

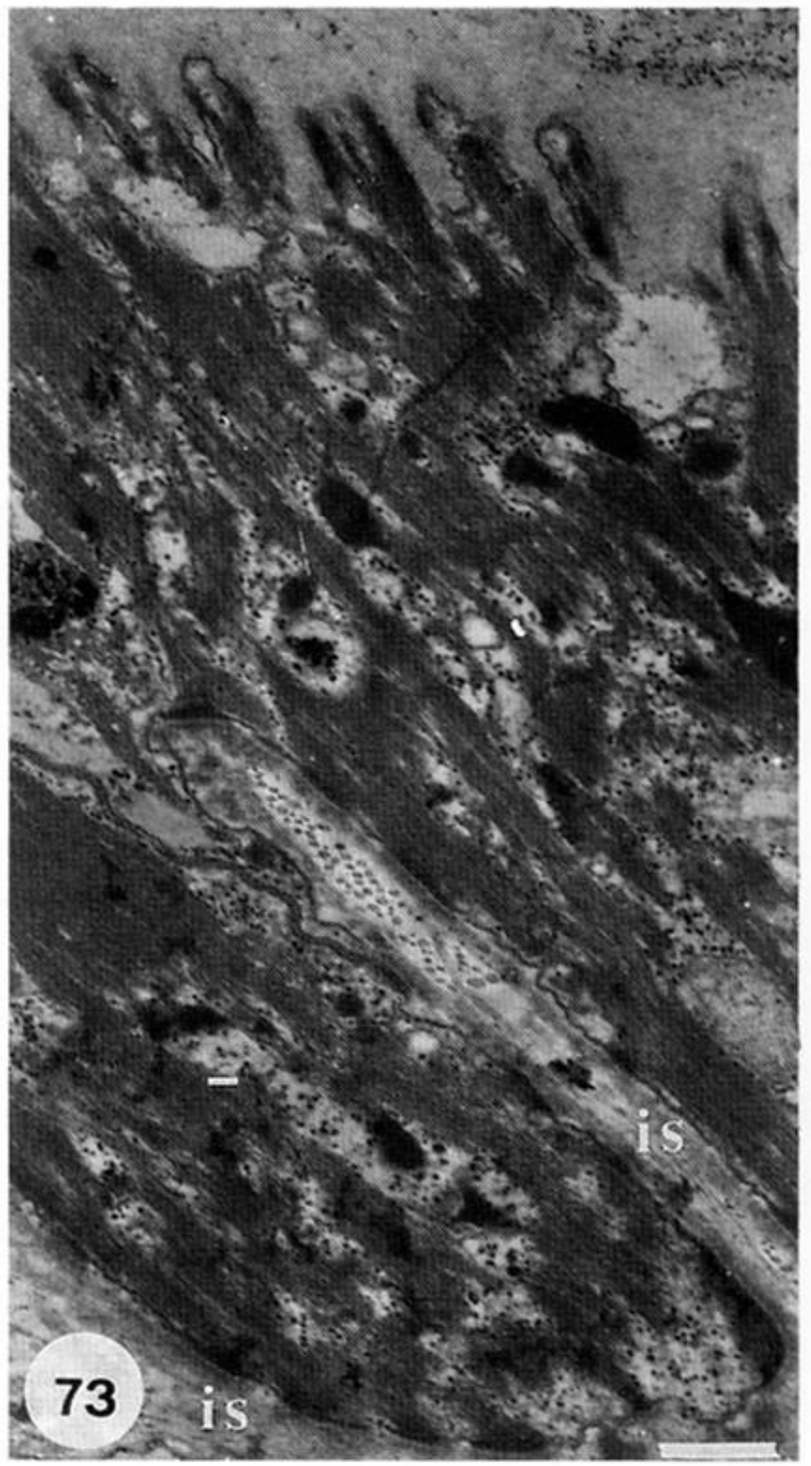

Figures 70–73. Transmission electron micrographs of sections of mineralized shell and mantle of *Lingula anatina*.

Figure 70. Section showing a rod and plate lamina (pl) secreted by digitate protrusions of apical plasmalemma (oe) of the secreting outer epithelium with a cluster of membrane-bound vesicles (vs), and connective tissue with collagen fibrils (co). Scale bar = 0.5 μm.

Figure 71. Detail of a vesicular cluster within the outer epithelium showing the mottled aspect of the vesicles and the abundance of glycogen granules and protein-coated electron-lucent components. Scale bar = 0.5 μm.

Figure 72. Detail of connective tissue showing the periodic banding of a collagen fibril. Scale bar = 100 nm.

Figure 73. Section of the outer epithelium peripheral to a muscle scar showing the pervasion of fibrils throughout the cells and the digitate protrusions of the apical plasmalemma and the intrusive sheets of connective tissue (is) between outer epithelial cells. Scale bar = 0.5 μm.

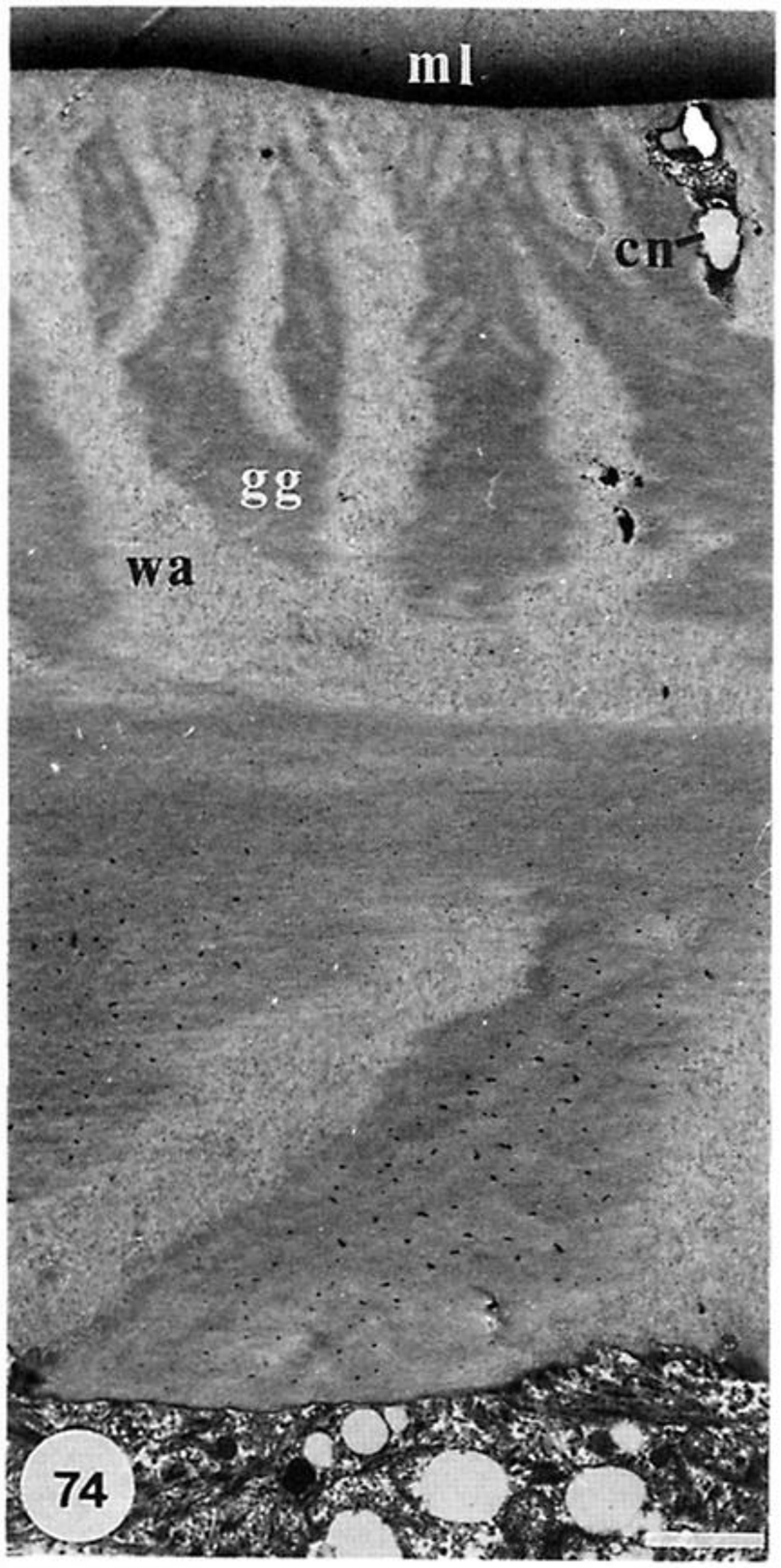

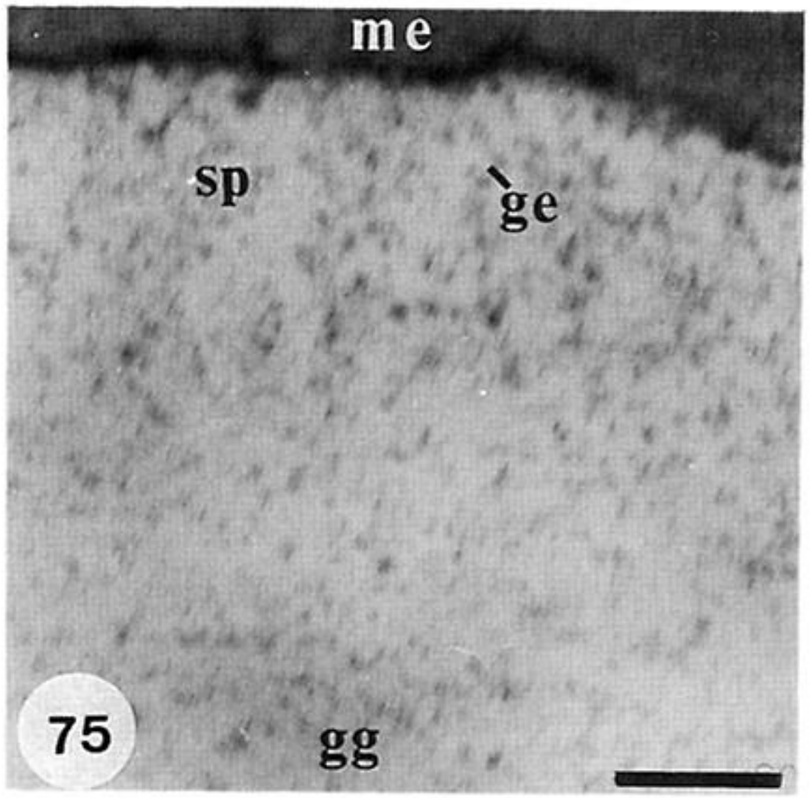

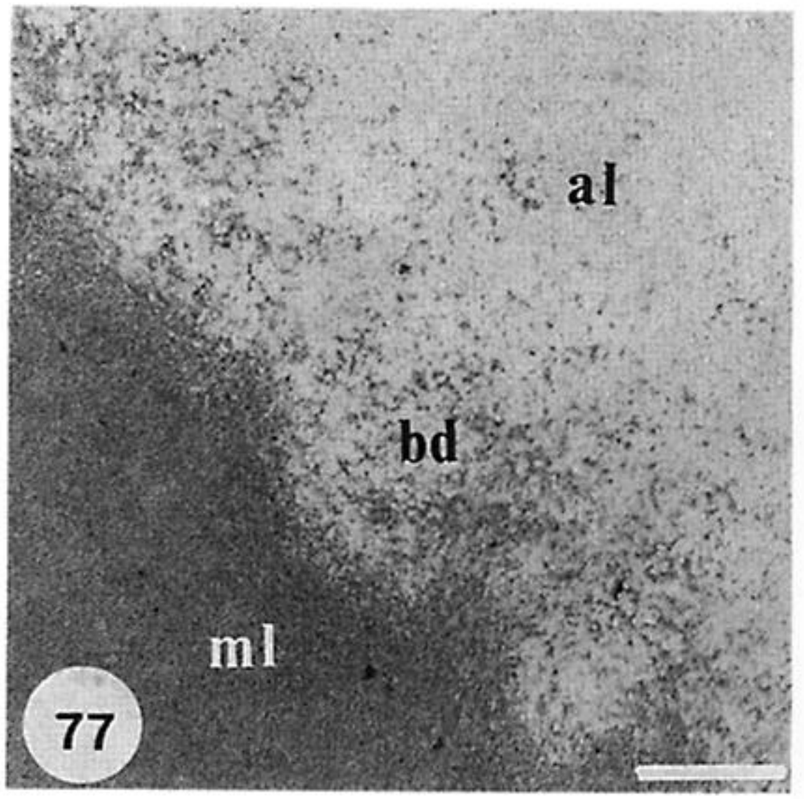

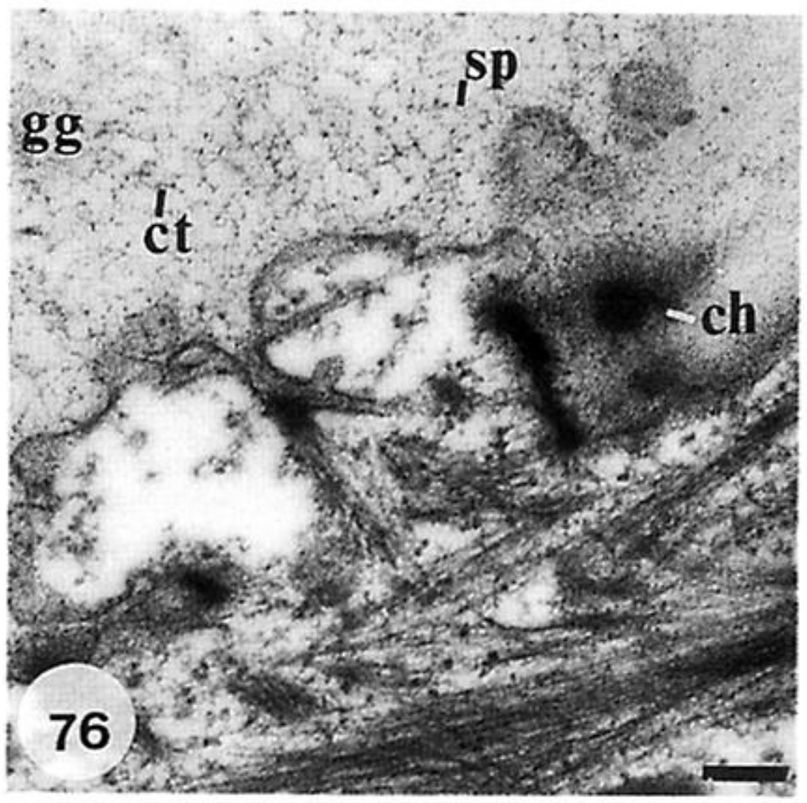

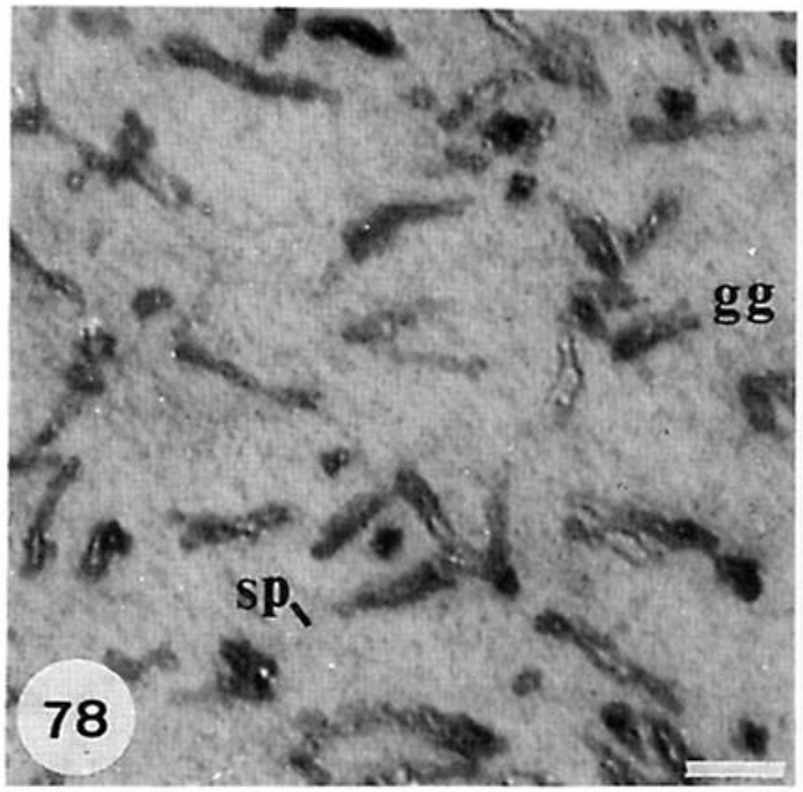

Figures 74–78. Transmission electron micrographs of demineralized valves and mantles of *Lingula anatina*.

Figure 74. Section of a walled set of laminae and secreting outer epithelium showing vesicular membranes within a canal (cn), a membranous lamina (ml) and alternating partitions of apatite (wa) and GAGs wih chitin (gg). Scale bar = 2 μm.

Figure 75. Detail of junction between a chitinoproteinous membrane (me) and a compact lamina composed of granules (ge) and spherules (sp) outlined by proteinaceous coats with chitin particles; concentrations of GAGs (gg) also occur. Scale bar = 100 nm.

Figure 76. Detail of digitate protrusions of an apical plasmalemma secreting chitinous fibrils (ch) and GAGs (gg) and apatitic granules and spherules (sp) with chitinoproteinaceous coats (ct). Scale bar = 200 nm.

Figure 77. Detail of interface between apatitic (al) and membranous (ml) laminae marked by the presence of botryoids (bd). Scale bar = 0.5 μm.

Figure 78. Detail of a demineralized lamina of rods and plates showing the chitinoproteinaceous strands associated with apatite (before it was removed by EDTA) in a GAGs (gg) matrix with outlines of spherules (sp). Scale bar = 50 nm.

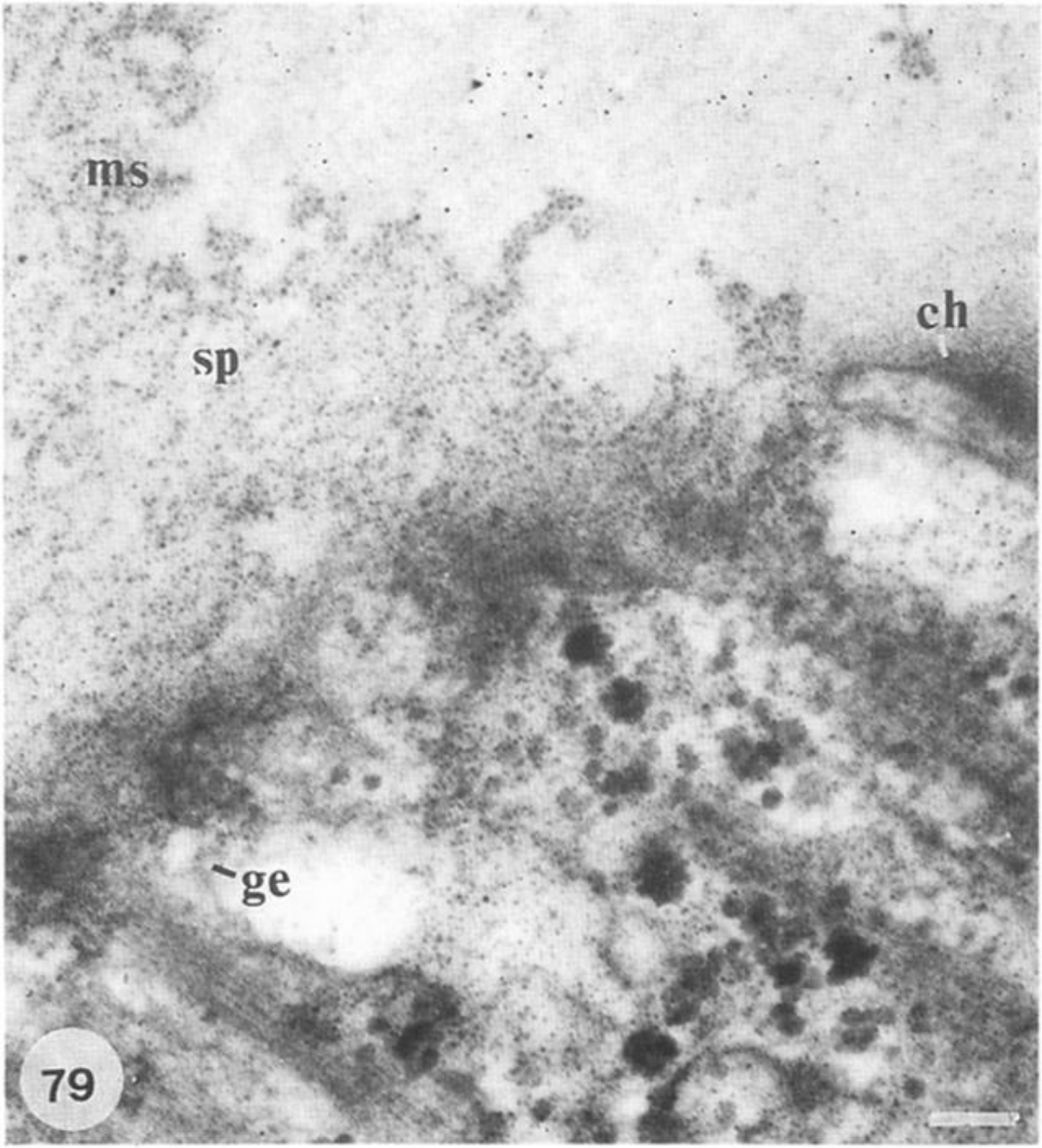

Figure 79. Transmission electron micrograph of a section of the apical plasmalemma of outer epithelium contiguous with a demineralized botryoidal lamina of *Lingula anatina* showing the exocytosis of granules (ge) and spherules (sp) to form mosaics (ms) in a GAGs matrix; chitinous fibrils (ch) were also secreted. Scale bar = 100 nm.

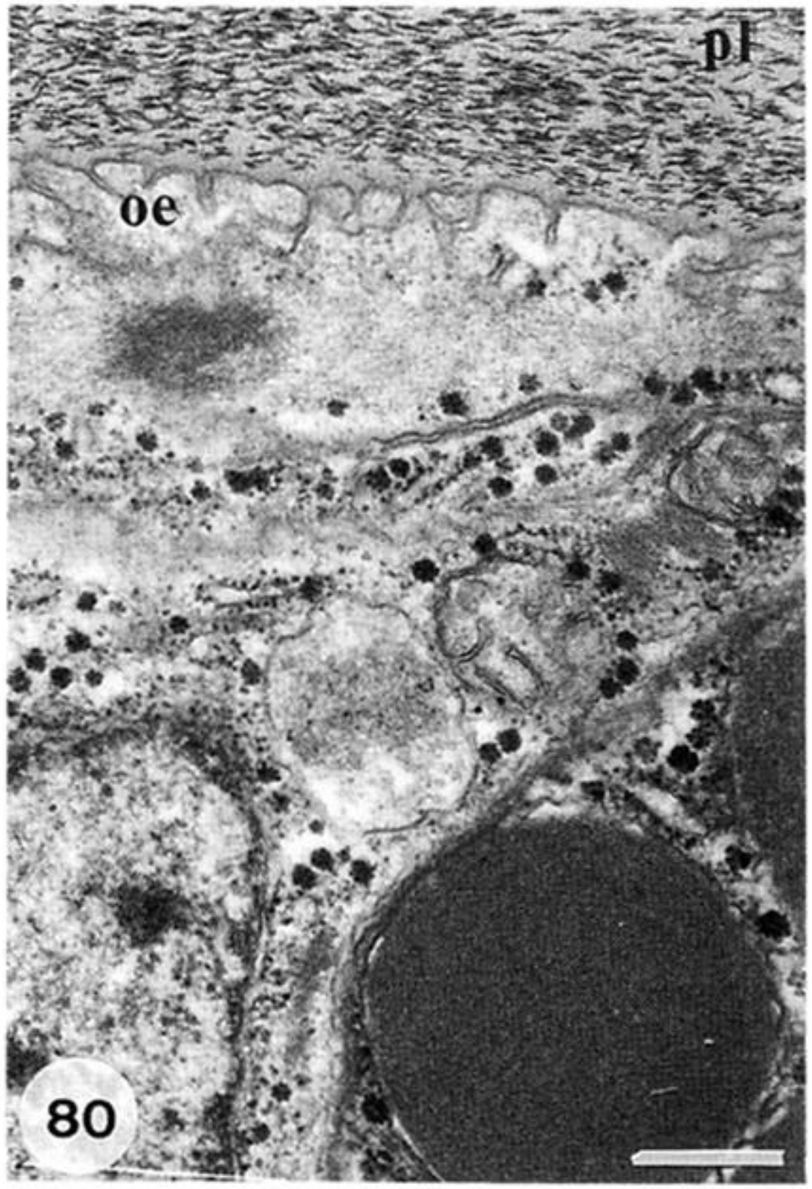

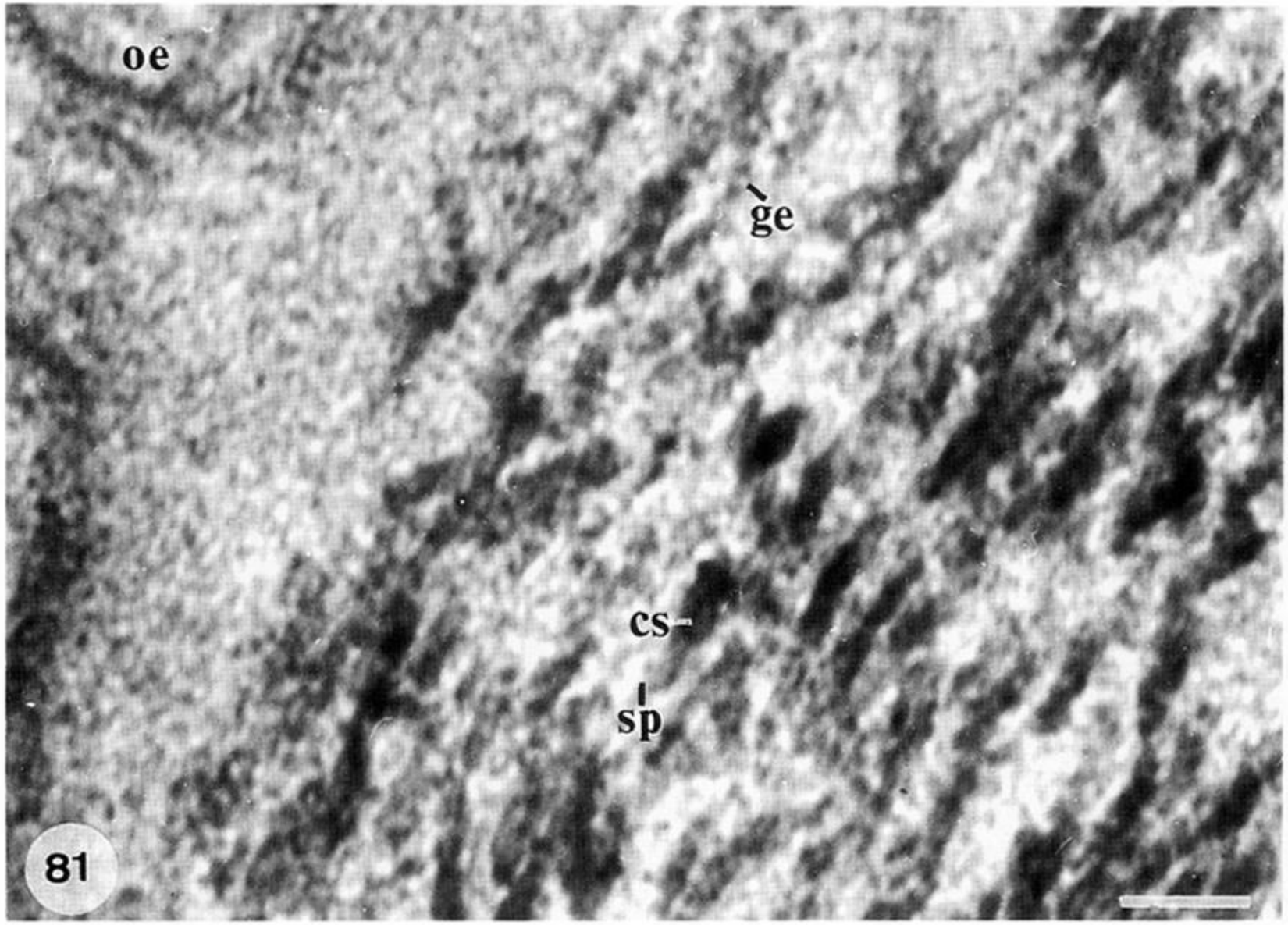

Figures 80–81. Transmission electron micrographs of a section of mineralized shell and secreting mantle of *Lingula anatina* stained with uranyl acetate and lead citrate.

Figure 80. Section of a rod and plate lamina (pl) with its secreting epithelium showing flattened protrusions of the apical plasmalemma (oe), glycogen granules, free ribosome particles, mitochondria and mottled vesicles. Scale bar = 0.5 μm.

Figure 81. Detail of the junction between the apical plasmalemma (oe) and the rod (and plate) lamina composed of granular (ge) and spherular (sp) apatite with coats of medium electron-dense protein and chitin particles, arranged linearly with strands of electron-dense material, assumed to be chitinoproteinaceous (cs). Scale bar 50 nm.

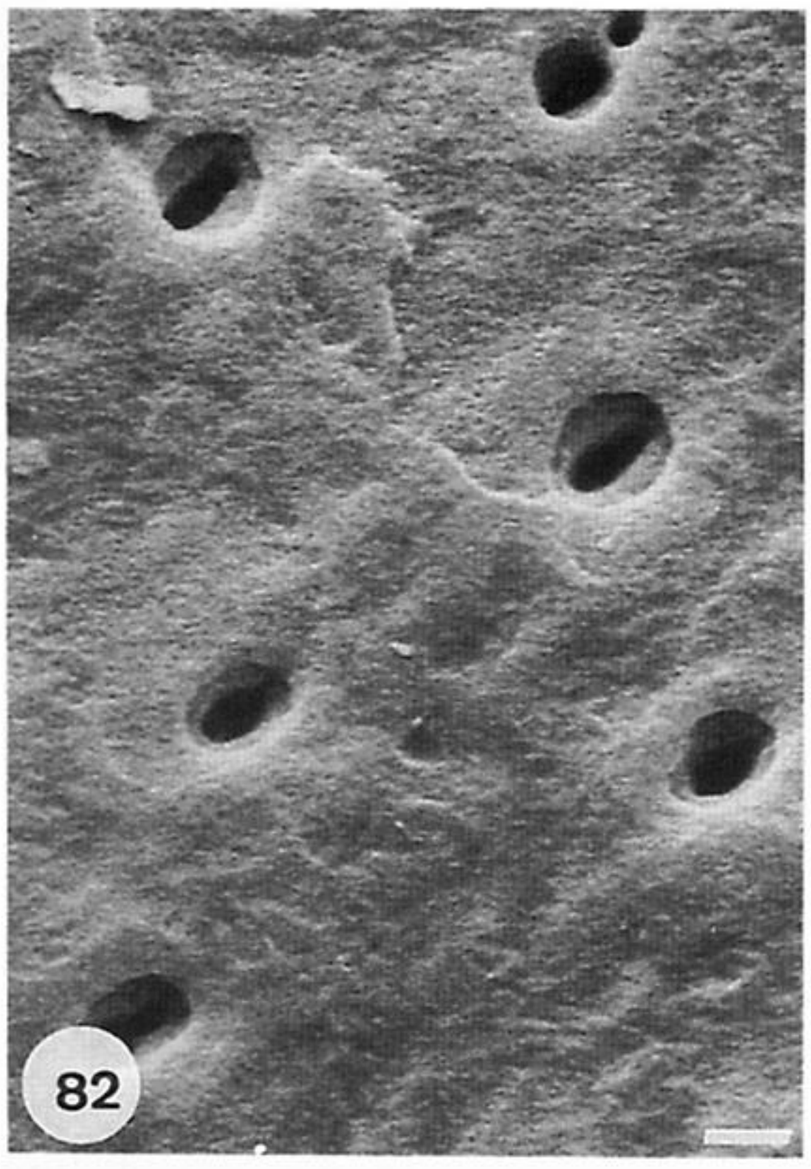

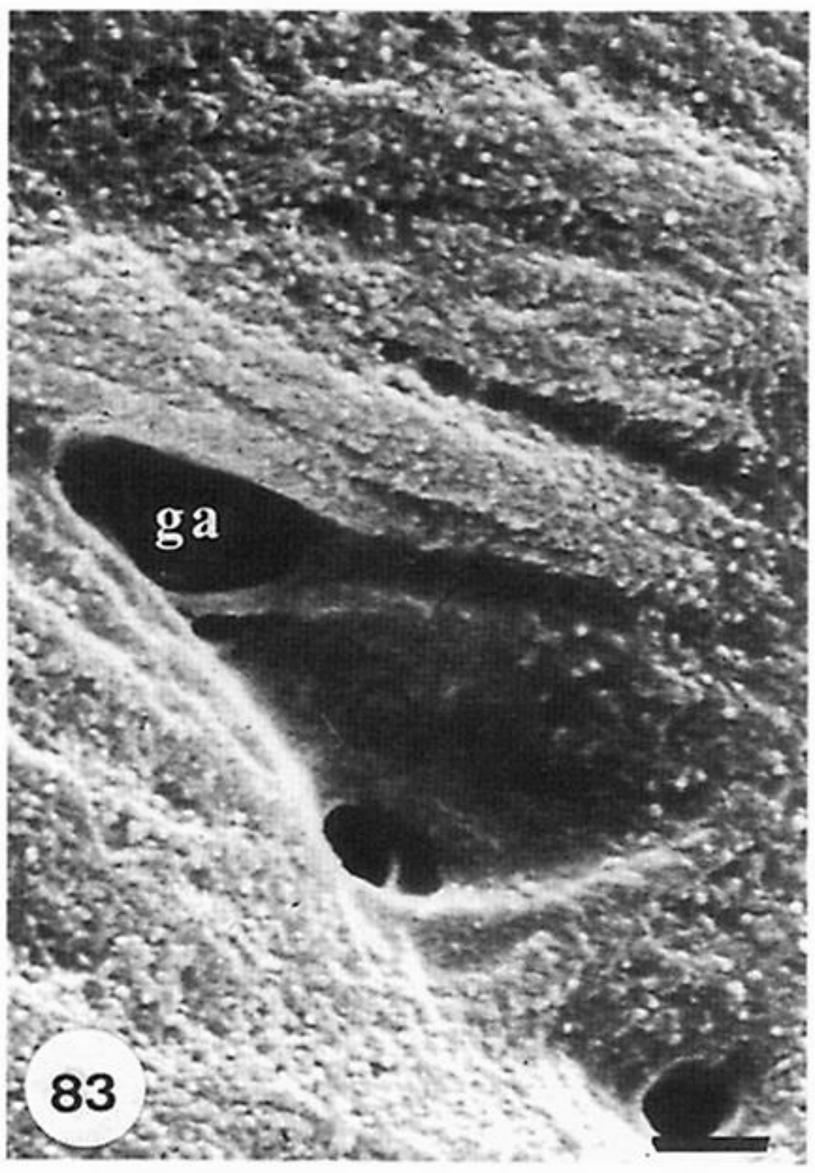

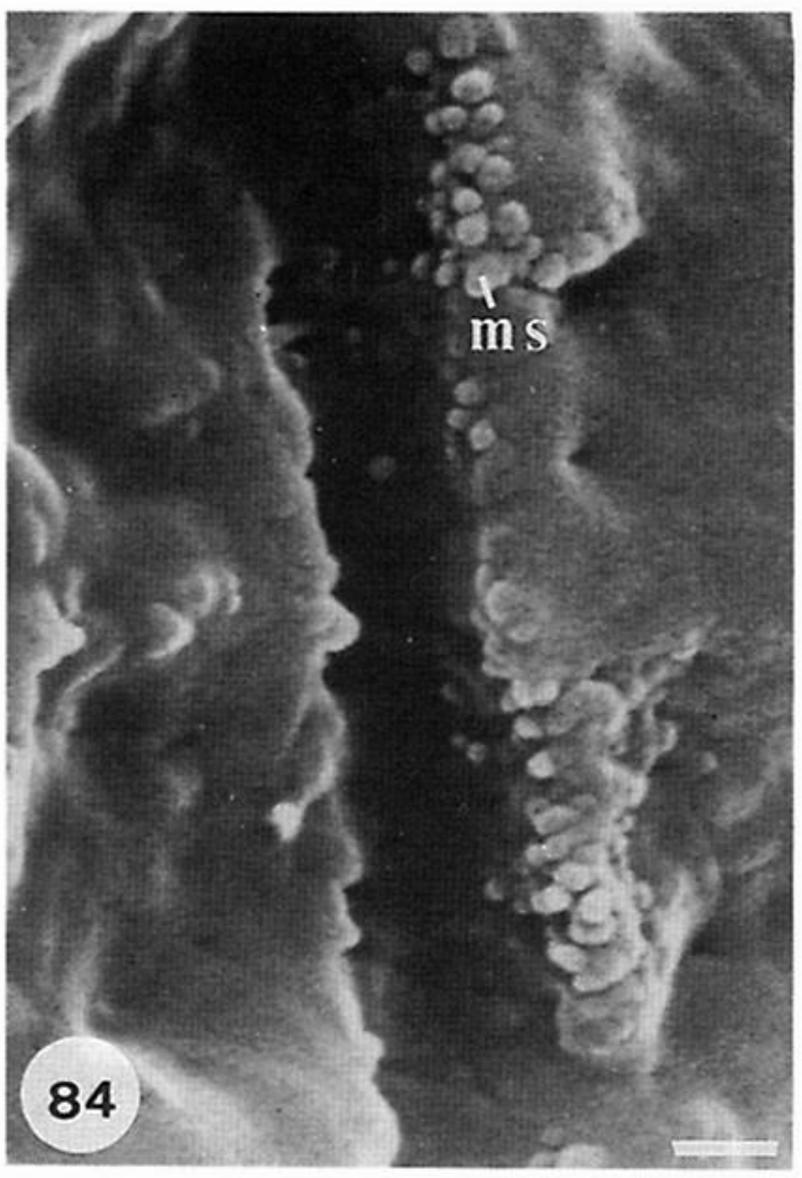

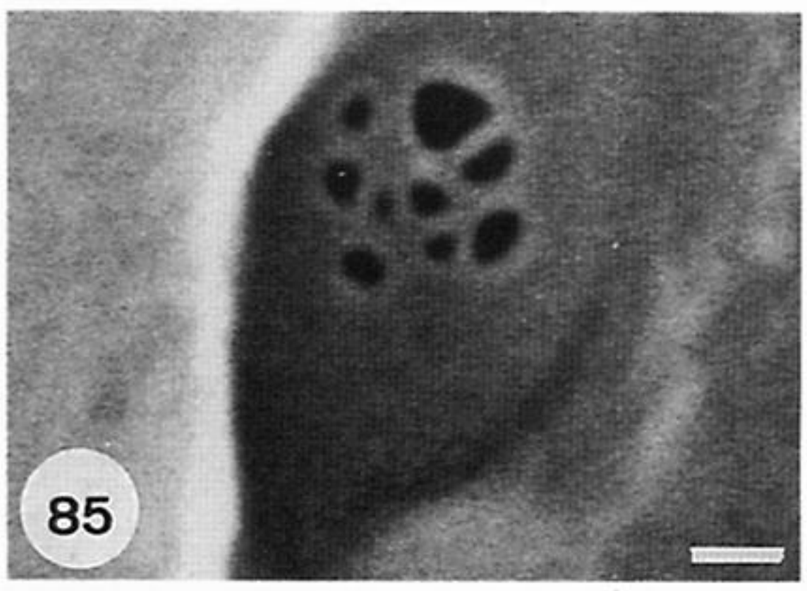

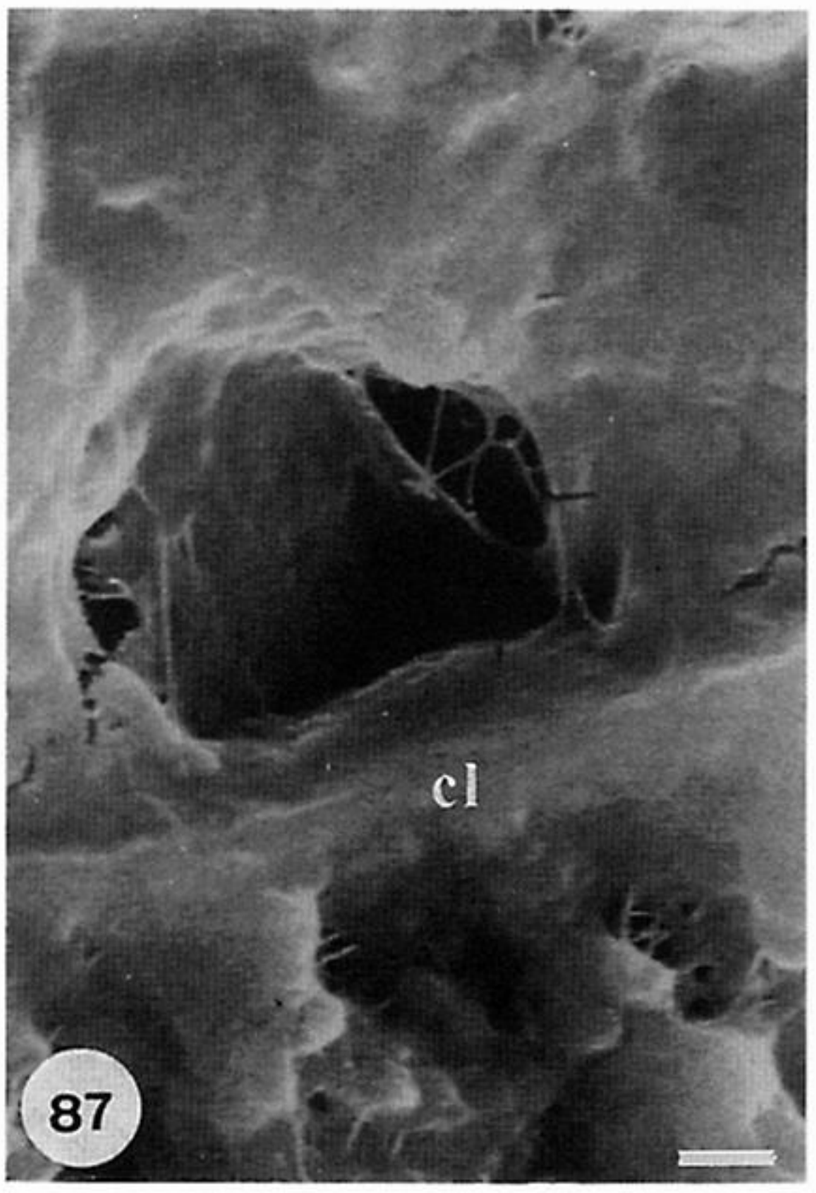

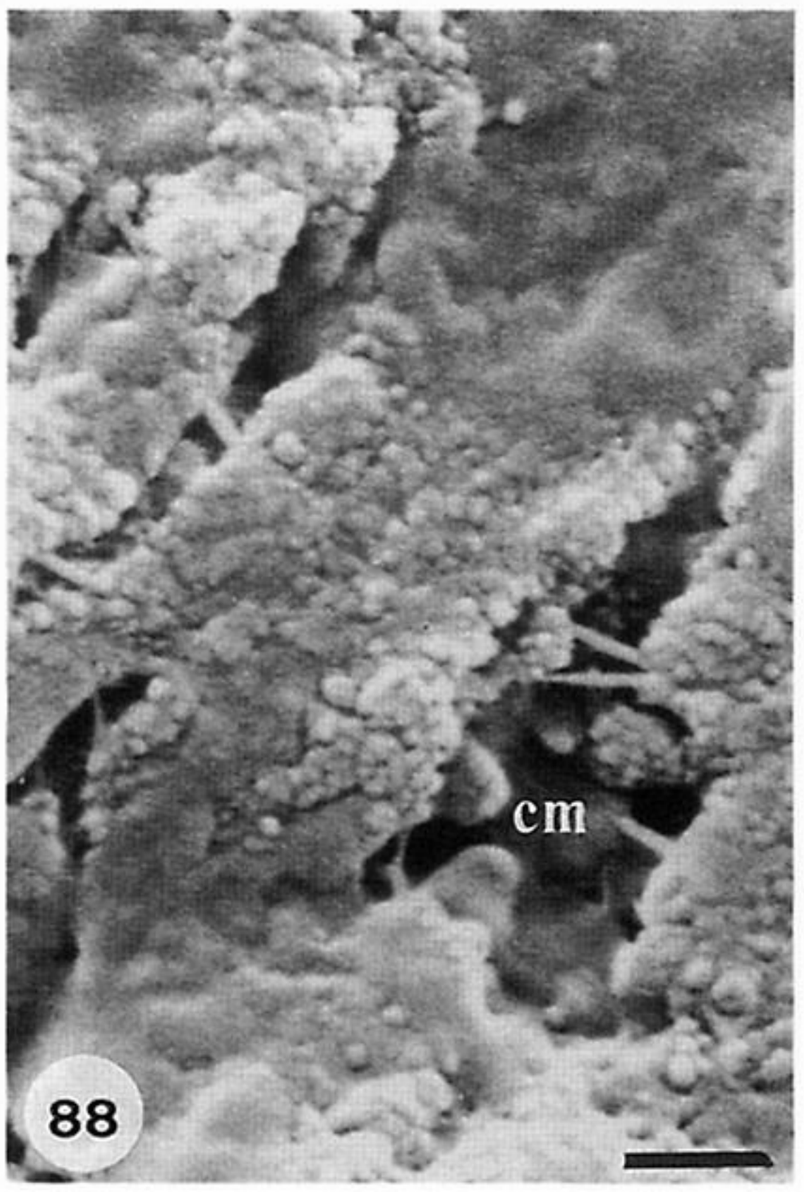

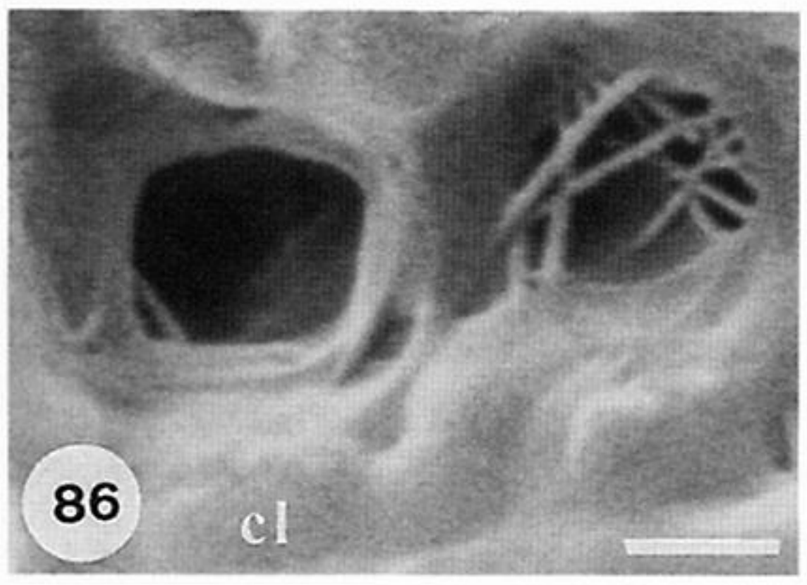

Figures 82–88. Scanning electron micrographs of gold-coated surfaces of the shell of *Lingula anatina*.

Figure 82. Radially arranged canal apertures in an apatitic compact lamina exposed on the internal surface of the mid-part of a valve digested in chitinase, with a converging pair of canals near the top right-hand corner. Scale bar = 2 μm.

Figure 83. Detail of a membrane-lined canal aperture in an apatitic compact lamina (with closely packed mosaics) exposed on the internal surface of the mid-part of a valve treated with phosphate buffer (100 mM, pH 7), with the beginnings of a horizontal gallery (ga) trailing laterally from the expanded opening of the canal, crossed by a collagen fibril strand. Scale bar = 1 μm.

Figure 84. Detail of a canal wall studded with mosaics (ms) in a botryoidal lamina exposed in a cut, vertical, posteromedian section of a valve digested in endoproteinase Glu-C. Scale bar = 0.5 μm.

Figure 85. Detail of a transverse membrane within the aperture of a canal in a compact lamina exposed on the internal surface of the mid-part of a valve treated with Tris buffer (80 mM, pH 8) with $CaCl_2$ (100 mM). Scale bar = 200 nm.

Figure 86. Detail of the openings of two horizontal galleries crossed and framed by collagenous fibrils immediately inward of an apatitic compact lamina (cl) exposed in a cut, vertical, median section in the mid-part of a valve digested in chitinase. Scale bar = 0.5 μm.

Figure 87. Transverse membrane across a horizontal gallery within a botryoidal lamina and immediately internal of an apatitic compact lamina (cl), exposed in a cut, vertical, median section in the mid-part of a valve digested in chitinase. Scale bar = 1 μm.

Figure 88. Detail of a vertical chamber intruded by mosaics (cm) and branching canals, all crossed by collagenous strands within a botryoidal lamina exposed in a cut, vertical posteromedian section of a valve treated with phosphate buffer (100 mM, pH 7). Scale bar = 1 μm.

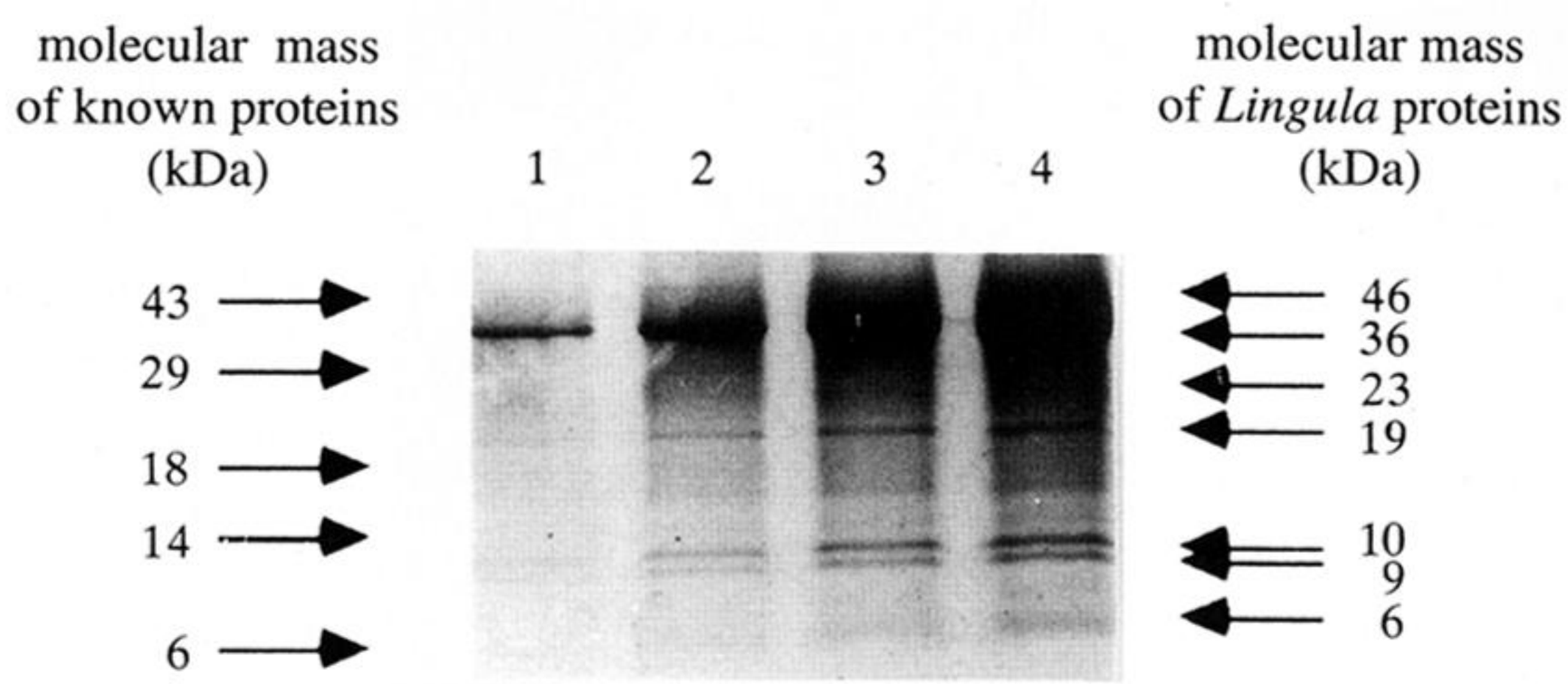

Figure 89. SDS PAGE analysis of the mineral-associated proteins from valves of *Lingula anatina*; the soluble fraction of the mineral-associated proteins was fractionated by SDS PAGE in a 15% polyacrylamide gel using the method of Schägger & Von Jagow (1987); Coomassie Brilliant Blue-R revealed the mixture of proteins present.

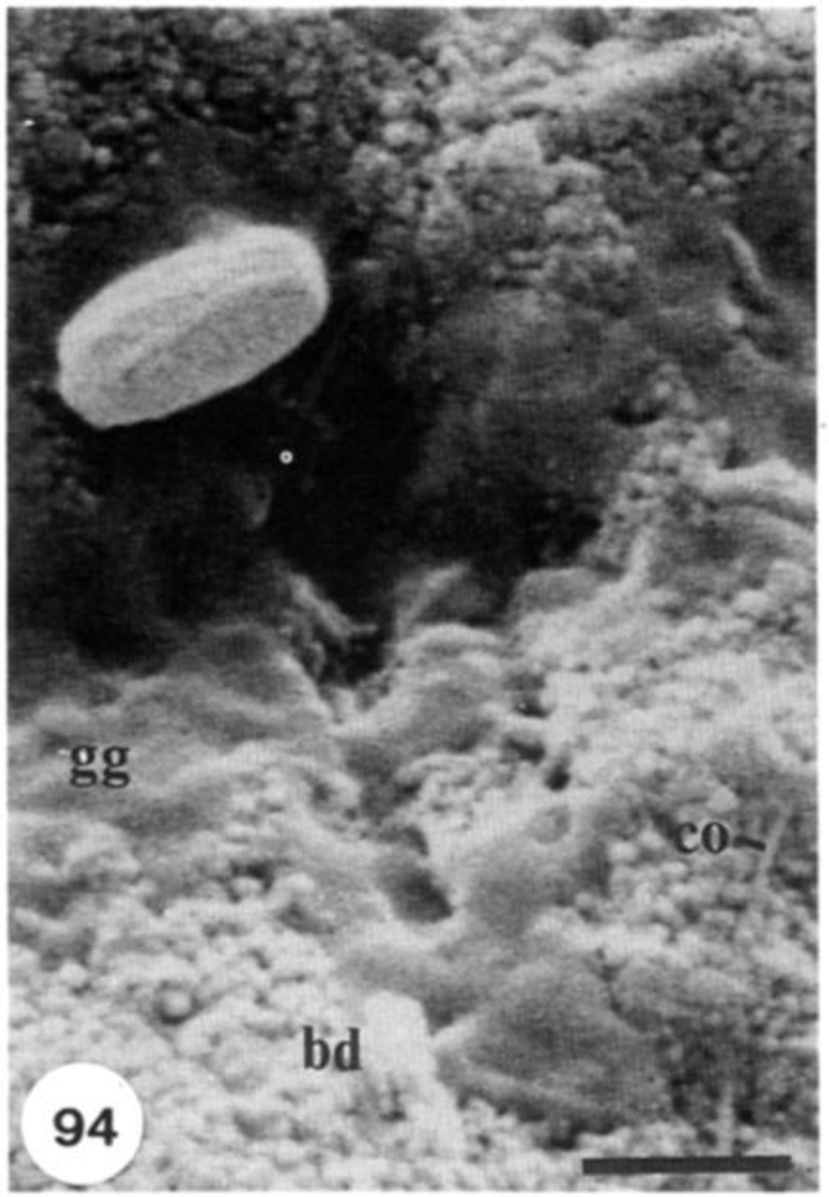

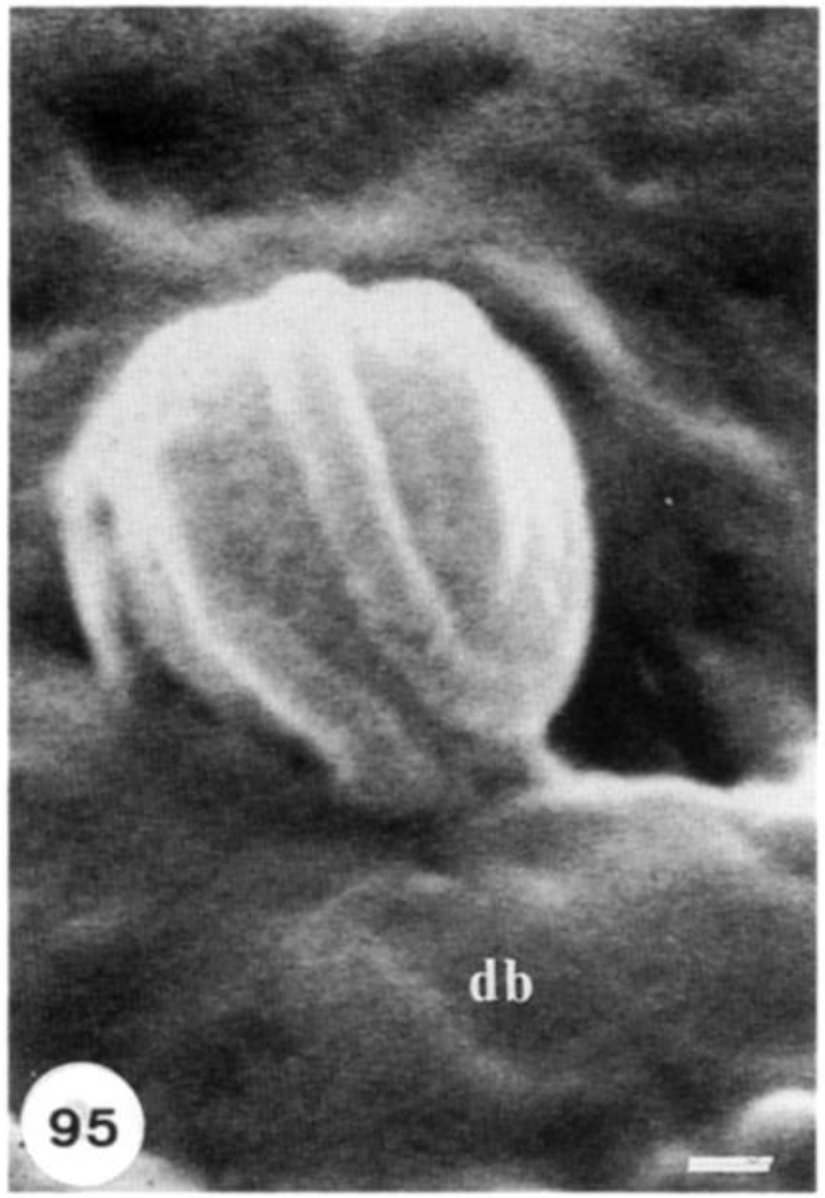

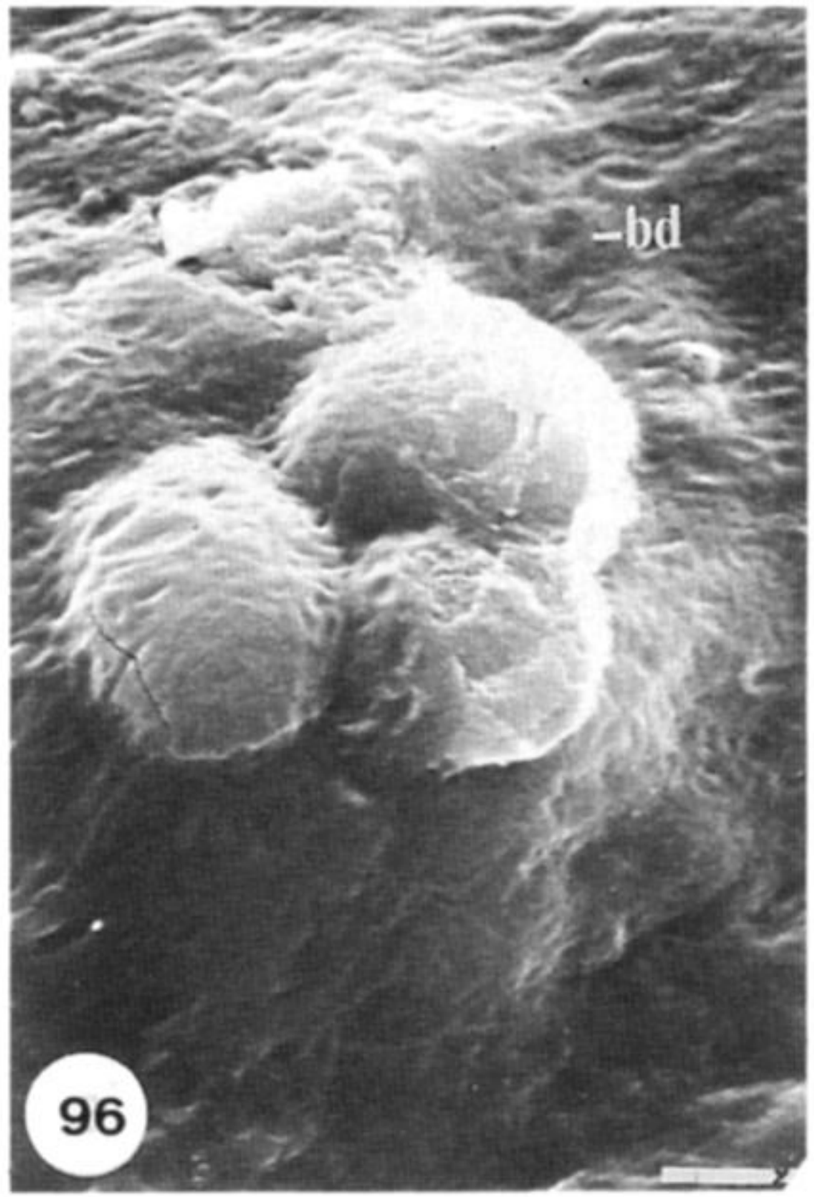

Figures 94–96. Scanning electron micrographs of gold-coated, extrinsic objects in the shell of *Lingula anatina*.

Figure 94. Banded vesicle developed in GAGs (gg) on a cut, vertical section of the body platform of a valve digested in subtilisin, with botryoidal apatite (bd) and collagen (co). Scale bar = 1 μm.

Figure 95. Hooped vesicle in GAGs with discoidal bodies (db) on a cut, vertical median section of the mid-part of a valve treated with MES buffer (100 mM, pH 6). Scale bar = 200 nm.

Figure 96. A cluster of large vesicles developed in GAGs with discoidal bodies (bd), on the internal surface of the marginal fold of a valve treated with phosphate buffer (100 mM, pH 7). Scale bar = 2 μm.